

# **Master Thesis**

Institute of Applied Geosciences  
Rechbauerstraße 12, 8010 Graz  
Graz University of Technology

## **Geological Conditions Favoring Extreme Scour of an Unlined Spillway at Ricobayo Dam, Zamora, Spain.**

by  
Markus Kaspar

Thesis presented in partial fulfilment of the requirements for the degree  
of Master of Earth Sciences  
at the Graz University of Technology

Reviewer:

Univ.- Prof. D. S. Kieffer, B.A., M.S., PhD.

Graz, March 2012

## Ehrenwörtliche Erklärung

Ich erkläre ehrenwörtlich, dass ich die vorliegende Arbeit selbstständig und ohne fremde Hilfe verfasst, andere als die angegebenen Quellen nicht benutzt und die den Quellen wörtlich oder inhaltlich entnommenen Stellen als solche kenntlich gemacht habe. Die Arbeit wurde bisher in gleicher oder ähnlicher Form keiner anderen Prüfungsbehörde vorgelegt und auch noch nicht veröffentlicht. Die vorliegende Fassung entspricht der eingereichten elektronischen Version.

Graz, März 2012

(Markus Kaspar)

## Acknowledgement

Herby I would like to thank any person who advised me in preparing this thesis. I thank my advisor D. S. Kieffer, Univ.-Prof. B.A. M.S. Ph.D. for his expert advice, ideas and friendly suggestions in preparing this thesis.

Further, I thank the employees of Iberdrola Rafael Landin Zorilla, Eduardo Rojo Martinez and Yolanda Diego Martin and the company of Iberdrola S.A for providing information about and access to their facilities and assisting during fieldwork.

I thank my parents for supporting me over the years during my education and my uncle Werner for helping me with the Spanish literature.

Graz, März 2012

(Markus Kaspar)

---

## Table of contents

1. Kurzfassung .....	1
1. Abstract .....	2
2. Introduction .....	3
3. Purpose and scope .....	4
4. Scour .....	5
4.1 Definition .....	6
4.2 Scour features in natural channels .....	6
4.3 Bedrock incision .....	7
4.4.1 Knickpoint migration .....	9
4.4.1.2 Geological factors influencing knickpoint migration .....	11
4.4.2 Erosion mechanisms at spillway structures .....	12
4.5 Scour models .....	16
4.5.1 Annandale's Erodibility Index method .....	16
5. The Ricobayo Dam .....	22
5.1 Introduction .....	22
5.2 The History of the Dam .....	25
5.2.1 Construction and layout .....	25
5.2.2 Spillway scour damage .....	28
5.2.3 Spillway repair .....	38
6 Geologic conditions .....	40
6.1 Regional conditions .....	40
6.2 Site conditions .....	44
6.2.1 Methods and description standards .....	44
6.2.2 Observations and Findings .....	58
7. Block removability analysis .....	82
7.1 Block Theory .....	82
7.2 Removability of Blocks .....	82
7.2.1 Finiteness .....	84
7.2.2 Removability of finite blocks .....	85
7.3 Removability using stereographic projection .....	86
7.3.1 The principle of the stereographic projection (equal angle) .....	86
7.4 Removability Plots .....	88
7.4.1 The factor of safety and friction cone concept .....	88
7.4.2 The Block Erodibility Spectrum .....	91
8. Discussion and Conclusions .....	114
9. References cited .....	117
10. Appendix .....	121
A1 Removable JPs .....	121
A2 Compound Friction Cones of Removable JPs .....	125
A3 Shapes of Removable Blocks .....	135

## Table of Figures

Fig.4.1: Formation of a strath (After Rance, 2007).....	7
Fig.4. 2: Plot of the ratio between tributary slope ( $S_t$ ) and primary stream slope ( $S_p$ ) against the ratio of principal valley drainage area ( $A_p$ ) to tributary drainage area ( $A_t$ ). Data from 16 coastal confluences in Oregon. The data indicate m/n values of essentially 1.0 and suggest that erosion is related linearly to stream power. The line drawn on the figure corresponds to a m/n value of 1.0 .....	9
Fig.4.3 : Profile through a stream channel bed showing features of knickpoint migration and associated bedrock terraces (T1, T2, T3) at Elder Creek, California (after Seidl & Dietrich, 1992). .....	10
Fig.4.4: Diagram showing the relationship of Vertical face height (H) and flow depth (d) at a knickpoint. $d_c$ is the critical depth at $d_1$ . Headcut migration will occur if at the critical depth ( $d_c$ ) the intersection of $d_c$ with the available channel slope ( $S_{1,2,3}$ ) lies above the orthogonal to the slope, defining the erodibility or critical shear stress of the material involved (after Leopold, 1964). .....	11
Fig.4.5: Most common failure modes at knickpoints (after May, 1989).....	12
Fig.4.6: Schematic longitudinal section of a spillway channel showing the domains of different scour processes (modified after Cameron et al, 1988). .....	14
Fig.4.7: Schematic sketch of the plucking mechanism. Large saltating clasts directly abrade the block by their impact, but more important contribute in generation and growth of new cracks. Those cracks subsequently loosen the blocks. Hydraulic clast wedging (debris accumulations) within the joints supports opening of the joints. Surface drag forces ( $F_f$ ), shear forces ( $\tau$ ) and differential pressures ( $p$ ) across the block act to lift loosened blocks. Where the downstream neighbour of a block has previously been removed, new modes of removal can be possible such as rotation and sliding and removal is greatly facilitated (after Whipple et al., 2000). .....	15
Fig.4. 8: Annandale's Erodibility Index and stream power with erosion threshold (Annandale, 2006) .....	17
Fig.4. 9: Influence of orientation on resistance against scour (after Annandale, 2006).....	21
Fig.5 1: Location of the study area. A detailed Satellite image of the Ricobayo Dam facility is shown in Fig.5.2 as indicated by the box (Google Maps, 2012). .....	22
Fig.5 2: Satellite image of the Ricobayo Dam facility. Labelled are the most important features related to the dam (modified after Google Maps, 2012).....	24
Fig.5 3: Alternative layout of the Ricobayo Dam in 1927 (Revista de Obras Públicas, 1933). .....	25
Fig.5 4: Map of the Ricobayo dam site showing the original topography of the area, the initial alignment of the spillway and the location of the consecutively formed plunge pool due to scouring. Scale 1: 3000. Section A-B is shown in Fig.5a. (modified after Rubio, 1940). .....	26
Fig.5 5:Original spillway situation .....	27
Fig.5 6: Open slot in the central part of the Ricobayo Dam, which was closed in 1933 for the construction of the power house (San Roman, 2006).....	28
Fig.5 7: Illustration of the 5 main stages of scour at the spillway. Note steepening of the natural rock slope and progressive upstream movement of erosion towards the reservoir (Guia Tecnica, 1997).....	29
Fig.5 8: The first major scour at the Ricobayo spillway. (a): View to the original front slope of the spillway in the first month of operation. The water flow was discharged unregulated over bare rock. (b): The original slope is already eroded after one month of operation leaving a gorge behind as the water works its way towards the reservoir (Pictures: Guia tecnica, 1997).....	30
Fig.5 9: An approx. 200m long gorge has developed working its way back to the reservoir..	31

---

Fig.5 10: Situation of the spillway during the 2nd major scour stage in March 1934. View upstream into the gorge. Sidewalls are almost vertically inclined and the front slope has steepened up compared to its original state, to form a waterfall at the exit of the spillway (Guia tecnica, 1997). .....	31
Fig.5 11: View downstream the spillway. The right curvature of the right wall at the end of the spillway was changed more to the middle of the plunge pool. The spillway surface was left unlined (Riesco Chueca, 2009). .....	32
Fig.5 12: Repair works on the spillway in summer of 1934. Construction of a concrete wall at the front slope of the spillway. Looking at the curvature of the wooden balk, the initial shape of the plunge pool can be recognized (Guia tecnica, 1997). .....	33
Fig.5 13: Situation of the spillway in 1935. Water release in January. By that time two waterfalls are developed. One in the back at the front slope of the spillway, the second one at the exit of the gorge. (Guia tecnica, 1997). .....	34
Fig.5 14: Only about one month later the vertical erosion has abraded the bottom of the channel. The second waterfall has disappeared (Guia tecnica, 1997). .....	34
Fig.5 15: Collapse of the front wall of the spillway. View upstream where the front wall and the spur dike were situated at. Note the huge amounts of crushed rock in the riverbed (Guia tecnica, 1997). .....	35
Fig.5 16: Look to the right wall of the plunge pool while the spillway is operating. The wall is already destroyed and the water impacting again right at the toe of the slope. Parts of the right sidewall are also damaged (Guia tecnica, 1997). .....	36
Fig.5 17: Shape and topography of the plunge pool without concrete. Note the deep hole right where the overtopping water impacted the rock. (Modified after Iberduero S.A, 1937) .....	37
Fig.5 18: Layout of the spillway after the reform as it was in 1947. The energy dissipating system with concrete teeth at the spillway edge was constructed in 1964 (redrawn and modified after Iberduero, 1947). .....	39
Fig.6 1: Geological map of the Alañines synform with its stratigraphic formations. The study area is located in the southeast of the synform within the syntectonic Ricobayo Granite. For lithologies within the study area see Fig.6.2 (after González Clavijo & Martínez Catalán, 2002). .....	42
Fig.6 2: Geologic map of the region around the Ricobayo Reservoir. Black circle indicates study area (after IGME, 1978). .....	43
Fig.6 3: Orientation of a plane as obtained with a geologic compass (left). Orientation of the hatched plane can be expressed as 330/60 (Strike/Dip) or 240/60 (Dip direction/Dip) (after Bell, 2007). Picture of a COCLA Compass (right) (Breithaupt.de, 2012). .....	45
Fig.6 4: Illustration of terms used in discontinuity statistics (modified after Wallbrecher, 1986) .....	46
Fig.6 5: Block diagrams showing the concept of persistence. The Persistence (K) is the jointed part of a discontinuity traced over a certain distance. The intact rock parts between the jointed sections are called rock bridges. (ISRM, 1981) .....	48
Fig.6 6: Assessment techniques for measuring roughness. a) Linear profiling of waviness (a = maximum amplitude, L = length of joint surface) (after Milne et al., 1992). b) Profile gauge. One side is pressed against the discontinuity plane and the pattern of the gauge is compared to the JRC chart (Fig.6.8) (after Milne et al., 1992). c) Compass and disc clinometer. ....	50
Fig.6 7: Roughness profiles and corresponding range of JRC values associated with each one (ISRM, 1981) .....	51
Fig.6 8: Typical roughness profiles and suggested nomenclature. The length of each profile is in the range 1-10m. The vertical and horizontal scales are equal (after Barton, 1978) .....	52
Fig.6 9: The terminology for discontinuity openings. Closed discontinuity (left), without filling (Aperture of open discontinuity; middle) and with filling (Width of filled discontinuity; right) (after ISRM, 1981). .....	55

Fig.6 10: -Example that demonstrates the effect of the number of joint sets on the mechanical behaviour and appearance of a rock mass. One set (left) and three systematic sets and one random set (R) (right) (ISRM, 1981).....	56
Fig.6 11: Sketch of rock masses illustrating (a) blocky, (b) irregular, (c) tabular and (d) columnar rock masses (ISRM, 1981).....	57
Fig.6 12: Topographic map of the Ricobayo Dam site indicating the most important lineaments and some mapped surface deposits (Topographic map by Iberduero S.A., 1984). .....	59
Fig.6 13: View to the area between the spillway and the river. The finer material dumped down on the left side of the picture forms fill deposits (arrows) for creating construction space. Location of the deposits is illustrated in Fig.6.12 above. ....	60
Fig.6 14: View to the fill deposit right at the end of the outlet of the plunge pool. Some raveling occurred where the shotcrete failed. ....	60
Fig.6 15: View to the right side of the spillway. End of the upper channel. The old wall is still visible in the back and was shifted towards the center of the spillway (left). Cut slope adjacent to the concrete wall of the spillway .....	61
Fig.6 16: The original spillway from 1934. Note the slight curvature at the tip of the right wall to prevent the overtopping water to erode the right wall of the plunge pool (circle). ..	61
Fig.6 17: Isolated blocks cropping out on the surface of the Ricobayo granodiorite. Both blocks shown above are weathered into a spheroidal shape. The block on the right is broken in half. ....	62
Fig.6 18: IUGS classification diagram for plutonic rocks. The highlighted field represents the rock type found at Ricobayo (after Streckeisen, 1973).....	62
Fig.6 19: Outcrop of the granodiorite of Ricobayo with iron oxide altered surfaces (arrow) (left). Hand specimen of the granodiorite (right). The rock is mostly composed of Quartz (grey) and Plagioclase (white), Potash feldspar (reddish) and Biotite (black). 2€ coin for scale.....	63
Fig.6 20: View to the right riverbank downstream of the dam, showing the appearance of the rock mass at the Ricobayo dam. Joint patterns of the five joint sets are illustrated. Numbers and colors correspond to the joint orientations in Tab.6.9. ....	66
Fig.6 21: Joint spacing.....	67
Fig.6 22: Outcrop at the left side of the river. Intense jointing of the rock resulting in the formation of blocks. Spacing (arrows) is well visible in this picture. Lines indicate joint set 5. Person for scale in front. ....	69
Fig.6 23: Outcrop situation at Ricobayo. Scanline along road cut (left). Estimates of the true persistence are difficult in this case. Large area of exposed rock along the river Esla right downstream of the dam (right). Some joints may be traced for more than 10 to 20m. ....	70
Fig.6 24: Terminations as they were observed during the scanline survey (28 observations). X = unknown/not visible, R = rock, D = discontinuity .....	71
Fig.6 25: JRC for the joints of Ricobayo. ....	72
Fig.6 26: Surface of joint set 1. Polished surface (Slickensides) is visible on the joint (left). Pencil for scale. Lineation measurements on the right. ....	75
Fig.6 27: Wall strength estimates. Note that rock material is either strong where it was unweathered to slightly weathered, or weak where weathered rock was tested. ....	76
Fig.6 28: Picture showing a strongly weathered rock.....	76
Fig.6 29: Weathering grades of the joint surfaces.....	77
Fig.6 30: Ranges of aperture of joints.....	78
Fig.6 31: Description of the type of filling encountered. ....	78
Fig.6 32: Filling of joint (~3cm wide; arrow) along joint set 1. Slightly reddish discolorations on vertical rock wall. Compass for scale. ....	79
Fig.6 33: View into the plunge pool. The left wall provides a large scale exposure of the rock at the site showing the joint patterns. Joint set colors refer to those of Tab.6.8. Note that failure plane on the left wall is bound by Joint set 4 and its surface follows approx. the orientation of joint set 2. Red line indicates location of profile shown in Fig.6.35.....	80

Fig.6 34: Transverse profile through the entrance of the outlet (view upstream). Plans from the 1940s show the original topography of the pool with step like bedrock terraces (straths) and the performed repair works (red and yellow anchors) (Iberduero S. A, 1940). .....	80
Fig.6 35: Right wall at the outlet channel downstream of the plunge pool. The wall exposures the joint pattern in this area where the first and third scour stage had occurred. Blue dashed line indicates approximate slope orientation after scour stage 1, yellow dashed line after stage 3. Joint set colors refer to those of Tab.6.9.....	81
Fig.7 1: Whole sphere stereonet. Red line marks the reference circle. Area within the reference circle refers to the standard lower hemisphere net (Goodman, 1989). .....	82
Fig.7 2: Types of blocks. Shapes of such blocks are illustrated in Fig.7.3 (redrawn from Goodman & Shi, 1986) .....	83
Fig.7 3: Types of blocks (a) infinite, (b) tapered, (c) stable, (d) potential keyblock, (e) keyblock (Goodman & Shi, 1986).....	83
Fig.7 4: Two dimensional example for the finiteness theorem to an infinite block. (a) situation before moving of the half spaces. (b) situation after moving of the half spaces to a common point. L and U define the lower and upper half spaces with respect to a plane, respectively. Infinite blocks share a common region and can not be shifted to only one common point (Goodman & Shi, 1985).....	84
Fig.7 5: Two dimensional example for the finiteness theorem to a finite block. (a) situation before moving of the half spaces. (b) situation after moving of the half spaces to a common point. L and U define the lower and upper half spaces with respect to a plane, respectively. The BP is empty, since all planes can be shifted to one single common point. The common part of a finite BP is the block itself. The JP (defined by $U_1$ and $U_2$ ) is not empty and totally within SP, which is important in terms of removability of finite blocks (Chap. 7.2.2)(Goodman & Shi, 1986).....	85
Fig.7 6: The removability theorem. (a) Illustration of the removability of different blocks depending on their shape. (b) Block A can never be formed only by joints and needs additionally a free surface. Its JP is not empty and therefore infinite. (c) Block B can be formed entirely by joints producing a finite block which has an empty JP.....	86
Fig.7 7: Principle of the stereographic projection (Upper focal point or lower hemisphere projection). A plane (red rectangle) intersecting the reference sphere. The great circle is project through the upper focal point (F) onto the projection plane. The section highlighted in blue is shown in Fig.7.8 (modified after Goodman, 1989).....	87
Fig.7 8: Section through the reference sphere. A plane inclined at an angle $\delta$ intersects the reference sphere at point P. P is projected through the upper focal point (F) on to the projection plane as (p). (-P) and (-p) refer to the plane projected into the upper hemisphere (Goodman, 1989) .....	87
Fig.7 9: Stability of a block on a slope for dry conditions. $W \cos\beta$ is the normal to the plane (N), $W \sin\beta$ is the parallel force to the plane (F) driving the block downslope. (-F) is the resisting force provided by the friction angle ( $\phi_a$ ) The weight vector acts vertically down under normal circumstances (modified after Price, 2009). .....	89
Fig.7 10: The friction cone concept. (a) A friction cone with an apex of the friction angle ( $\phi_j$ ) around the normal to a plane. Any resulting force plotting within the friction cone will cause no movement of the block. (b) The friction cone as a small circle (friction circle) on the stereonet with the radius of the friction angle ( $\phi_j$ ) (Goodman, 1989). .....	90
Fig.7 11: Whole sphere stereographic projection for the front slope of the spillway at Ricobayo. The removable JPs are highlighted, slope (red dashed circle), reference circle (black circle). Orientations of joints (first 5 entries) and slope (last entry) are listed in the top left corner. The original slope orientation was estimated from old maps. The corresponding failure modes are shown in Fig.7.12. ....	92
Fig.7 12: Failure modes for JPs shown in Fig.7.11. However, failure mode of a JP is distinct from the removability of a block. (note that some JPs that have a number assigned are not entirely within SP). .....	93
Fig.7 13: Shape of Block 00000. Numbers 1 to 5 indicate the joint planes, 6 the free surface. ....	95



---

Fig.7 14: Compound friction cone for JP 00000. Blue line indicates the 30° friction line. Black dashed lines in 5° steps, reference circle shown as dashed orange circle. Orientation of spillway is indicated by arrow. The principle of obtaining the angles is shown in Fig.7.15 below, which is a cross section through the reference sphere along red line. ....	96
Fig.7 15: The principle of transferring the measured distances (ov') from the friction plots to angle of rotation employing Eq.7.11.....	96
Fig.7 16: Block diagram showing Block 00000 on the spillway surface (6). J1 to J5 refer to the joints involved in forming the block. Blue arrow indicates direction of water flow. Red line AB indicates cross section shown in Fig.7.17. W (weight vector), R (Resultant after rotation), $\theta$ (Angle of rotation) .....	97
Fig.7 17: Cross section of the block diagram showing the principle of shifting the resulting force (i.e. weight vector (W)) by the angle of rotation ( $\theta$ ) to trigger a different failure mode. ....	98
Fig.7 18: Schematic illustration of the front slope, spillway surface and compound slope. The dip vectors (-D1 & D1) should show how the mobilization takes place into the upper hemisphere along J1. In classic stability analysis this would not be possible since the plane of J1 doesn't daylight. 0 & 1 refer to joint halfspaces, $\theta$ (Angle of rotation), $\phi$ (friction angle), W (Weight vector), n1 (normal to J1). ....	98
Fig.7 19: Block Erodibility Spectrum for the JPs of the front slope at $\phi = 30^\circ$ . The spillway flow is oriented at 216 (vertical red line). Note that in this alignment the angle of rotation is close to its minimum for most blocks. ....	99
Fig.7 20: Block Erodibility Spectrum for the JPs of the front slope showing ratios of weight of individual blocks vs. the Fmin at different azimuth orientations. In sections where the angle of rotation is small as shown in Fig.7.19 above, accordingly less force is required to mobilize block. Flow at vertical red line. ....	99
Fig.7 21: Block Erodibility Spectrum for the JPs of the front slope at $\phi = 40^\circ$ . Plot is similar to the one shown in Fig.7.19 with 30° friction, but shifted to slightly higher values. The spillway flow is indicated by vertical red line.....	100
Fig.7 22: Block Erodibility Spectrum for the JPs of the front slope showing ratios of weight of individual blocks vs. the Fmin at different azimuth orientations. The spillway flow is indicated by vertical red line.....	100
Fig.7 23: Block Erodibility Spectrum Envelope for the front slope for friction angles of 30° and 40°. Also here in the stability envelope it is visible how the angle of rotation drops to lower values in the orientation of the spillway at 216°(vertical red line). ....	101
Fig.7 24: Minimal force envelope for the front slope for friction angles of 30° and 40°. The spillway flow is indicated by vertical red line.....	102
Fig.7 25: Block Erodibility Spectrum for the spillway surface. The minimum angle of rotation is not as critical as for the front slope. Vertical red line shows flow direction. ....	104
Fig.7 26: Block Erodibility Spectrum for the JPs of the spillway surface showing ratios of weight of individual blocks vs. the Fmin at different azimuth orientations. Much more force is needed to mobilize blocks here than on the front slope. The spillway flow is indicated by vertical red line.....	105
Fig.7 27: Block Erodibility Spectrum for the JPs of the spillway surface at $\phi = 40^\circ$ . Plot is similar to the one shown in Fig.7.26 with 30° of friction, but shifted to slightly higher values. The spillway flow is indicated by vertical red line. ....	105
Fig.7 28: Block Erodibility Spectrum for the JPs of the spillway surface showing ratios of weight of individual blocks vs. the Fmin at different azimuth orientations. The spillway flow is indicated by vertical red line.....	106
Fig.7 29: Block Erodibility Spectrum Envelope of the angle of rotation for the spillway surface for friction angles of 30° and 40°. The point of the first mobilization is quite uniform over the entire spectrum. The spillway flow is indicated by vertical red line.....	106
Fig.7 30: Minimal force envelope for the spillway surface for friction angles of 30° and 40°. The spillway flow is indicated by vertical red line.....	107
Fig.7 31: Block Erodibility Spectrum for the compound slope for a friction angle of 30°. Vertical red line indicates flow direction.....	109

---

Fig.7 32: Block Erodability Spectrum for the JPs of the compound slope showing ratios of weight of individual blocks vs. the Fmin at different azimuth orientations. The spillway flow is indicated by vertical red line.....110

Fig.7 33: Block Erodability Spectrum for the compound slope for a friction angle of 40°. The spillway flow is indicated by vertical red line.....110

Fig.7 34: Block Erodability Spectrum for the JPs of the compound slope showing ratios of weight of individual blocks vs. the Fmin at different azimuth orientations. The spillway flow is indicated by vertical red line. ....111

Fig.7 35: Block Erodability Spectrum Envelope of the angle of rotation for the compound slope for friction angles of 30° and 40°. The spillway flow is indicated by vertical red line.111

Fig.7 36: Stability Envelope of Fmin for the compound slope. The spillway flow is indicated by vertical red line.....112

Fig.8 1: Photograph showing the size of scoured blocks after scour stage 2 in 1934..... 115

Fig.8 2: Schematic profiles illustrating the scour processes believed having shaped the appearance of the spillway in the years between 1933 and 1934 – 35, respectively. ....116

## List of Tables

Tab.4.1: Chart with typical values of the Mass Strength Number (Ms) (Kirsten, 1982 in Annandale, 2006). .....	18
Tab.4 2: Values for the Joint Number (Jn) (Kirsten, 1982 in Annandale, 2006).....	19
Tab.4 3: Joint roughness (Jr) values for different joint conditions (Kirsten, 1982 in Annandale, 2006). .....	20
Tab.4 4: Joint alteration numbers (Ja) for different joint separations (Kirsten, 1982 in Annandale, 2006). .....	20
Tab.4 5: Relative ground structure number depending on the dipdirection and dip of least favorable joint set orientation (Kirsten, 1982 in Annandale, 2006).....	21
Tab.5 1: Ricobayo scheme specifications- excerpt (from Iberdrola, 2011b) .....	23
Tab.6 1: Spacing terminology (after ISRM, 1981) .....	48
Tab.6 2: Description of persistence (ISRM, 1981) .....	49
Tab.6 3: Chart for the weathering classification of rock masses (ISRM, 1981). .....	53
Tab.6 4: Chart for the weathering description of rock material (ISRM, 1981).....	53
Tab.6 5: Chart for the description of the strength of weathered material. S1 – S6 are applied to cohesive soils, R0 – R6 are applied to rock (ISRM, 1981).....	54
Tab.6 6: Chart for the classification of aperture (ISRM, 1981). .....	55
Tab.6 7: Table showing the Jv and related block sizes (ISRM, 1981).....	57
Tab.6 8: adjective terms used to describe the appearance of a rock mass (ISRM, 1981). ....	57
Tab.6 9: Joint orientation statistics for the Ricobayo Dam site. Full circles are compass measurements, empty circles are measurements obtained by ShapeMetrix3D.....	65
Tab.6 10: Mean and standard deviation for the joint set spacings measured at the scanline. ....	66
Tab.7 1: Range of Friction angles for different rock types (Barton, 1973). Granite as it occurs at Ricobayo is in the high friction class. For the Erodibility Spectrum plots ranges from 30° to 40° were used to cover a broad range of friction.....	91
Tab.7 2: JP properties for the 5 joint sets of Ricobayo.....	92
Tab.7 3: Listing of failure modes for removable JPs. ....	93
Tab.7 4: List of the removable JPs for the front slope, the spillway surface and the compound slope. The compound slope is the combination of the first two.....	94
Tab.7 5: Radar plots for the JPs of the front slope for friction angles of 30° and 40°. Angle of Rotation (left) and Fmin (right). .....	103
Tab.7 6: Radar plots for the 3 JPs of the spillway surface that are different from the front slope for friction angles of 30° and 40°. Angle of Rotation (left) and Fmin (right).....	108

### 1. Kurzfassung

Seitdem der Mensch Bauaktivitäten in Gebieten durchführt, die durch die Aktivität von Wasser geprägt sind, stellt Kolkbildung im Gesteinsuntergrund ein Problem dar. Dies betrifft insbesondere Gebiete, wo starke Oberflächenabflüsse vorhanden sind, die während und nach Fertigstellung einer Anlage den Untergrund auskolken. Jedes Objekt, das in einem Flussbett errichtet wird, stellt ein Hindernis für das darin fließende Wasser dar und wird daher einerseits vom Wasser selbst, aber auch von den mit ihm transportierten Partikeln angegriffen. Zusätzlich stören anthropogene Änderungen der Fließgeometrie das natürliche System, was zu erhöhten Erosionsraten führen kann.

Heutzutage wird oberflächennahe Erosion durch fließendes Wasser als ein eher langsamer, kontinuierlicher Prozess gesehen, der überwiegend weniger kompetentes Gestein (Sedimente) bzw. Böden betrifft. Verschiedenste Untersuchungen haben bereits versucht das Phänomen Kolk zu erforschen, um dessen Mechanismen und Raten zu erfassen.

Kolkbildung im Festgestein ist bisher jedoch wenig beachtet worden und noch schlecht erfasst. Mittels Fallstudien wird dieses Problem in den letzten Jahren vermehrt untersucht.

Der untersuchte Fall am Staudamm von Ricobayo stellt den wohl Verheerendsten dar, der bisher dokumentiert wurde. Insgesamt wurde in den 1930er Jahren über 1 Million m<sup>3</sup> Gestein innerhalb weniger Jahre von dem Entlastungsgerinne erodiert, während überschüssiges Wasser vom Staubecken abgelassen wurde. Dies führte in weiterer Folge dazu, dass die ursprüngliche Böschung des Entlastungsgerinnes stromaufwärts migrierte und schlussendlich ein Tossbecken formte.

Diese Arbeit versucht das Phänomen Kolk im Zusammenhang mit ingenieurgeologischen Gebirgseigenschaften und der Anwendung von ‚Block Theorie‘ zu verstehen. Es werden außerdem geomorphologische Aspekte des Fließverhaltens von natürlichen Flusssystemen betrachtet, die Parallelen zu den Beobachtungen vor Ort aufweisen.

Das so genannte ‚Erodibility Spectrum‘ wird vorgestellt, um eine richtungsabhängige Evaluierung der Mobilisierung von Blöcken vorzunehmen. Die Untersuchungen ergeben, dass die ursprüngliche Ausrichtung des Entlastungsgerinnes im Bezug auf seine Widerstandsfähigkeit gegen Kolkbildung unvorteilhaft gewählt wurde. Zusätzlich erleichterten die Gegebenheiten durch das aufgelockerte Gebirge die Entfernung von Blöcken, die Bildung eines Gerinnes im Festgestein bzw. des Tossbeckens. All dies legt nahe, dass die geologischen Bedingungen vor Ort einen großen Einfluss auf die Kolkbildung haben, wobei nicht die Festigkeit des Gesteins, sondern das lokale Trennflächengefüge ausschlaggebend ist.

### 1. Abstract

Rock scour has been an issue ever since human structures were established near or directly at environments with high water presence. Especially on sites where high rates of surface water discharge occur, scouring of the underlying material has been a problem during and after construction. Any object that is constructed in a river flow regime forms an obstacle to the flow of water and is therefore attacked not only by the water itself, but also the sediment load transported within the stream. Additionally, manmade changes in flow geometries of a river can lead to massive disturbances of the naturally formed system, causing high rates of erosion.

To date, most of the erosion phenomena caused by the surface flow of water is mostly considered as a slow, continuous process that takes place in soft rock (mostly sedimentary rocks) or soil, respectively. Many studies dealing with this kind of problem considering scour at bridges have been published over the years (e.g. Richardson & Davis, 2001). Studies carried out by different organisations such as the USGS (United States Geological Survey) or USACE (United States Army Corps of Engineers) have attempted to understand the mechanisms involved with scour and estimation of its rates (e.g. May, 1989, Langley, 2006). Conversely, scour in hard bedrock has not received as much attention and is therefore not well understood yet. Case studies at selected dam sites where hard rock erosion has occurred have been published by various authors (e.g. Annandale, 2005; Bollaert & Mason, 2006; Bollaert & Schleiss, 2003a; Li & Liu, 2010).

The Ricobayo Dam provides a severe case of scour damage in so far documented at manmade structures. In total more than 1 million cubic meters of rock were removed within only a few years from the spillway. This led to upstream migration of the front slope of the spillway and subsequent, to formation of a 100m deep plunge pool.

This work contributes to the understanding of rock scour, based on engineering geologic ground conditions and the application of block theory by Goodman and Shi (1985). Aspects of natural stream channel formation in geomorphology are also considered, which show similar features to those encountered at Ricobayo Dam.

The 'Block Erodability Spectrum Analysis' (Kieffer, 2011) is introduced to evaluate direction dependant mobilization of blocks. The analysis reveals that the alignment of the spillway was unfavorably chosen in terms of resistance against scour. Additionally, the blocky rock mass conditions facilitated block removal resulting in the formation of a bedrock channel and a plunge pool, respectively. The scour features indicate a strong connection between rock mass conditions and erosion behaviour.

## 2. Introduction

Construction of dams is a challenge to all project partners involved, in terms of planning, design, construction, maintenance and monitoring. The interaction of rock, water and synthetic materials make dams a very sensitive structure that have to be designed in a way so they will stay in place, operating properly for a long time.

Sound engineering and geologic investigation and evaluation of the ground and underground are necessary to ensure an adequate design of the facility. Although the dam site itself is usually investigated enough to know the underground conditions, other structures involved in the dam site are may receive far less scrutiny. Spillway channels, for example, are designed to release excess water from the reservoir in case of a high water. Their design may prove appropriate for the flow conditions anticipated, but the geometry, alignment and slope gradient with respect to the rock mass conditions are not fully considered in three dimensions. Strong flows that are released downstream may result in massive removal of material within a short period of time (Annandale, 2005; Bollaert, 2002).

Since dams are structures that have to be monitored and observed from the first day on, they provide a lot of information collected over the years and stored in the archives. The Ricobayo Dam provides a case where massive scour has affected the spillway of the dam. It occurred in hard rock over a short period of time and is one of the most severe cases of scour documented.

### 3. Purpose and scope

Geologic assessment and interpretations of the Ricobayo Dam Scour event may help understanding scour phenomena in general. Geomorphologic features created by river flow caused by knickpoint migration and associated head cutting can be observed in short term erosion as well as at spillway channels. Although those processes that can be found for example at the Niagra gorge or the Grand Canyon are way slower some implications on the mechanisms of scour could be inferred.

This thesis deals with scour at the Ricobayo dam site in the province of Castile and León, Spain. The thesis is done with cooperation and support of Iberdrola SA, which provided access to their facilities and kindly allowed the use of historical records, pictures and plans of the dam.

Works performed include:

- Study of the existing data provided by Iberdrola S.A. in the historical archives of Ricobayo.
- Collecting of the rock mass parameters and mapping of surface features.
- Evaluation of the susceptibility of the rock to scour applying Block Theory (Goodman & Shi, 1985)

### 4. Scour

Scouring is a process that has affected rocks ever since they were exposed to the force of water. Geomorphology and landscape evolution are strongly linked to exogenous processes on the surface of the earth. Many landscapes of today were created and shaped by this process. The Grand Canyon in Arizona developed over a very long time due to the interaction of tectonic activity, lithological properties and the flow of water. Other examples are the Niagara Gorge or the Channelled Scablands.

Also the construction of hydraulic structures such as dams, bridges and piers by human activity has always challenged the engineers to deal with the different uses of water and its interaction with the ground.

It is still not very well understood how the scouring process works and general rules seem to be missing to be applied for an evaluation. Especially the rate of scour is something that can vary strongly. Erosion is usually considered by geologists as a slow, continuous process that changes the appearance of the earth's surface over a long period of time. Nevertheless, some cases nowadays present a whole different perspective of the erosion by water, i.e. scour, with extremely high rates of material removal, mostly occurring at manmade structures. Natural cases with similar features are only observed in context with catastrophic events as documented in the Channelled Scablands.

Considering the processes observed in natural fluvial environments can be a hint in understanding the issue of scour at manmade structures. Some aspects of landscape evolution related to rivers will be discussed in this chapter and the attempt is made to draw parallels to the scour case at Ricobayo with creation of a gorge, a waterfall and a plunge pool, respectively.

For engineering purposes some semi-empirical formulas and approaches for the study of scour have been established in the last few years. Some of them will be presented in this chapter as well.

The explanation of bedrock erosion (scour) is not satisfied with single transport laws or erosion theories. The variety of influencing factors such as ground conditions, flow rates, flow depth, slope gradients, climate make it difficult to develop comprehensive models. Different mechanisms are acting at different settings as described in the precedent chapters (Seidl & Dietrich, 1992).



### 4.1 Definition

Scour is a phenomenon that can not be assigned to one single process. It is the interaction of the water and its load with the ground. There are some definitions so far describing “scour”:

“...Scour can be defined as the flow- or wave-induced lowering of a (sediment) bed that could result in damage to the natural or built environment. Scour is classified as generally occurring in coastal and river environments, or locally in the vicinity of, and as a consequence of, the presence of various types of hydraulic structures. The extent of scour is determined by the interaction between the flow of water, the presence of hydraulic structures, and the response of earth material to the applied forces...”

(Annandale et al, 2002)

Another definition is provided by Bollaert (2002) describing scour with:

“...Erosion of the downstream rock mass...”

“...Scouring is a complex three-phase (gas-liquid-solid) interactive problem, governed by a multitude of hydraulic, hydrodynamic and geomechanical phenomena that are strongly dependent on both time and space...”

(Bollaert, 2002)

### 4.2 Scour features in natural channels

Scour features in natural channels typically indicate high energy conditions. These features are shaped by existing control factors such as structural and lithological considerations and the influence of major flood events. Rivers with steep slope gradients typically develop such features (Brierley & Fryirs, 2005).

The formation of such features depends on the conditions at a specific site as a function of the slope, flow conditions (discharge characteristics), bedrock properties, change in gorge alignment and sediment load and size, respectively. Erosion of bedrock occurs via the chemical action of water (corrosion), the mechanical (hydraulic and abrasive) action of water armed with particles (corrasion), and the effects of shock waves generated through the collapse of vapor pockets in a flow with marked pressure changes (cavitation; Knighton, 1998 in Brierley & Fryirs, 2005). A comprehensive explanation of these processes is found in the spillway erosion chapter. The biggest blocks are exposed above the water surface and their diameter is usually about the depth of the channel. These features act to a certain extend as energy dissipaters during high flood events (Brierley & Fryirs, 2005).

### Strath

Straths (Fig.4.1) are features encountered in fluvial settings. A definition is given by Brierley & Fryirs (2005):

Typically a relatively flat, valley marginal feature that is perched above the contemporary channel or floodplain. These erosional surfaces have a bedrock core often with a thin alluvial overburden. Strath terraces often confine the channel, analogous to valley margins.

Their occurrence reflects incision and valley expansion associated with down cutting into bedrock and subsequently abandoning terrace surfaces. In many cases, an associated floodplain develops and becomes inset within these terraces. In other cases, where incision occurs with little lateral expansion, a confined valley is formed.

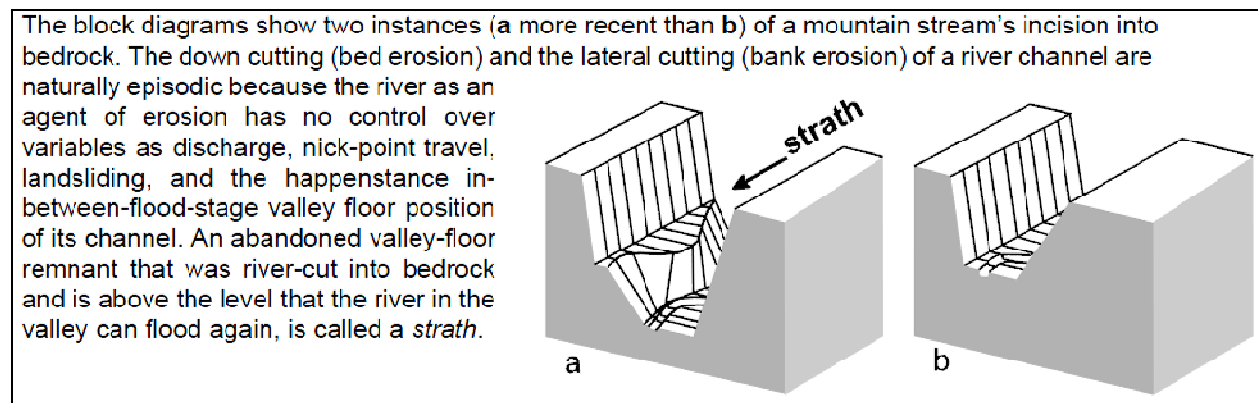


Fig.4.1: Formation of a strath (After Rance, 2007)

### 4.3 Bedrock incision

Relatively little is known about bedrock incision by streams, and no general rules to describe the phenomenon of bedrock scour exist. The application of a single scour law seems not appropriate for all the processes involved. However, some attempts have been made to explain the scour of bedrock. According to Seidl and Dietrich (1992) three major mechanisms are responsible for rivers eroding (scouring) into bedrock:

- Vertical wearing of the channel bed due to stream flow and consequent abrasion by transported particles and dissolution.
- Scour by periodic debris flows
- Knickpoint propagation

Investigation of primary streams and their tributaries were performed by Seidl and Dietrich (1992) to establish formulas describing the scour mechanisms in bedrock. Their attempt was to do describe the type of mechanism by plotting drainage area ratios against slope gradient

#### 4. Scour

---

ratios (Fig.4.2). It was shown that erosion is linearly related to stream power (Eq.4.1, Eq.4.2) in areas with low gradients (slopes up to ~ 11°) yielding m/n ratios of 1.0 (Eq. 4.3). Vertical incision of the bed is dominated by abrasion and dissolution.

Stream power (P) is defined as:

$$P = \frac{\gamma \cdot Q \cdot \Delta E}{A} \quad (\text{Eq.4.1})$$

Where: P = Stream Power (kW/m<sup>2</sup>)

γ = Unit weight of water (9,81KN/m<sup>3</sup>)

Q = Discharge rate (m<sup>3</sup>/s)

ΔE = Energy dissipation (expressed as hydraulic head, m/m)

A formula used to describe bedrock evolution of a channel is the shear stress (or stream power) erosion law (Eq.4.2) (e.g. Whipple et al., 2000):

$$\mathcal{E} = KA^m S^n \quad (\text{Eq.4.2})$$

Where:  $\mathcal{E}_t$  = Total erosion of all processes

K = Coefficient of erosion (comprising effects due to lithology, climate, channel width, hydraulics, and sediment load)

A = Upstream catchment area (proxy for discharge)

m, n = positive constants depending on depend on erosion process, basin hydrology, and channel hydraulic geometry

For areas with steeper slopes the erosion processes are proportional to slope gradient. Debris flow scour becomes dominate as the slope steepens, and the slope gradient exerts more control, than drainage area. This probably indicates debris flow scour acts more locally than abrasion and dissolution processes.

For debris flow scour, the m/n ratio is typically around 0.7. Additionally, the area term would be a substitute for frequency and size of the debris flow. In general, debris scours at steep slopes would yield a higher erosive capacity moving faster and imposing higher drag forces on the bed.

This implicates a transition from a debris flow scour regime to a stream flow scour regime in the downstream direction where slopes become gentler as they approach base level.

The formula used to describe the relationship is written below (Eq.4.3):

$$A_p^m S_p^n = A_t^m S_t^n \quad \text{or} \quad \left(\frac{A_p}{A_t}\right)^m = \left(\frac{S_t}{S_p}\right)^n \quad \text{or} \quad \left(\frac{A_p}{A_t}\right) = \left(\frac{S_t}{S_p}\right)^{\frac{m}{n}} \quad (\text{Eq.4.3})$$

Where: A = Drainage area

S = Surface slope

m, n = Constants (m/n ratio determinable via plotting the ratio of channel gradient vs. drainage area ratio for principal and tributary channels. For areas with similar geology and climate).

The subscripts indicate primary (p) and tributary valley (t)

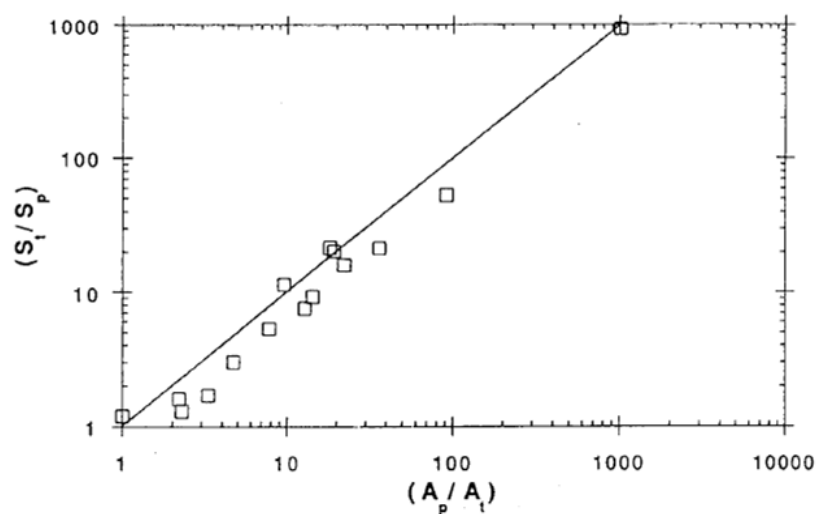


Fig.4. 2: Plot of the ratio between tributary slope ( $S_t$ ) and primary stream slope ( $S_p$ ) against the ratio of principal valley drainage area ( $A_p$ ) to tributary drainage area ( $A_t$ ). Data from 16 coastal confluences in Oregon. The data indicate m/n values of essentially 1.0 and suggest that erosion is related linearly to stream power. The line drawn on the figure corresponds to a m/n value of 1.0 (after Seidl and Dietrich, 1992)

#### 4.4.1 Knickpoint migration

Because the above erosion mechanisms could not sufficiently describe all scour features encountered in the field, Seidl and Dietrich (1992) introduced the third mechanism of knickpoint propagation. It is referred to it as knickpoint propagation. The term "knickpoint" refers to a point along the longitudinal profile of a stream channel at which there is an abrupt change in gradient (Fig.4.3). Knickpoint propagation is a process observed in many bedrock types, and is often associated with straths (bedrock terraces) (Fig.4.3). The process of upstream migration of the front face of the knickpoint is referred to as headcutting. It is one of the most unpredictable scour phenomena, since it is highly dependant on local geologic site conditions (May, 1989).

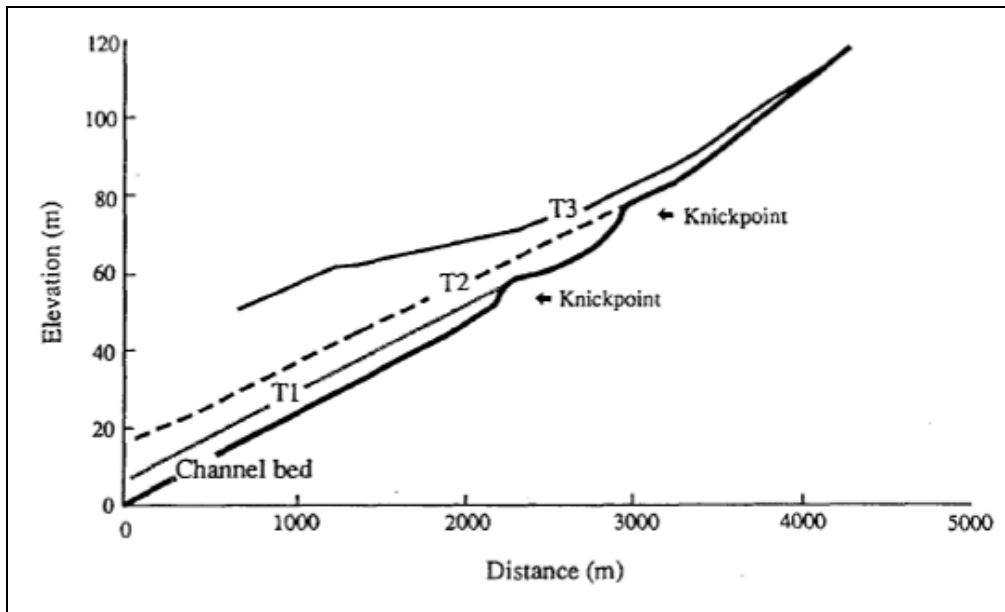


Fig.4.3 : Profile through a stream channel bed showing features of knickpoint migration and associated bedrock terraces (T1, T2, T3) at Elder Creek, California (after Seidl & Dietrich, 1992).

Leopold et al., (1964) stated that knickpoints in competent materials would migrate upstream if the following criteria are satisfied:

- A vertical face is preserved, if the ratio between height of the slope face ( $H$ ) and flow depth ( $d$ ) is greater than one, and a plunge pool or hydraulic jump is produced (Fig.4.4).
- The resistance of the material building up the bed at the knickpoint has to be larger than the shear stress imposed by the flow.
- Stream flow must be able to remove material downstream at the base of the waterfall.

However, headcutting at knickpoints is a far more complex process than considering only the criteria mentioned above. Seepage from above, water pressure changes within the rock due to seeping of the front face, and changes in the water table of the plunge pool may contribute also to the removal of material at the knickpoint. Undercutting of the vertical front face due to plunge pool action during high magnitude flood events also facilitates removal of material at the knickpoint.

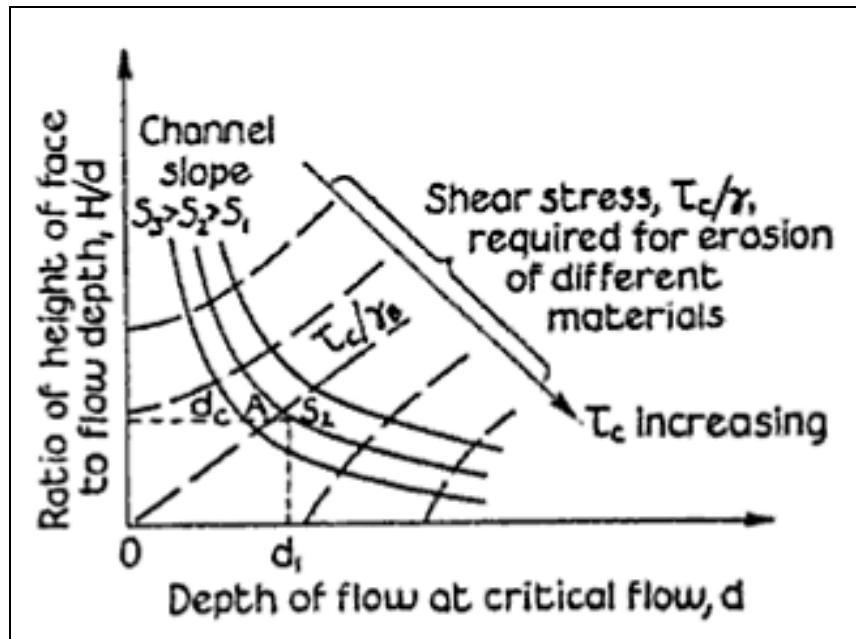


Fig.4.4: Diagram showing the relationship of Vertical face height ( $H$ ) and flow depth ( $d$ ) at a knickpoint.  $d_c$  is the critical depth at  $d_1$ . Headcut migration will occur if at the critical depth ( $d_c$ ) the intersection of  $d_c$  with the available channel slope ( $S_1, 2, 3$ ) lies above the orthogonals to the slope, defining the erodibility or critical shear stress of the material involved (after Leopold, 1964).

The higher the  $H/d$  ratio gets, the steeper the slope has to be to produce upstream migration (headcutting). Below  $H/d = 1$  no migration will occur. Material with high shear resistance will be eroded first in steep slopes. As shown in the diagram at point  $d_1$  the intersection lies above the line of slope  $S_3$ , which is steeper than  $S_2$ . Hence,  $S_3$  is already steep enough to trigger migration, whereas  $S_2$  is right at the intersection.

#### 4.4.1.2 Geological factors influencing knickpoint migration

Traditional understanding of knickpoint development usually involves abrupt changes in lithology or structure such as faults across the river (Seidl & Dietrich, 1992). Miller (1991) pointed out the importance of geological features in knickpoint formation and migration. Knickpoints can form when the channel alignment changes relative to strata dip, and upstream knickpoint propagation is controlled by channel gradient and geologic structure. Even when knickpoints form due to changes in bedrock resistance, they may propagate through the more resistant parts and adapt their rate of upstream migration according to the resistance of the rock. This can lead to episodes of more rapid migration and incision. Another factor triggering knickpoint formation and increased upstream migration is a drop in base level by shoreline migration, tectonic uplift or differential incision against more resistant bedrock (Seidl & Dietrich, 1992). The influence of geologic structure on knickpoint migration is shown in Fig.4.5.

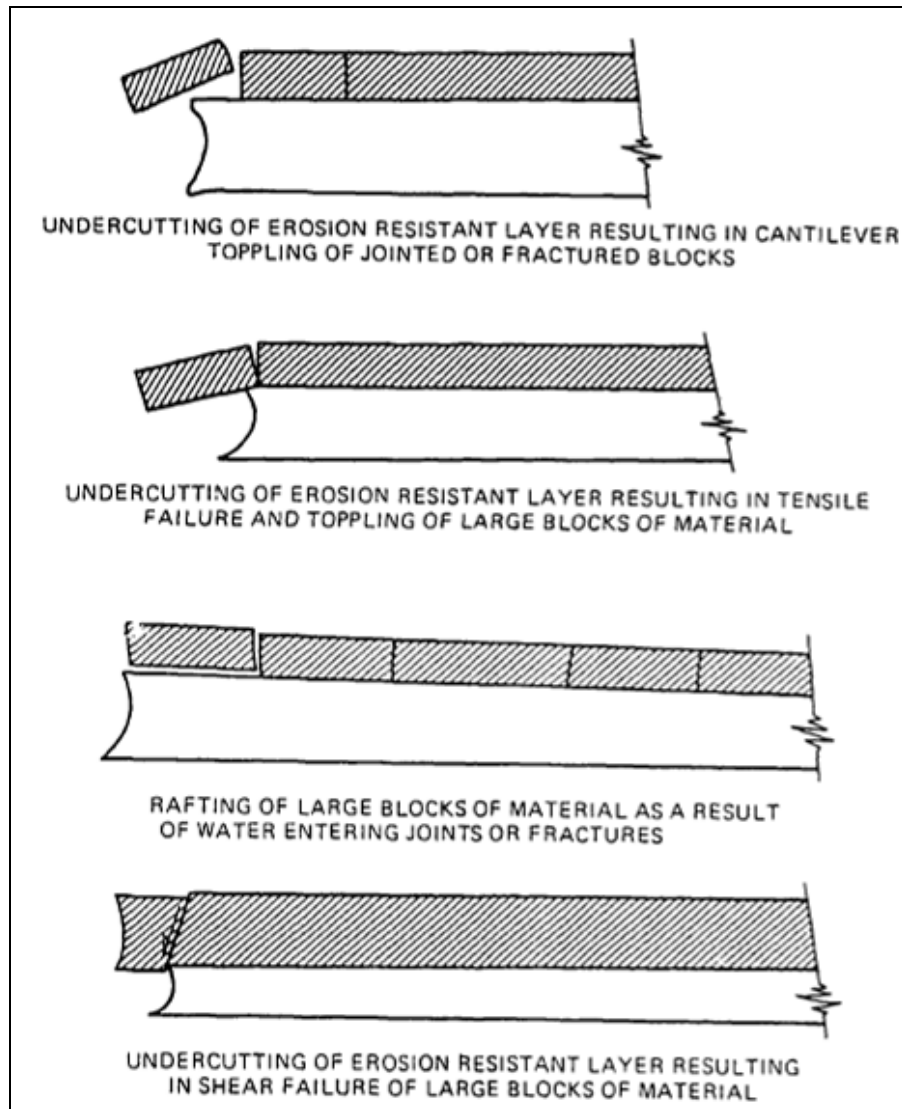


Fig.4.5: Most common failure modes at knickpoints (after May, 1989)

#### 4.4.2 Erosion mechanisms at spillway structures

Knickpoint migration is also one of the most common mechanisms of damage to unlined spillway constructions at dam sites. Spillway erosion is controlled by a variety of complex geological and hydraulic factors including (May, 1989):

- Flood frequency, magnitude and duration
- Channel design
- Channel gradient
- Rock discontinuity characteristics
- Rock erodibility

#### 4. Scour

---

The USACE (1970) provides a table with maximum permissible flow velocities for certain earth materials. For channels in metamorphic or igneous rocks, which correspond to the highest quality of rock a threshold value of 20ft/s (~6m/s) is given.

Studies on the influence of stratigraphy and structure on knickpoint erosion revealed many mechanisms of retreat, including mass movements such as cantilever toppling, but also removal by horizontal shear forces and pore pressure. Although the mass movements associated with upstream migration are complex, they generally can be assigned to the following categories:

- Undercutting of cap- rock resulting in cantilever toppling of jointed or fractured cap-rock.
- Undercutting of cap- rock resulting in tensile failure and toppling of cap- rock.
- Rafting of large blocks of jointed material as a result of water entering joints or fractures.
- Undercutting of a thick erosion resistant top layer resulting in shear failure of large block of material.

Emergency spillways can be considered as small parts of a stream system. The erosion in emergency spillways is controlled by phenomena that occur upstream and downstream of their immediate vicinity. The unlined portion of the emergency spillway is subject to vertical degradation and headcutting associated with various scour phenomena (Fig.4.6).

Emergency spillways are subject to violent, turbulent, short-lived flow events. The downstream end of emergency spillways commonly drops into a natural stream valley, thus producing a severe oversteepened reach or knickpoint (May, 1989).



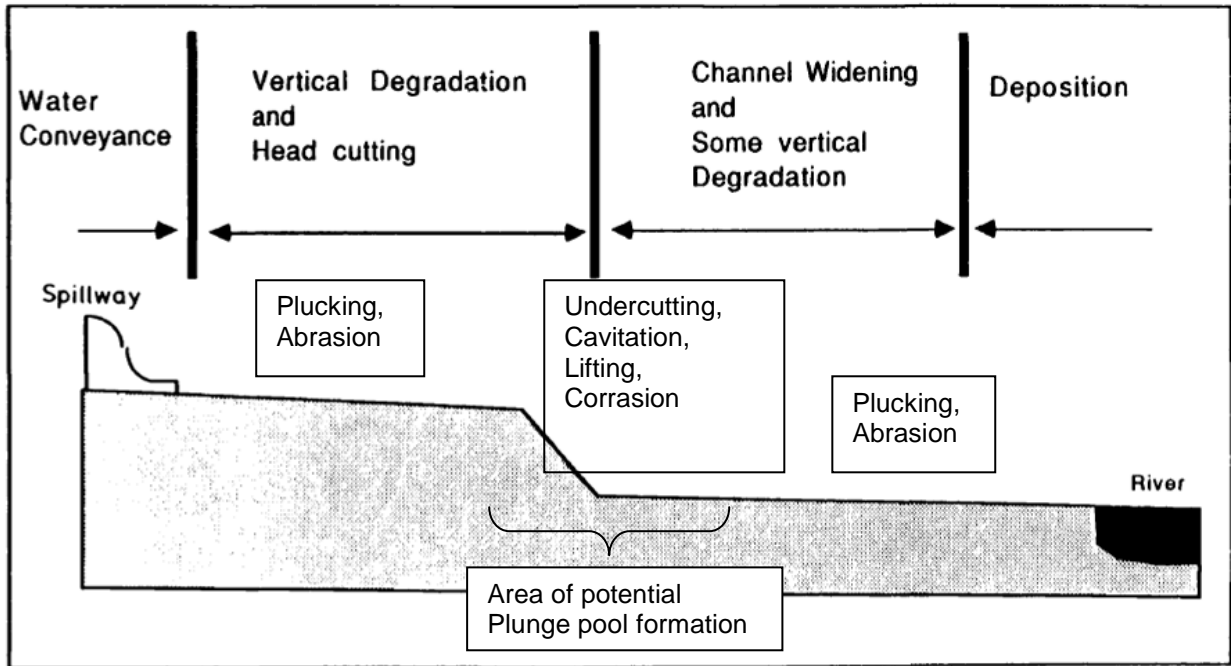


Fig.4.6: Schematic longitudinal section of a spillway channel showing the domains of different scour processes (modified after Cameron et al, 1988).

Within the spillway channel, many processes are responsible for the scourbedrock, including.

- Block plucking/ lifting of blocks
- Abrasion
- Undercutting
- Cavitation
- Corrasion

Processes that are able to remove large blocks are referred to as *dynamic block scour*. The removal of large blocks can occur in many ways including plucking (Fig.4.7) or lifting of fractured blocks, cantilever toppling, tension failure of the capping layer, or shear failure of large homogeneous masses of material. In fractured bedrock, water can propagate into the cracks resulting in a build-up of pressure within them.

The loosening, fracturing and plucking of joint blocks can be assigned to basically four processes (Whipple et al., 2000):

- Chemical and physical weathering along joints (e.g., frost shattering of exposed surfaces in winter).

#### 4. Scour

- hydraulic wedging of sand, pebbles, and fine gravel into progressively opening cracks.
- Vertical and lateral crack propagation induced by high instantaneous differential stresses associated with impacts of large saltating clasts.
- Crack propagation induced by flexing of the bed associated with instantaneous pressure fluctuations in intense turbulent flows.

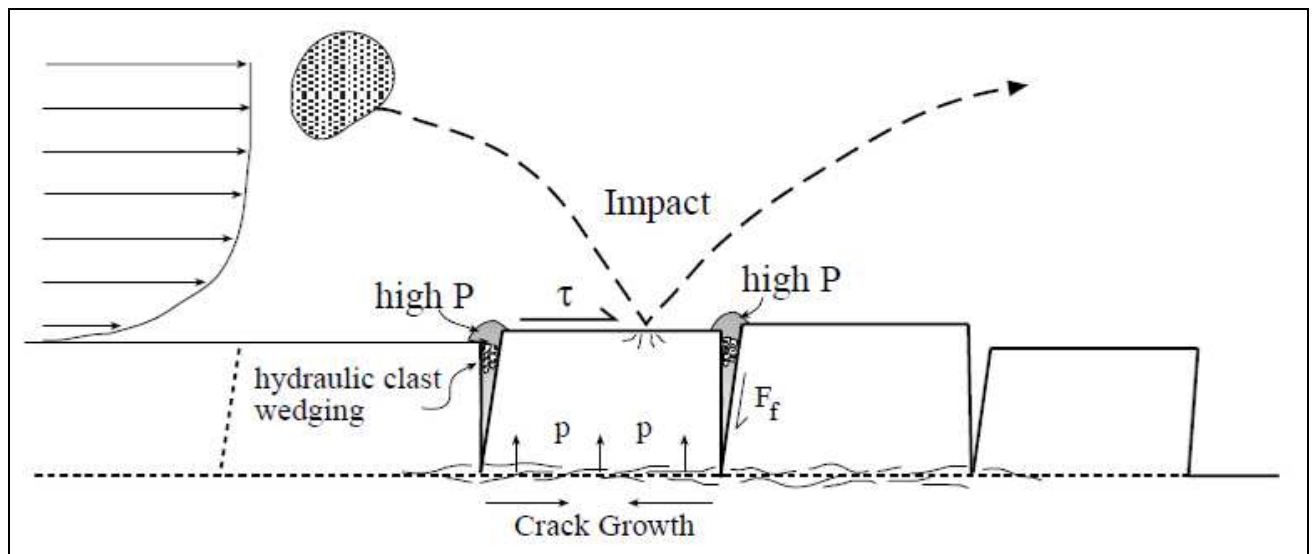


Fig.4.7: Schematic sketch of the plucking mechanism. Large saltating clasts directly abrade the block by their impact, but more important contribute in generation and growth of new cracks. Those cracks subsequently loosen the blocks. Hydraulic clast wedging (debris accumulations) within the joints supports opening of the joints. Surface drag forces ( $F_f$ ), shear forces ( $\tau$ ) and differential pressures ( $p$ ) across the block act to lift loosened blocks. Where the downstream neighbour of a block has previously been removed, new modes of removal can be possible such as rotation and sliding and removal is greatly facilitated (after Whipple et al., 2000).

Removal and entrainment is more difficult for blocks that are surrounded by neighbouring neighbour blocks (Fig.4.7). Those blocks where their adjacent downstream neighbour has been removed previously, more failure modes such as sliding and rotating become feasible and easier removal is possible. Moreover the downstream resistance is greatly reduced and the block is free to slide. Also drag forces ( $F_f$ ) increase as the block rotates out of his position.

Whether a block is removed depends on the balance of stabilizing (resisting) and destabilizing forces acting on a single block. Resisting forces are the normal component of block buoyant weight, friction on the lateral ( $F_{fyi}$ ), upstream ( $F_{fyu}$ ) and downstream ( $F_{fyd}$ ) block edges, and the instantaneous averaged spatial pressure force across the upper surface of the block ( $p$ 's). The forces acting at the base of the block ( $p$ 'b) together with drag forces associated with upwelling at the downstream margin are the only ones that are apt to lift the block up. Whipple et al., (2000) provided a formula describing the criterion for plucking of

joint blocks in bedrock (Eq. 4.4). It describes that this mechanism of removal is especially efficient for blocks with small length : thickness ratios.

$$p'b - p's \geq g(\rho_s - \rho)h + (F_{fxu} + F_{fxd})\frac{h}{l} + 2(F_{yl})\frac{h}{w} \quad (\text{Eq.4.4})$$

Where:  $p'b$  = Pressure at the base of the block

$p's$  = Pressure at the surface of the block

$g$  = Gravity

$\rho_s$  = Density of the block

$\rho$  = Density of water

$F_{x,y}$  = Friction on the block (l = lateral; u = upstream; d = downstream)

w, l, h = Width, length and height of block

The formula indicates that if the surface pressure on the block is subtracted from the pressure at the base, the latter must be larger than the buoyant weight of the block and the friction forces acting along the vertical surfaces.

## 4.5 Scour models

### 4.5.1 Annandale's Erodibility Index method

One of the most comprehensive scour models so far was developed by Annandale (2006). He takes into account a number of factors that influence the scour process. It is a semi-empirical approach based on approximately 150 field observations at spillways regarding the ability of ground material to resist erosion in context with stream power (P) (Eq.4.1). The Erodibility Index (K) (Eq.4.6) to evaluate scour was developed out of it by observing whether scour damages did, or did not occur (Fig.4.8).

The erodibility Index is defined by the following formula (Eq.4.6):

$$K = M_s \cdot K_b \cdot K_d \cdot J_s \quad (\text{Eq. 4.6})$$

Where:  $M_s$  = mass strength number (UCS)

$K_b$  = block size number (RQD/Jn)

$K_d$  = discontinuity bond shear strength number (Jr/Ja)

$J_s$  = relative ground structure number (dependant on relative strike and dip with respect to flow direction)

#### 4. Scour

The Erodibility Index (K) is dimensionless. The method incorporates many rock mass parameters and takes geological structure into account in the evaluation of scour susceptibility.

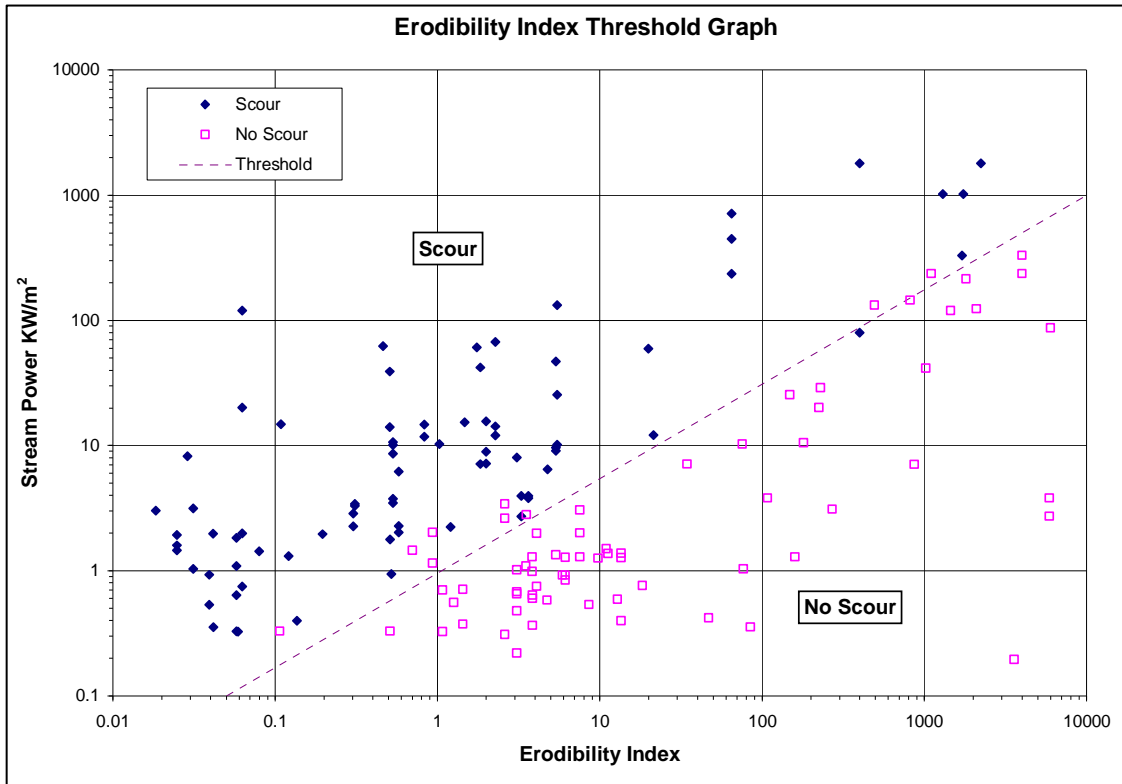


Fig.4. 8: Annandale's Erodibility Index and stream power with erosion threshold (Annandale, 2006)

#### Mass strength number ( $M_s$ )

This number is obtained from the product of the uniaxial compressive strength (UCS > 10 MPa) (Eq.4.7) of the rock and its coefficient of relative density ( $C_r$ ) (Eq.4.8). The UCS is usually obtained by field estimates or laboratory tests and expressed in MPa. The value of  $M_s$  is not constant over time since weathering affects the strength of the rock. Tab.4.1 shows typical values of the Mass Strength Number for rock.

$$M_s = C_r \cdot UCS \quad (\text{Eq. 4.7})$$

Where: UCS = Uniaxial Compressive Strength (MPa)

$C_r$  = relative density coefficient

$$C_r = \frac{g \cdot \rho_r}{27 \cdot 10^3} \quad (\text{Eq. 4.8})$$

Where:  $g$  = acceleration due to gravity (9,81m/s<sup>2</sup>)

$\rho_r$  = density of the rock (kg/m<sup>3</sup>)

27 10<sup>3</sup> = reference unit weight of the block (N/m<sup>2</sup>)

#### 4. Scour

Hardness	Identification in profile	UCS (MPa)	Mass strength number ( $M_s$ )
Very soft rock	Material crumbles under firm (moderate) blows with sharp end of geological pick and can be peeled off with a knife; is too hard to cut tri-axial sample by hand	Less than 1.7 1.7 – 3.3	0.87 1.86
Soft rock	Can just be scraped and peeled with a knife; indentations 1 mm to 3 mm show in the specimen with firm (moderate) blows of the pick point.	3.3 – 6.6 6.6 – 13.2	3.95 8.39
Hard rock	Cannot be scraped or peeled with a knife; hand-held specimen can be broken with hammer end of geological pick with a single firm (moderate) blow.	13.2 – 26.4	17.70
Very hard rock	Hand-held specimen breaks with rock hammer end of pick under more than one blow.	26.4-53.0 53.00-106.0	35.0 70.0
Extremely hard rock	Specimen requires many blows with hard rock geological pick to break through intact material.	Larger than 280.0	212.0

Tab.4.1: Chart with typical values of the Mass Strength Number ( $M_s$ ) (Kirsten, 1982 in Annandale, 2006).

#### Block size number ( $K_b$ )

This factor is controlled by the number of systematic and random joints ( $J_n$ ) (Tab.4.2) and the RQD (Rock Quality Designation; Eq. 4.9), a standard parameter for drill core logging and a measure for joint spacing of the rock. It is defined as the ratio between the sum of the lengths of pieces of rock that are longer than 0.1m and the total core run length. It was introduced by Deere & Deere (1988). The  $K_b$  is defined by Eq.4.10.

$$RQD = \frac{\sum \text{Length of core pieces} > 10\text{cm}}{\text{Total core run length (cm)}} \cdot 100 \quad (\text{Eq. 4.9})$$

The block size number is expressed as:

$$K_b = \frac{RQD}{J_n} \quad (\text{Eq. 4.10})$$

#### 4. Scour

---

Where: RQD = Rock quality designation (% of pieces longer than 0.1m)  
 $J_n$  = Joint number (number of joint sets in a rock mass)

The  $J_n$  values are given in Tab.4.2.

Number of joint sets	Join set number ( $J_n$ )
Intact, no, or few joints/fissures	1.00
One joint/fissure set	1.22
One joint/fissure set plus random	1.50
Two joint/fissure sets	1.83
Two joint/fissure sets plus random	2.24
Three joint/fissure sets	2.73
Three joint/fissure sets plus random	3.34
Four joint/fissure sets	4.09
Multiple joint/fissure sets	5.00

Tab.4 2: Values for the Joint Number ( $J_n$ ) (Kirsten, 1982 in Annandale, 2006).

Alternatively, if no drill core is available, Palmström (1982) suggested the RQD estimate by a formula using the Volumetric Joint count ( $J_v$ ) (Eq.4.11 & 4.12).

$$J_v = \frac{1}{S_1} + \frac{1}{S_2} + \dots + \frac{1}{S_n} \quad (\text{Eq. 4.11})$$

Where:  $S_{1,2,\dots,n}$  = Spacing of the respective joint sets

The relation of  $J_v$  to the RQD is given below:

$$RQD = 115 - 3.3J_v \quad (\text{Eq. 4.12})$$

#### Discontinuity bond shear strength number ( $K_d$ )

This number indicates the shear strength of joint interfaces in rocks. It is determined by characteristics of the joint surface: the ratio of the joint roughness ( $J_r$ ) and the joint alteration number ( $J_a$ ) (Eq. 4.13). It is a factor describing the shear strength of a joint since the roughness or waviness (a matter of scale) of a joint and its weathering stage have an impact on the resistance against shear.

$$K_d = \frac{J_r}{J_a} \quad (\text{Eq. 4.13})$$

Typical values for the Joint roughness ( $J_r$ ) and Joint alteration number ( $J_a$ ) are listed in Tab.4.3. and Tab.4.4, respectively.

#### 4. Scour

Joint separation	Condition of joint	Joint roughness number
Joints/fissures tight or closing during excavation	Stepped joints/fissures	4.0
	Rough or irregular, undulating excavation	3.0
	Smooth undulating	2.0
	Slickensided undulating	1.5
	Rough or irregular, planar	1.5
	Smooth planar	1.0
	Slickensided planar	0.5
Joints/fissures open and remain open during excavation	Joints/fissures either open or containing relatively soft gouge of sufficient thickness to prevent joint/fissure wall contact upon excavation.	1.0
	Shattered or micro-shattered clays.	1.0

Tab.4 3: Joint roughness ( $J_r$ ) values for different joint conditions (Kirsten, 1982 in Annandale, 2006).

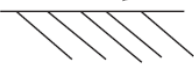

Description of gouge	Joint alteration number ( $J_a$ ) for joint separation (mm)		
	1.0	1.0 – 5.0	5.0
Tightly healed, hard, non-softening impermeable filling	0.75	-	-
Unaltered joint walls, surface staining only	1.0	-	-
Slightly altered, non-softening, non-cohesive rock mineral or crushed rock filling	2.0	2.0	4.0
Non-softening, slightly clayey non-cohesive filling	3.0	6.0	10.0
Non-softening, strongly over consolidated clay mineral filling, with or without crushed rock	3.0	6.0	10.0
Softening or low friction clay mineral coatings and small quantities of swelling clays	4.0	8.0	13.0
Softening moderately over consolidated clay mineral filling, with or without crushed rock	4.0	8.0	13.0
Shattered or micro-shattered (swelling) clay gouge, with or without crushed rock	5.0	10.0	18.0

Tab.4 4: Joint alteration numbers ( $J_a$ ) for different joint separations (Kirsten, 1982 in Annandale, 2006).

#### Relative ground structure number ( $J_s$ )

This parameter is inferred to account for the complexity of the ground structure and depends on the joint set spacing and their dip angles and dip directions, respectively. It is also a factor that describes the shape of the material and the ability of water to penetrate the ground and dislodge individual blocks (Fig.4.9). It is defined by the dip and dip direction of the least favourable joint set with respect to the flow direction. The values for the ground structure number are shown in Tab.4.5.

#### 4. Scour

Dip direction of closer spaced joint set (degrees)	Dip angle of closer spaced joint set (degrees)	Ratio of joint spacing, r			
		1:1	1:2	1:4	1:8
180/0	Vertical 90	1.14	1.20	1.24	1.26
In direction of stream flow 	89	0.78	0.71	0.65	0.61
	85	0.73	0.66	0.61	0.57
	80	0.67	0.60	0.55	0.52
	70	0.56	0.50	0.46	0.43
	60	0.50	0.46	0.42	0.40
	50	0.49	0.46	0.43	0.41
	40	0.53	0.49	0.46	0.45
	30	0.63	0.59	0.55	0.53
	20	0.84	0.77	0.71	0.67
	10	1.25	1.10	0.98	0.90
	5	1.39	1.23	1.09	1.01
	1	1.50	1.33	1.19	1.10
0/180	Horizontal 0	1.14	1.09	1.05	1.02
Against direction of stream flow 	-1	0.78	0.85	0.90	0.94
	-5	0.73	0.79	0.84	0.88
	-10	0.67	0.72	0.78	0.81
	-20	0.56	0.62	0.66	0.69
	-30	0.50	0.55	0.58	0.60
	-40	0.49	0.52	0.55	0.57
	-50	0.53	0.56	0.59	0.61
	-60	0.63	0.68	0.71	0.73
	-70	0.84	0.91	0.97	1.01
	-80	1.25	1.41	1.53	1.61
	-85	1.39	1.55	1.69	1.77
	-89	1.50	1.68	1.82	1.91
180/0	Vertical 90	1.14	1.20	1.24	1.26

Tab.4 5: Relative ground structure number depending on the dipdirection and dip of least favorable joint set orientation (Kirsten, 1982 in Annandale, 2006).

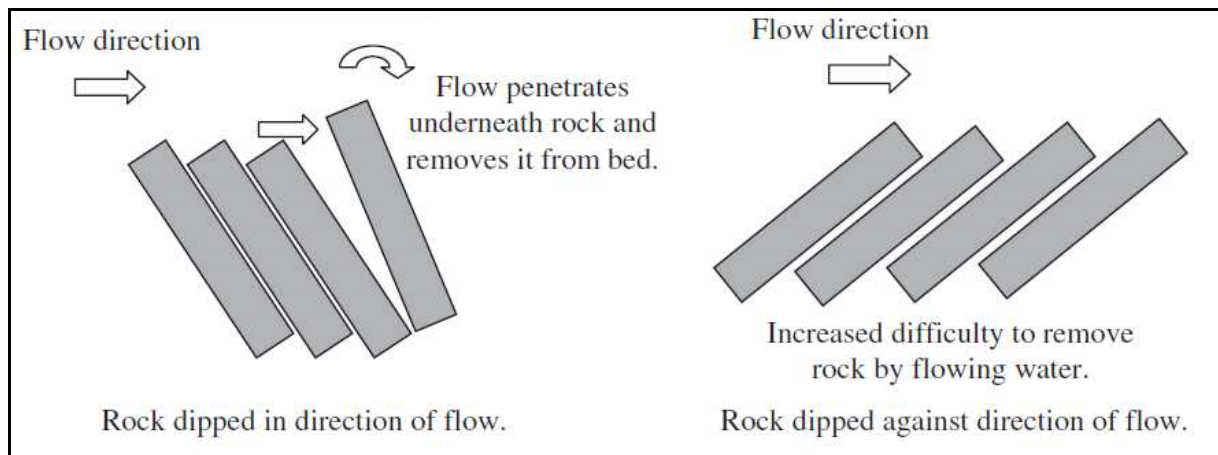


Fig.4. 9: Influence of orientation on resistance against scour (after Annandale, 2006).



### 5. The Ricobayo Dam

#### 5.1 Introduction

The Ricobayo Dam (sp.: Presa de Ricobayo or Salto de Ricobayo) is located in north-western Spain, about 20km from the Portuguese border and approx. 10km west of the city of Zamora in the autonomous community of Castile and León (Fig.5.1). The nearest village to the dam is Muelas del pan. The dam is installed at the Rio Esla (Esla River), which belongs to the Duero River system. The elevation is between 710m and 600m (Iberdrola, 2011a).

The construction of Ricobayo dam started in the late 1920s, and was completed in 1933. Ricobayo dam was the first large hydroelectric installation in Spain, and at the time of constructing had the largest reservoir in Europe. (Diego Martín, 2007). The dam was designed as a gravity dam, with an unlined spillway channel. The scheme information of the present facility is shown in Tab.5.1.

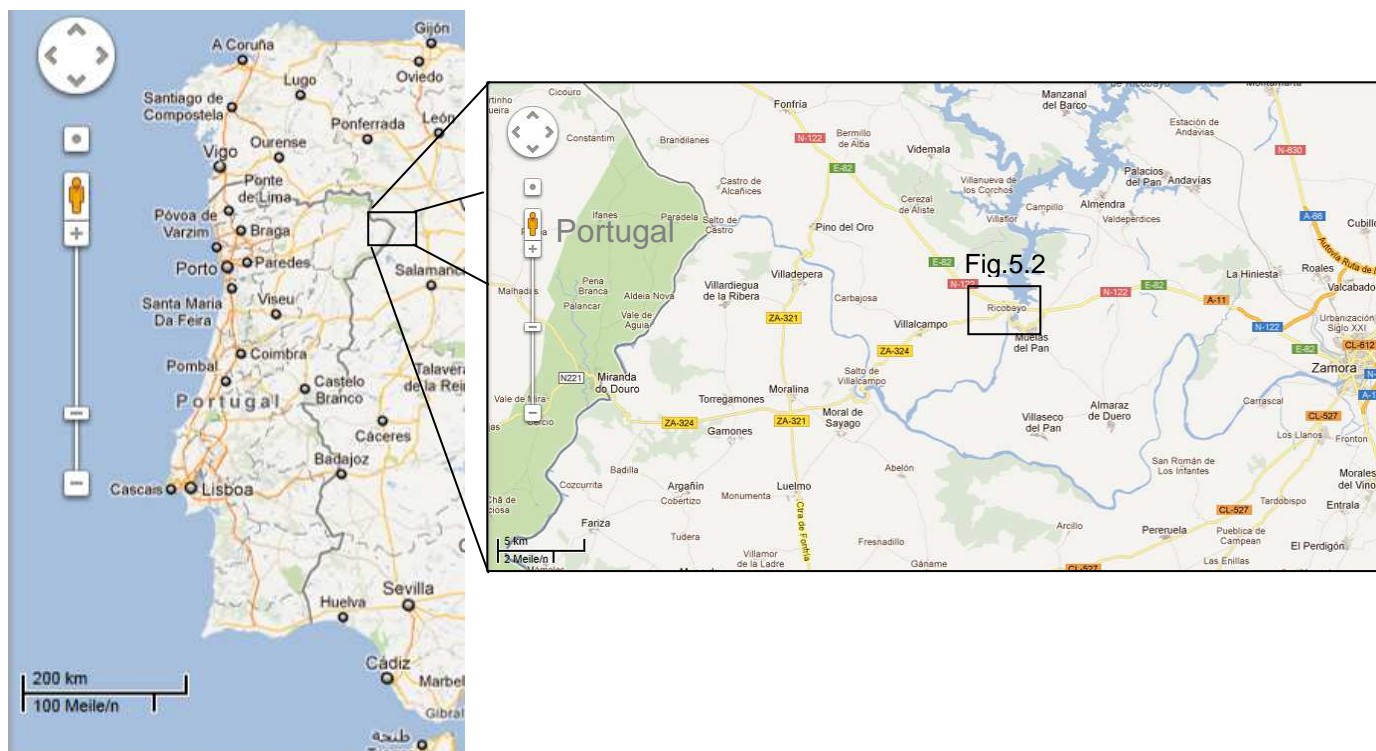


Fig.5 1: Location of the study area. A detailed Satellite image of the Ricobayo Dam facility is shown in Fig.5.2 as indicated by the box (Google Maps, 2012).

## 5. The Ricobayo Dam

---

### General Information

Location	Muelas del Pan
River	Esla
River basin	Duero
Catchment area	17,020km <sup>2</sup>
Average annual flow	4,639hm <sup>3</sup>
Year of completion	1933

### Reservoir

Storage capacity	1,178.88hm <sup>3</sup>
Active storage	1,078.40hm <sup>3</sup>
Maximum normal level (MNL)	684.00m
Minimum operating level	641.00m
Reservoir surface	5,725ha
Electricity capacity	840GWh

### Dam

Type	Gravity
Height above foundation	99.57m
Crest length	270.00m
Crest level	685.00m
Dam volume	398,000m <sup>3</sup>
Foundation rock	Granite

### Spillway

Type	Channel
Number of gates	4
Type of gates	Roller gates 20.84m x 10.50m
Discharge capacity at MNL	4,743m <sup>3</sup> /s
Discharge capacity at level 864.60	5,187m <sup>3</sup> /s
Energy dissipation system	Stilling basin

### Power Stations

<b>Ricobayo I Hydro Power Station (Exterior)</b>	
Number of units	4
Total nominal discharge	240m <sup>3</sup> /s
Maximum head	83.00m
Installed capacity	133.20MW
<b>Ricobayo II Hydro Power Station (Cavern)</b>	
Number of units	1
Total nominal discharge	217m <sup>3</sup> /s
Maximum head	75.00m
Installed capacity	158.04MW

Tab.5 1: Ricobayo scheme specifications- excerpt (from Iberdrola, 2011b)

## 5. The Ricobayo Dam

The layout of the study area is shown in Fig.5.2. Adjacent to the dam on the east side lies the city of Muelas del Pan, where the historical archives of Ricobayo (Archivo historico de Ricobayo) are situated. To the west side of the dam the village of Ricobayo is situated. The power station of Ricobayo I is situated right at the dam, whereas Ricobayo II is a cavern underneath the operating center.



Fig.5 2: Satellite image of the Ricobayo Dam facility. Labeled are the most important features related to the dam (modified after Google Maps, 2012).

### 5.2 The History of the Dam

#### 5.2.1 Construction and layout

As this thesis deals with the issue of rock scour, it is crucial to reconstruct the stages of the extreme scour at the Ricobayo spillway. Therefore, historical data such as original photographs, construction plans, reports and personal comments by employees of Iberdrola SA were used to set up a detailed timeline of the scour events. This chapter illustrates how the scouring has affected the operation of the spillway and the countermeasures that have been taken to overcome this problem. The following description is closely related to the Spanish Guia tecnica paper translated by Rocha (2012).

The first plans from 1927 showed alternative designs for the facility. The alignment of the spillway was initially planned to be much more curved and should have merged with the Elsa River at an approximately 60° angle (Fig.5).

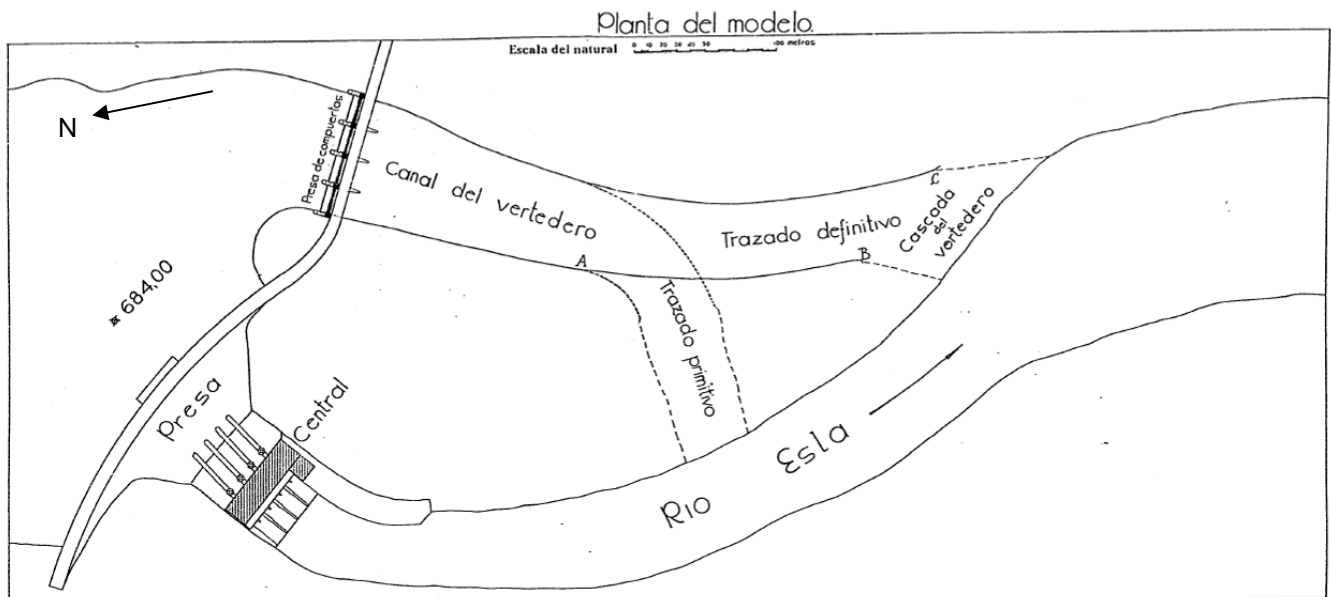


Fig.5 3: Alternative layout of the Ricobayo Dam in 1927 (Revista de Obras Públicas, 1933).

The final design then was to align the spillway straighter, and lead parallel to the Elsa River. The power station and the intake were shifted to the middle of the river right in front of and behind the dam, respectively (Fig.5.4). Construction of the dam was finished by 1933 (Guia tecnica, 1997).

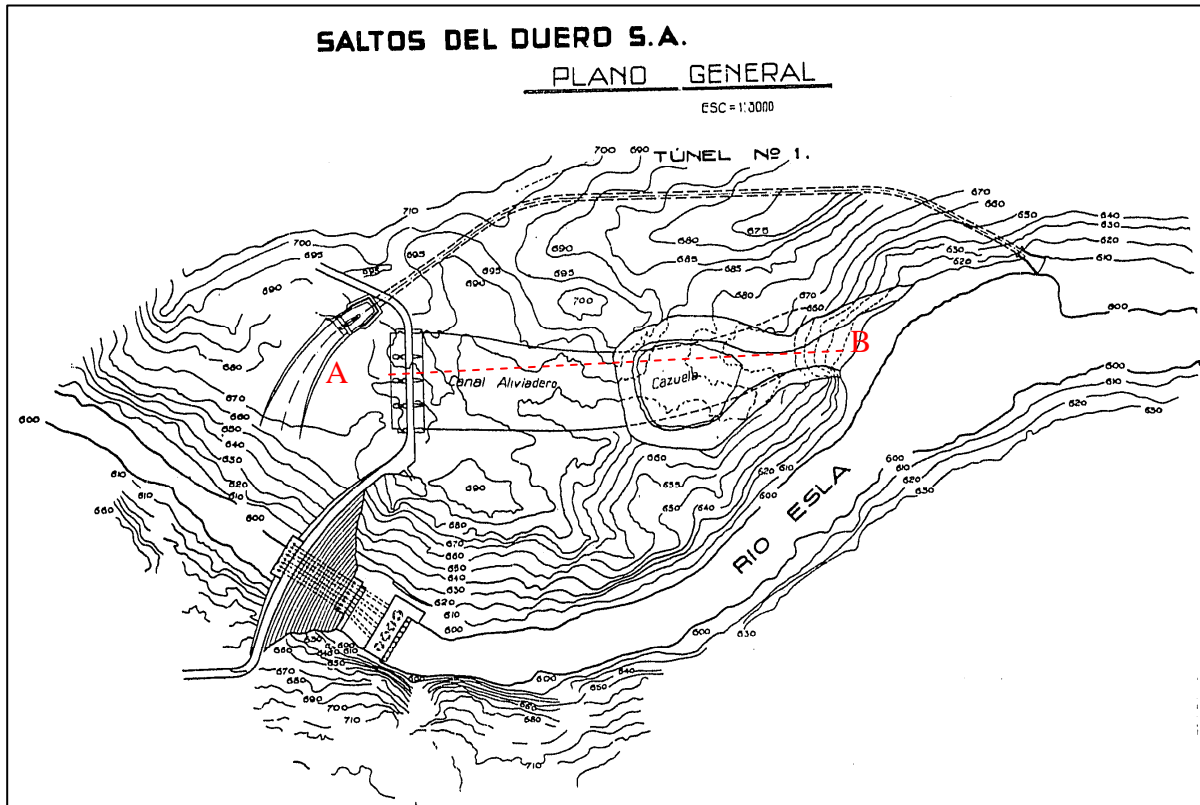
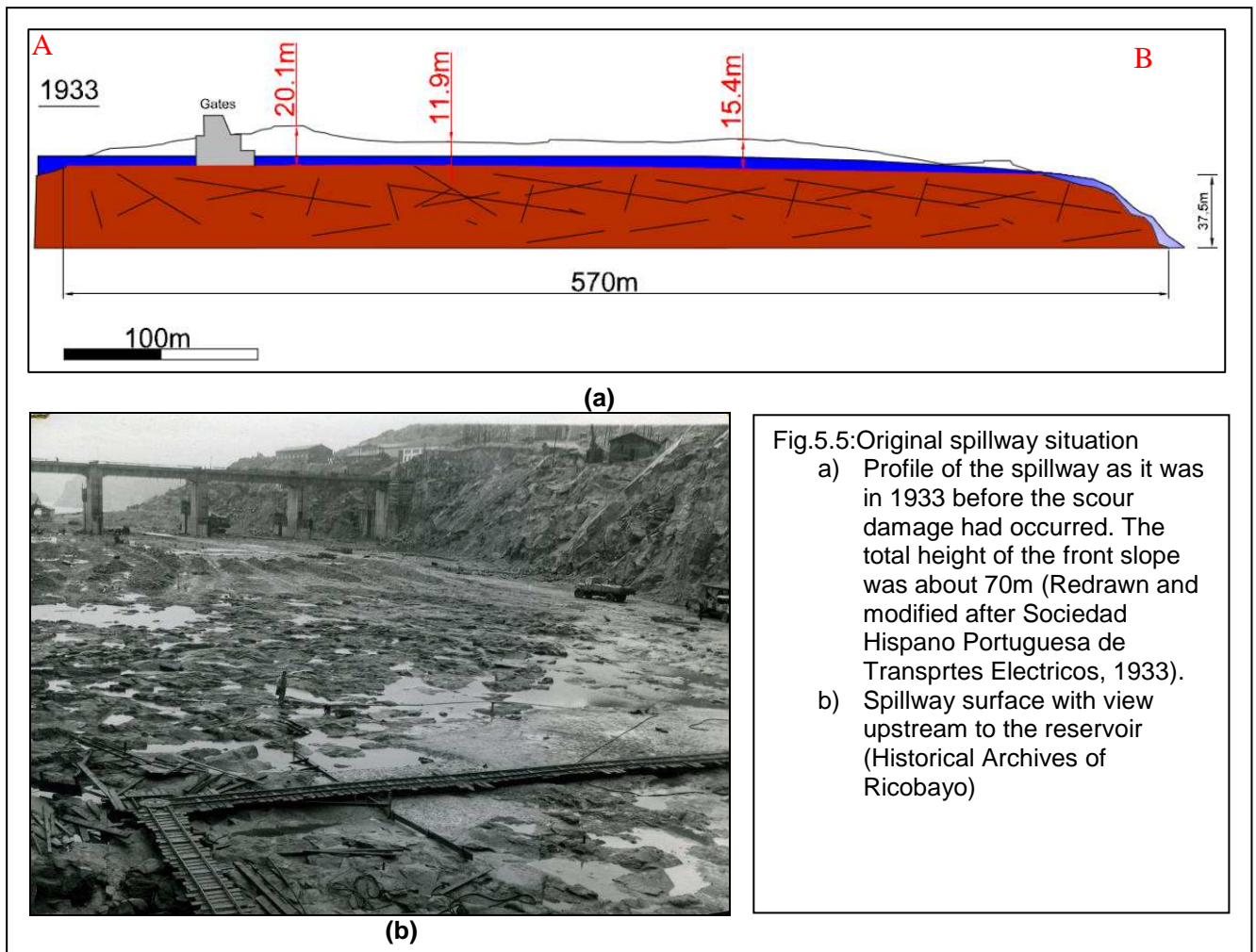


Fig.5 4: Map of the Ricobayo dam site showing the original topography of the area, the initial alignment of the spillway and the location of the consecutively formed plunge pool due to scouring. Scale 1: 3000. Section A-B is shown in Fig.5a. (modified after Rubio, 1940).

For the construction of the spillway, the granodioritic bedrock was excavated over a total length of more than 400m (Iberduero S.A., year unknown, Guia tecnica, 1997). In total the spillway, including the untreated rock sections, was more than 0.5km long and 75m wide (Iberduero S.A., year unknown). Up to 20m of overburden were excavated to create an even surface with about 0.5 degrees of inclination over the total distance (Fig.5.5a). The elevation of the surface is at 670m (Guia tecnica, 1997). The surface of the spillway was left unlined after the excavation because it was believed that the hard bedrock would sustain the water flows (Fig.5.5b). Also the low inclination of the spillway surface should ensure that flow velocities stay moderate not to damage the underlying rock, but clean up the excavated rock surface. Even back then the blocky characteristics of the rock mass were recognized, but not considered to be a problem. At the end of the spillway the water was supposed to flow over the natural existing 70m high slope, merging again with the Esla River (Guia tecnica, 1997). The spillway was dimensioned for water flows up to 5000m<sup>3</sup>/s (Iberduero S.A, year unknown).



The design of the spillway was based on the flow conditions of the Esla River, which are highly irregular. Peak flow conditions occur mostly in winter time during rain season and in springtime at the snowmelt in the closer vicinity of the catchment area of the Duero River system. Due to that, flow rates ranging from  $6800\text{m}^3/\text{s}$  (500 years maximum) to only  $5\text{m}^3/\text{s}$  in dry season are encountered in the area (Guia tecnica, 1997, Diego Martín, 2007). The 6 months flow amount of the Esla River is documented to be  $5 \times 10^9 \text{m}^3$  (Diego Martín, 2007). The average annual precipitation at Ricobayo is 503mm (SEPREM, 2012).

In the first years when the spillway was constructed, extraordinary intense rainfalls occurred in the area, which exceeded the maximum capacity of the reservoir and made it necessary to release huge amounts of water. From December 1933 to June 1934, for half a year, the spillway was permanently used (Guia tecnica, 1997).

## 5. The Ricobayo Dam

---

During construction of the dam, a slot just a few meters wide was left open in its middle of the dam until 1933 (Fig.5.6). In that year, it was closed to fill up the reservoir and to establish the power house at the toe of the dam. During this time, the spillway was already finished and ready for use, if necessary (Guia tecnica, 1997).

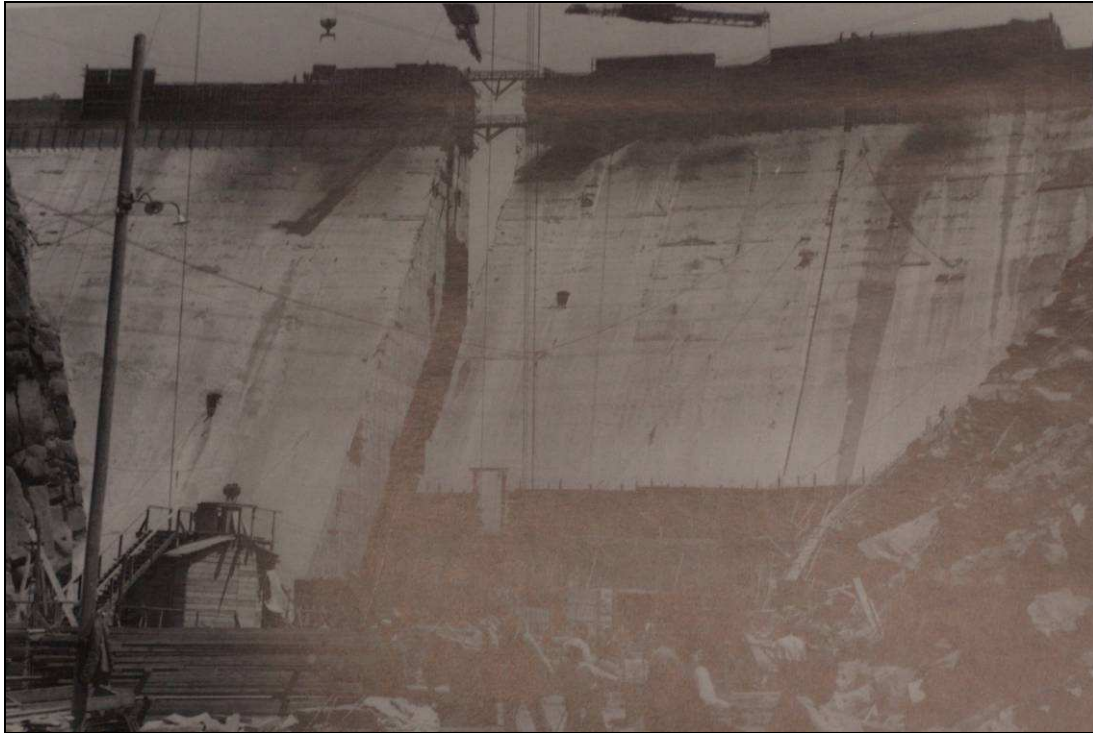


Fig.5 6: Open slot in the central part of the Ricobayo Dam, which was closed in 1933 for the construction of the power house (San Roman, 2006)

### 5.2.2 Spillway scour damage

From 1933 to 1939, 5 major scour events occurred along the spillway, eroding approximately  $1.1 \times 10^6 \text{m}^3$  of rock (Iberduero S.A., year unknown). The different stages of scour are illustrated in Fig.5.7. During the spill events the amount of discharge did not exceed  $1900 \text{m}^3/\text{s}$ , which is below the designed maximum capacity of the spillway.

The most severe damages occurred in the following 5 stages:

1. January, 1934
2. March, 1934
3. March, 1935
4. March, 1936
5. January, 1939

## 5. The Ricobayo Dam

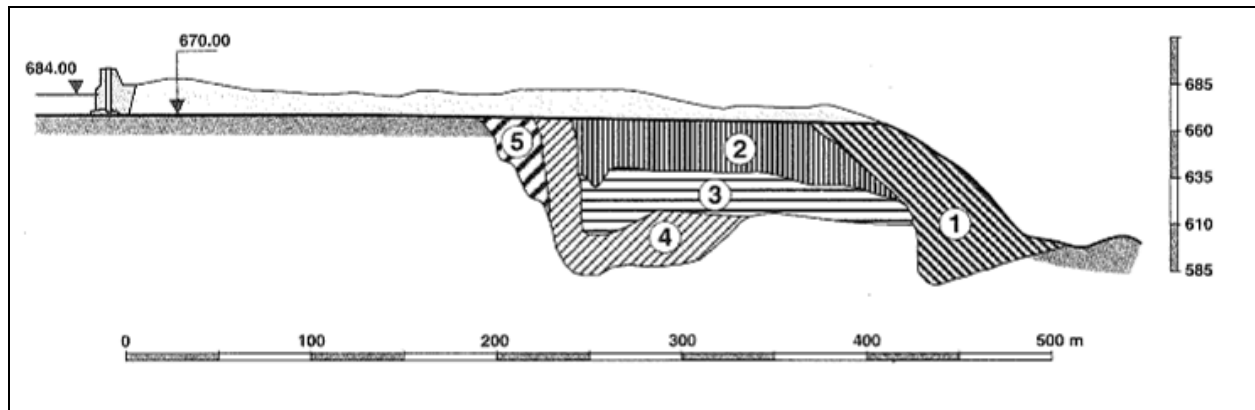


Fig.5 7: Illustration of the 5 main stages of scour at the spillway. Note steepening of the natural rock slope and progressive upstream movement of erosion towards the reservoir (Guia Tecnica, 1997)

### Scour Stage 1 (January, 1934)

Already in the first year when the spillway and the dam were finished (1933) and the reservoir filling began, the spillway had to be used. As mentioned above, strong rainfalls in winter time of 1933 and 1934 lead to a rapid fill up of the storage reservoir, which made it necessary to release water.

The first time the spillway operated was in December of 1933 discharging  $100\text{m}^3/\text{s}$  leading to the first scour damage on January 10th in a way that resembled a landslide (Iberduero S.A. year unknown)(Fig.5.8a/b). From that time on, water was released without any interruption until June 1934. In that time span the first two major scour events occurred. Material from the front slope was removed by the overflowing water and created a small plunge pool at the toe of the slope. The material eroded was deposited in the downstream riverbed. Additionally, the spillway was also reduced in length, due to the progressive upstream erosion resulting in the formation of a gorge at the exit of the spillway (Fig.5.8b). Gradually, the slope angle steepened up. At the beginning the water was simply flowing over the spillway surface and the untreated rock of the front slope. But as more and more material was removed and the slope angle became steeper, the water flow got more characteristics of a water fall.



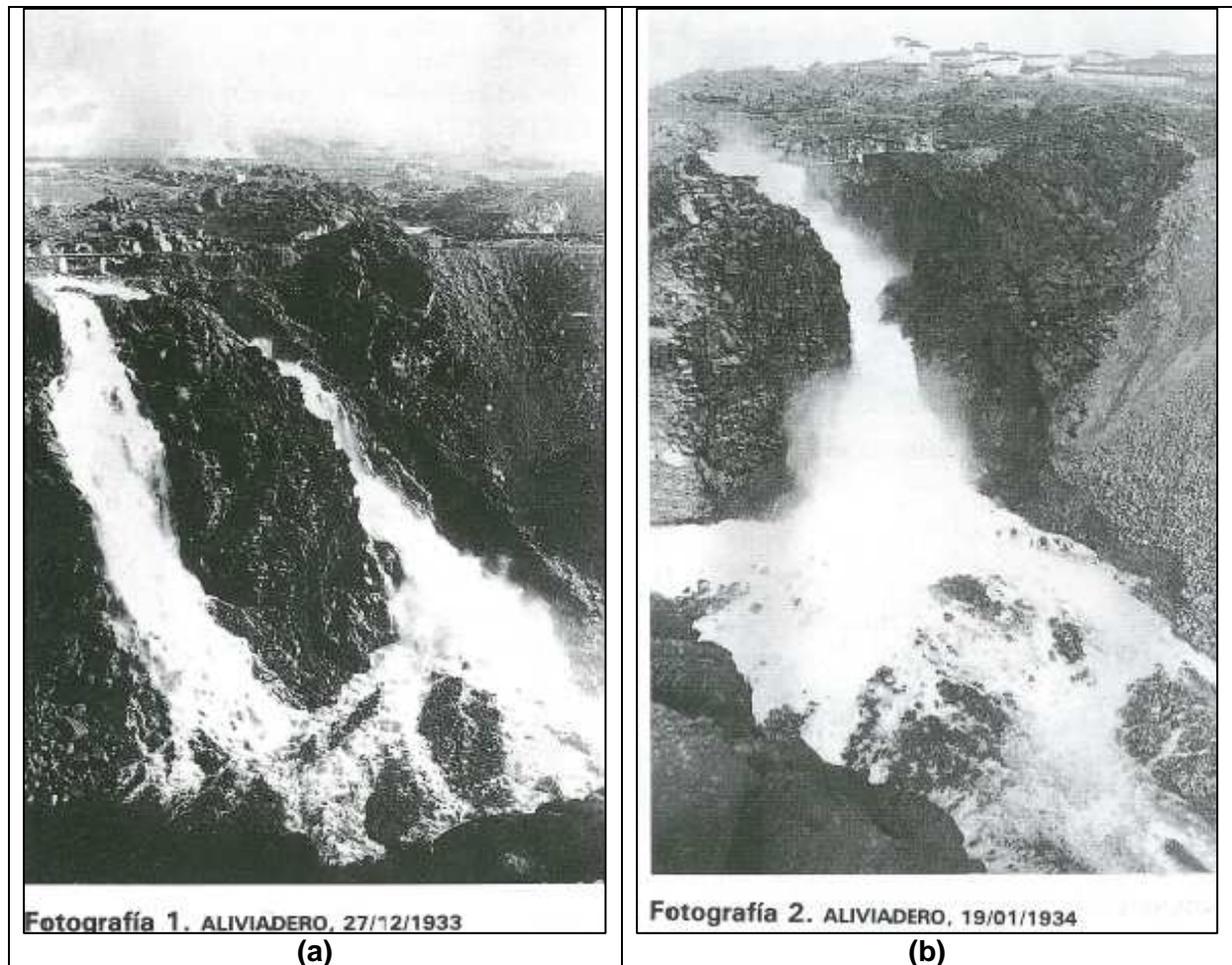


Fig.5 8: The first major scour at the Ricobayo spillway. (a): View to the original front slope of the spillway in the first month of operation. The water flow was discharged unregulated over bare rock. (b): The original slope is already eroded after one month of operation leaving a gorge behind as the water works its way towards the reservoir (Pictures: Guia tecnica, 1997).

### Scour Stage 2 (March 1934)

Despite the fact that the spillway was operating all the time from December to June, the removal of the material occurred in a sudden event rather than in continuous erosion. This means that there were some periods where no scouring was encountered, but then larger amounts of material were removed at once in some sort of rock fall character. Only two months after the first scour stage major scour damage happened again. This time the rate of erosion was so high, that the spillway lost material over a length of approximately 200m (Guia tecnica, 1997). Discharge raised up to  $400\text{m}^3/\text{s}$ . Erosion in vertical direction caused a deepening of the gorge of 30 to 40m (Iberduero S. A., year unknown). By summer of 1934, a new river bed had formed in front of the spillway channel (Fig.5.9 & 5.10). Additionally the gorge became wider and more circular in shape, forming a plunge pool. Those severe damages required immediate repair measurements because loss of the whole spillway and the reservoir would have killed the whole dam project. In summer of 1934, repair works on the spillway were conducted when the spills ended.

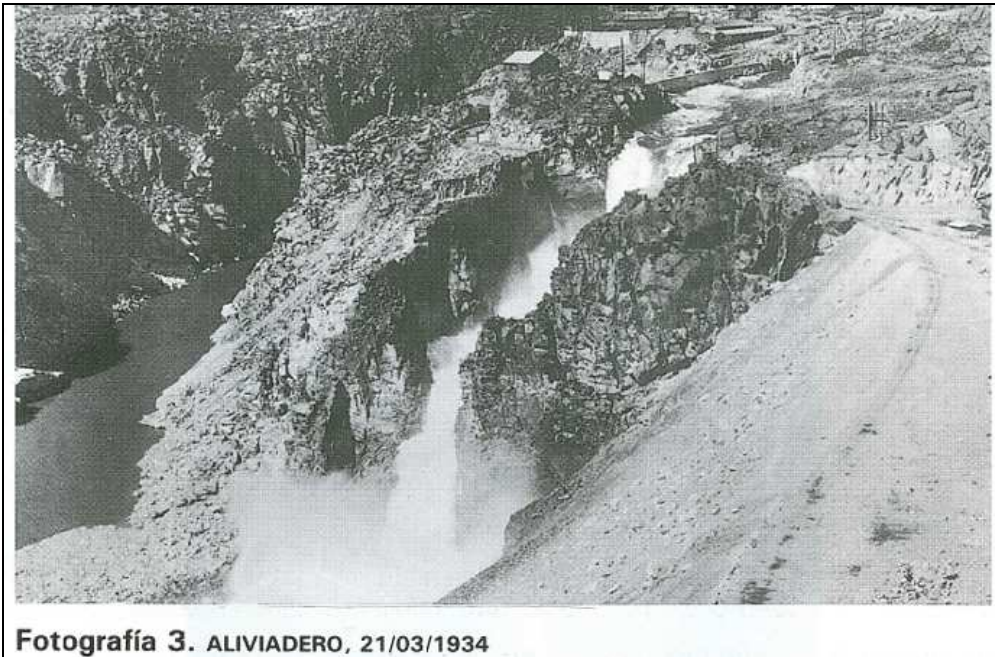


Fig.5 9: An approx. 200m long gorge has developed working its way back to the reservoir

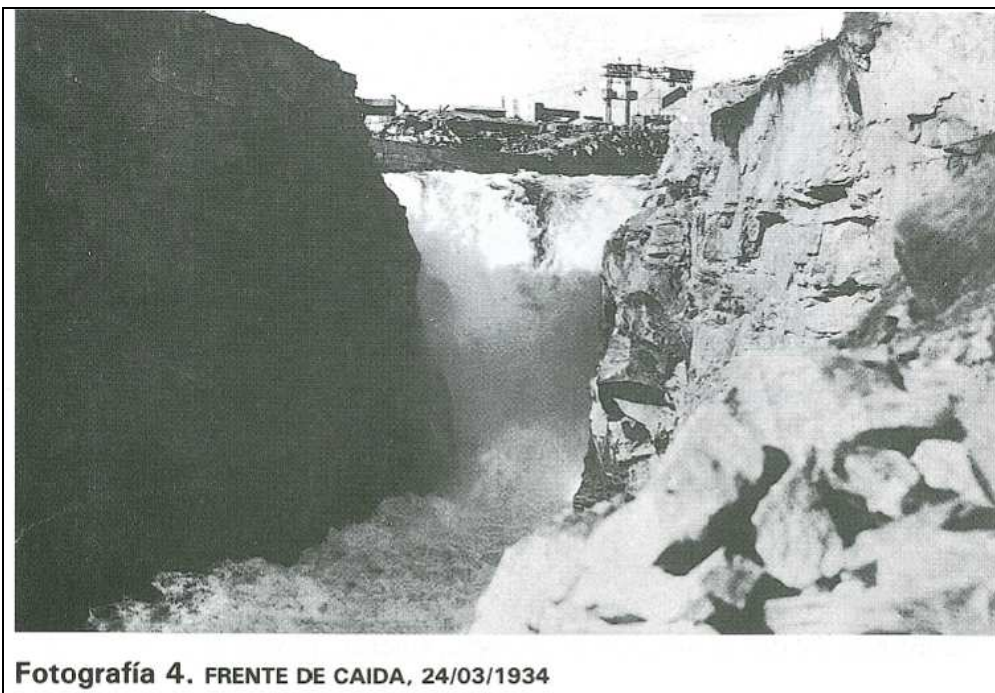


Fig.5 10: Situation of the spillway during the 2<sup>nd</sup> major scour stage in March 1934. View upstream into the gorge. Sidewalls are almost vertically inclined and the front slope has steepened up compared to its original state, to form a waterfall at the exit of the spillway (Guia tecnica, 1997).

## 5. The Ricobayo Dam

---

Reformation of the spillway had to be done very quickly during the drier season, before larger amounts of water were expected to occur again in the following winter. The repairs included the following measures:

- a) Realignment of the spillway wall on the right side (view downstream). The curvature of the wall was changed towards the formed plunge pool to prevent the water from attacking the right wall of the pool (Fig.5.11).
- b) The right wall of the pool was reinforced with concrete as a protection against further erosion (Guia tecnica, 1997). A big concern was the jut at the tip of the right wall of the newly formed gorge and the Elsa River at the very end of the outlet. A loss would have completely destroyed the spilling system (Personal comments by Iberdrola employees).
- c) Construction of a steel concrete wall at the front slope of the spillway channel to stop the progressive advance towards the reservoir (Fig.5.12).
- d) Installation of a wall at the exit of the gorge to create a higher water level inside the plunge pool. This should provide a water cushion which allows the impinging water fall to dissipate its energy before reaching the bottom of the channel (Guia tecnica, 1997).

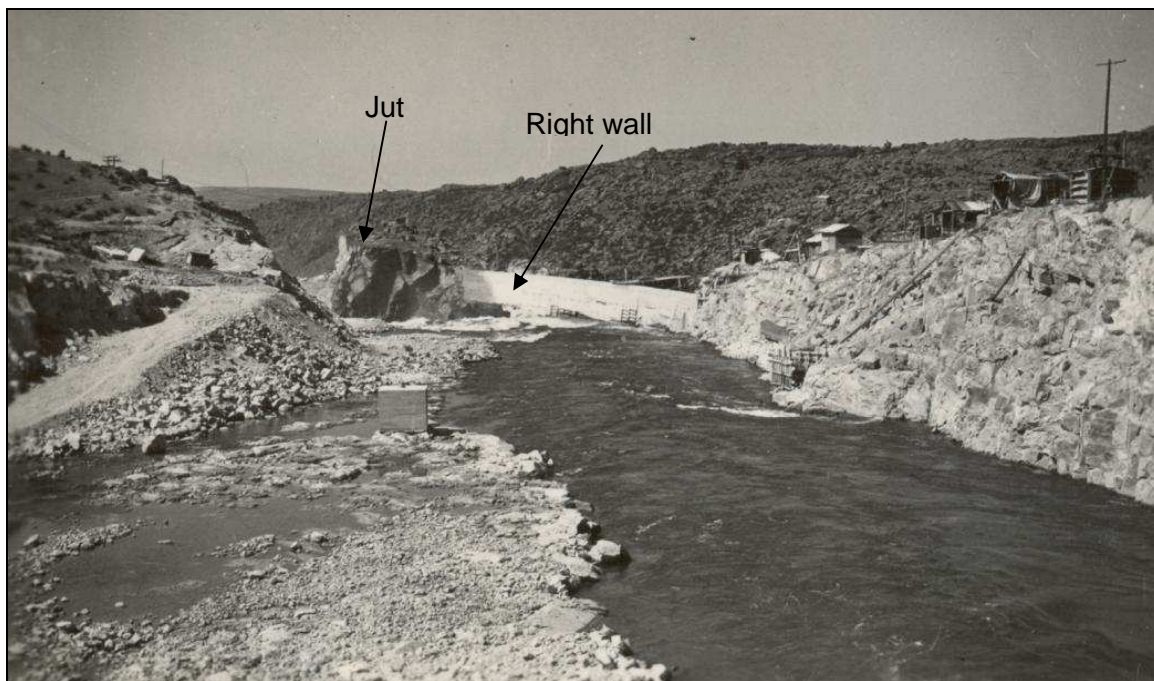


Fig.5 11: View downstream the spillway. The right curvature of the right wall at the end of the spillway was changed more to the middle of the plunge pool. The spillway surface was left unlined (Riesco Chueca, 2009).



Fig.5 12: Repair works on the spillway in summer of 1934. Construction of a concrete wall at the front slope of the spillway. Looking at the curvature of the wooden balk, the initial shape of the plunge pool can be recognized (Guia tecnica, 1997).

### Scour Stage 3 (March 1935)

In 1935, the discharge raised to  $1000\text{m}^3/\text{s}$  (Iberduero S. A., year unknown). Massive scour damage occurred to the spillway again. During that third stage the wall at the exit of the gorge collapsed resulting in loss of the water cushion. This triggered erosion that affected more the bottom of the channel and the right wall of the plunge pool (Fig.5.13 & Fig.5.14). The concrete wall constructed at the front slope in the summer before at least prevented the water from eroding progressively upstream. Right in front of the wall where the water jet impingement took place, the plunge pool grew significantly in depth (Fig.5.8). The bottom of the channel was lowered from 630m to 608m (Iberduero S. A., year unknown). On January 4th 1935 the power station started producing electricity for the customer Hidroeléctrica Ibérica and the market of Bilbao (Diego Martín, 2007).

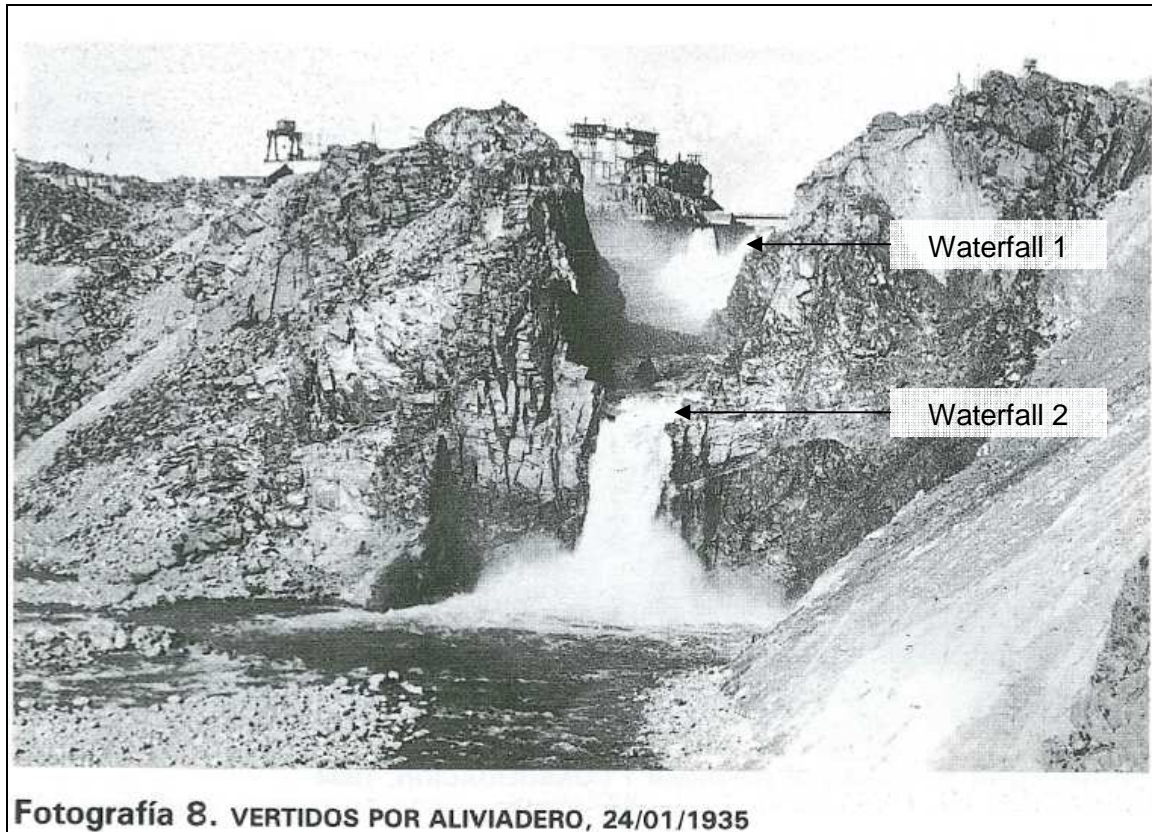


Fig.5 13: Situation of the spillway in 1935. Water release in January. By that time two waterfalls are developed. One in the back at the front slope of the spillway, the second one at the exit of the gorge. (Guia tecnica, 1997).

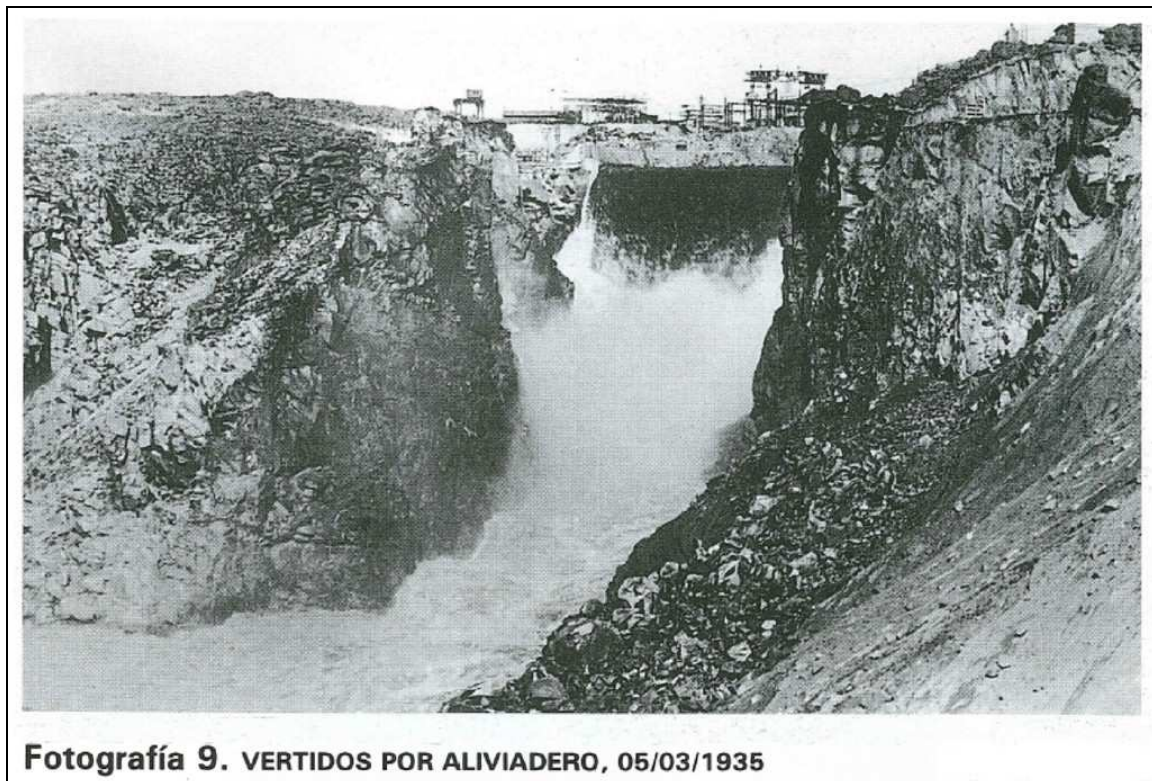


Fig.5 14: Only about one month later the vertical erosion has abraded the bottom of the channel. The second waterfall has disappeared (Guia tecnica, 1997).

## 5. The Ricobayo Dam

---

In summer of 1935 additional repairs were performed, including:

- a) Changing the geometry of the spillway edge to ensure the impact of the water jet to be farther away from the wall.
- b) A spur dike is installed at the river bed so no material can be deposited in the Esla River upstream to the power house, which started operating in November of the same year.

### Scour Stage 4 (March, 1936)

In winter of 1935/36 the plunge pool grew in diameter and depth, but no upstream regression occurred (Iberduero S. A., year unknown). At this stage the front wall collapsed, that had been constructed in summer of 1934 after the 2nd scour stage (Fig.5.15 & Fig.5.16). As a consequence upstream erosion was triggered again. Moreover the spur dike was destroyed. Up to 1280m<sup>3</sup>/s were discharged at this period (Annandale, 2006). Since the power station was already operating, the water table in the reservoir could be controlled to a certain extend over the intake making it not necessary to use the spillway.



Fig.5 15: Collapse of the front wall of the spillway. View upstream where the front wall and the spur dike were situated at. Note the huge amounts of crushed rock in the riverbed (Guia tecnica, 1997).

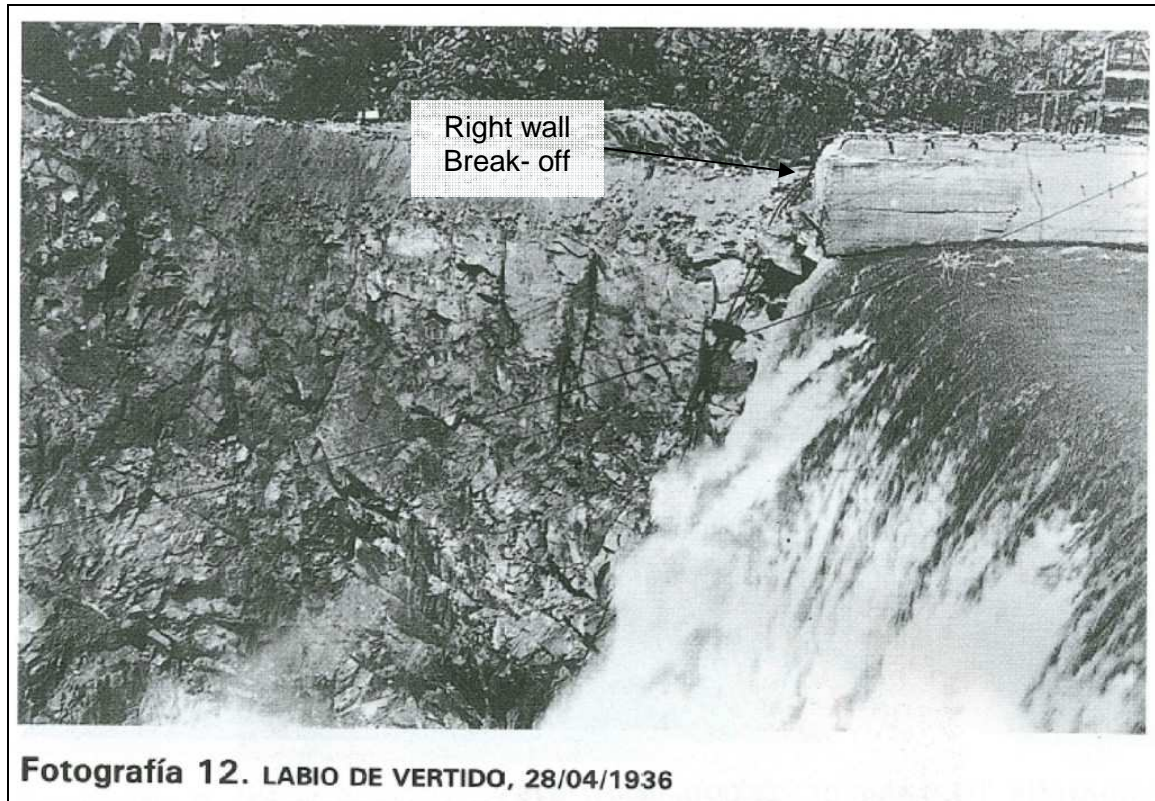


Fig.5 16: Look to the right wall of the plunge pool while the spillway is operating. The wall is already destroyed and the water impacting again right at the toe of the slope. Parts of the right sidewall are also damaged (Guia tecnica, 1997).

#### Scour Stage 5 (March, 1939)

For 3 years after the last scour no major damage occurred at the spillway. In 1939 the last event of scour affected the spillway at its edge. Not much is documented about this last stage. Peak flows of more than 3200m<sup>3</sup>/s are reported for this event (Annandale, 2006). The topography of the plunge pool as it was in 1937 is shown in Fig.5.17

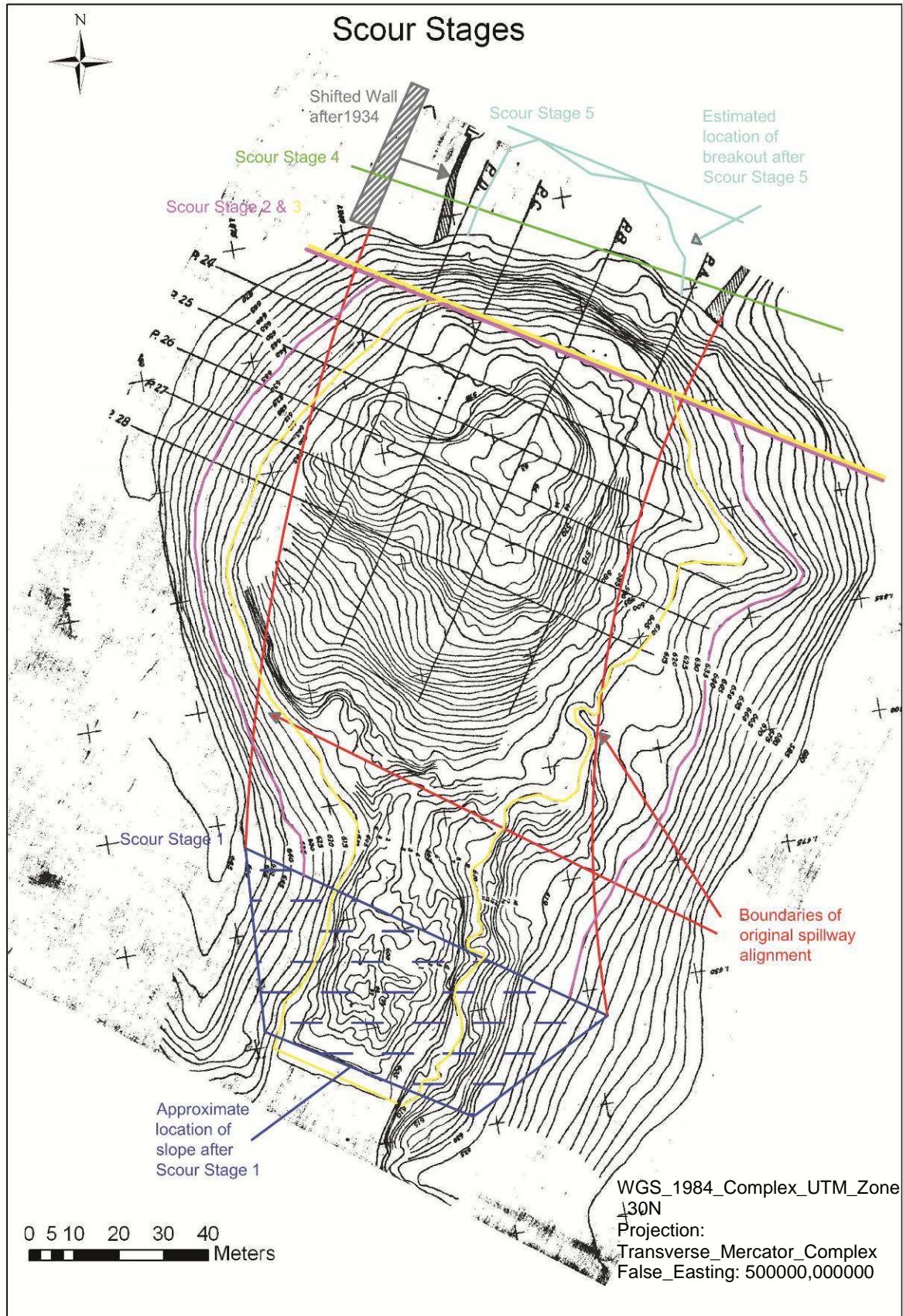


Fig.5 17: Shape and topography of the plunge pool without concrete. Note the deep hole right where the overtopping water impacted the rock. Profile lines are meaningless in this figure (Modified after Iberduero S.A, 1937)



### Further measures against scour

The spillway has caused problems for 6 years of operation, not only because of the numerous repairs, but also making it difficult to run the power station during periods of high water table. The eroded rock that was deposited in the Esla River caused backwater affecting the power station. To overcome this problem, a tunnel was constructed on the left side of the spillway bypassing water and material, merging with the river again some few hundred meters downstream the power station. The capacity of that tunnel is 874m<sup>3</sup>/s. By this the operation of the spillway was limited only to very high water tables in the reservoir, which allowed more comprehensive works on the spillway.

### **5.2.3 Spillway repair**

For the repair of the spillway 4 options were considered.

1. One option was to construct a channel with a supercritical regime, leading the water back to the river.
2. Construction of a hydraulic jump to create energy dissipation so that the plunge pool would not be needed. This option involved some difficulties in terms of handling the flow from the spillway and modification of the gorge to lead the water back to the river.
3. In the 3<sup>rd</sup> option it was planned to build 2 tunnels underneath the right side of the spillway with a capacity of 2000m<sup>3</sup>/s each. With this solution the original spillway would have had no purpose any more.
4. The 4<sup>th</sup> option was to use the plunge pool that had already formed due to the scour process as a stilling basin. The water inside the pool should act as an energy dissipater.

From an economical and practical point of view, option 4 was chosen to be realized. It used the shape of the plunge pool created by scouring. The final design of the spillway consisted of two independent complexes, an upper channel with the original spillway surface and a lower channel consisting of the plunge pool and the outlet to the river. The transition from the upper to the lower channel is a waterfall (Fig.5.18).

The spillway, from the gates to the edge, is about 92m long and situated at an elevation of 670m. The spillway is divided by a concrete sill, which creates a basin to collect water, in case not all of the gates are open. This device ensures uniform flow over the entire width of the spillway. Further downstream of the sill the water level is lowered creating a supercritical flow. Additionally the final part at the spillway edge shows a higher curvature (approx. 30°), speeding up the water flow. This way it should be ensured the water impacts the plunge pool far enough away from the front slope wall of the spillway. As the waterfall overtops the edge

## 5. The Ricobayo Dam

of the spillway its lower part gets aerated and impacts away from the slope of the spillway (Guia tecnica, 1997). The impact of the water creates eddies inside the pool which rotate towards the front wall. These conditions were considered to be dangerous in terms of stability. The situation improved in 1964 when the “teeth” (hydraulic splitters) at the spillway edge were constructed. The splitters had two effects: first was to split up the waterfall before it overtopped the edge of the spillway, second it induced two contrarily turning eddies in the plunge pool. This system improved tremendously the energy dissipating system (Iberduero S.A., year unknown).

The concrete lining of the spillway edge, the upper part of the slope and the side walls of the plunge pool is much thicker than in the rest of the pool. Those were the parts most affected by the scouring process. The bottom of the pool is reinforced with a concrete slab with a thickness of 0.8 to 1.5m. At the bottom deflector walls were constructed to reorient the flow of the water to the outlet (Guia tecnica, 1997). In the outlet channel again supercritical flow conditions were achieved by a small cavity. So the accelerated water was released over a ramp structure to the Esla River without having to widen the gorge (Iberduero S.A., year unknown)

Until 1962 the spillway operated satisfyingly when the bottom concrete slab of the plunge pool failed during a flood with a discharge up to  $4800\text{m}^3/\text{s}$ . (Annandale, 2006). After installation of the above mentioned hydraulic splitters the operation of the spillway has been successful up to now.

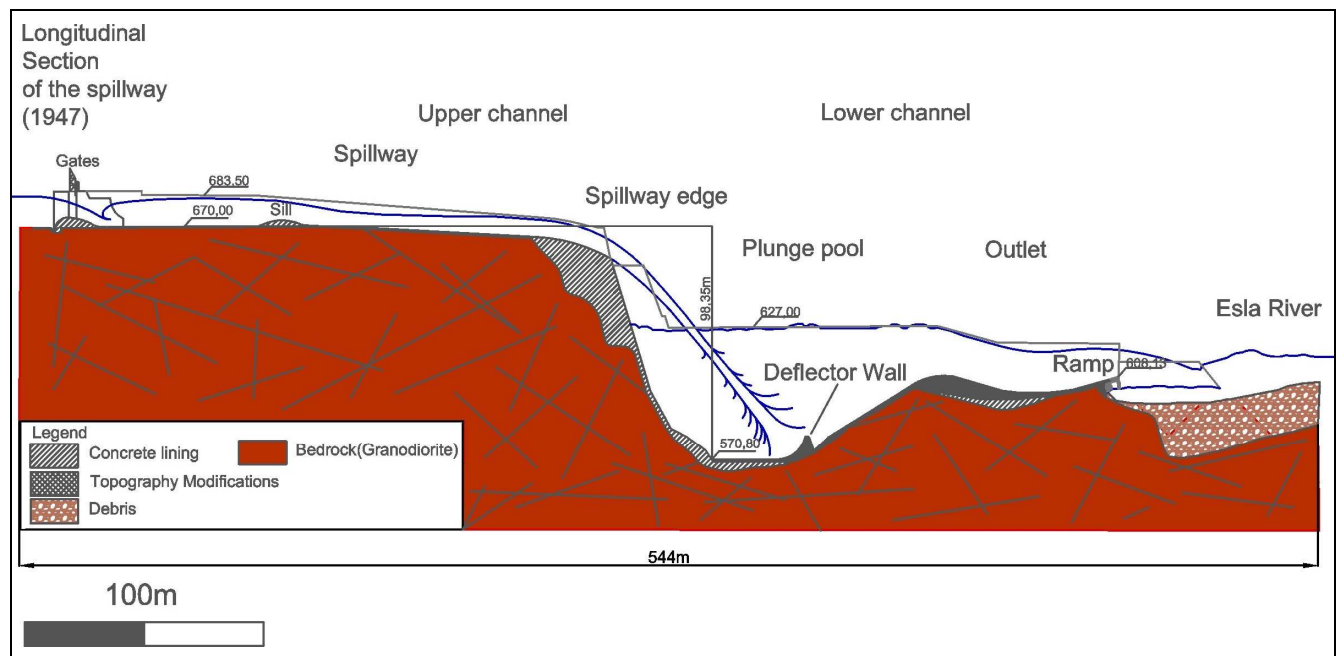


Fig.5 18: Layout of the spillway after the reform as it was in 1947. The energy dissipating system with concrete teeth at the spillway edge was constructed in 1964 (redrawn and modified after Iberduero, 1947).

## 6 Geologic conditions

### 6.1 Regional conditions

The study area is geologically located within the northwestern part of the Iberian Massif at the SE margin of the Alañcines Synform (Fig.6.1). The Ricobayo Batholith is of hercynian (variscan) age ( $324\pm 12$  Ma; K- Ar dating, Toros, 1981) and is build up of two syntectonic, peraluminous granites (Fernandez- Turiel et al., 1991). The Carbajosa leucogranite and the Ricobayo two- mica granite form the magmatic bodies in the southern part of the Alañcines Synform. The Ricobayo Granite is the larger one covering an area of approx. 150km<sup>2</sup>. Its composition is various containing different lithological types such as biotitic granite, garnet-sillimanite bearing leucogranite and amphibolitic diorites.

Both intrusive bodies, the Cabajosa and the Ricobayo granite were deformed by the Villacampo Shear System. It consists of right lateral ductile shear bands than can be traced over 40km at the surface striking about NE- SW. In the Duero Basin it is covered by Cenozoic clastic sediments (González Clavijo & Martínez Catalán, 2002). In its NE part the shear system splays into several faults, which merge towards the SW in an approx. 1km wide shear zone at the boarder of the Ricobayo Granite. The age of the system has been estimated to be Upper Carboniferous based on the relationship to the Ricobayo Granite.

The Alañcies Synform is a variscian, NW- SE striking feature developed in the Central Iberian Zone containing metasedimentary rocks from the late Proterozoikum (Vendian) to the Devonian. Those rocks are divided in four main units (Fig.6.1): (a) Río Duero Unit (b) Bajo Río Esla Unit (c) Río Aliste Unit (d) Río Manzanas Unit.

The rocks were deposited at the northern passive continental margin of the Gondwana continent and experienced deformation, metamorphism and granitic intrusions before and during the variscan orogeny. In the regional vicinity of the investigated area, 6 formations build up the ground, all belonging to the Río Duero Unit.

#### The Villacampo Schist

This unit contains the oldest rocks in the area and is one of the main host rocks for the Ricobayo Granite. A small part of it crops out to the northwest of the Granite and shows a sharp contact to it. Entering the village of Muelas del Pan from the highway to Zamora, the contact is traversed. The major occurrence of this rock unit is encountered southwest of the Ricobayo Granite and around the Carbajosa Granite. The schist is uniformly composed and up to 2000m thick. Some constituents of greywackes, some calc- silicates and quartzites are present in the formation (González Clavijo & Martínez Catalán, 2002).

### Villadepera Gneiss

Together with the Villacampo Schist this unit represents the oldest sequence of the Spanish part of the Alañcines synform. It is not as abundant in the area, but overlies the schist in some parts of the area. It is a porphyric fine grained, strongly foliated orthogneiss with a thickness of 250m (González Clavijo & Martínez Catalán, 2002).

### Santa Eufemia Formation

The base of the Ordovician rocks is formed by the approx. 1000m thick metapelites (Schists) and quartzites of the Santa Eufemia Fm, which are separated by an unconformity from the Villadepera gneisses (González Clavijo & Martínez Catalán, 2002).

### Peña Gorda Formation

Farther north, separated by a conformity the quartzites of the Peña Gorda Fm. overly the metasediments of the Santa Eufemia Fm (González Clavijo & Martínez Catalán, 2002).

### Villaflor and Campillo Formation

With up to 600m thick slates and some quartzites the Villaflor Fm. and the Campillo Fm. with schists and minor sandstones represent the upper Ordovician in the region. Glacial pebbles and olistholites are present in the Campillo Fm. The formations thickness varies strongly from 150 to 450m due to tectonic activity (González Clavijo & Martínez Catalán, 2002).

The rocks within the Río Duero Unit represent the autochthon within the Alañcines synform. The younger rocks of the Bajo Río Esla Unit, the Río Aliste Unit and the Río Manzanas Unit, which are all of Slurian- Devonian age, were thrust to the northeast over the Río Duero Unit (González Clavijo & Martínez Catalán, 2002).

## 6 Geologic conditions

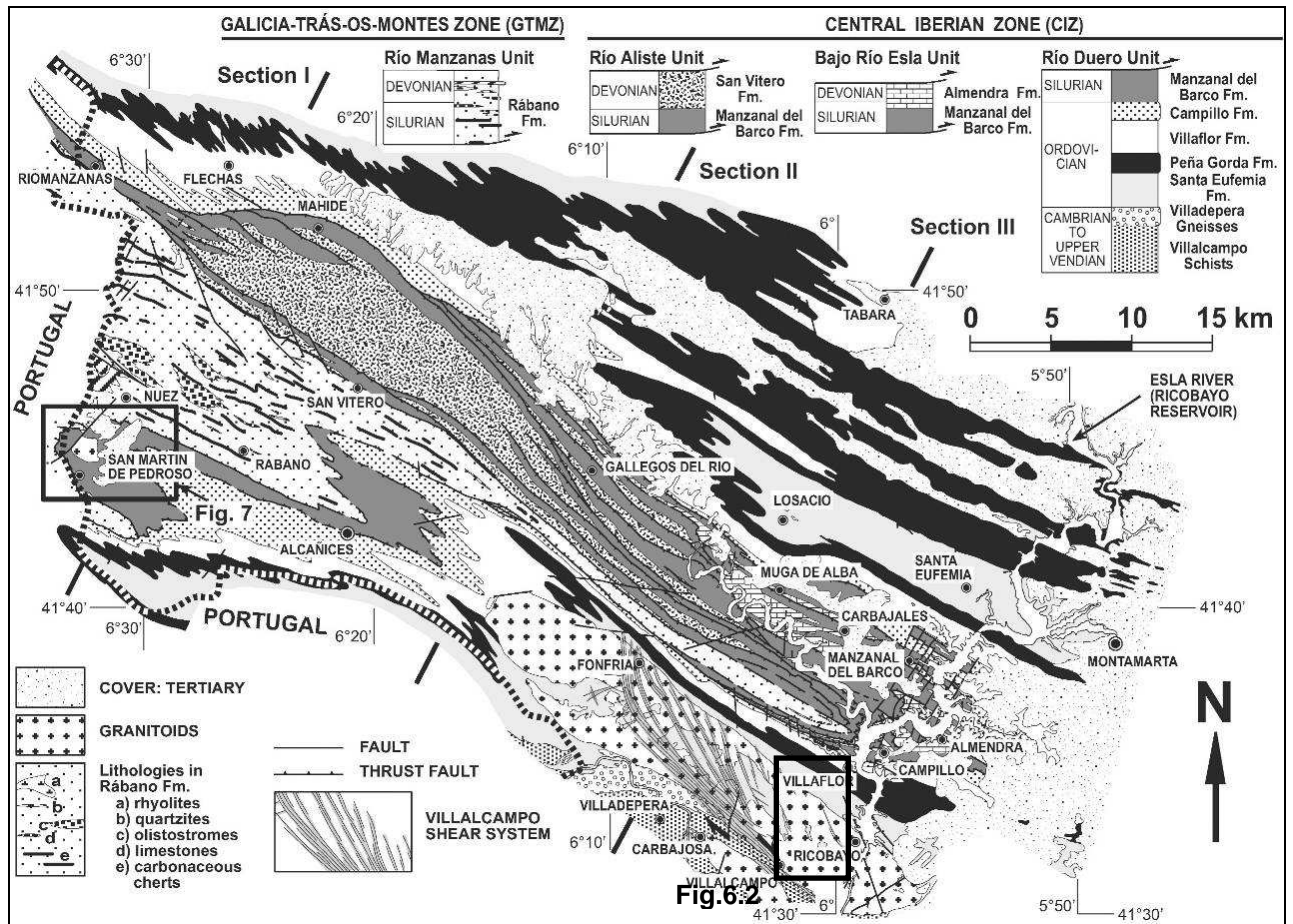


Fig.6 1: Geological map of the Alañines synform with its stratigraphic formations. The study area is located in the southeast of the synform within the syntectonic Ricobayo Granite. For lithologies within the study area see Fig.6.2 (after González Clavijo & Martínez Catalán, 2002).

## 6 Geologic conditions

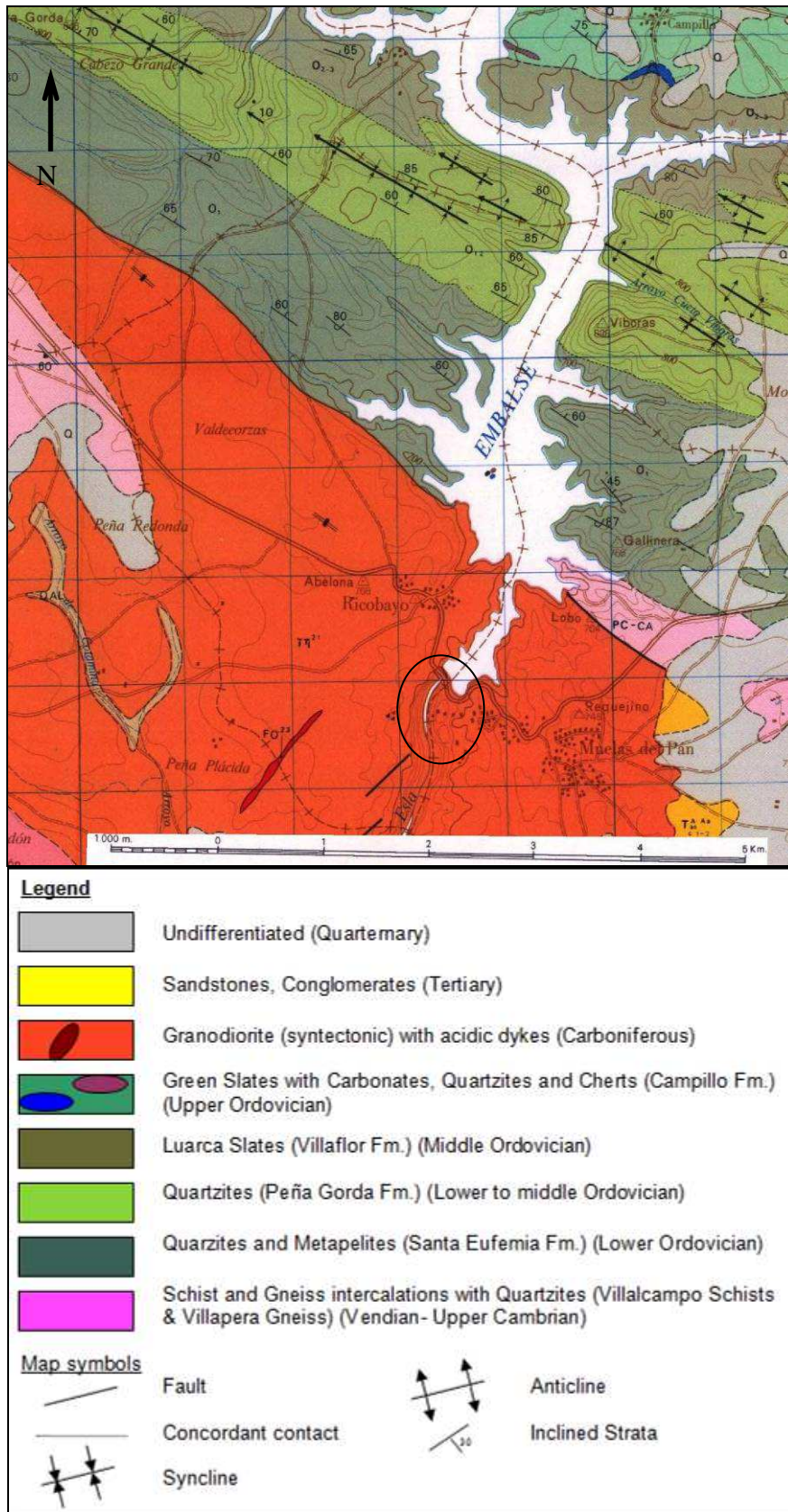


Fig.6 2: Geologic map of the region around the Ricobayo Reservoir. Black circle indicates study area (after IGME, 1978)

### 6.2 Site conditions

#### 6.2.1 Methods and description standards

The field work included a characterization of the geology on site using equipment to gain the needed data for further analysis. The following equipment was used in the field: A geologic compass, profile gauges, hammer, knife, measuring tape, look up charts for rock mass properties at a scanline survey (Roughness, strength, spacing,...), pencil, topographic maps, camera, photogrammetric methods (ShapeMetrix<sup>3D</sup>).

One focus was to gather information about the joint system of the investigated site to use it for a block theory analysis (Chap.7). Dip direction and dip were measured using a Breithaupt compass (Fig.6.3). The data gathered on site include field mapping of morphological units and surface features, measurements of rock mass properties (Joint orientation, roughness, spacing, weathering) and historical records from the archives of Ricobayo (Plans, cross sections, reports).

#### Definitions of the most important terms

For the evaluation of on site conditions the following guidelines were used. Definitions of the most important terminological terms are given below. All descriptions of the rock mass made in the field were done according to the ISRM (1981) suggestions and are described in this chapter.

#### Discontinuity

A collective term used for all structural breaks in geologic materials which usually have zero to low tensile strength. Discontinuities also may be healed. Discontinuities comprise fractures (including joints), planes of weakness, shears/faults, and shear/fault zones. Depositional or erosional contacts between various geologic units may be considered discontinuities (USB, 2001).

#### Fracture

A term used to describe any natural break in geologic material, excluding shears and shear zones (USB, 2001). An example for such a feature is a joint.

#### Joint

A fracture which is relatively planar along which there has been little or no obvious displacement parallel to the plane. In many cases, a slight amount of separation normal to the joint surface has occurred. A series of joints with similar orientation form a joint set. Joints may be open, healed, or filled; and surfaces may be striated due to minor movement.

Fractures which are parallel to bedding are termed bedding joints or bedding plane joints. Those fractures parallel to metamorphic foliation are called foliation joints (USBR, 2001).

Joints can be described by a number of parameters. The most important ones are defined below together with their classification charts according to this ISRM (1981).

### Orientation

Attitude of discontinuity in space. Described by the dip direction (azimuth; angle clockwise from North) and dip (angle below horizontal) of the line of steepest declination in the plane of the discontinuity. Example: (240/60) (Fig.6.3).

The line of steepest declination is called the true dip. Any cross section at an arbitrarily chosen angle to a discontinuity would give smaller angles (apparent dip). Strike is perpendicular to the dip direction.

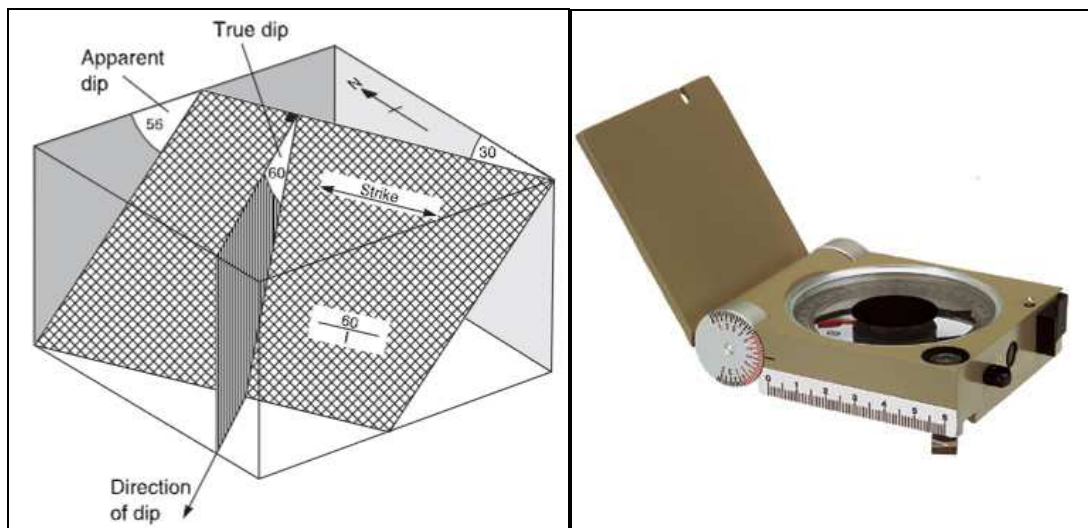


Fig.6 3: Orientation of a plane as obtained with a geologic compass (left). Orientation of the hatched plane can be expressed as 330/60 (Strike/Dip) or 240/60 (Dip direction/Dip) (after Bell, 2007). Picture of a COCLA Compass (right) (Breithaupt.de, 2012).

The cover of the compass is held against the plane of interest and adjusted until the compass is horizontally aligned (indicated by a bubble tube). The dip angle is read on the side at the hinge and the coloured values correspond to the needle of the compass where to read the azimuth. The azimuth can be read from the compass as soon as the needle is stopped by an automatic brake.

### Evaluation terms for discontinuity orientations

Fig.6.4 below illustrates the statistical features during discontinuity orientation analysis. Their explanation is also given below. Definitions are from Wallbrecher (1986).



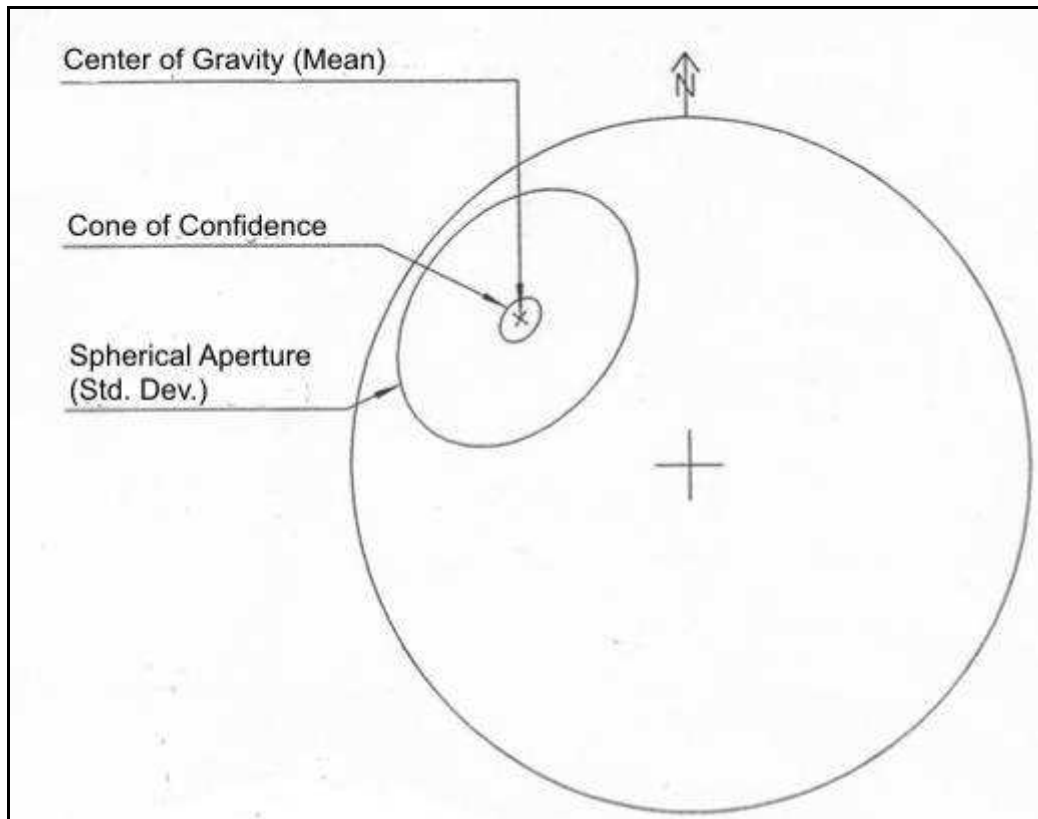


Fig.6 4: Illustration of terms used in discontinuity statistics (modified after Wallbrecher, 1986)

### Confidence

Chosen level of confidence for the probability that the statistical estimate (e.g. the calculated mean orientation, center of gravity) lies within certain angular range. Makes sense only when >90%.

### Percent Degree of Orientation

( $0 \leq R\% \leq 100$ ): Data concentration parameter derived from the sum vector divided by the number of data:  $R\% = R_{sn} \cdot 100$ ; the higher the value gets, the more parallel are the fabric elements.

### Parameter of Concentration

( $0 \leq k \leq \infty$ ): The relation of the data concentration density of the mode and the least concentration density ("anti-mode") on a sphere is an exponential function with the term "ek". Orientation statistics makes sense only with  $k > 4$  (better  $k > 6$ ) and with symmetrical normal distributions (circular or spherical).

### Cone of Confidence

Small circle, within which the estimate of the mean orientation is situated with a certain probability (see Confidence). Higher levels of confidence accordingly render larger cones of confidence. In cases that the cone of confidence reaches or exceeds the Spherical-Aperture (see below) further statistical considerations are meaningless.

### Spherical (circular) Aperture

Gives the angular range of a small circle (or great circle section) which would have the same concentration parameter (k) and the same eigenvalues as the actual sample, however with uniformly distributed data points. Depending on the value of k the area represents between 64 % and 69% of the data and hence can be understood as equivalent to the standard deviation (representing 68.27% of data within  $2\sigma$ ).

### Center of Gravity

The plane having the gravity vector S as pole (mean plane orientation).

### Cluster Distribution

Is always the case if a certain preferred orientation is recognized around which all the other fabric elements are distributed. Deviation can already occur due to measurement errors. The model this distribution is based on is the Spherical Normal Distribution, which is often referred to as Fisher Distribution after its inventor.

### **Spacing**

Spacing controls the size of blocks formed by discontinuities. It also influences the permeability of the rock mass. Spacing refers to the perpendicular distance between single discontinuities of the same set. If that is not possible it can be corrected by the following formula (Eq.6.1):

$$S = d_m \sin \alpha \quad (\text{Eq.6.1})$$

Where: S = spacing

$d_m$  = most common (modal) distance measured

$\alpha$  = smallest angle between measuring tape and discontinuity

The suggested terminology after ISRM (1981) is given below (Tab.6.1)

Description	Spacing
Extremely close spacing	< 20mm
Very close spacing	20- 60mm
Close spacing	60- 200mm
Moderate spacing	200- 600mm
Wide spacing	600- 2000mm
Very wide spacing	2000- 6000mm
Extremely wide spacing	> 6000mm

Tab.6 1: Spacing terminology (after ISRM, 1981)

**Persistence (continuity)**

Persistence describes the areal extend or size of a discontinuity. It is the rate between the jointed area to the total area of a plane (Fig.6.5). The shear strength along the discontinuity is dependent on the persistence. Intact rock has to be broken before displacement can take place if the discontinuity ends in intact rock. It is usually considered to be one dimensional. However it extends in two dimensions (Price & De Freitas, 2009).

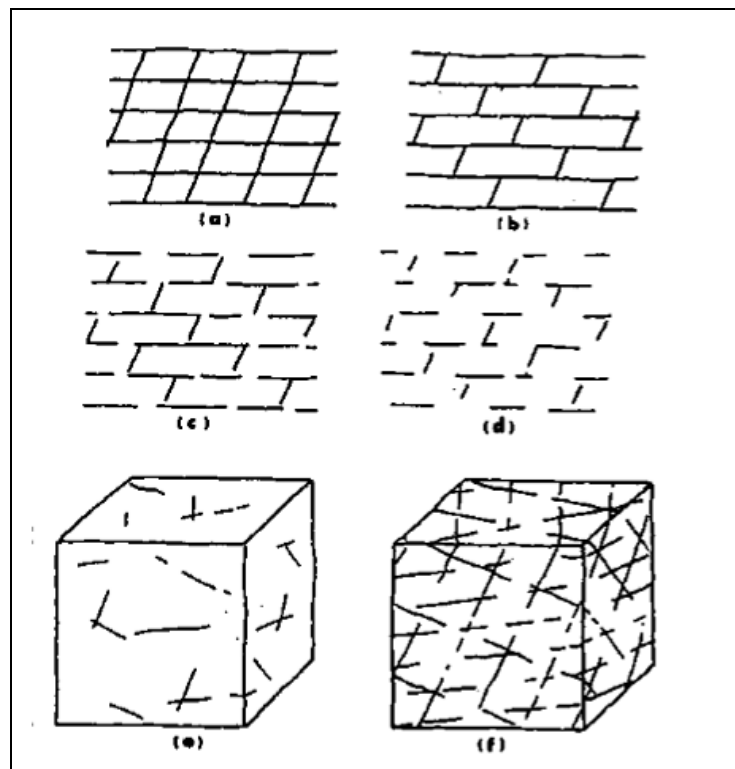


Fig.6 5: Block diagrams showing the concept of persistence. The Persistence (K) is the jointed part of a discontinuity traced over a certain distance. The intact rock parts between the jointed sections are called rock bridges. (ISRM, 1981)

Rather than giving a ratio of areas, which is usually impossible to obtain in the field length measurement of the discontinuity at an outcrop are performed (Tab.6.2).

Description	Persistence
Very low persistence	< 1m
Low persistence	1- 3m
Medium persistence	3- 10m
High persistence	10- 20m
Very high persistence	> 20m

Tab.6 2: Description of persistence (ISRM, 1981)

### Termination

This term is closely related to the persistence observations, since as the persistence is recorded the discontinuity has an end somewhere in the field. Three letters are used to describe the termination of a discontinuity: (D) indicates a termination in another discontinuity, (R) the termination within the intact rock and (X) is used if the end of the discontinuity is not visible and hence unknown.

The so called Termination Index ( $T_r$ ) is used to describe the percentage of discontinuities ending in rock (Eq.6.2).

$$T_r (\%) = \frac{(\sum R) \cdot 100}{2 \cdot (\text{no. of discontinuities observed})} \quad (\text{Eq.6.2})$$

This formula is used if both ends of a discontinuity are known. In cases where only the upper or lower termination is determined (semi trace length) the “2” in the formula is removed. The smaller the value of  $T_r$  is, the more blocky the rock mass tends to be. It is an index for permeability and strength of the rock mass.

### Roughness

The surface conditions have great influence the shear strength, especially where joints are unfilled. Roughness can be described as waviness or unevenness (asperities), which are scale dependant. Waviness describes large-scale undulations, which, if interlocked and in contact, cause dilation during shear displacement since they are too large to be sheared off. Unevenness or asperities describe small-scale roughness that can be sheared off (Wyllie & Mah, 2004).

Assessment of roughness can be done by linear profiling of a plane, a compass and disc clinometer or the profile gouge (Fig.6.6). For the measurement of the roughness at Ricobayo the Profile gauge was used assigning JRC values to the measures profiles (Fig.6.7).

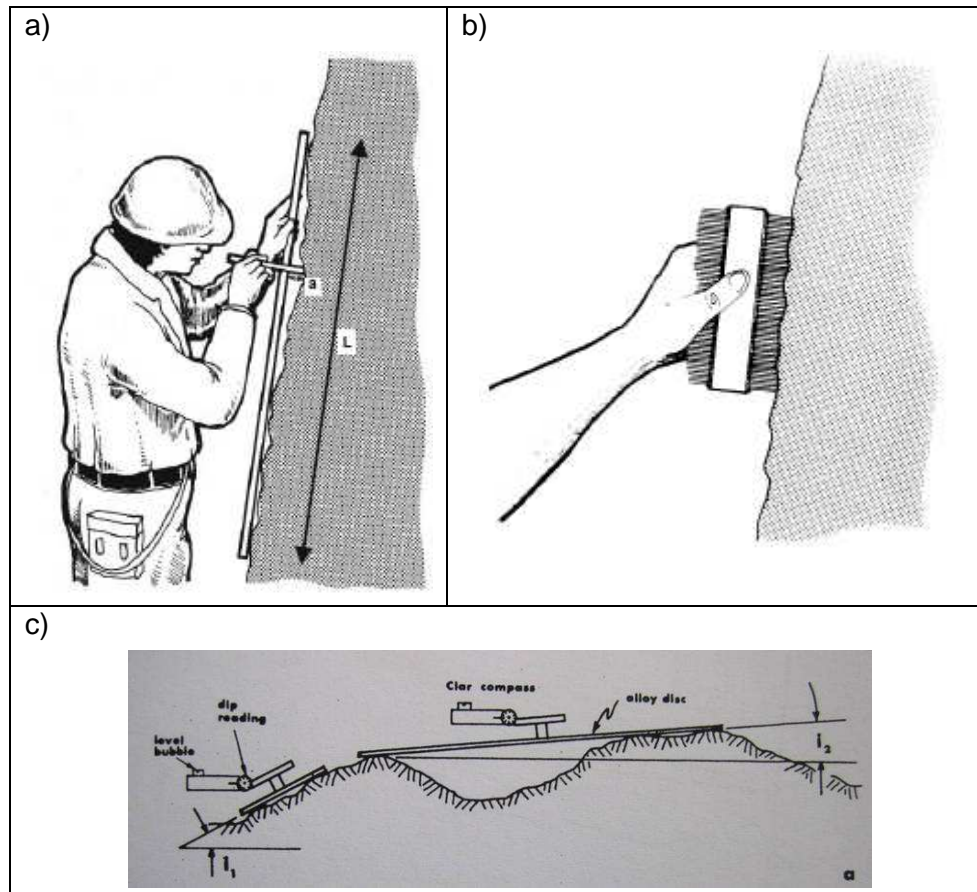


Fig.6 6: Assessment techniques for measuring roughness. a) Linear profiling of waviness ( $a$  = maximum amplitude,  $L$  = length of joint surface) (after Milne et al., 1992). b) Profile gauge. One side is pressed against the discontinuity plane and the pattern of the gauge is compared to the JRC chart (Fig.6.8) (after Milne et al., 1992). c) Compass and disc clinometer.

Barton (1978) suggested some descriptive terms to be used where the above mentioned methods are not applicable or a quick interpretation is made. It is based upon two scales of observations. Small scale (several centimetres) including rough, smooth, slickensided, and larger scale (several meters) including stepped, undulating, planar. The smaller scale features are imposed on the larger ones (Fig.6.8).

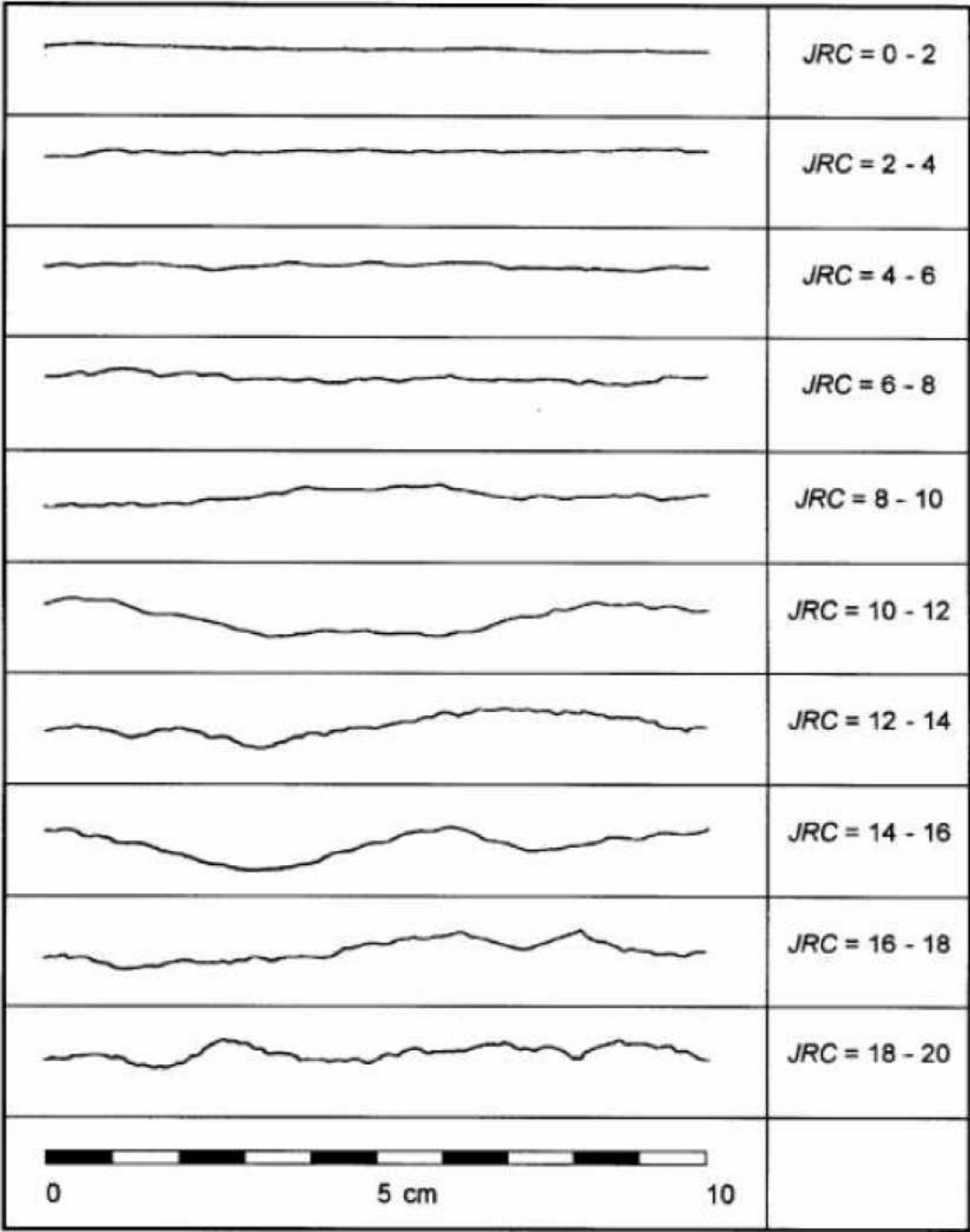


Fig.6 7: Roughness profiles and corresponding range of JRC values associated with each one (ISRM, 1981)

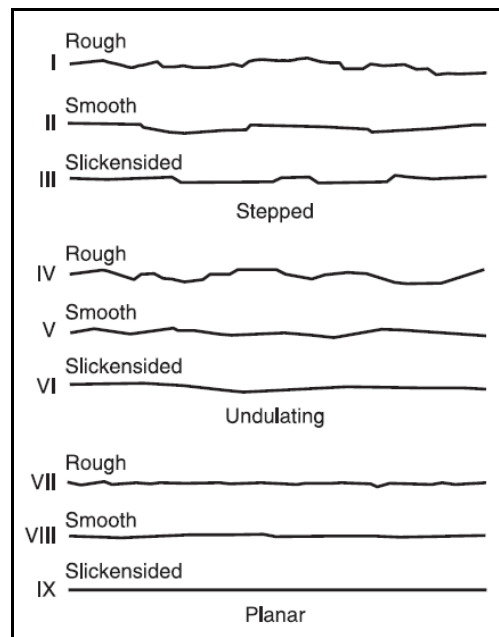


Fig.6 8: Typical roughness profiles and suggested nomenclature. The length of each profile is in the range 1-10m. The vertical and horizontal scales are equal (after Barton, 1978)

## Wall Strength

Rocks at the surface are exposed to alteration processes resulting in weathering of the rock. Weathering may occur due to meteoric waters, hydrothermal waters or other, mostly acidic fluids resulting in decomposition (transformation of components and discoloration). Mechanical effects on the rock lead to disintegration (grain by grain separation). Discontinuities are in general stronger affected by these processes than the interior of the rock. Climatic conditions are the controlling factor on the rate and type of weathering. The ISRM provides two charts for the description of weathering for rock masses and rock material, respectively (Tab.6.3 &6.4).

## 6 Geologic conditions

Term	Description	Grade
Fresh	No visible sign of rock material weathering; perhaps slight discoloration on major discontinuity surfaces.	I
Slightly weathered	Discoloration indicates weathering of rock material and discontinuity surfaces. All the rock material may be discolored by weathering and may be somewhat weaker externally than in its fresh condition.	II
Moderately weathered	Less than half of the rock material is decomposed and/or disintegrated to a soil. Fresh or discolored rock is present either as a continuous framework or as corestones.	III
Highly weathered	More than half of the rock material is decomposed and/or disintegrated to a soil. Fresh or discolored rock is present either as a discontinuous framework or as corestones.	IV
Completely weathered	All rock material is decomposed and/or disintegrated to soil. The original mass structure is still largely intact.	V
Residual soil	All rock material is converted to soil. The mass structure and material fabric are destroyed. There is a large change in volume, but the soil has not been significantly transported.	VI

Tab.6 3: Chart for the weathering classification of rock masses (ISRM, 1981).

Term	Description
Fresh	No visible sign of weathering of the rock material
Discolored	The color of the original fresh rock material is changed. The degree of change from the original color should be indicated. If the color change is confined to particular mineral constituents this should be mentioned.
Decomposed	The rock is weathered to the condition of a soil in which the original material fabric is still intact, but some or all of the material grains are decomposed.
Disintegrated	The rock is weathered to the condition of a soil in which the original material fabric is still intact. The rock may be friable, but the material grains are not decomposed.

Tab.6 4: Chart for the weathering description of rock material (ISRM, 1981).

To estimate the strength of the rock walls or soils the manual index test can be used. It can be estimated by the use of a geological hammer, a knife or the thumb depending on the weathering conditions of the rock (Tab.6.5).



## 6 Geologic conditions

Grade	Description	Field identification	Approx. range of UCS (MPa)
S1	Very soft clay	Easily penetrated several inches by fist.	<0.025
S2	Soft clay	Easily penetrated several inches by thumb	0.025- 0.05
S3	Firm clay	Can be penetrated several inches by thumb with moderate effort.	0.05–0.1
S4	Stiff clay	Readily indented by thumb but penetrated only with great effort..	0.1–0.25
S5	Very stiff clay	Readily indented by thumbnail,	0.25–0.5
S6	Hard clay	Indented with difficulty by thumbnail	>0.5
R0	Extremely weak rock	Indented by thumbnail	0.25–1
R1	Very weak rock	Crumbles under firm blows with point of geological hammer; can be peeled by a pocket knife.	1–5
R2	Weak rock	Can be peeled with a pocket knife; shallow indentations made by firm blow with point of geological hammer.	5–25
R3	Medium strong rock	Cannot be scraped or peeled with a pocket knife; specimen can be fractured with single firm blow of geological hammer.	25–50
R4	Strong rock	Specimen requires more than one blow with a geological hammer to fracture it.	50–100
R5	Very strong rock	Specimen requires many blows of geological hammer to fracture it.	100–250
R6	Extremely strong rock	Specimen can only be chipped with geological hammer.	> 250

Tab.6 5: Chart for the description of the strength of weathered material. S1 – S6 are applied to cohesive soils, R0 – R6 are applied to rock (ISRM, 1981).

## Aperture and Filling

Aperture is the perpendicular distance separating the adjacent rock walls of an open discontinuity, in which the intervening space is air or water filled. If the discontinuity is filled with other materials such as clays it is referred to as width of the filled discontinuity (Fig.6.9). Apertures may result from outwash of material, displacement along discontinuities or opening due to stress relief. The extent of the aperture is determined by direct measurements with a tape or feeler gauge. The classification of aperture is shown below (Tab.6.6).

Aperture	Description	
< 0.1mm	Very tight	"closed" features
0.1 – 0.25mm	Tight	
0.25 – 0.5mm	Partly open	
0.5 – 2.5mm	Open	"gapped" features
2.5 – 10mm	Moderately wide	
> 10mm	Wide	
1 – 10cm	Very wide	"open" features
10 – 100cm	Extremely wide	
> 1m	Cavernous	

Tab.6 6: Chart for the classification of aperture (ISRM, 1981).

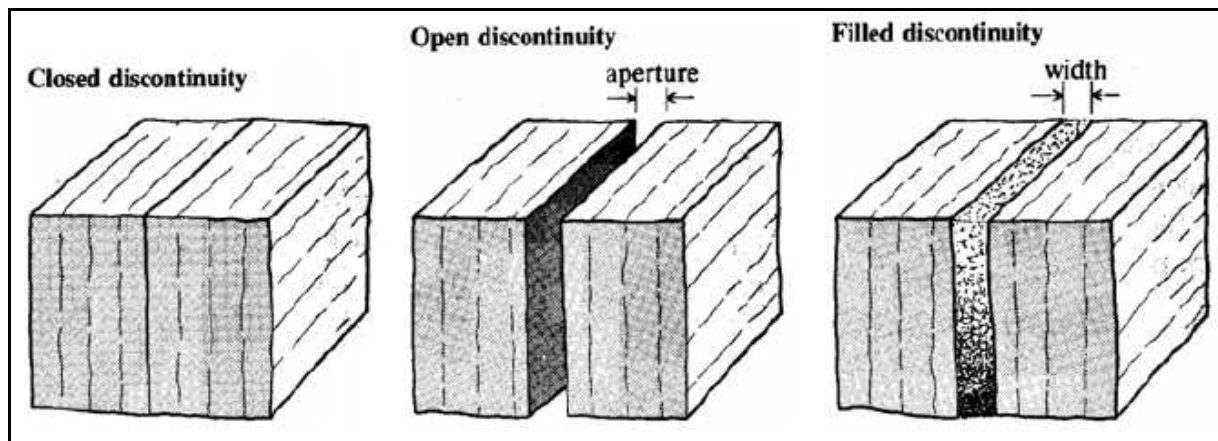


Fig.6 9: The terminology for discontinuity openings. Closed discontinuity (left), without filling (Aperture of open discontinuity; middle) and with filling (Width of filled discontinuity; right) (after ISRM, 1981).

Filling comprises many features that should be described in a quantitative manner. The most important factors are: Mineralogy of the filling material, grain size, water content and permeability, width and fracturing of wall rock. Also the weathering classification mentioned above can be applied to filling material.

### Seepage

Water flow can occur at discontinuities that act as a conduit. The assessment of water flow and seepage at an investigation site is mostly done by visual inspection in the field and hydrological records.

### Number of sets

The number of sets of discontinuities controls the mechanical behaviour and appearance of the rock mass (Fig.6.10). Their intersection, spacing and persistence form the shape and size of resulting blocks. The recognition of sets will occur simultaneously with the orientation measurements and are identified by plotting on equal area nets (see further above). The labelling of the sets can be according to their dominance. For example the most systematic set can be labelled as Set No. 1.

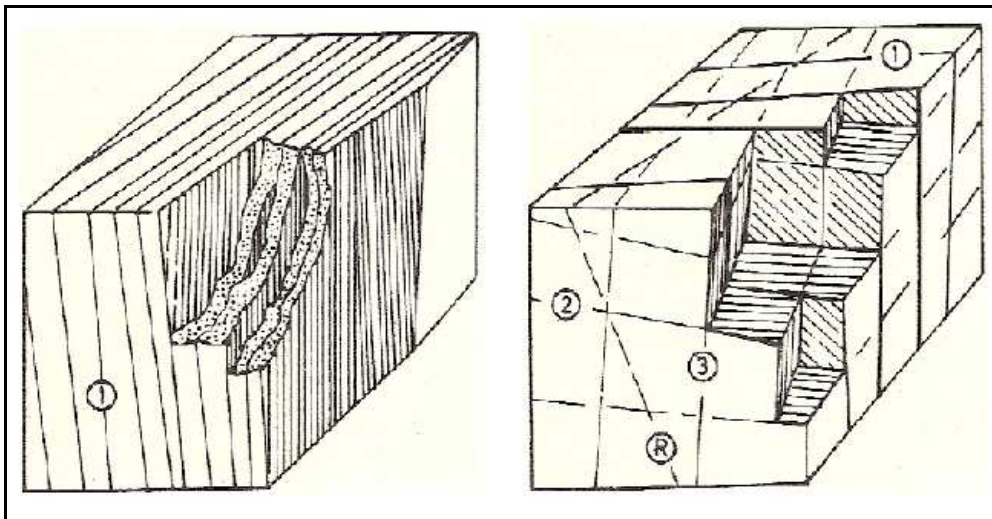


Fig.6 10: -Example that demonstrates the effect of the number of joint sets on the mechanical behaviour and appearance of a rock mass. One set (left) and three systematic sets and one random set (R) (right) (ISRM, 1981).

### Block size

The block size and their shape is controlled by the joint patterns on site. The resulting shapes may vary from cubic to rhomboidal or sheet like, although a regular geometry is seldom, since the sets are not always consistently parallel. In general, rock masses comprising big blocks tend to be less deformable. A way to describe the block size is the volumetric joint count ( $J_v$ ) (Eq.4.3). It is the number of joints intersecting a unit rock mass. As an impression for the size of the blocks, the  $J_v$  gives the following values (Tab.6.7).

## 6 Geologic conditions

Description	$J_v$ (Joints/m <sup>3</sup> )
Very large blocks	< 1.0
Large blocks	1 – 3
Medium-sized blocks	3 – 10
Small blocks	10 – 30
Very small blocks	> 30
Crushed rock (clay free)	> 60

Tab.6 7: Table showing the  $J_v$  and related block sizes (ISRM, 1981).

Rock masses can be described by a series of adjectives to give an impression of block size and shape (Tab.6.8). Examples for them are shown in Fig.6.11.

Adjective	Description
Massive	few joints or very wide spacing
Blocky	approximately equidimensional
Tabular	one dimension considerably smaller than the other two
Columnar	one dimension considerably larger than the other two
Irregular	wide variations of block size and shape
Crushed	heavily jointed to “sugar cube”

Tab.6 8: adjective terms used to describe the appearance of a rock mass (ISRM, 1981).

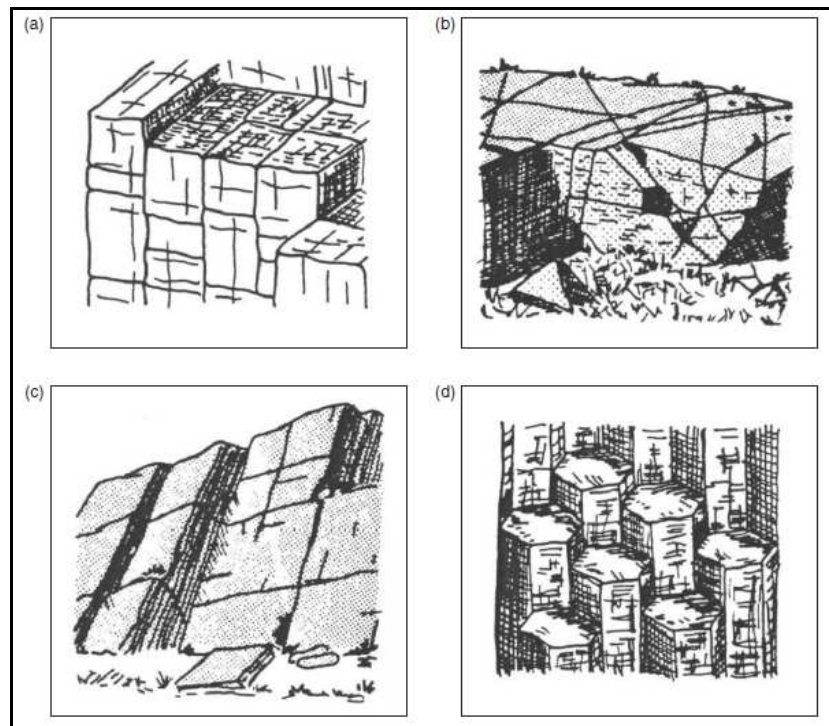


Fig.6 11: Sketch of rock masses illustrating (a) blocky, (b) irregular, (c) tabular and (d) columnar rock masses (ISRM, 1981).

### 6.2.2 Observations and Findings

#### General information

The investigated area includes outcrops on the left and right side of the river Esla, where the plunge pool and the spillway are located. Most of the data collected were sampled along road cuts within the Ricobayo Dam area, but also in underground excavations such as the tunnel below the spillway or the tunnel leading to the power station of Ricobayo I.

#### Surface features

The area studied site is characterized by a massive granodioritic rock mass that is incised by the Esla river. Vegetation is scarce with mostly grassy or bushy cover. Also surface water occurs, except for the river itself only on a few spots along major joints.

Additionally to the major lineaments, surface features have been mapped and are shown in Fig.6.12. Large amounts of fill from the construction were dumped on the area between the spillway and the river Esla to create even surfaces for the high voltage facilities (Fig.6.13). Also adjacent to the east of the plunge pool, a huge fill deposit was encountered, that extended from the river up to the street leading to the hydraulic laboratory (Fig.6.14). Parallel to the Spillway channel, the original cut slope from the construction in the 1930s can still be recognized in the field (Fig.6.15). The spillway channel is now shifted about 10 to 15m away from the cut slope and stabilized by a concrete wall. The difference in elevation as it is now is the result of the final scour stage when the edge of the spillway collapsed and was reshaped in more curved fashion.

## 6 Geologic conditions

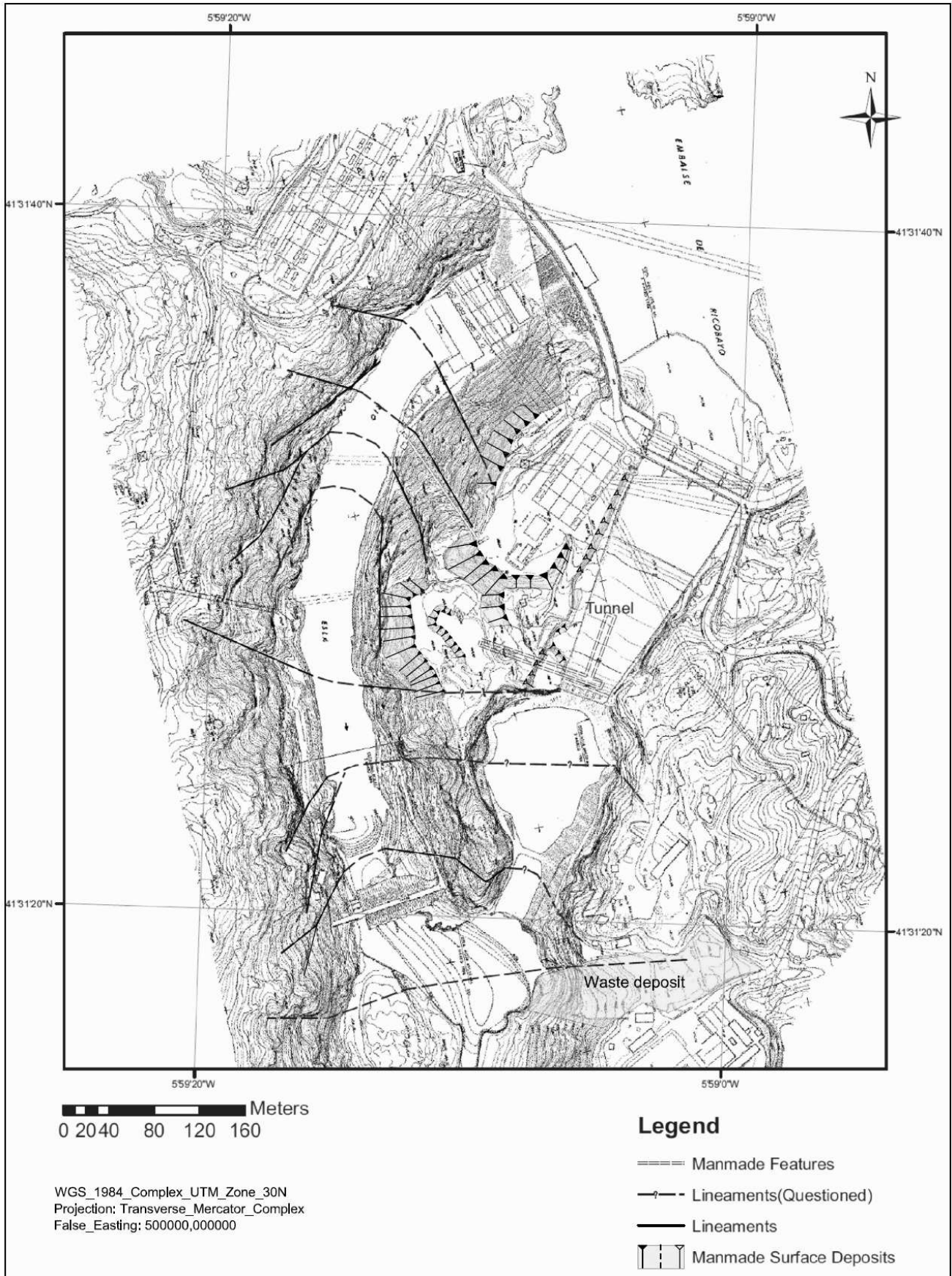


Fig.6 12: Topographic map of the Ricobayo Dam site indicating the most important lineaments and some mapped surface deposits (Topographic map by Iberduero S.A., 1984).



Fig.6 13: View to the area between the spillway and the river. The finer material dumped down on the left side of the picture forms fill deposits (arrows) for creating construction space. Location of the deposits is illustrated in Fig.6.12 above.

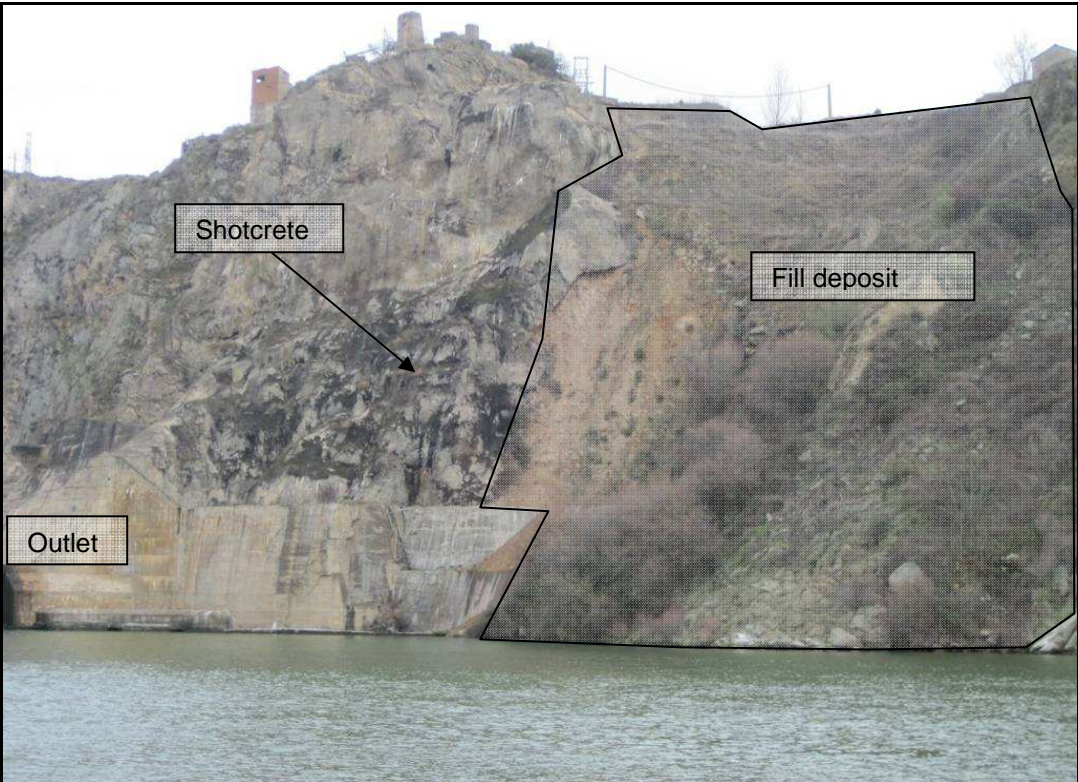


Fig.6 14: View to the fill deposit right at the end of the outlet of the plunge pool. Some raveling occurred where the shotcrete failed.



Fig.6 15: View to the right side of the spillway. End of the upper channel. The old wall is still visible in the back and was shifted towards the center of the spillway (left). Cut slope adjacent to the concrete wall of the spillway

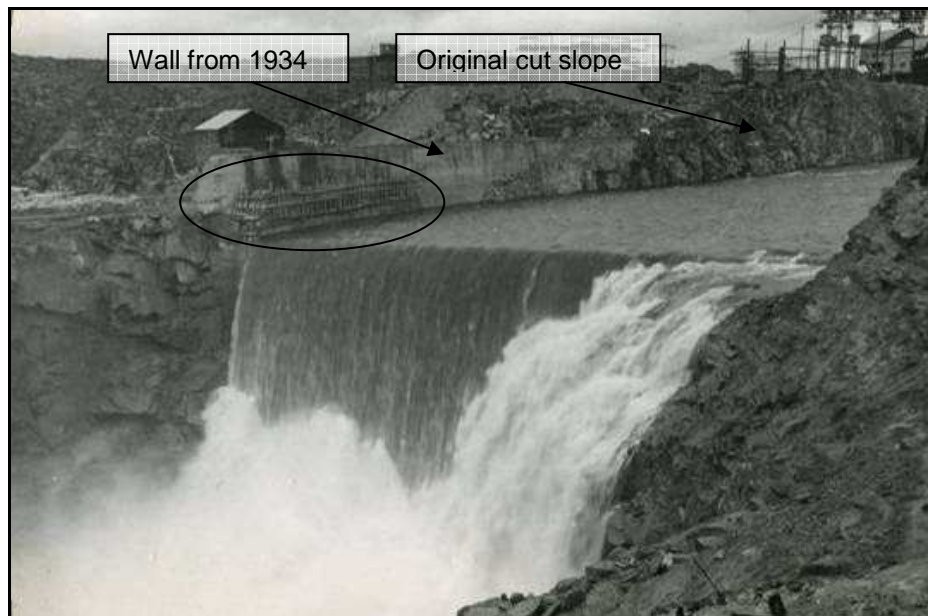


Fig.6 16: The original spillway from 1934. Note the slight curvature at the tip of the right wall to prevent the overtopping water to erode the right wall of the plunge pool (circle).

Some blocks exposed at the surface show spheroidal weathering features, which results in rounding of edges and corners. Also the upper few meters of the rock are subject to weathering and show therefore signs of strong discoloration due to iron oxide formation and disintegration. Single blocks are split in half (Fig.6.17). Some blocks are already isolated and, others are still in assemblage with the surrounding blocks showing initiations of spherical weathering where water can access the rock via joints.



## 6 Geologic conditions



Fig.6 17: Isolated blocks cropping out on the surface of the Ricobayo granodiorite. Both blocks shown above are weathered into a spheroidal shape. The block on the right is broken in half.

### Composition and Fabric

The entire site of Ricobayo Dam is situated within a granitic Intrusive body. It is composed of mainly granodiorite (Fig.6.18), which consists of Plagioclase, Potash feldspar, Quartz and two types of micas- Biotite and Muskovite. The Plagioclase is present in the rock as the Nar-rich variety Oligoclase (Iberduero, 1986).

Accessory minerals such as Apatite, Tourmaline and Zircon are present in the rock too. The texture of the rock is holocrystalline with hypidiomorphic crystals. The grain size is not uniform within the granodiorite and varies from medium (1- 5mm) to coarse grained (>5mm). The fabric of the rock appears to be massive with no major recognizable foliation. The fresh rock shows a light gray color with some red discolorations on the surface (Fig.6.19).

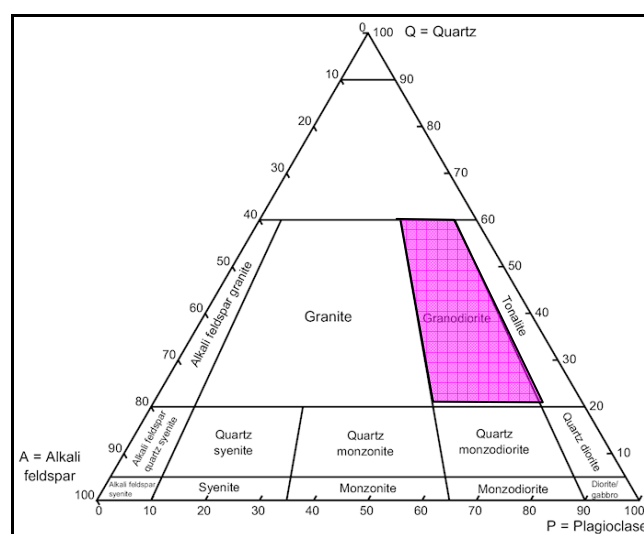


Fig.6 18: IUGS classification diagram for plutonic rocks. The highlighted field represents the rock type found at Ricobayo (after Streckeisen, 1973).



Fig.6 19: Outcrop of the granodiorite of Ricobayo with iron oxide altered surfaces(arrow) (left). Hand specimen of the granodiorite (right). The rock is mostly composed of Quartz (grey) and Plagioclase (white), Potash feldspar (reddish) and Biotite (black). 2€ coin for scale.

### Intact Rock properties

According to the geotechnical report for the Ricobayo II Powerhouse the rock at Ricobayo has an uniaxial compressive strength (UCS) between 77 MPa (789 kg/cm<sup>2</sup>) and 125 MPa (1280 kg/cm<sup>2</sup>) with a most frequently measured value of 98 MPa (1000 kg/cm<sup>2</sup>). The medium density is 2.62 t/m<sup>3</sup>.

### Rock mass characteristics

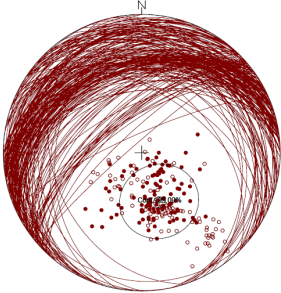
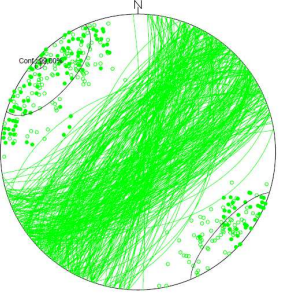
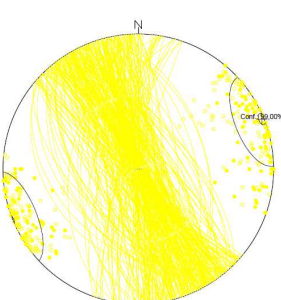
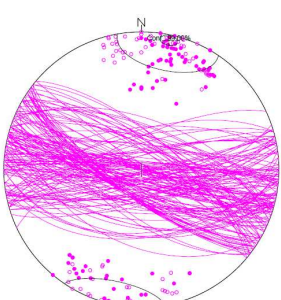
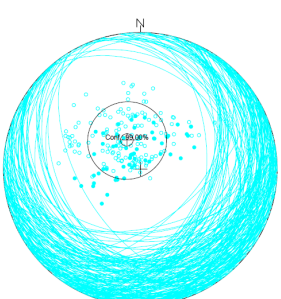
Many of the rock mass parameters were collected with a scanline survey and at selected outcrops. The results of those parameters will be shown in this section. Classifications after ISRM (1981) (see further above).

### Joint Properties

The Ricobayo granodiorite in this area is characterized by strong and intense jointing resulting in the formation of joint bound blocks with a few cubic meters in volume. The joint orientations and properties were measured at different locations at the Ricobayo dam site. In the following sections a general description of the rock mass will be provided together with some selected outcrops.

### Joint orientations

In total 516 joint orientations were measured in the field and additionally 688 measurements were performed using ShapeMetrix<sup>3D</sup>. The orientations were plotted in Sphaira and are shown in Tab. 6.9. The data are compiled from own measurements together with those from Rocha (2012). The joint sets encountered on site are characterized by 5 systematic joint sets that occur quite consistently within the entire site. The joint sets comprise two medium steep, approx. N to NW and S to SE dipping sets, which are represented as joint set 1 and joint set 5, respectively. The other three sets are sub vertical to almost vertical inclined striking NE-SW (Joint set 2), NW- SE (Joint set 3) and approx. E- W (Joint set 4). Joint set one is the most dominant set as it can be seen on map scale. The mapped lineaments are mostly assigned to joint set one (Fig. 6.20). From crosscutting relations joint set 1 is considered to be the youngest joint system.

 <p>Joint Set 1</p>	Amount of Data	212
	Confidence Limit	99,00%
	Percent degree of orientation	85,21%
	Parameter of concentration	13,46
	Cone of confidence	3,40°
	Spherical Aperture	22,61°
	Center of gravity	340,36° / 31,21°
 <p>Joint Set 2</p>	Amount of Data	324
	Confidence Limit	99,00%
	Percent degree of orientation	81,25
	Parameter of concentration	10,66
	Cone of confidence	3,21°
	Spherical Aperture	25,62°
	Center of gravity	132,29° / 85,11°
 <p>Joint Set 3</p>	Amount of Data	315
	Confidence Limit	99,00%
	Percent degree of orientation	87,34%
	Parameter of concentration	15,752
	Cone of confidence	2,56°
	Spherical Aperture	20,84°
	Center of gravity	247,96° / 88,24°
 <p>Joint Set 4</p>	Amount of Data	162
	Confidence Limit	99,00%
	Percent degree of orientation	85,37°
	Parameter of concentration	13,59
	Cone of confidence	3,88°
	Spherical Aperture	22,48°
	Center of gravity	192,00° / 85,46
 <p>Joint Set 5</p>	Amount of Data	191
	Confidence Limit	99,00%
	Percent degree of orientation	84,25°
	Parameter of concentration	12,63
	Cone of confidence	3,71°
	Spherical Aperture	23,38
	Center of gravity	155,36° / 19,14°

Tab.6 9: Joint orientation statistics for the Ricobayo Dam site. Full circles are compass measurements, empty circles are measurements obtained by ShapeMetrix<sup>3D</sup>.



Fig.6 20: View to the right riverbank downstream of the dam, showing the appearance of the rock mass at the Ricobayo dam. Joint patterns of the five joint sets are illustrated. Numbers and colors correspond to the joint orientations in Tab.6.9.

### Joint Spacing

The joint spacing histograms are shown below for all sets together and for each set separately (Fig.6.21a-e). Only joint set one does not appear on this diagrams as it was encountered only once in the scanline survey. The data show that most of the spacing lies in the range of 0.2 to 2m with some up to 6m. The true spacing was determined from the scanline survey using Eq.6.1. Also the variation within the sets is not very strong implying that the resulting blocks formed by approximately equal spacing will be equidimensional (Tab.6.10). This is indeed confirmed by the general appearance of the rock mass on site, where blocky rocks are present (Fig.6.22).

	<b>Joint set 2</b>	<b>Joint set 3</b>	<b>Joint set 4</b>	<b>Joint set 5</b>
Mean (m)	0.7	0.3	0.7	0.8
Std. dev. (m)	0.4	0.2	0.5	0.2

Tab.6 10: Mean and standard deviation for the joint set spacings measured at the scanline.

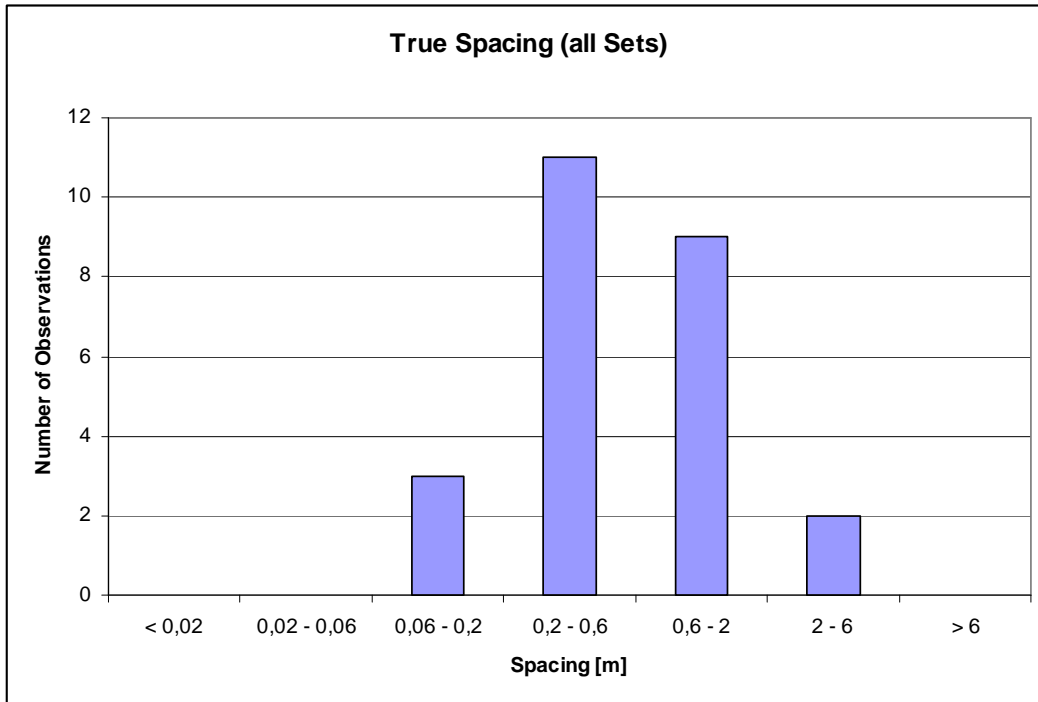


Fig.6.21a: True spacing for all sets

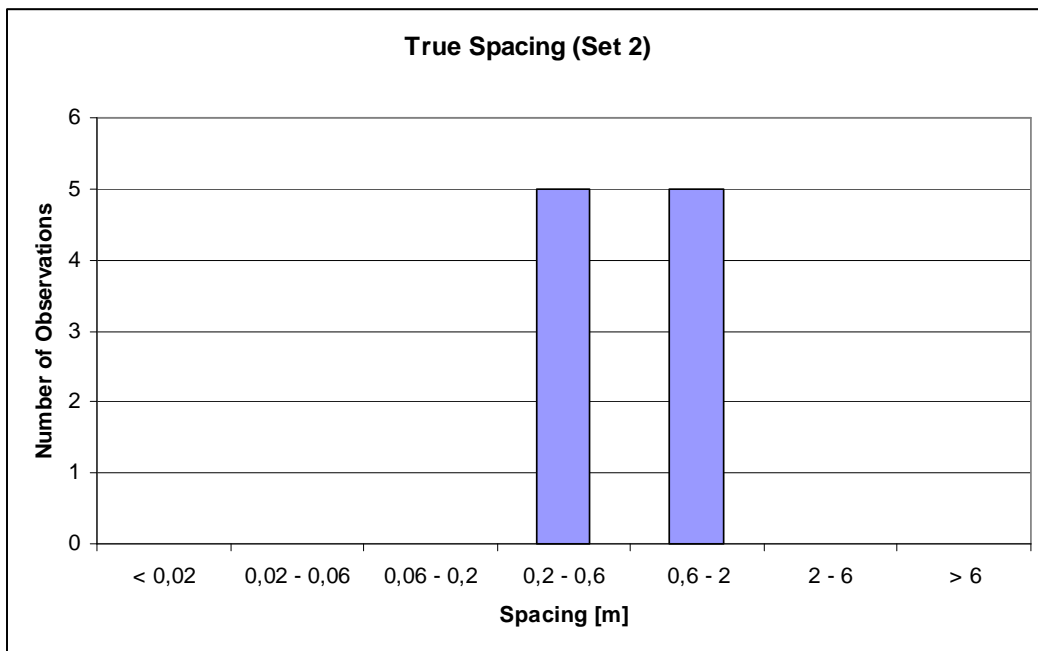


Fig.6.21b: True spacing for set 2

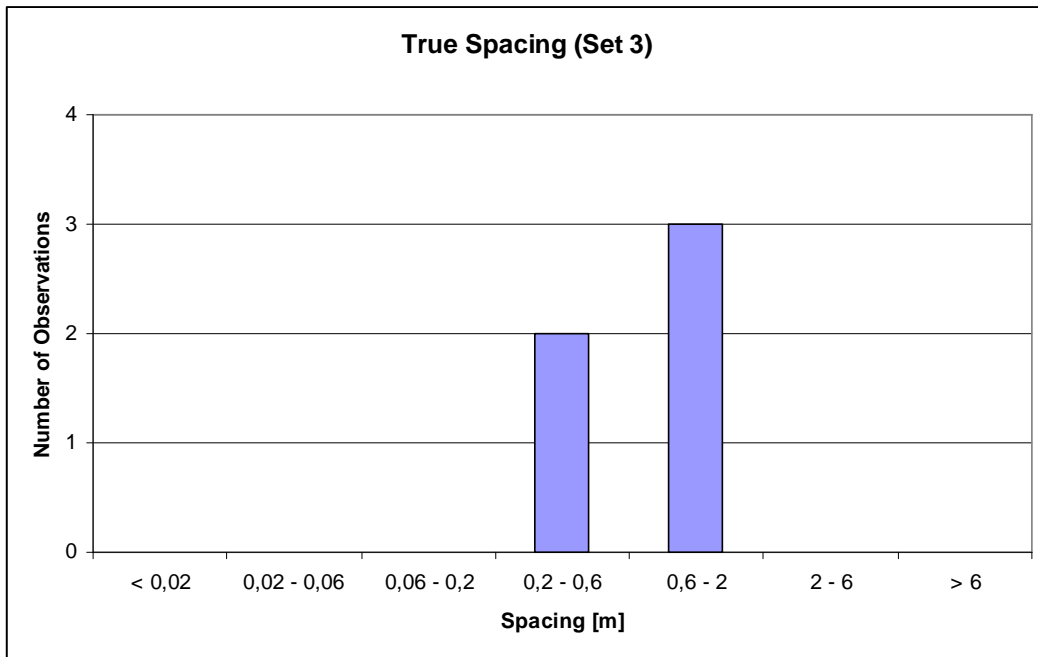


Fig.6.21c: True spacing for set 3

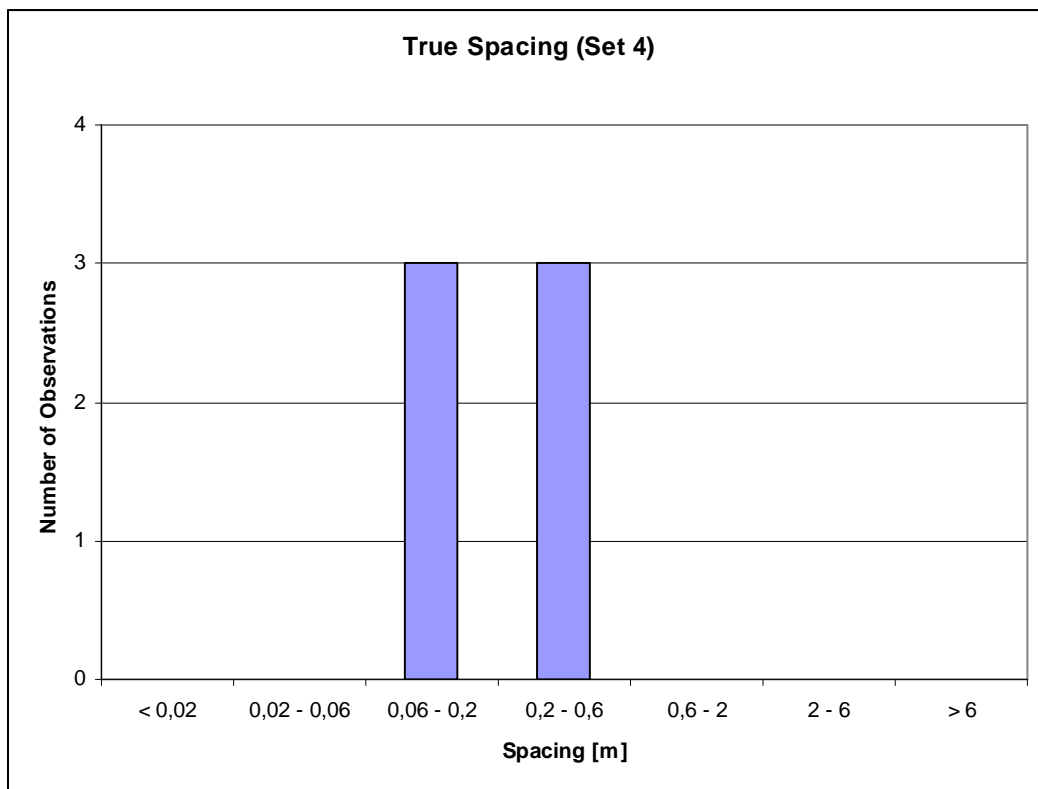


Fig.6.21d: True spacing for set 4

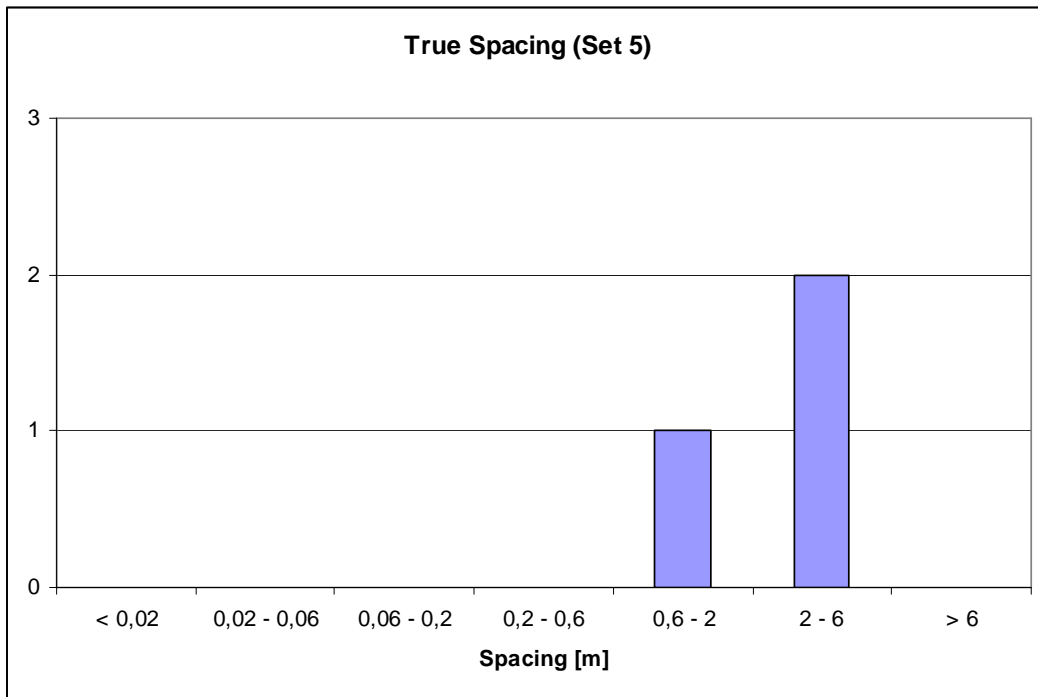


Fig.6.21e: True spacing for set 5



Fig.6 22: Outcrop at the left side of the river. Intense jointing of the rock resulting in the formation of blocks. Spacing (arrows) is well visible in this picture. Lines indicate joint set 5. Person for scale in front.



### Persistence

The outcrop situation also allowed only measurements or estimates, respectively, of the persistence in the apparent dip direction, but not along strike. The persistence at the scanline was considered as not representative, due to its small scale and is therefore estimated by observations on a larger scale. (Fig.6.23). Although those areas had bad accessibility to directly measure the trace length, it could be estimated that the persistence was high to very high, in some cases over 100m. The observations of the persistence were combined with recording the type termination (Fig.6.24). The Termination Index ( $T_r$ ) is estimated from these observations to get an impression of blockiness of the rock mass.



Fig.6 23: Outcrop situation at Ricobayo. Scanline along road cut (left). Estimates of the true persistence are difficult in this case. Large area of exposed rock along the river Esla right downstream of the dam (right). Some joints may be traced for more than 10 to 20m.

The observation of the termination of joints revealed that most of the joints terminated in another joint (see Fig.6.23 above). The terminations are shown in Fig.6.24.

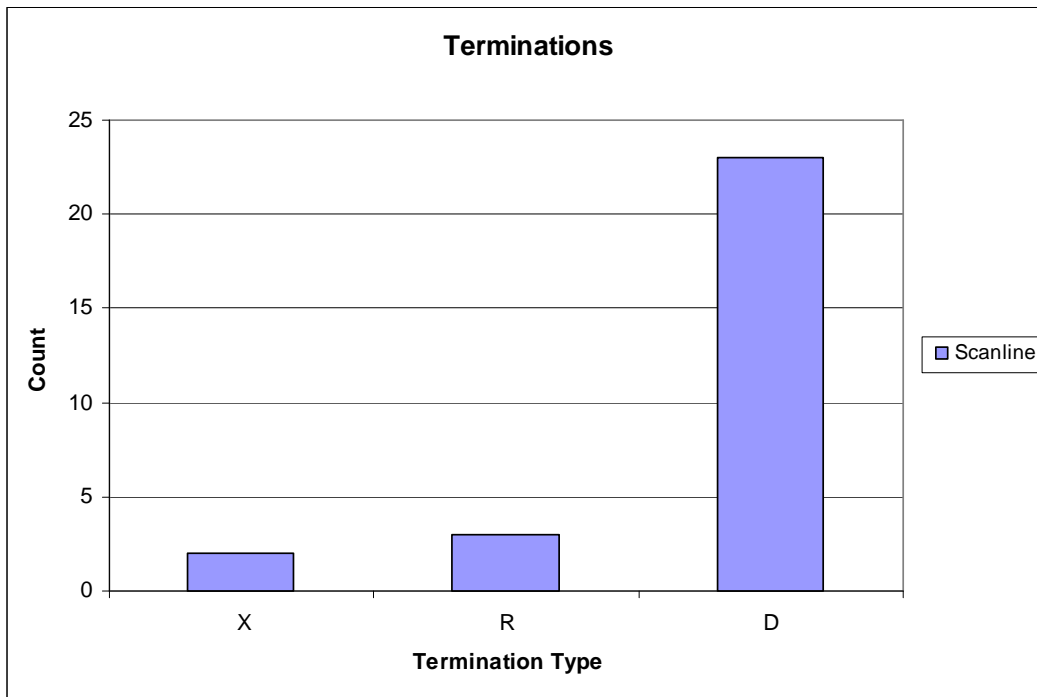


Fig.6 24: Terminations as they were observed during the scanline survey (28 observations). X = unknown/not visible, R = rock, D = discontinuity

The Termination Index ( $T_r$ ) calculated from those data applying Eq.6.4 modified for semi trace length yielded an  $T_r$  of 10.7%.

### Roughness

The roughness profiles were measured with a profile gauge and assigned to the JRC chart. All sets together show a wide range of roughness profiles with dominance of 4 to 10 on the JRC chart (Fig.6.25a- f).

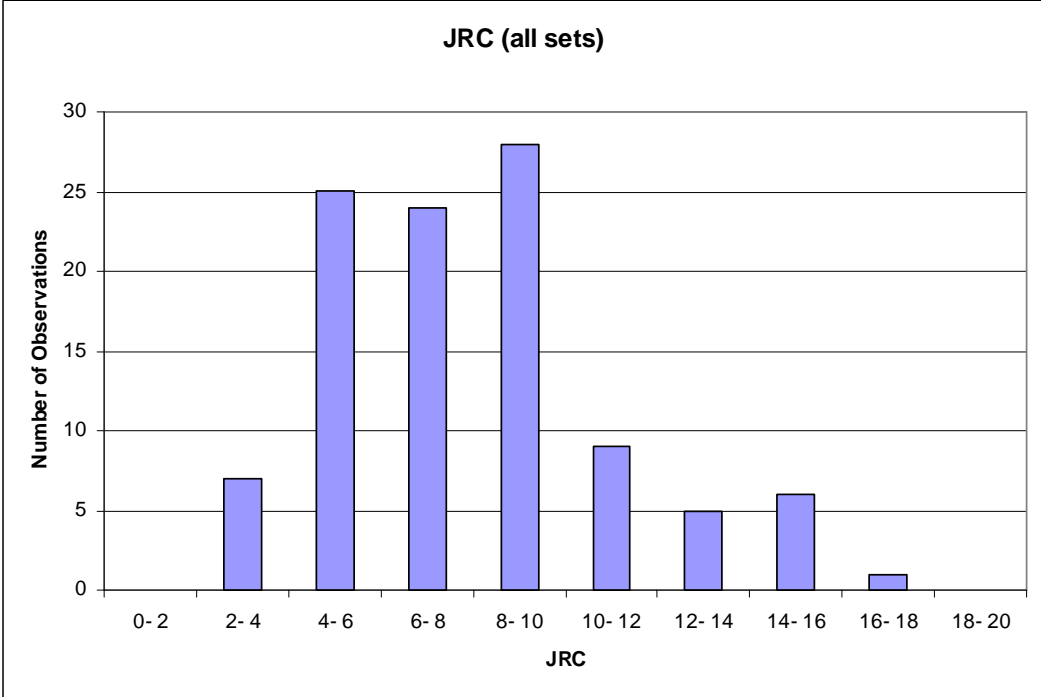


Fig.6.25a: Histogram of the measured JRC of all joint sets (105 measurements).

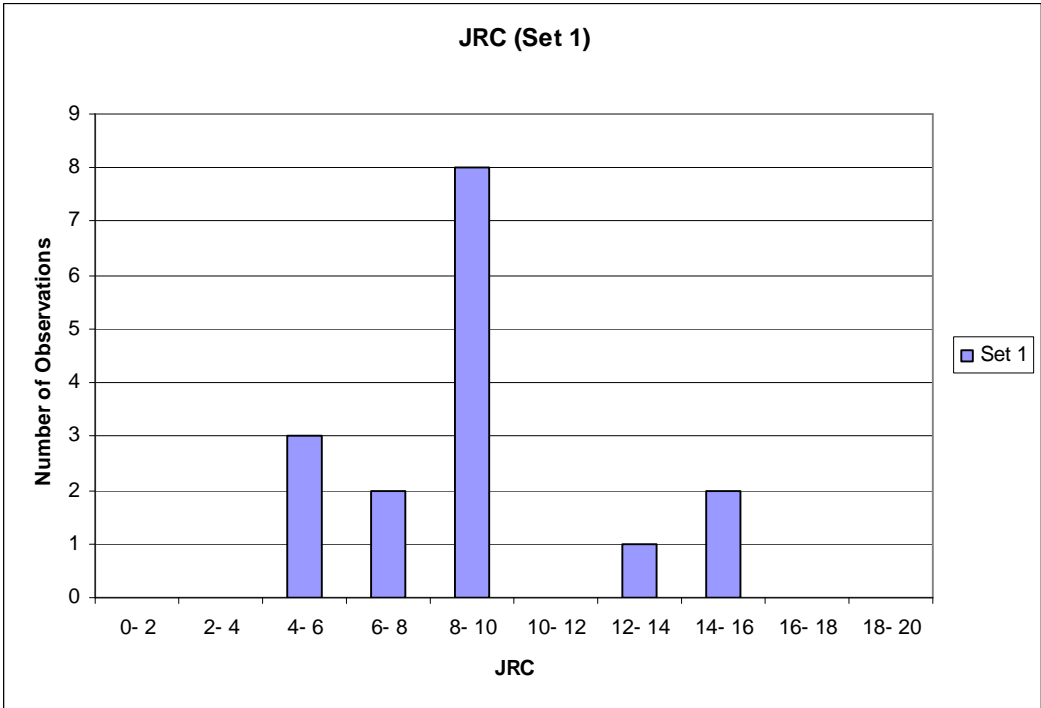


Fig.6.25b: Histogram of the measured JRC of joint set 1.

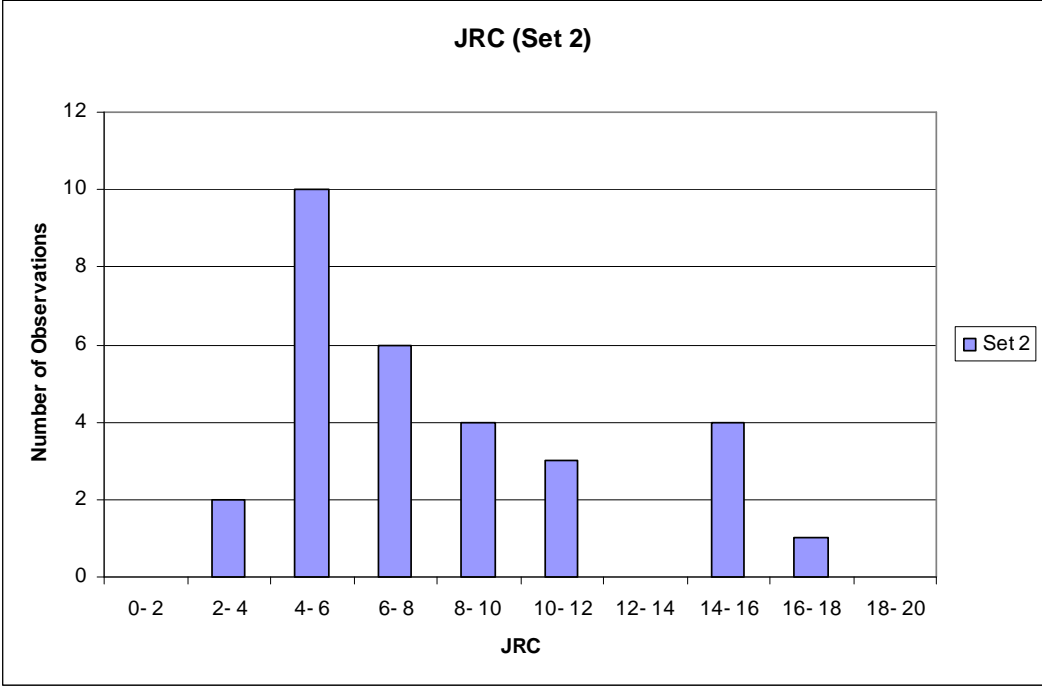


Fig.6.25c: Histogram of the measured JRC of joint set 2.

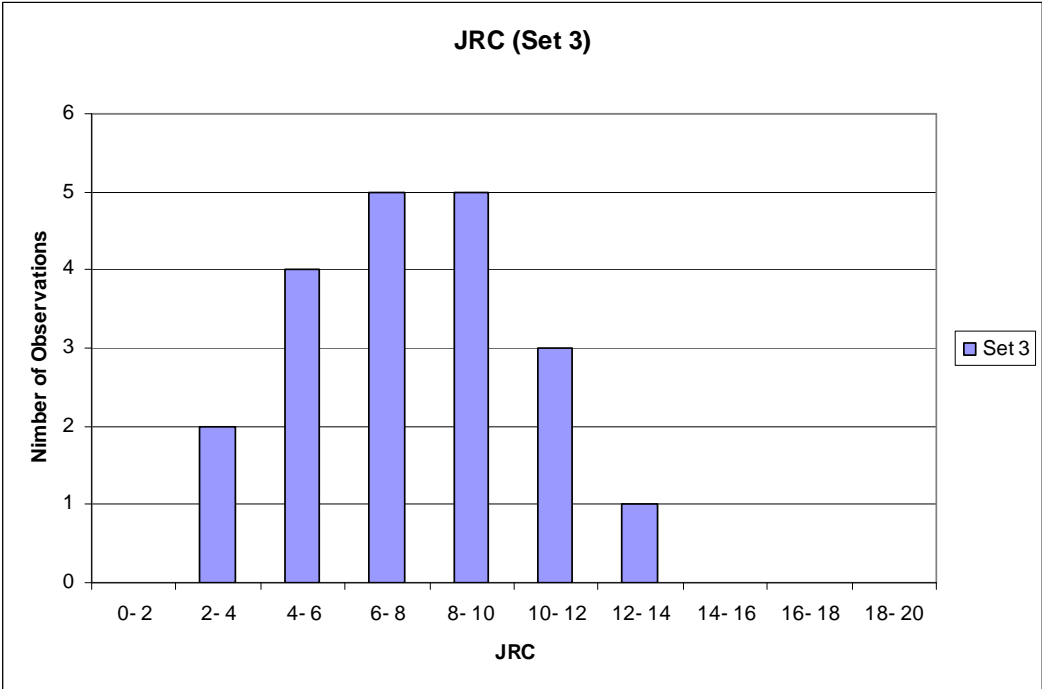


Fig.6.25d: Histogram of the measured JRC of joint set 3.

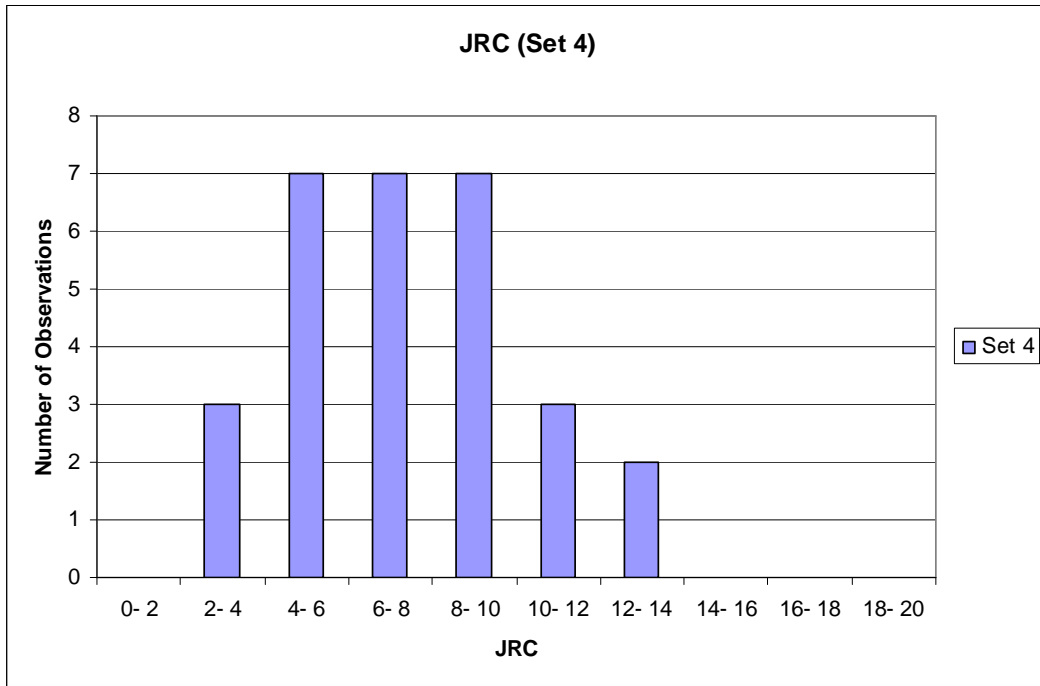


Fig.6.25e: Histogram of the measured JRC of joint set 4.

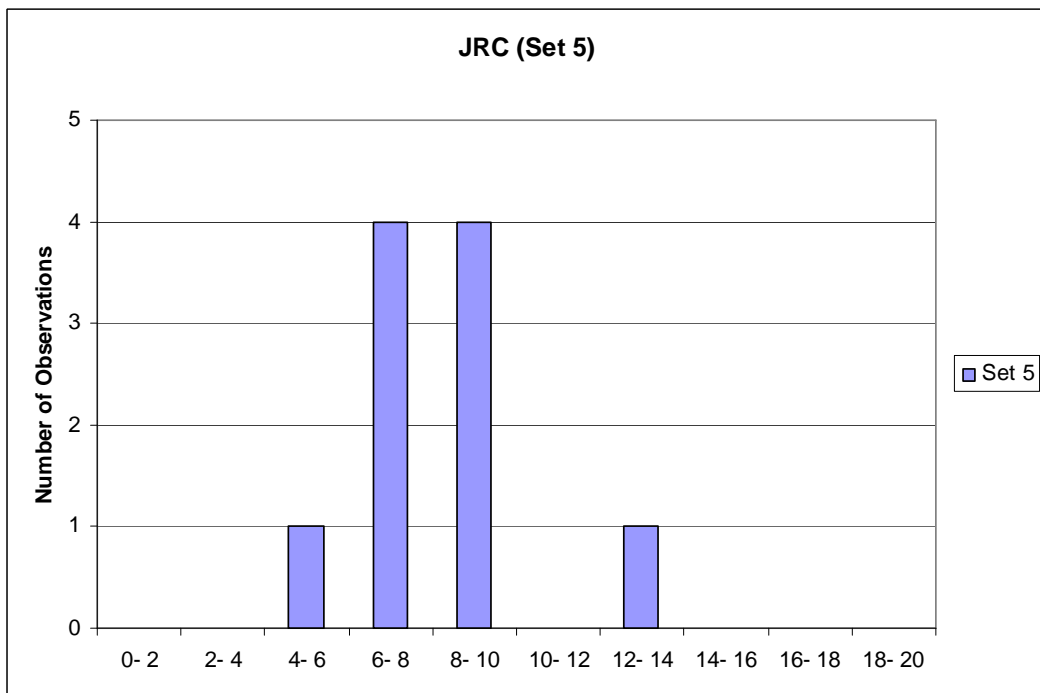


Fig.6.25f: Histogram of the measured JRC of joint set 4.

The surface of joint set 1 shows slickenside features, that can be found on the entire site. The measurements of 8 lineations on the surface of joint set 1 tend to be quite consistently oriented plunging shallow towards west. A possible displacement occurred against the direction of the trend towards east (Fig.6.26).


	Trend	Plunge
	270	10
	295	4
	265	20
	252	31
	280	15
	266	20
	260	15
	283	11

Fig.6 26: Surface of joint set 1. Polished surface (Slickensides) is visible on the joint (left). Pencil for scale. Lination measurements on the right.

Wall strength and weathering

With aid of a geologic hammer, a knife and the thumb the wall strength was estimated (Fig.6.27). As the test was made it was obvious that those joint surfaces affected by weathering have lower strength compared to fresh rock. In general the rock exposed near or at the surface was stronger affected by weathering. Strength determined at the tunnel of Ricobayo II or at steep unaltered rock walls yielded high strength estimates. At some outcrops the intense weathering had resulted in strong disintegration of the rock that could easily be ripped by hand. In such spots the rock was decomposed to a soil like material, although the original fabric was still visible (Fig.6.28)

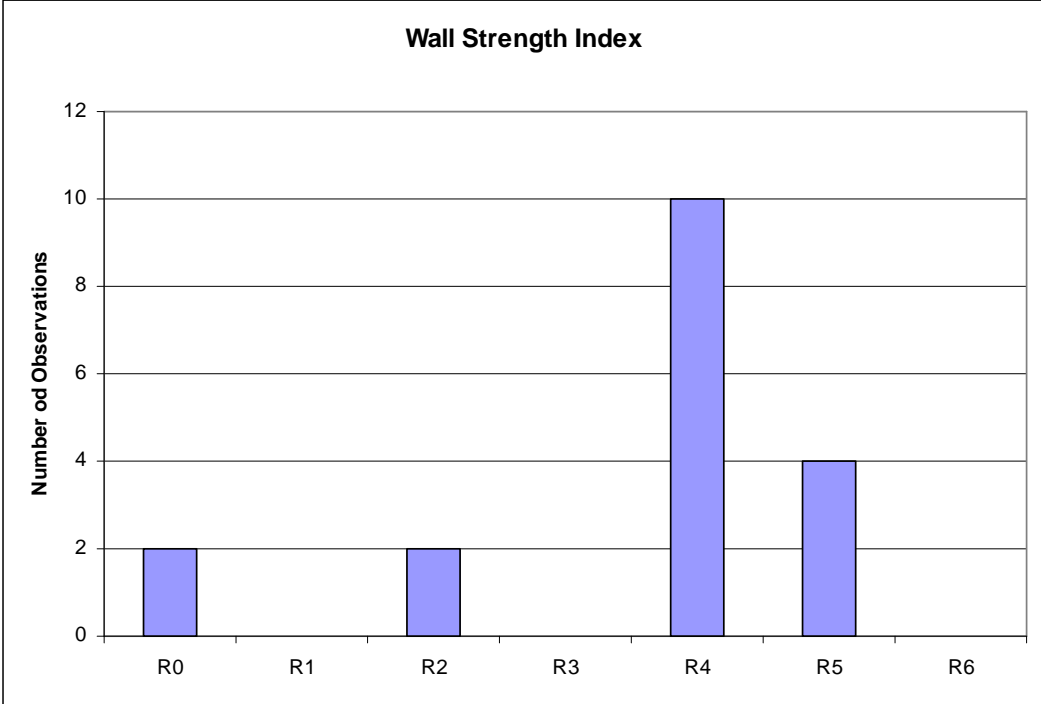


Fig.6 27: Wall strength estimates. Note that rock material is either strong where it was unweathered to slightly weathered, or weak where weathered rock was tested.



Fig.6.28: Picture showing a strongly weathered rock (R0 to R1). Geologic hammer could be indented without great effort and ripped by hand.

The weathering grades are shown in the histogram below (Fig.6.39). Again the generally good condition of the rock material itself is visible. Discolorations on the joint surfaces appear all over the area, but have only little influence on the strength of the rock.

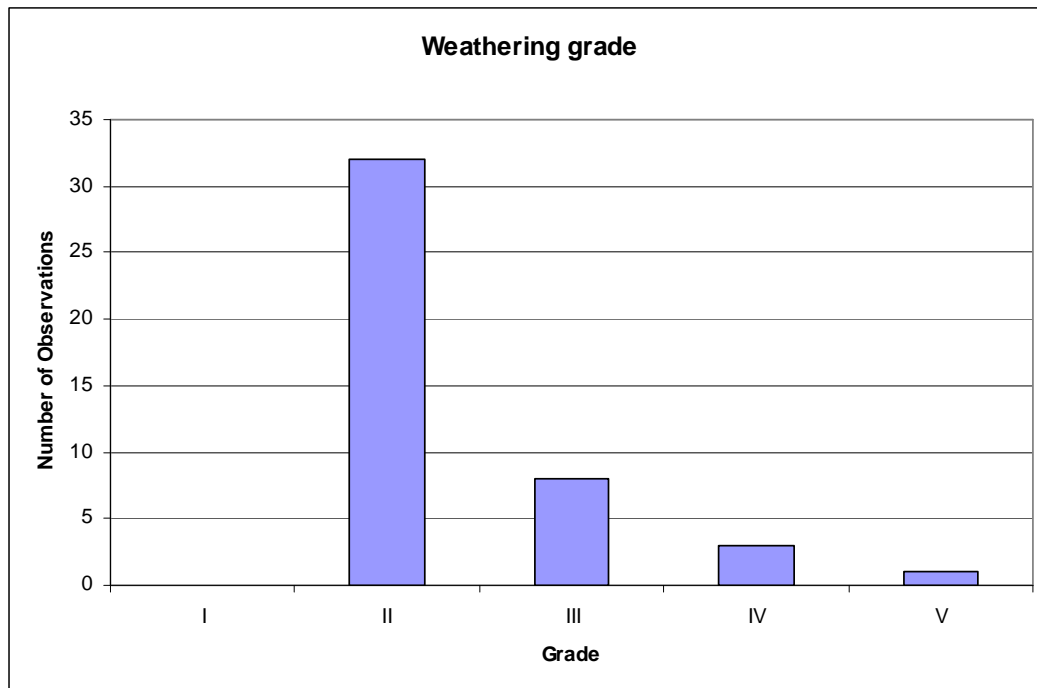


Fig.6 29: Weathering grades of the joint surfaces.

### Aperture and Filling

The joints at the investigated site are usually closed to gapped, in some cases open (Fig.6.30). Therefore filling is scarce or completely absent (Fig.6.31). Those joints that have material interfaces are typically characterized by a clayey to rock powder like material (Fig.6.32). Joints without filling are mostly characterized by surface staining. Few joints show minor water seepage.



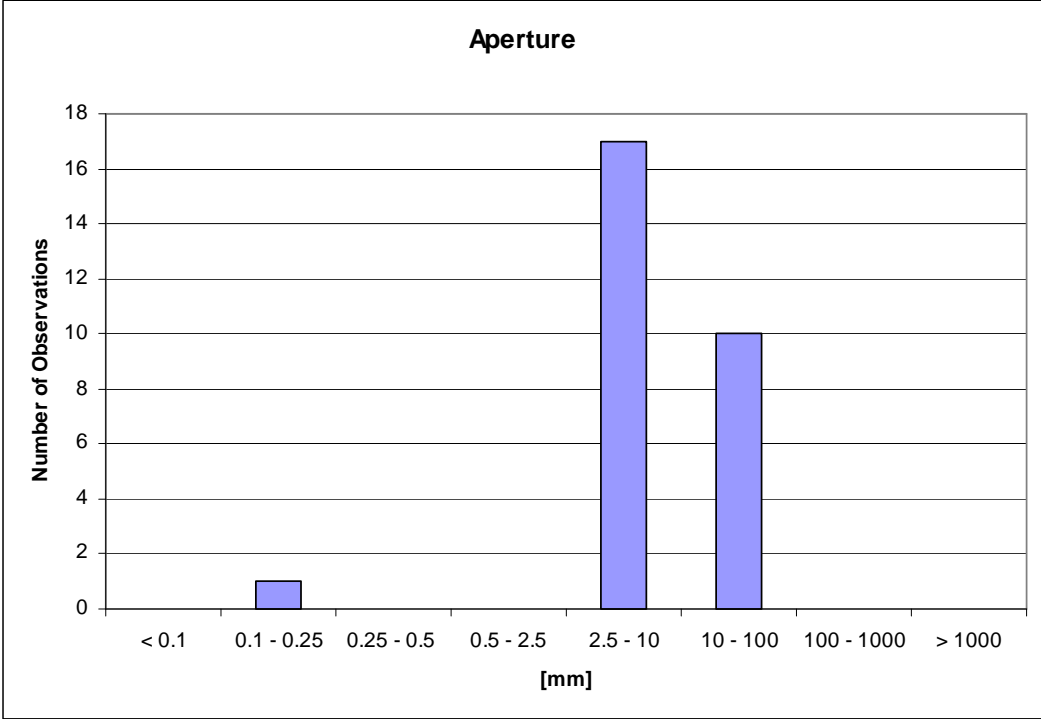


Fig.6 30: Ranges of aperture of joints

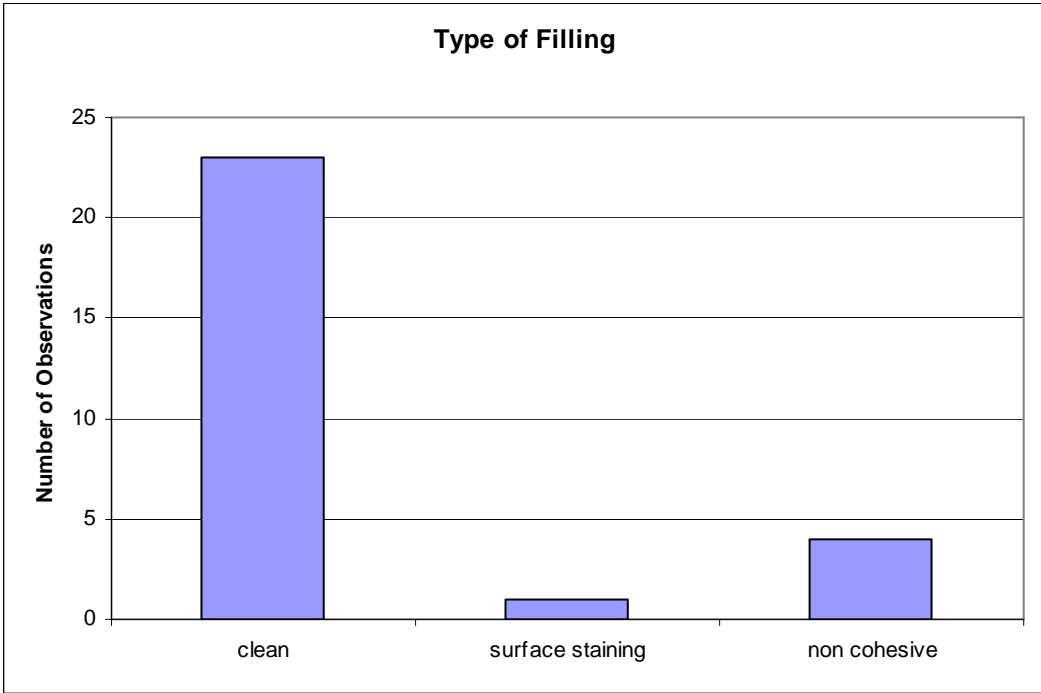


Fig.6 31: Description of the type of filling encountered.



Fig.6 32: Filling of joint (~3cm wide; arrow) along joint set 1. Slightly reddish discolorations on vertical rock wall. Compass for scale.

### Plunge Pool conditions

The plunge pool has a roughly circular to slightly elliptic shape approximately 160m long by 100m wide. It leads into a narrow approximately 30m wide and 40m long outlet channel that discharges the water back to the Esla river. The shape of the pool is not symmetric, with the right wall of the pool being more curved with respect to the spillway, while the left wall appears more parallel to it. About half of the total depth of the 100m deep plunge pool is filled with water. The water surface in the pool remains constant during dry season and acts as a water cushion for the overtopping water from the spillway. The sidewalls are mostly covered with concrete and shotcrete. However, the underlying structure of the bedrock can still be hypothesized. Planes of joint set 1 can be seen at the right wall right above the water table and the vertical joints of joint set 2 and 3 can be seen on the left wall (Fig.6.33).

Especially at the base of the left wall above the water table, a bench or terrace shaped feature is developed. At that elevation the steep walls stop abruptly and the morphology of the pool becomes more stepped (Fig.6.34). Those benches are related to joint set 1 orientations. On the vertical walls more or less continuous, persistent surfaces are exposed. Those surfaces reflect to a certain extend the local joint pattern (Fig.6.35).

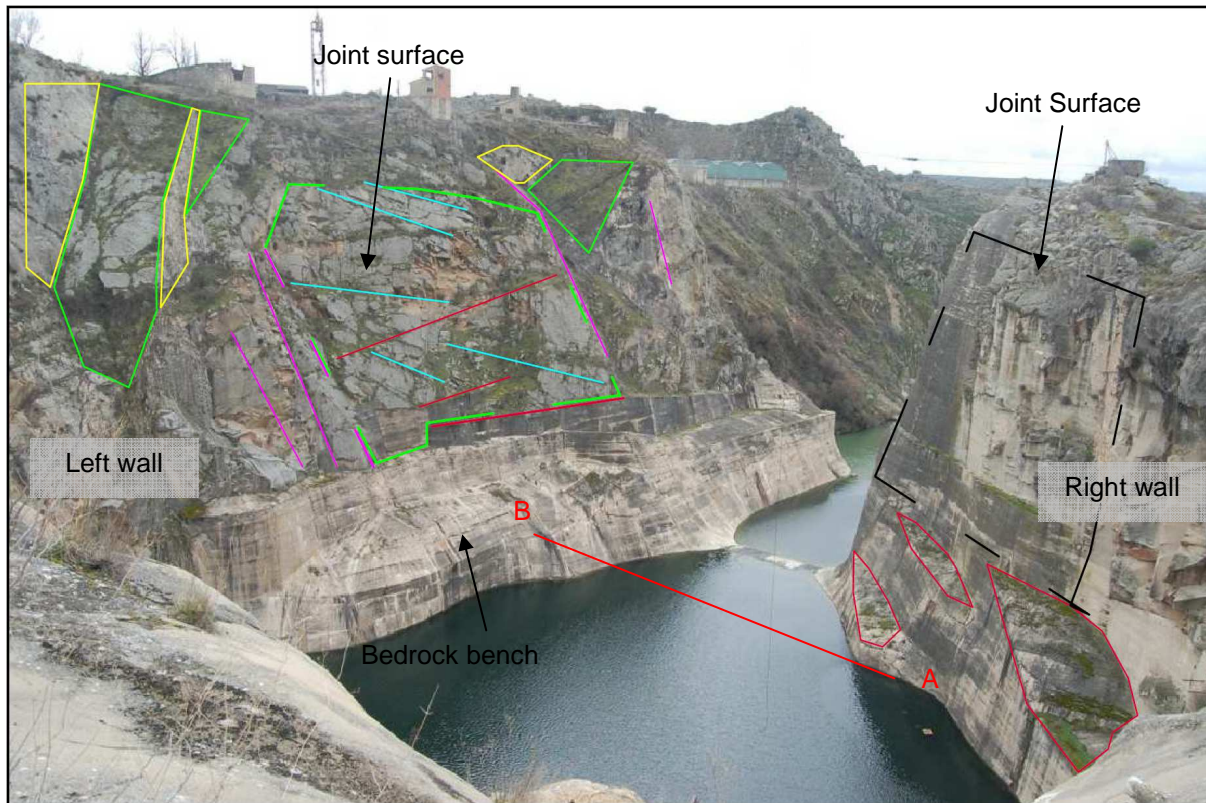


Fig.6 33: View into the plunge pool. The left wall provides a large scale exposure of the rock at the site showing the joint patterns. Joint set colors refer to those of Tab.6.8. Note that failure plane on the left wall is bound by Joint set 4 and its surface follows approx. the orientation of joint set 2. Red line indicates location of profile shown in Fig.6.35.

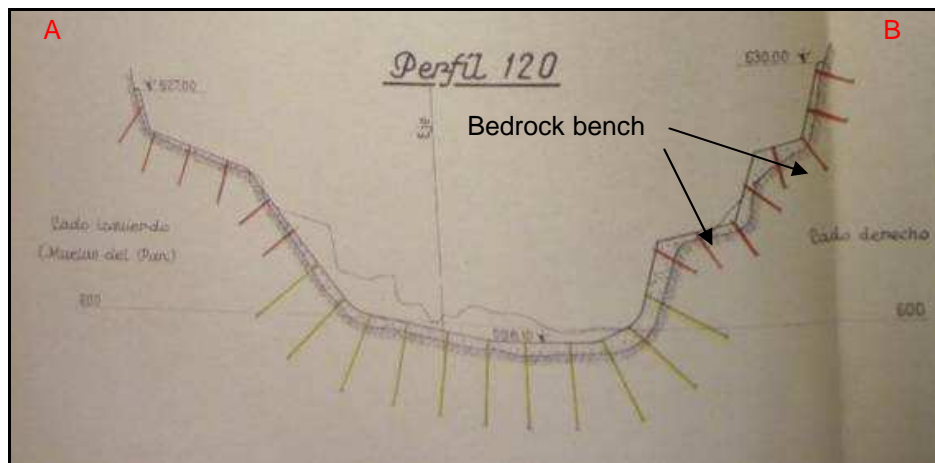


Fig.6 34: Transverse profile through the entrance of the outlet (view upstream). Plans from the 1940s show the original topography of the pool with step like bedrock terraces (straths) and the performed repair works (red and yellow anchors) (Iberduero S. A, 1940).

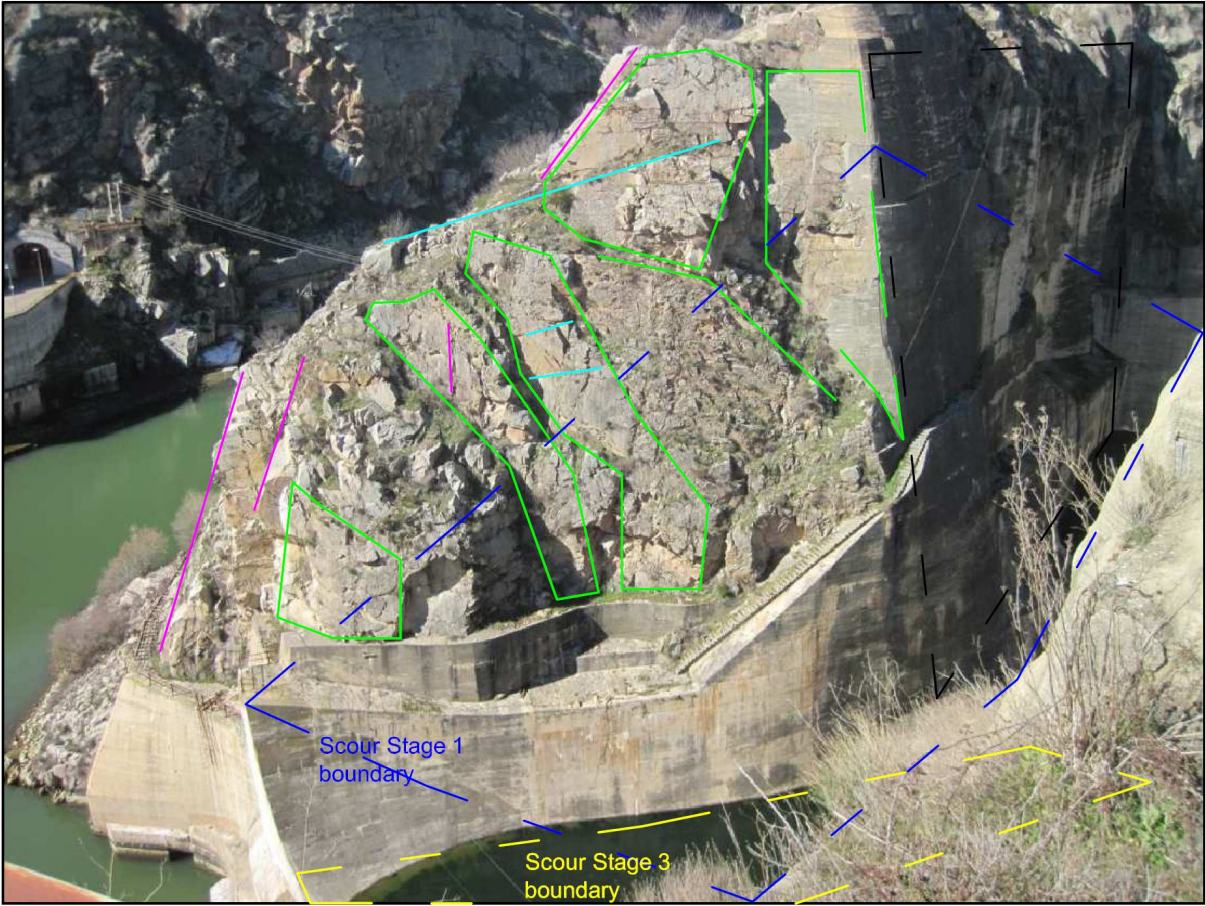


Fig.6 35: Right wall at the outlet channel downstream of the plunge pool. The wall exposures the joint pattern in this area where the first and third scour stage had occurred. Blue dashed line indicates approximate slope orientation after scour stage 1, yellow dashed line after stage 3. Joint set colors refer to those of Tab.6.9.

## 7. Block removability analysis

### 7.1 Block Theory

To evaluate the block removability in combination with the scour phenomenon, the concept of Block Theory (Goodman & Shi, 1985) was used. The concept of Block Theory is to determine a solution for the removability of block from the rock mass. It uses a combination of joint sets and free surfaces to determine the number and type of removable blocks. Each joint divides the three dimensional space into an upper and lower half space. Graphically the determination of removability is done by plotting the joint set and free surface orientations on a whole sphere stereonet (Fig.7.1) to identify if or if not a block is removable from all kinds of possible combinations of joints. The assumptions made are that: (1) a block is perfectly rigid, (2) joints are infinite and parallel with negligible apertures, (3) joints are parallel within a set and (4) no fracturing of rock is allowed.

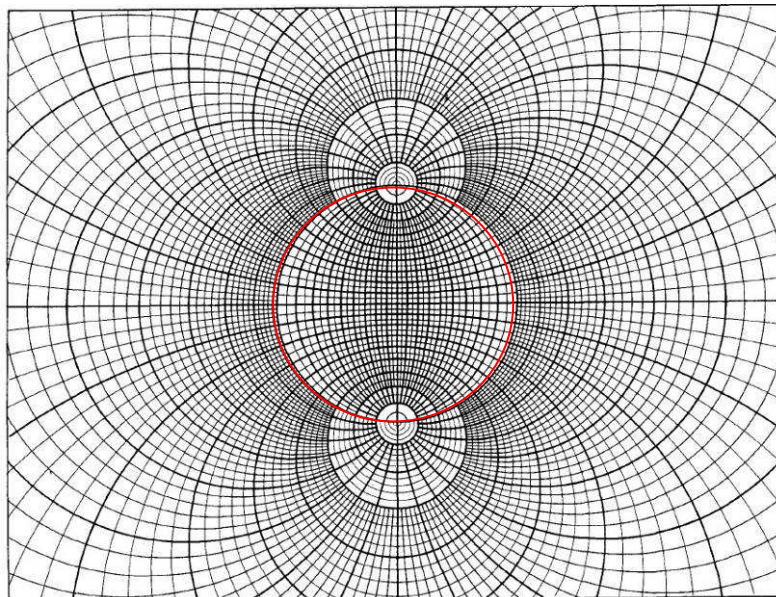


Fig.7 1: Whole sphere stereonet. Red line marks the reference circle. Area within the reference circle refers to the standard lower hemisphere net (Goodman, 1989).

### 7.2 Removability of Blocks

As mentioned above, the intersections of joints control the formation of blocks. There are  $2^n$  unique half space intersections, where  $n$  is the number of joints. The blocks formed can be classified as finite and infinite blocks (Fig.7.2). Infinite blocks such as the Type V block provide no hazard, since the block cannot slide toward the free space. Finite blocks can further be separated into removable and non-removable blocks.

Type IV blocks are tapered and not removable because of their shape. The removable blocks are represented by three different types. Type III is removable, but stable due to its

## 7. Block removability analysis

favorable orientation with respect to the excavation. It does not mobilize friction under gravity. Type II blocks are called potential keyblocks, since they are stable with friction and have the tendency to move in direction of the free space. Type I blocks are true keyblocks that will move if no support is provided (Fig.7.3).

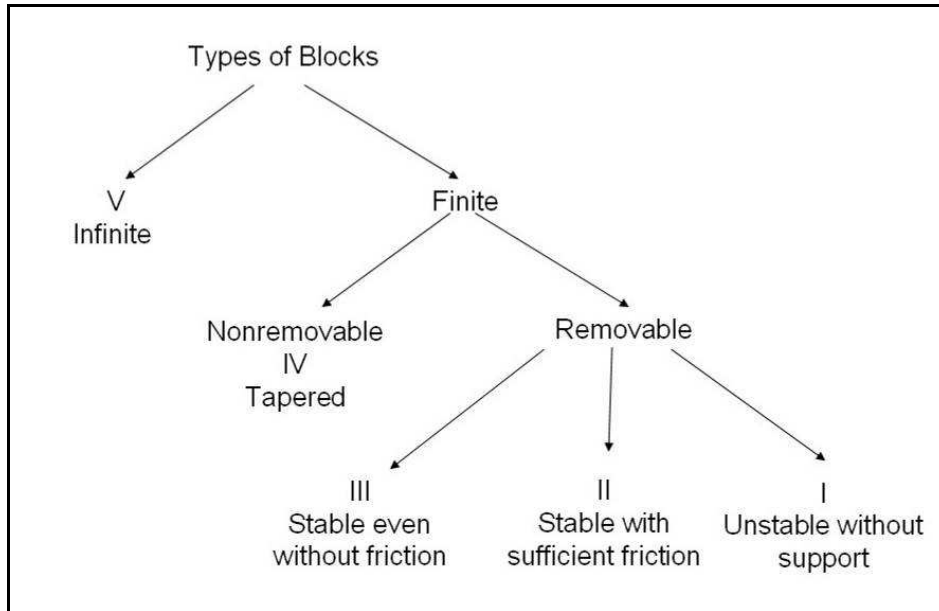


Fig.7 2: Types of blocks. Shapes of such blocks are illustrated in Fig.7.3 (redrawn from Goodman & Shi, 1986)

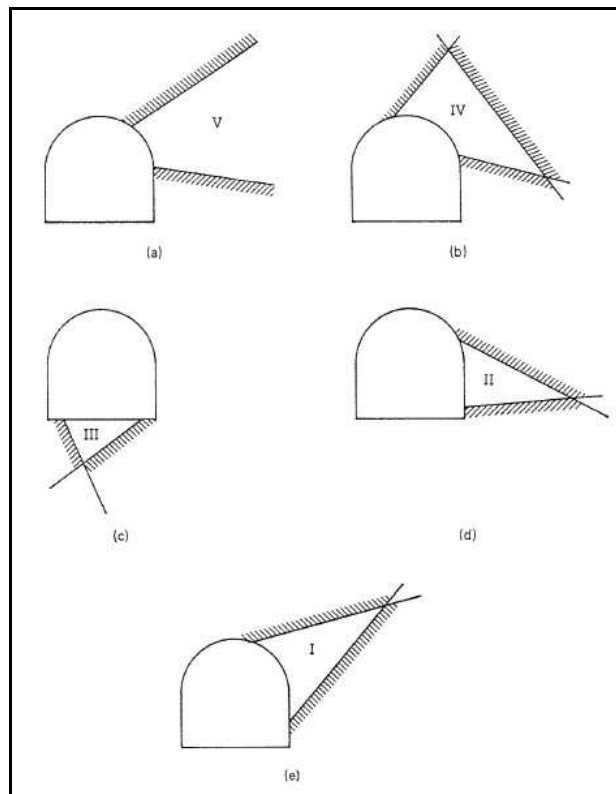


Fig.7 3: Types of blocks (a) infinite, (b) tapered, (c) stable, (d) potential keyblock, (e) keyblock (Goodman & Shi, 1986).

Blocks exposed to a free surface are referred to as Block Pyramids (BPs) which are formed by the intersection of a Joint Pyramid (JP) and the Excavation Pyramid (EP) (Eq.7.1). The excavation pyramid (EP) represents the rock, and the space pyramid (SP) represents the free space. A JP is the joint subset of a BP (only the joints without the free face).

$$BP = JP \cap EP \tag{Eq.7.1}$$

### 7.2.1 Finiteness

According to Shi's Theorem, a block is finite if its BP is empty (Eq.7.2) or in other words if its JP subset is totally contained within the Space Pyramid (SP) (Eq.7.3). The SP refers to that part of the excavation plane that is the "free space". It's the complimentary to the EP.

$$JP \cap EP = \text{empty} \tag{Eq.7.2}$$

or

$$JP \subset SP \tag{Eq.7.3}$$

Conversely a block is infinite (Type V) if the BP is not empty. The BP is not empty as shown in Fig.7.4, since it has a common region within the EP (below L3). An empty pyramid has no edges. Since in Fig 7.4 the JP is not entirely included within the SP it is not empty. In Fig 7.5 the JP is included in the SP and therefore empty. And since it is empty it is a finite block.

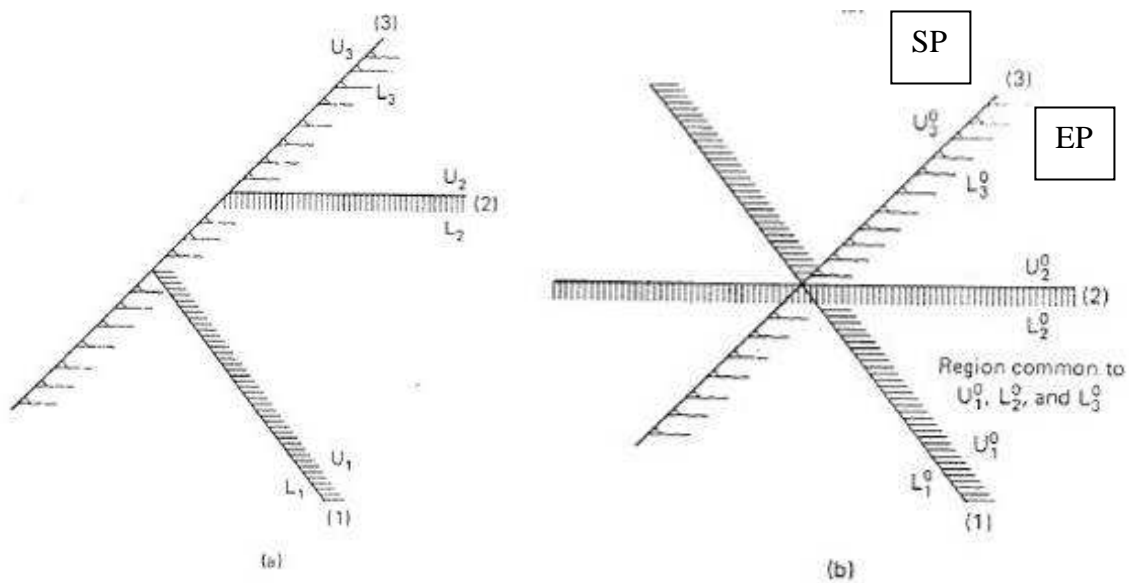


Fig.7 4: Two dimensional example for the finiteness theorem to an infinite block. (a) situation before moving of the half spaces. (b) situation after moving of the half spaces to a common point. L and U define the lower and upper half spaces with respect to a plane, respectively. Infinite blocks share a common region and can not be shifted to only one common point (Goodman & Shi, 1985).

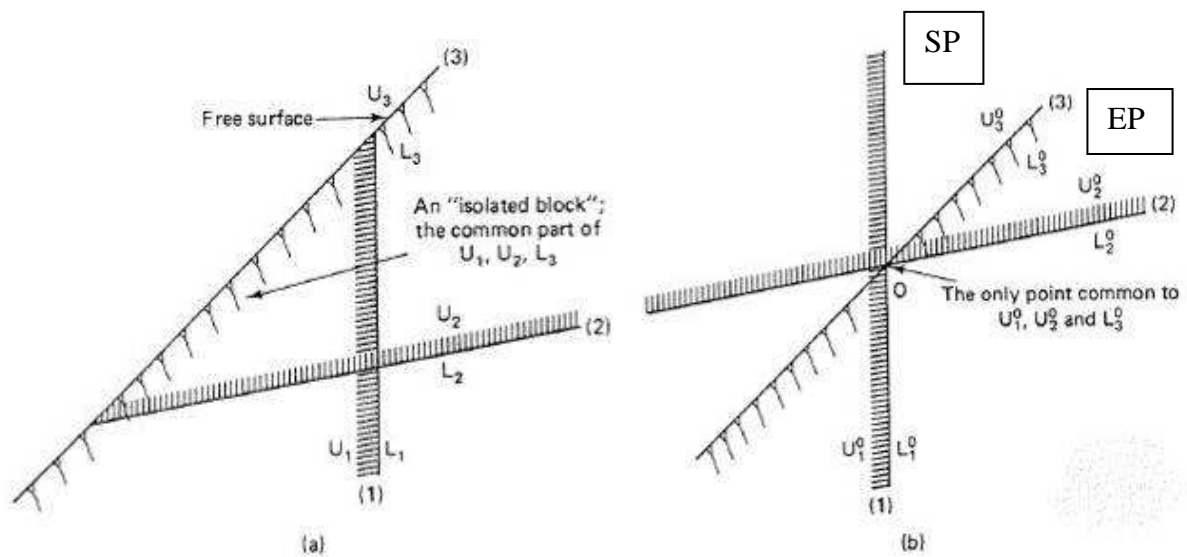


Fig.7 5: Two dimensional example for the finiteness theorem to a finite block. (a) situation before moving of the half spaces. (b) situation after moving of the half spaces to a common point. L and U define the lower and upper half spaces with respect to a plane, respectively. The BP is empty, since all planes can be shifted to one single common point. The common part of a finite BP is the block itself. The JP (defined by U1 and U2 ) is not empty and totally within SP, which is important in terms of removability of finite blocks (Chap. 7.2.2)(Goodman & Shi, 1986).

### 7.2.2 Removability of finite blocks

The removability of a block depends on its shape and orientation with respect to the excavation surface (Fig.7.5a). The theorem for the removability is given below:

*A convex block is removable if its block pyramid (BP) is empty and its joint pyramid (JP) is not empty. A convex block is not removable (tapered; Type IV) if its BP is empty and its JP is also empty.*

If a finite block is entirely defined by joint half spaces (Fig.7.5c) its JP is empty (finite) and the block is tapered. Also the BP is empty. Those JPs can not be represented on the stereographic projection. The determination of finiteness was shown in Fig. 7.4 & 7.5 above. If the joint half spaces define an infinite block (Fig.7.5b), the JP is not empty and they have a common region to the joint planes. Their BPs are empty and they are removable. Infinite (non empty) JPs are visible on the projection as Type I, II, III or V blocks. Infinite Blocks on the projection, where their JPs are partly or completely within the EP are named Type V. Their JPs are and BPs are both not empty (infinite) and therefore not removable. Type V blocks may only become finite through rock fracturing. Another type of block is the joint-block. It's a block defined only by joints that exists inside a rock mass without any contact to the surface. It can be seen as a tapered (Type IV) block without a free surface.



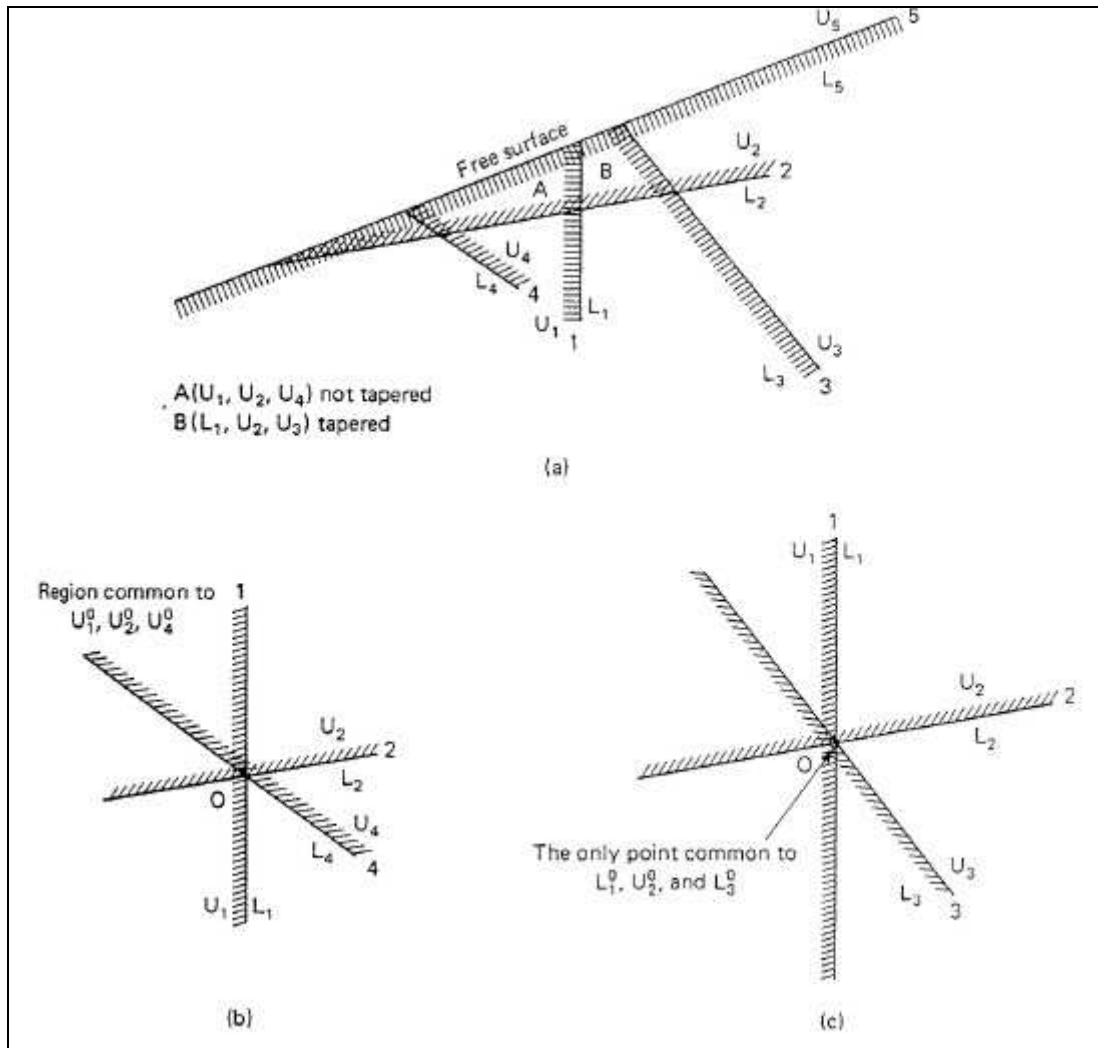


Fig.7 6: The removability theorem. (a ) Illustration of the removability of different blocks depending on their shape. (b) Block A can never be formed only by joints and needs additionally a free surface. Its JP is not empty and therefore infinite. (c).Block B can be formed entirely by joints producing a finite block which has an empty JP.

### 7.3 Removability using stereographic projection

#### 7.3.1 The principle of the stereographic projection (equal angle)

In Chapter 6 the principle of the equal area stereonet was discussed, which is used for the joint statistics orientations. Here, the equal angle stereonet will be introduced, which is used for the block theory evaluation. In the equal angle projection the projection plane lies in the equator (Fig.7.7).

## 7. Block removability analysis

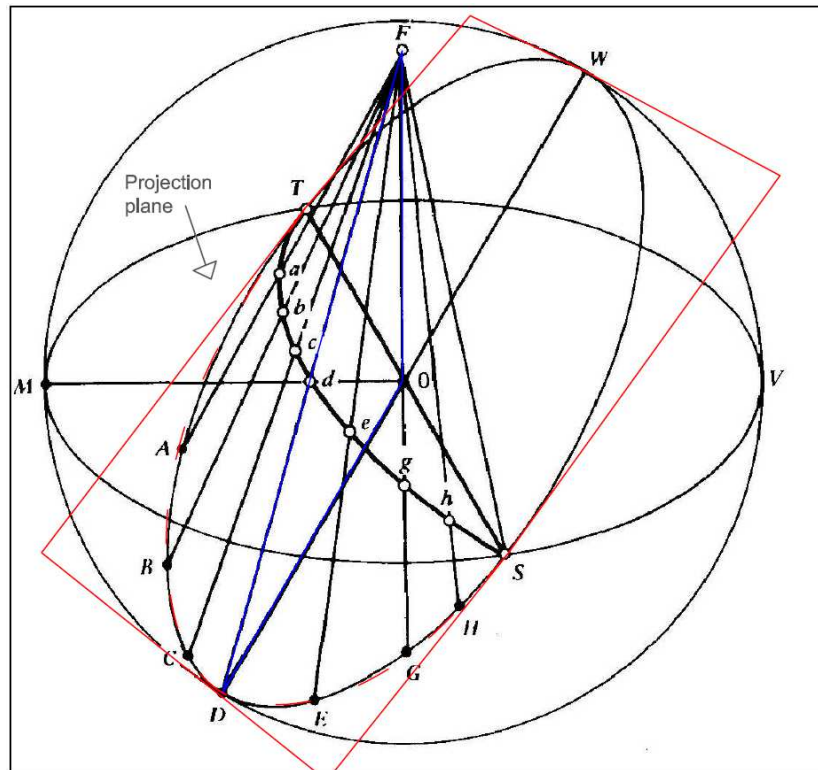


Fig.7 7: Principle of the stereographic projection (Upper focal point or lower hemisphere projection). A plane (red rectangle) intersecting the reference sphere. The great circle is project through the upper focal point (F) onto the projection plane. The section highlighted in blue is shown in Fig.7.8 (modified after Goodman, 1989)

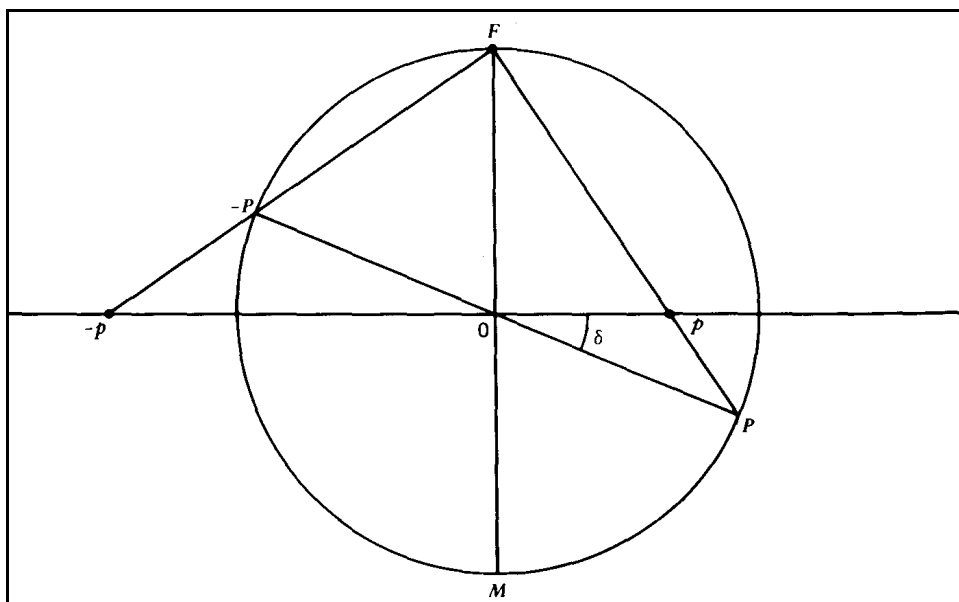


Fig.7 8: Section through the reference sphere. A plane inclined at an angle  $\delta$  intersects the reference sphere at point P. P is projected through the upper focal point (F) on to the projection plane as (p). (-P) and (-p) refer to the plane projected into the upper hemisphere (Goodman, 1989)

## 7. Block removability analysis

---

The number of JPs appearing on the stereographic projection depends on the number of nonparallel joints.

The following formulas illustrate the relationships of the number of joints and the JPs on the stereographic projection.

The number of JPs is given by Eq.7.4.

$$\text{Number of JPs} = 2^n \quad (\text{Eq.7.4})$$

Where:  $n$  = number of joints in a rock mass

The number of JPs appearing on the stereographic projection ( $N_R$ ) is given by Eq.7.5.

$$N_R = n(n - 1) + 2 \quad (\text{Eq.7.5})$$

The number of JPs absent from the stereographic projection ( $N_T$ ) is given by Eq.7.6.

$$N_T = 2^n - n(n - 1) + 2 \quad (\text{Eq.7.6})$$

To identify the blocks, so called JP codes are assigned to the areas on the stereonet enclosed by joint half spaces. A binary digit code with  $n$  positions. For example a block can be named 01110. The position of the number on this code refers to the joint half space where it is formed. A “1” indicates the lower half space, a “0” the upper half space. For this example the block would be formed in the upper half space of joint 1, the lower half space of joint 2 to 4 and the upper half space of joint 5. Such projections will be presented in the Erodibility spectrum (Chap. 7.4)

### 7.4 Removability Plots

In order to understand the block removal at the spillway of the Ricobayo dam, a limit equilibrium analysis using Block Theory is done. It comprises a direction dependant investigation on the mobilization of blocks with compound friction cones. This concept is named “Erodibility Spectrum” (Kieffer, personal comment) and will be discussed further in this chapter.

#### 7.4.1 The factor of safety and friction cone concept

The factor of safety (FS) is defined by the ration of available friction angle to required friction angle (Eq.7.7), or in other words resisting forces versus driving forces. Fig.7.9 illustrates the factor of safety concept.

## 7. Block removability analysis

$$FS = \frac{\tan \phi_a}{\tan \phi_r} \quad (\text{Eq.7.7})$$

Where:  $\phi_a$  = available friction angle adopted for a discontinuity  
 $\phi_r$  = required friction angle to be mobilized for a certain FS.

In terms of forces the factor of safety can be expressed as follows (cohesion is not considered here):

$$FS = \frac{W \cdot \cos \beta \cdot \tan \phi_a}{W \cdot \sin \beta} \quad (\text{Eq.7.8})$$

Where:  $W$  = Weight vector  
 $\beta$  = Slope angle (mobilizing angle for the block)

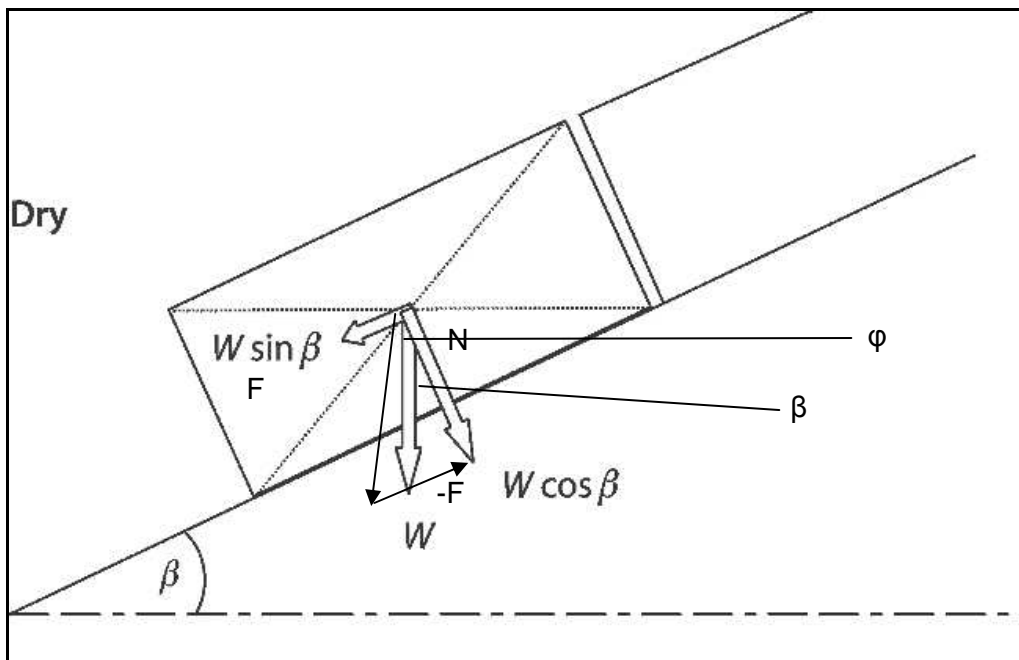


Fig.7 9: Stability of a block on a slope for dry conditions.  $W \cos \beta$  is the normal to the plane ( $N$ ),  $W \sin \beta$  is the parallel force to the plane ( $F$ ) driving the block downslope. ( $-F$ ) is the resisting force provided by the friction angle ( $\phi$ ) The weight vector acts vertically down under normal circumstances (modified after Price, 2009).

The resisting force on the plane is given by:

$$-F = N \cdot \tan \phi \quad (\text{Eq.7.9})$$

## 7. Block removability analysis

Substituting  $F$  and  $N$  by the expressions of Fig.7.9 the formula can be transformed into  $\tan\beta = \tan\phi$  for limit equilibrium conditions.

The angle of friction acts in three dimensions and forms a friction cone which appears as a small circle on the stereonet (Fig. 7.10).

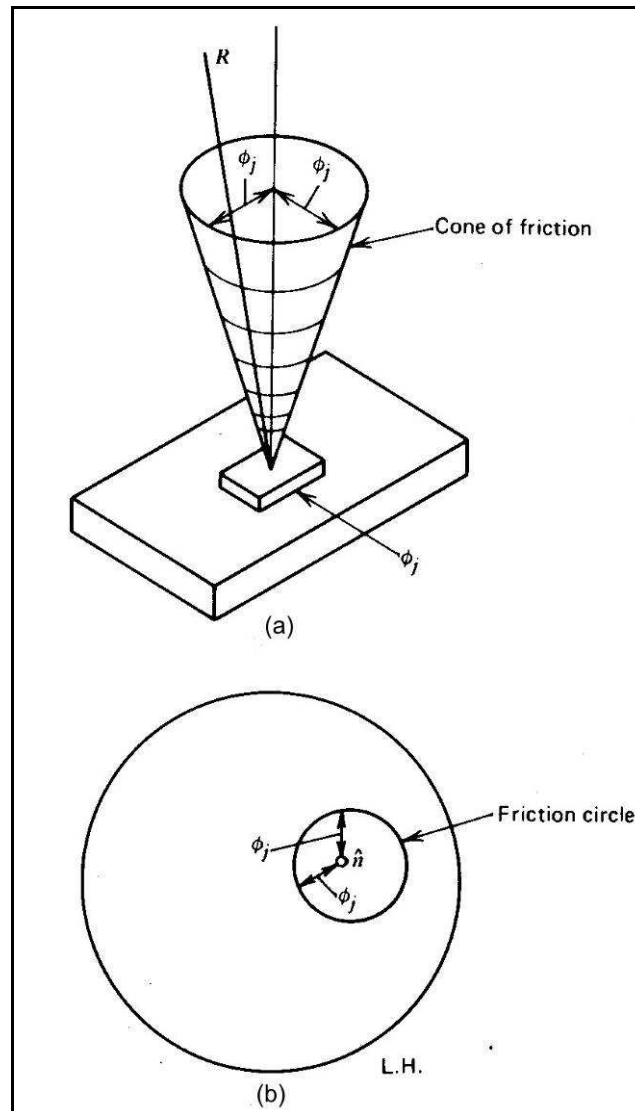


Fig.7 10: The friction cone concept. (a) A friction cone with an apex of the friction angle ( $\phi_j$ ) around the normal to a plane. Any resulting force plotting within the friction cone will cause no movement of the block. (b) The friction cone as a small circle (friction circle) on the stereonet with the radius of the friction angle ( $\phi_j$ ) (Goodman, 1989).

For a planar discontinuity without filling, shear strength will be controlled by the friction angle. The friction angle of the rock material depends on the size and shape of the grains exposed on the surface of the discontinuity. Thus, a fine-grained rock, and rock with a high mica content aligned parallel to the surface, such as a phyllite, will tend to have a low friction angle, while a coarse-grained rock such as granite, will have a high friction angle. Table 7.1 shows typical ranges of friction angles for a variety of rock types (Wyllie & Mah, 2004).

## 7. Block removability analysis

---

Rock Class	Friction angle range	Rock type
Low friction	20–27	Schists (high mica content), shale, marl
Medium friction	27–34	Sandstone, siltstone, chalk, gneiss, slate
High friction	34–40	Basalt, <u>granite</u> , limestone, conglomerate

Tab.7 1: Range of Friction angles for different rock types (Barton, 1973). Granite as it occurs at Ricobayo is in the high friction class. For the Erodibility Spectrum plots ranges from 30° to 40° were used to cover a broad range of friction.

### 7.4.2 The Block Erodibility Spectrum

The Block Erodibility Spectrum (Kieffer, 2011) includes is a more complex representation of compound friction cones of different joint planes. It helps determining in which direction a block is more susceptible to sliding. For the analyses, Block Theory Software has been utilized (Goodman & Shi, 1989) In order to determine this for the Ricobayo spillway the following steps are performed to create the Erodibility Spectra.

- 1.) Plotting of the mean joint orientations on a whole sphere stereonet to identify the removable blocks and their associate failure mode under gravity to determine the block type. This is done for the flat spillway surface, the front slope and the compound slope using the Keyblock program.
- 2.) Drawing of the shape of the removable blocks using the Keyblock program.
- 3.) Drawing of the compound friction cone for each removable block.
- 4.) Importing the plots from (3) into AutoCAD to measure distances from the resulting force (R) to the 30° and 40° friction cone boundary . This has to be done since no degree contours are drawn on these plots to directly count the amount of degrees that are necessary to destabilize the block.
- 5.) Calculation of the Angle of Rotation ( $\theta$ ) from the in (4) measured distances for of the resulting force using an Excel worksheet and generation of the Erodibility Spectra.

The total procedure following the above described steps will be demonstrated with an example.

From the joint orientations in Chapter 6 we know that there are 5 joint sets present at Ricobayo. The following table (Tab.7.2) gives an overview of the average joint orientation and the implied considerations for Block Theory analysis.

## 7. Block removability analysis

Number of joint sets	Total Number of JPs ( $2^n$ )	Number of JPs appearing on projection ( $N_R$ )	Number of JPs absent from projection ( $N_T$ )
5	32	22	10

Tab.7 2: JP properties for the 5 joint sets of Ricobayo.

### Identification of removable blocks

For the front slope 6 removable blocks have been identified. Eq. 7.10 also shows this. The JPs that are removable are highlighted in Fig.7.11.

$$(n^2 - 3n + 2)/2 \quad (\text{Eq.7.10})$$

Where  $n$  = number of joints

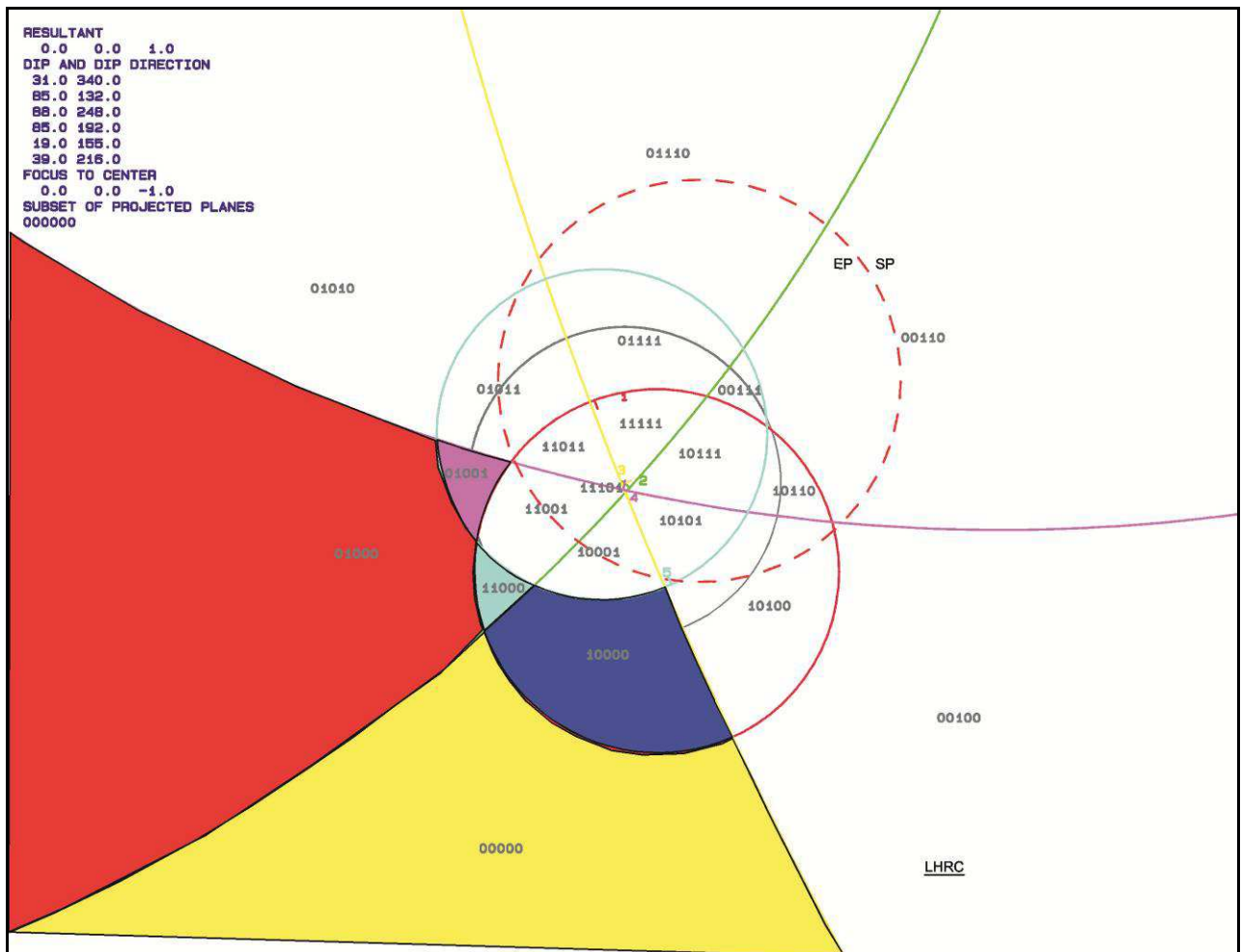


Fig.7 11: Whole sphere stereographic projection for the front slope of the spillway at Ricobayo. The removable JPs are highlighted, slope (red dashed circle), reference circle (black circle). Orientations of joints (first 5 entries) and slope (last entry) are listed in the top left corner. The original slope orientation was estimated from old maps. The corresponding failure modes are shown in Fig.7.12.

## 7. Block removability analysis

The failure modes are computed for gravity acting on the blocks. The numbers indicate the type of failure mode which is characteristic for a certain JP (Tab.7.3). The developed type of failure depends on where the resultant force plots for each JP. E.g. if the resultant plots on Joint plane 1, the digit 1 indicates sliding on 1 (Fig.7.12). This can be shown for each block and will be discussed in step 3 of the removability analysis with the compound friction cones.

Number on projection	Block type	Failure mode
0	I	Lifting or Falling
1, 2,.. (single- digit number)	II	Plane sliding
12, 24, (two- digit number)	II	Wedge sliding
- (number absent)	III	No failure mode

Tab.7 3: Listing of failure modes for removable JPs.

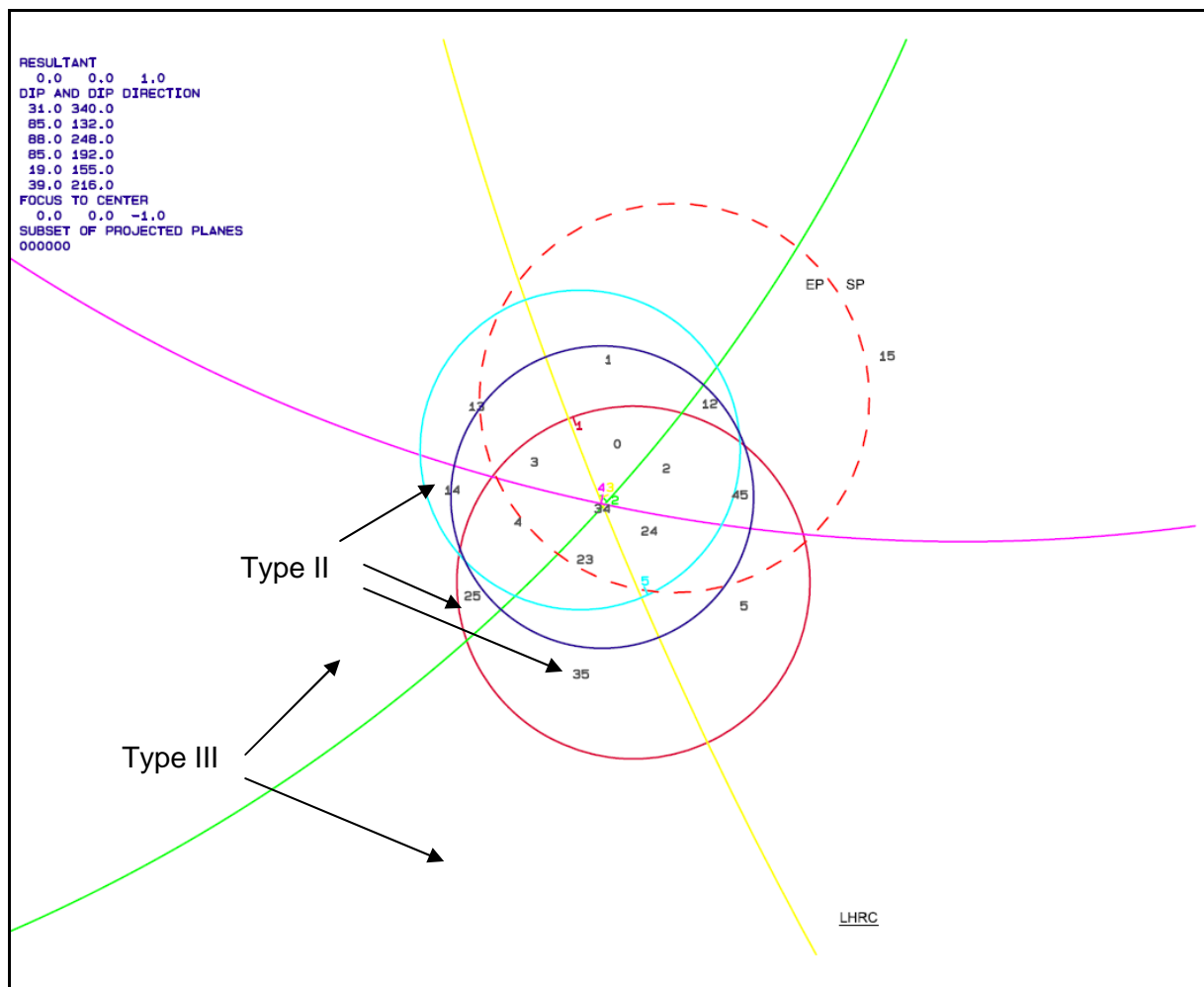


Fig.7 12: Failure modes for JPs shown in Fig.7.11. However, failure mode of a JP is distinct from the removability of a block. (note that some JPs that have a number assigned are not entirely within SP).



## 7. Block removability analysis

---

Since tapered blocks do not appear on the stereographic projection, the JPs within the EP are type IV (infinite) blocks. Removable blocks are finite blocks with infinite, non empty JPs. Tab.7.4 lists the removable JPs for the front slope, the spillway surface and the compound slope. The according Figures are found in the appendix.

Location	Removable JPs	Block Type
Front Slope	00000	III
	01000	III
	01001	II
	10000	II
	11000	II
	00010	III
Spillway surface	00000	III
	01000	III
	01010	III
	00100	III
	01110	III
	00010	III
Compound slope	00000	III
	01000	III
	01001	II
	10000	II
	11000	II
	01010	III
	01110	III
	00100	III
	00010	III

Tab.7 4: List of the removable JPs for the front slope, the spillway surface and the compound slope. The compound slope is the combination of the first two.

### Shape of the blocks

The Keyblock program (Goodman & Shi, 1989; Liu, 2004) computed the shapes of the removable blocks at the different locations. For the block computations spacing measurements from the ShapeMetrix<sup>3D</sup> software were used (adopted from Rocha, 2012). As an example the Block with the JP code 0000 is shown below (Fig.7.13). The other blocks can be found in the appendix.

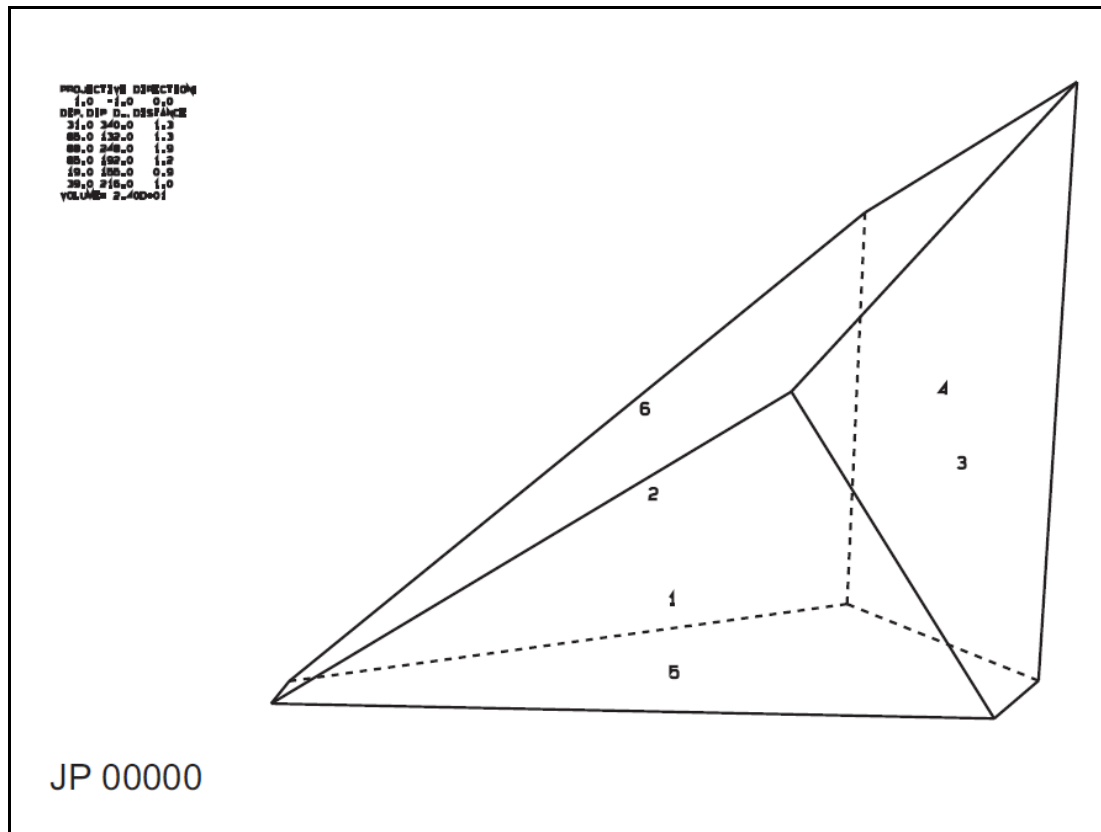


Fig.7 13: Shape of Block 00000. Numbers 1 to 5 indicate the joint planes, 6 the free surface.

### Compound friction cones and angle of rotation

The limit equilibrium analysis is performed for each block with a friction of 30° and 40° which covers a broad range of friction for granitic rocks (Tab.7.1). Considering again the plot of JP00000 (Fig.7.14) the friction cone for 30° is shown. We know from step (2) that this block is a Type III, which is stable. This can also be seen in this plot where the resultant force (R) is gravity acting vertically down and no failure mode is indicated. As soon as R is shifted to the line of limit equilibrium, it plots on different fields mobilizing friction. In some directions this might only be some degrees, whereas in other cases more than 90° are necessary to move the block (i.e. lifting).

For JP00000 in the direction of the spillway it can be seen that the distance from the resultant (R) to the line of limit equilibrium is short compared to other directions. To get the actual angle of rotation ( $\Theta$ ) from these plots, the distances obtained from AutoCAD have to be transferred into angles (Eq. 7.11). The angles are determined in 10° steps.

$$\theta = 2 \cdot \arctan\left(\frac{ov'}{R}\right) \quad (\text{Eq.7.11})$$

Where:  $\theta$  = Angle of rotation

R = Radius of the reference sphere/circle

ov' = Distance from center to projected point

## 7. Block removability analysis

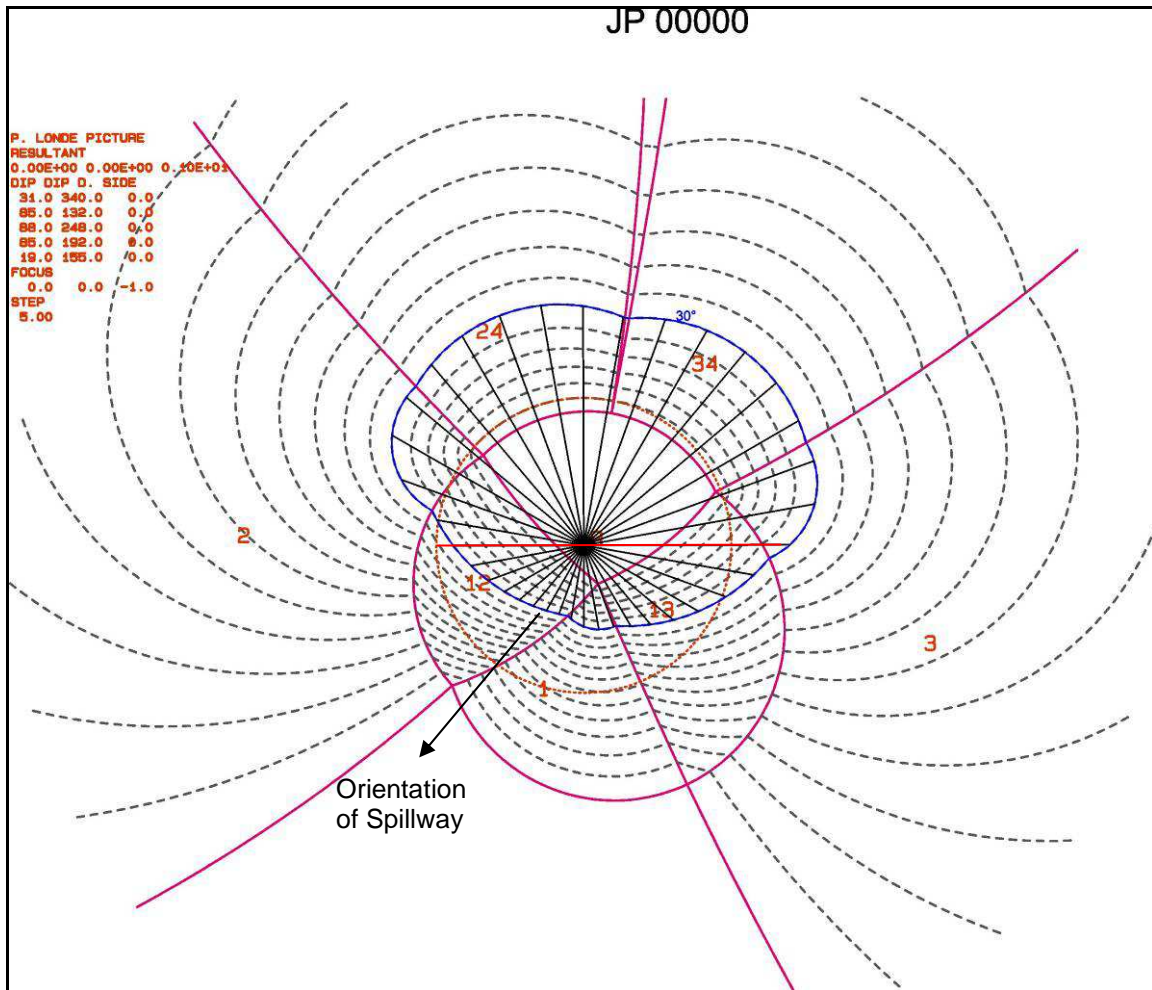


Fig.7 14: Compound friction cone for JP 00000. Blue line indicates the 30° friction line. Black dashed lines in 5° steps, reference circle shown as dashed orange circle. Orientation of spillway is indicated by arrow. The principle of obtaining the angles is shown in Fig.7.15 below, which is a cross section through the reference sphere along red line.

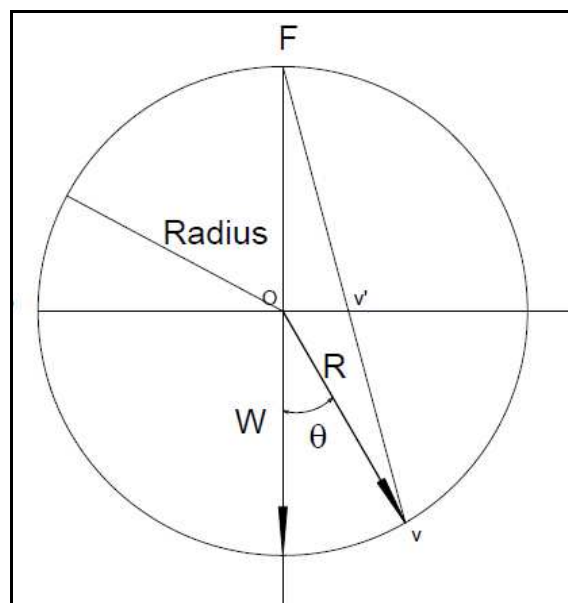


Fig.7 15: The principle of transferring the measured distances ( $ov'$ ) from the friction plots to angle of rotation employing Eq.7.11.

Block Erodibility Spectrum Plots

In this section the plots from the Block Erodibility Spectrum (Kieffer, 2011) will be presented. Plots are generated for the front slope, the spillway surface and the compound slope, showing all JPs together. For each JP a radar plot is generated showing the angle of rotation ( $\theta$ ) and the minimum force with respect to the weight of the block.

The basic idea of the Block Erodibility Spectrum is illustrated in Fig.7.18. It compiles the angle of rotation ( $\theta$ ) versus the azimuth for different JPs to identify their susceptibility of being mobilized (Kieffer, personal comment). The resultant force (R) is obtained by rotating the weight vector (W) by the angle of rotation ( $\theta$ ) to trigger a failure mode in a certain direction (Fig.7.16 & Fig.7.17). We again consider JP0000, which is formed in the upper half spaces of all joints and by the free surface of the spillway in this case. The minimum Force ( $F_{min}$ ) is expressed in Eq. 7.12.

$$F_{min} = W \cdot \sin \theta \tag{Eq.7.12}$$

Where: W = Weight of the block  
 $\theta$  = Angle of rotation

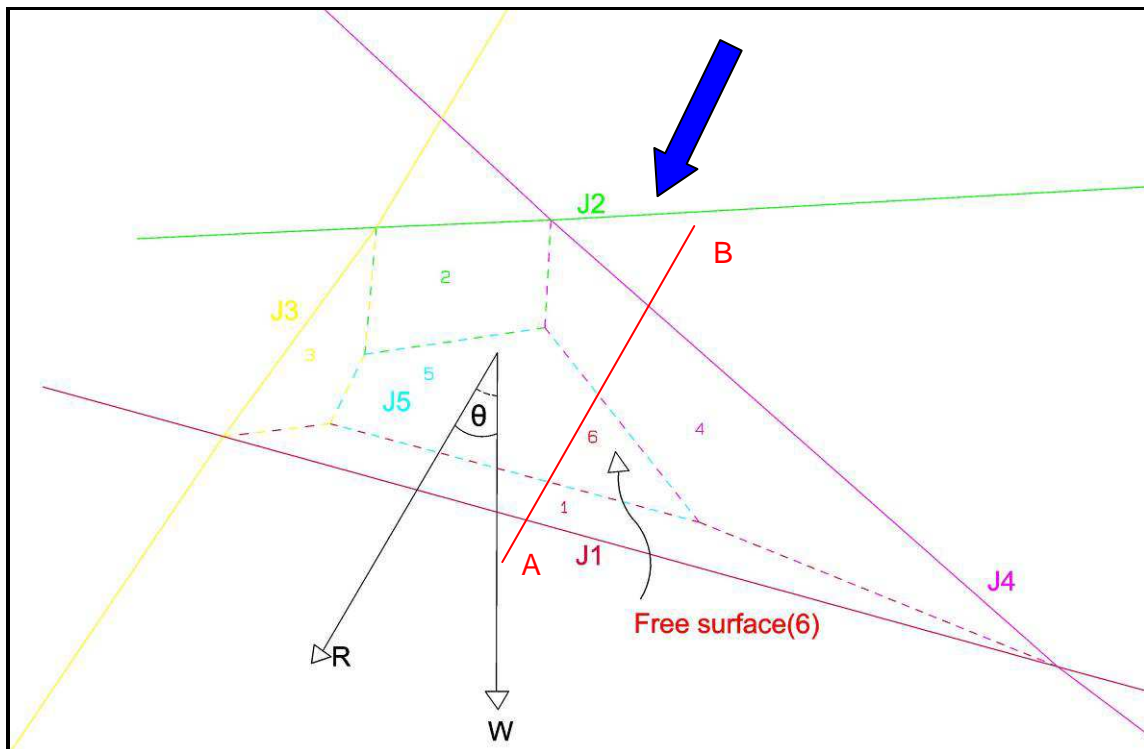


Fig.7 16: Block diagram showing Block 00000 on the spillway surface (6). J1 to J5 refer to the joints involved in forming the block. Blue arrow indicates direction of water flow. Red line AB indicates cross section shown in Fig.7.17. W (weight vector), R (Resultant after rotation),  $\theta$  (Angle of rotation)

## 7. Block removability analysis

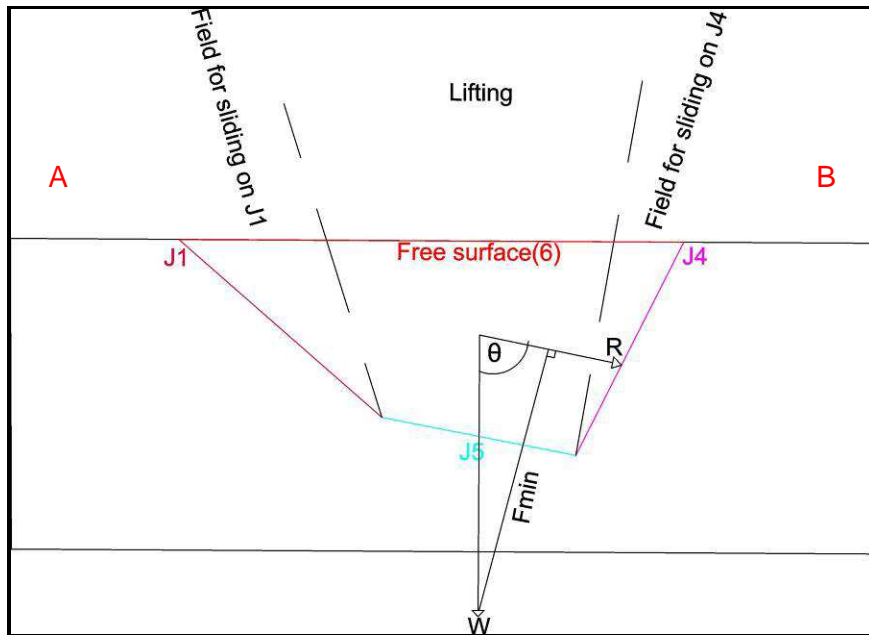


Fig.7 17: Cross section of the block diagram showing the principle of shifting the resulting force (i.e. weight vector (W)) by the angle of rotation ( $\theta$ ) to trigger a different failure mode.

In the following diagrams the Erodibility Spectra for the front slope, the spillway surface and the compound slope (Fig.7.18) will be presented for a friction angle ( $\phi$ ) of  $30^\circ$  and  $40^\circ$  (Fig.7.18 – 7.23).  $\theta$  values larger than  $90^\circ$  imply lifting for as a mode of failure. Nevertheless, the plot extends further, since the information if removal in a certain direction is possible at all would be lost. Not all JPs cover the whole spectrum from  $0 - 360^\circ$  (e.g. JP 10000, Fig.7.18).

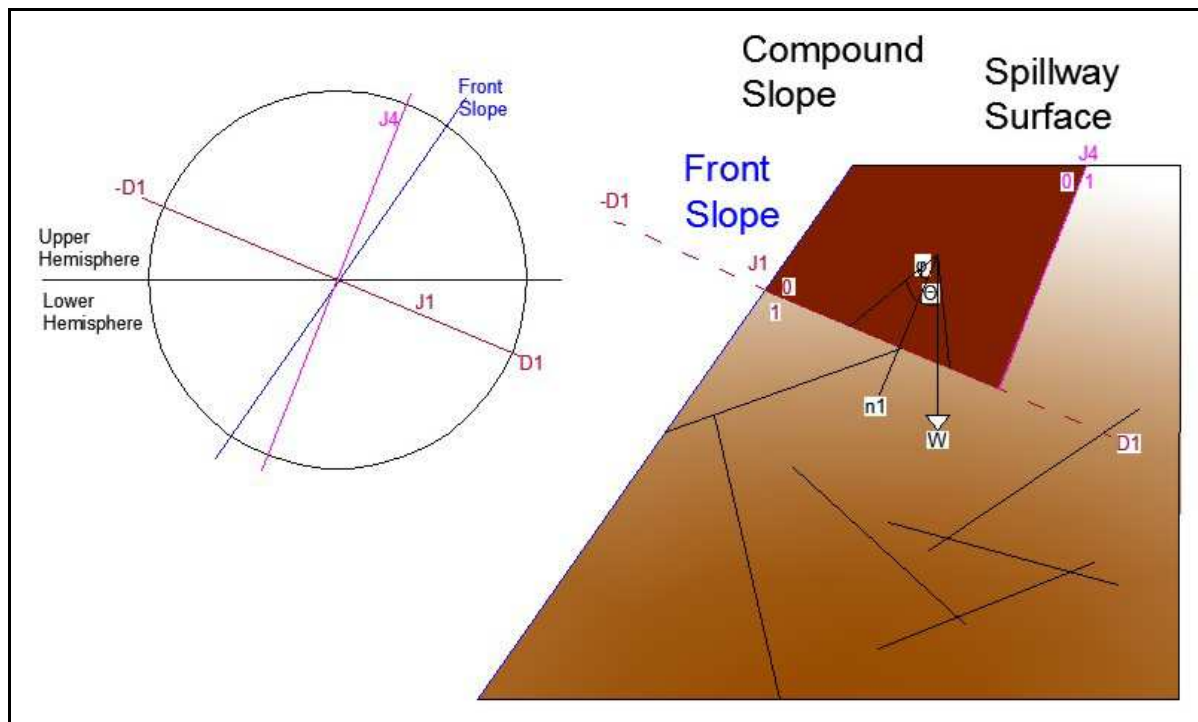


Fig.7 18: Schematic illustration of the front slope, spillway surface and compound slope. The dip vectors (-D1 & D1) should show how the mobilization takes place into the upper hemisphere along J1. In classic stability analysis this would not be possible since the plane of J1 doesn't daylight. 0 & 1 refer to joint halfspaces,  $\theta$  (Angle of rotation),  $\phi$  (friction angle), W (Weight vector), n1 (normal to J1).

## 7. Block removability analysis

### Front Slope

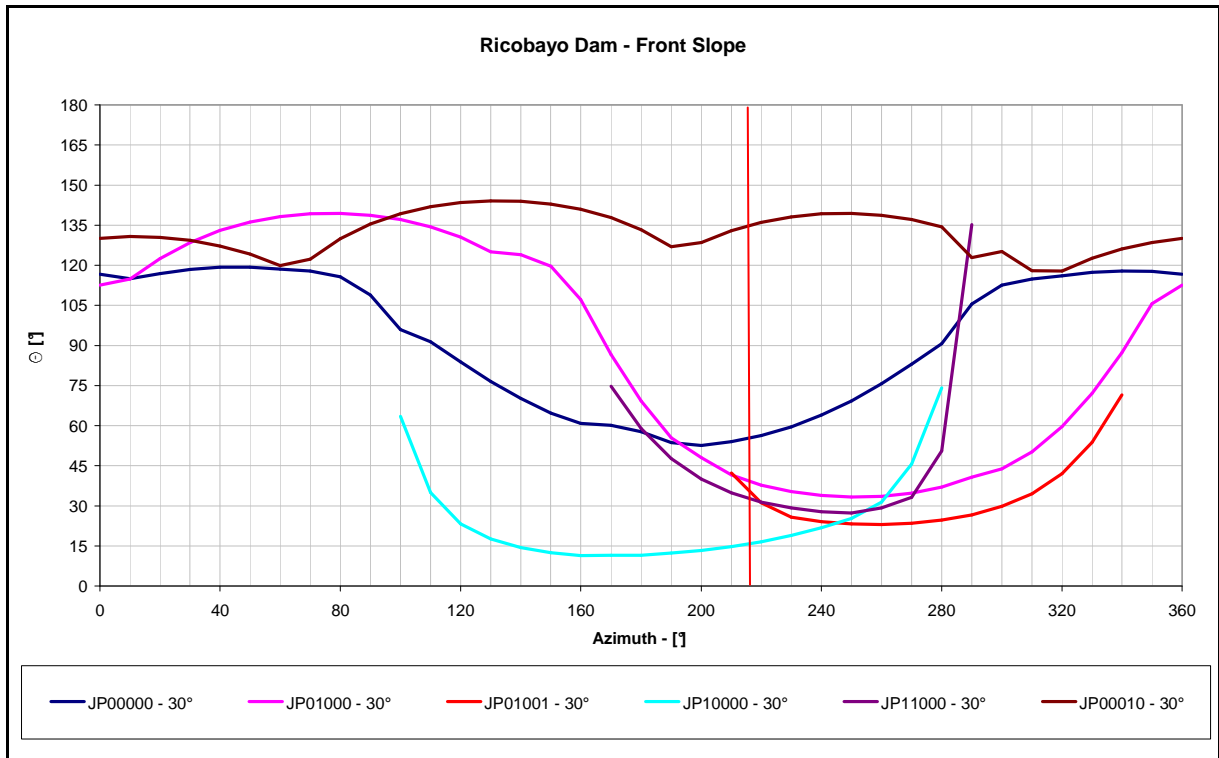


Fig.7 19: Block Erodibility Spectrum for the JPs of the front slope at  $\phi = 30^\circ$ . The spillway flow is oriented at 216 (vertical red line). Note that in this alignment the angle of rotation is close to its minimum for most blocks.

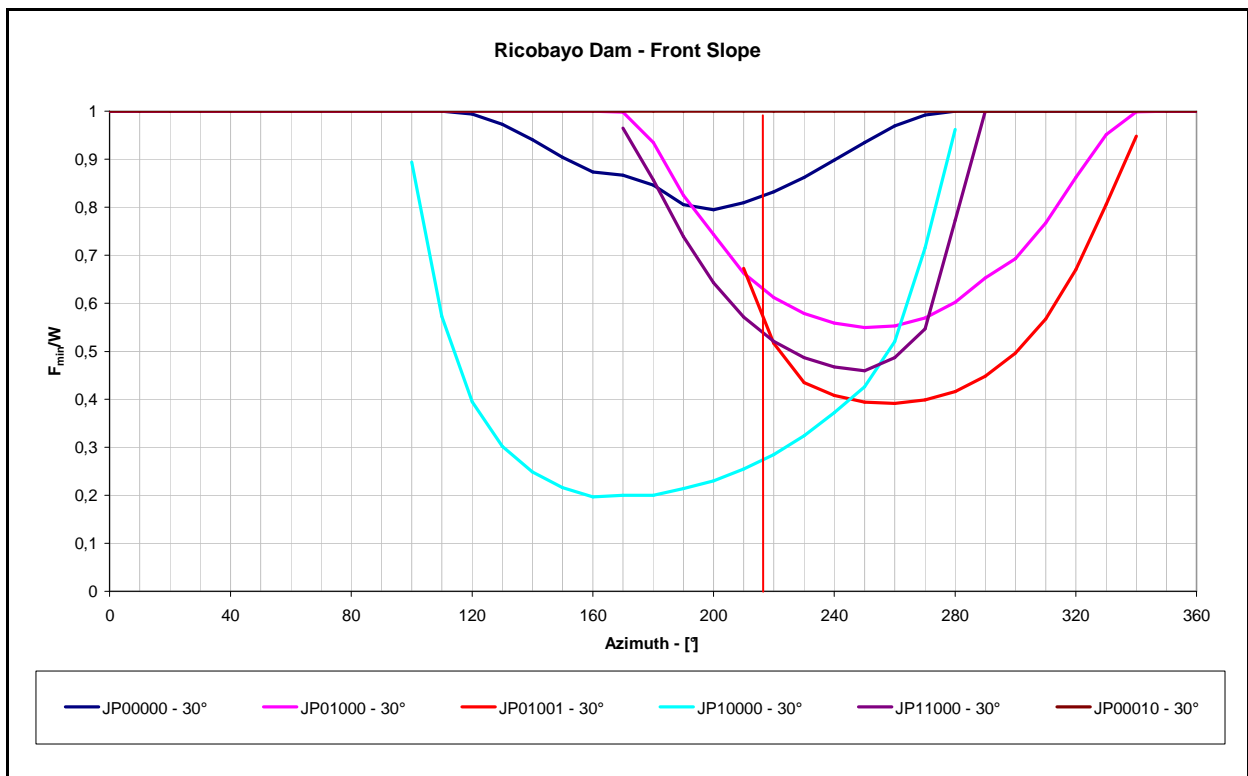


Fig.7 20: Block Erodibility Spectrum for the JPs of the front slope showing ratios of weight of individual blocks vs. the  $F_{min}$  at different azimuth orientations. In sections where the angle of rotation is small as shown in Fig.7.19 above, accordingly less force is required to mobilize block. Flow at vertical red line.

## 7. Block removability analysis

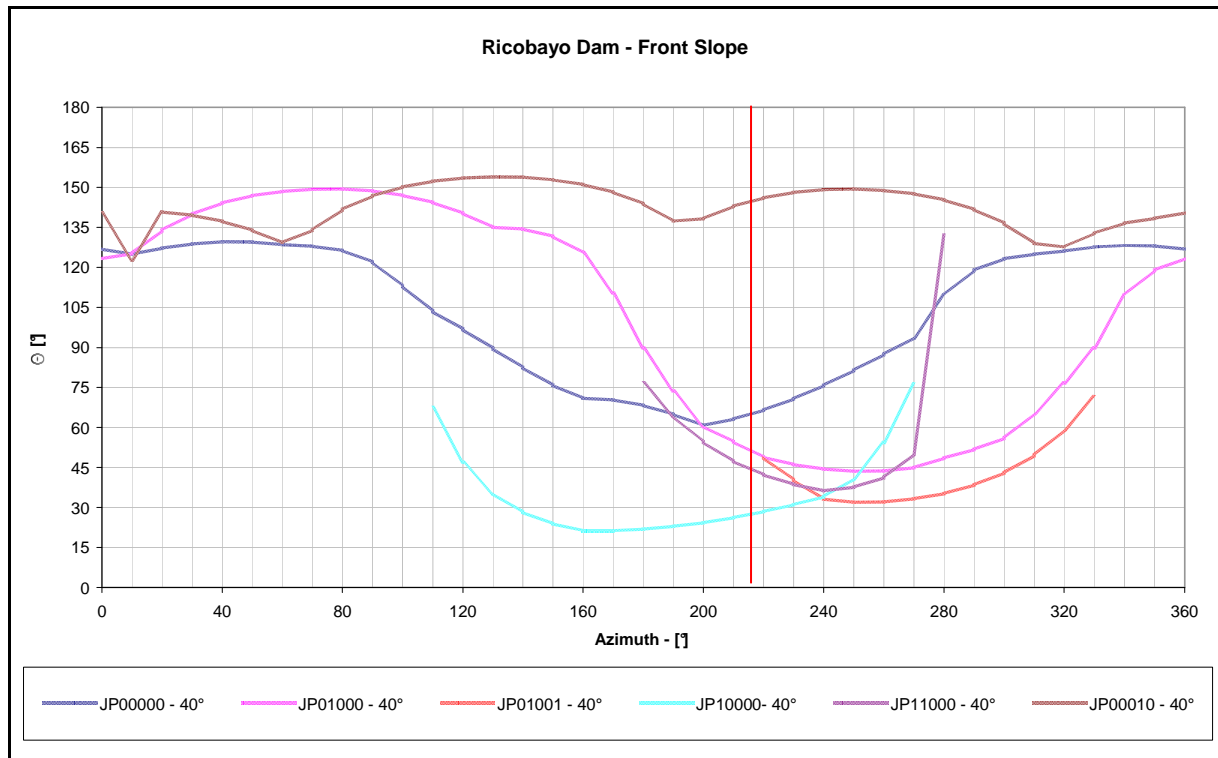


Fig.7 21: Block Erodibility Spectrum for the JPs of the front slope at  $\phi = 40^\circ$ . Plot is similar to the one shown in Fig.7.19 with  $30^\circ$  friction, but shifted to slightly higher values. The spillway flow is indicated by vertical red line.

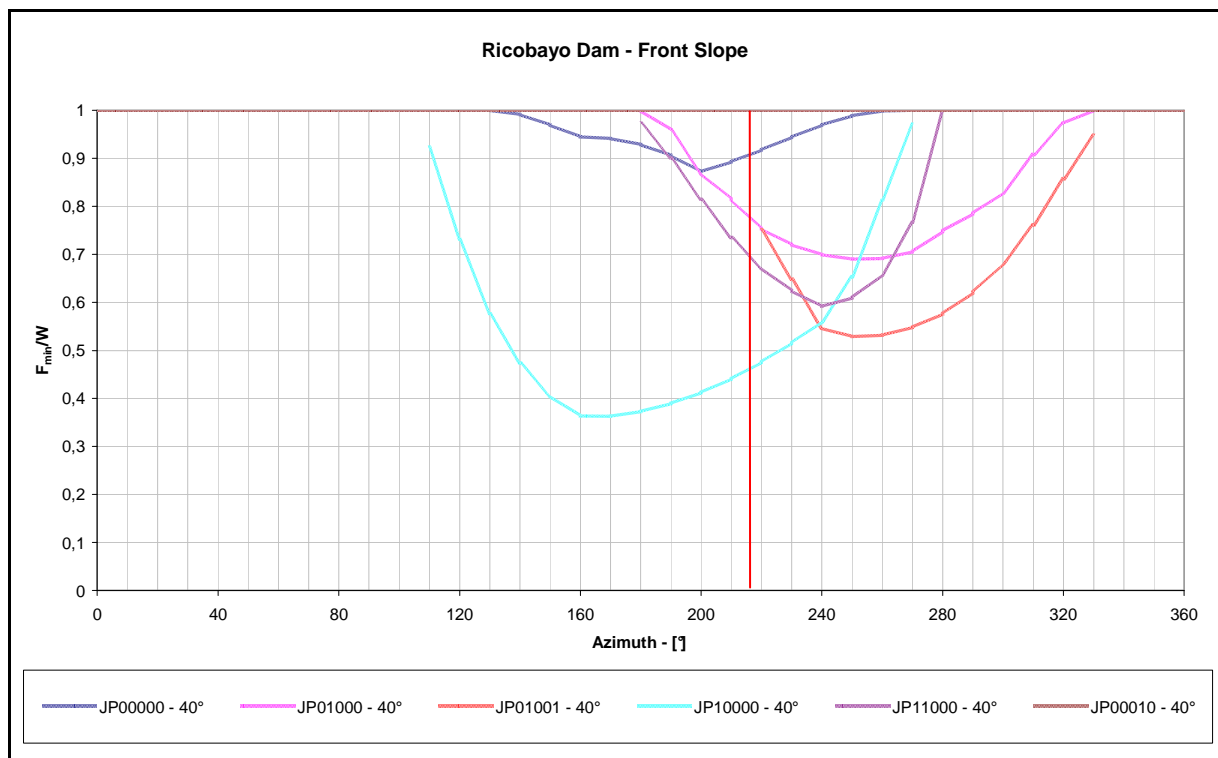


Fig.7 22: Block Erodibility Spectrum for the JPs of the front slope showing ratios of weight of individual blocks vs. the  $F_{min}$  at different azimuth orientations. The spillway flow is indicated by vertical red line.

7. Block removability analysis

From the above shown diagrams, the Block Erodibility Spectrum Envelope (Kieffer, 2011) is compiled to show the minimum composite requirements for the removal of any block type, i. e. where the first mobilization occurs (Fig.7.23). The related force envelope is shown in Fig.7.24.

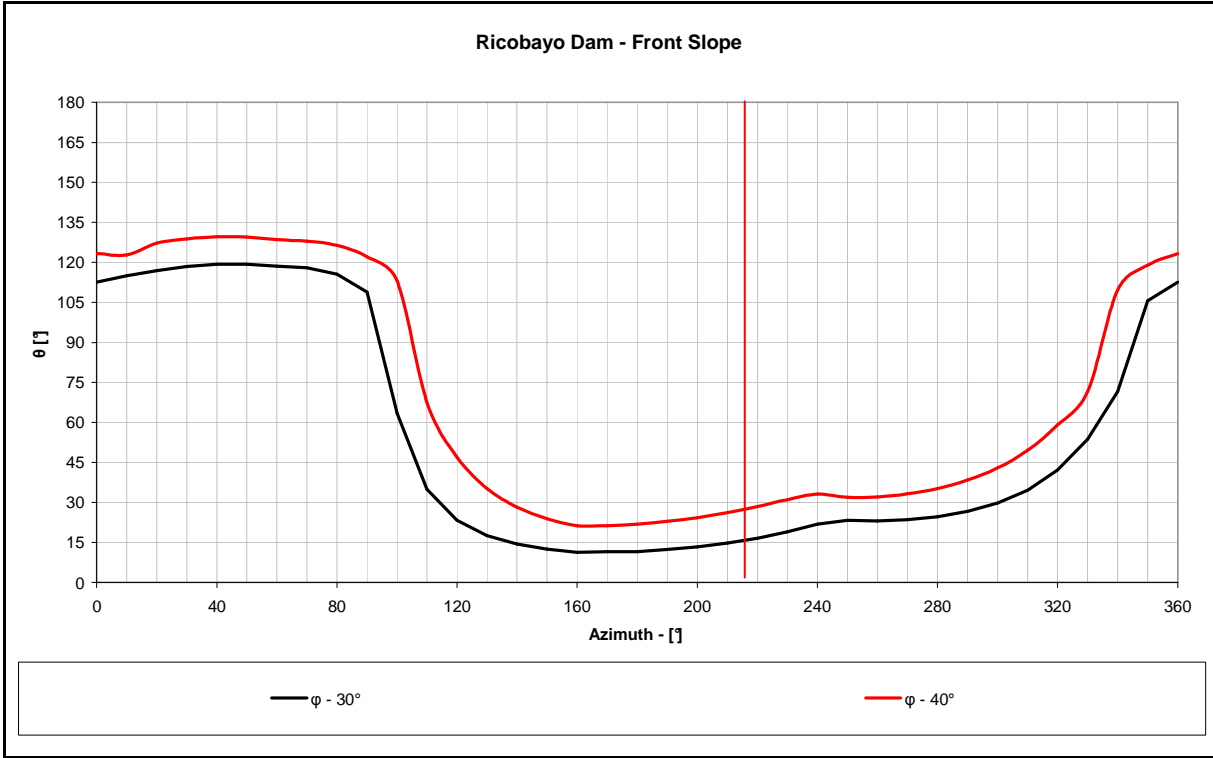


Fig.7 23: Block Erodibility Spectrum Envelope for the front slope for friction angles of 30° and 40°. Also here in the stability envelope it is visible how the angle of rotation drops to lower values in the orientation of the spillway at 216° (vertical red line).



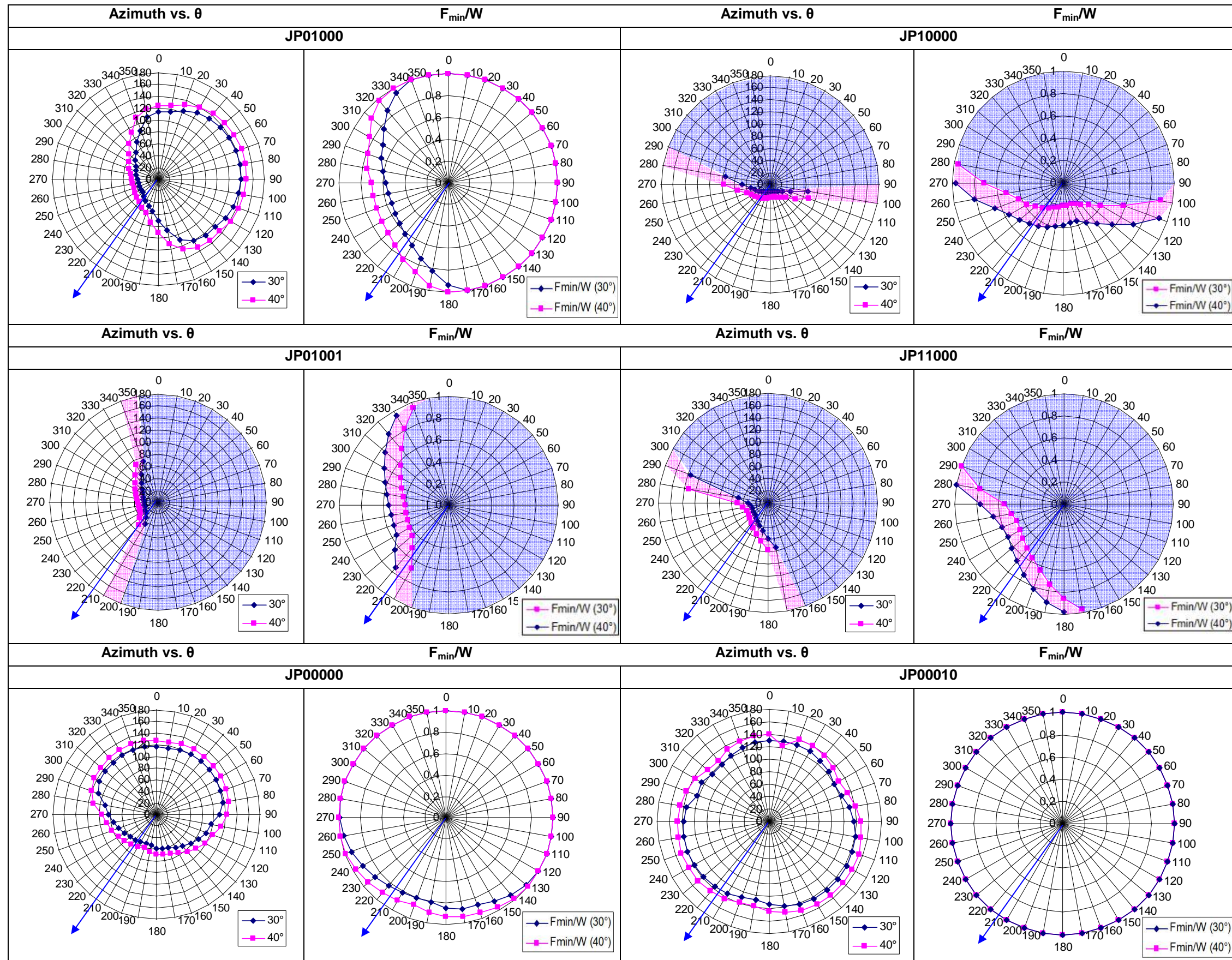
7. Block removability analysis



Fig.7 24: Minimal force envelope for the front slope for friction angles of 30° and 40°. The spillway flow is indicated by vertical red line.

For each JP, radar plots were computed to provide an alternative depiction of the orientation dependant requirements for block removal. The results are shown in Tab.7.5

7. Block removability analysis



Tab.7 5: Radar plots for the JPs of the front slope for friction angles of 30° and 40° and the related  $F_{min}/W$ . Blue arrow indicates the flow direction; shaded areas indicate fields of unconditionally stable conditions.

## 7. Block removability analysis

### Spillway Surface

In the following figures the Block Erodibility Spectra for the spillway surface are presented (Fig.7.25 - 7.29).

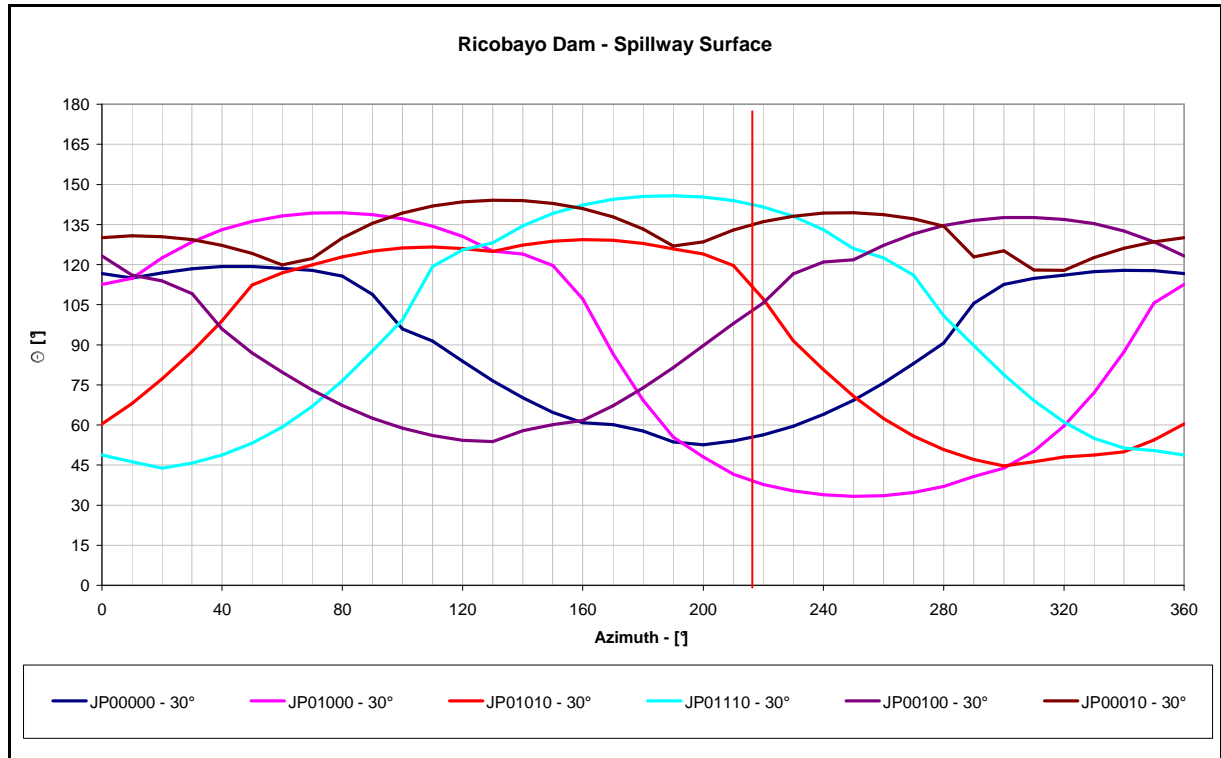


Fig.7 25: Block Erodibility Spectrum for the spillway surface. The minimum angle of rotation is not as critical as for the front slope. Vertical red line shows flow direction.

## 7. Block removability analysis

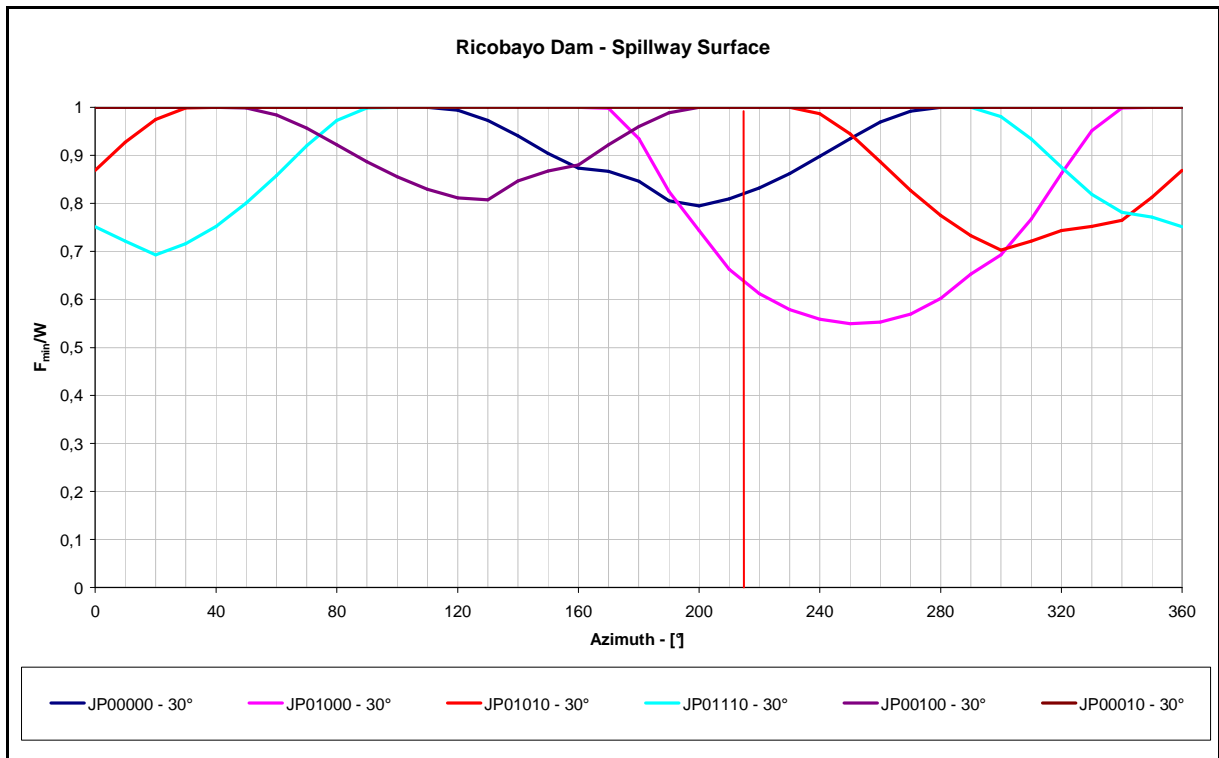


Fig.7 26: Block Erodibility Spectrum for the JPs of the spillway surface showing ratios of weight of individual blocks vs. the  $F_{min}$  at different azimuth orientations. Much more force is needed to mobilize blocks here than on the front slope. The spillway flow is indicated by vertical red line.

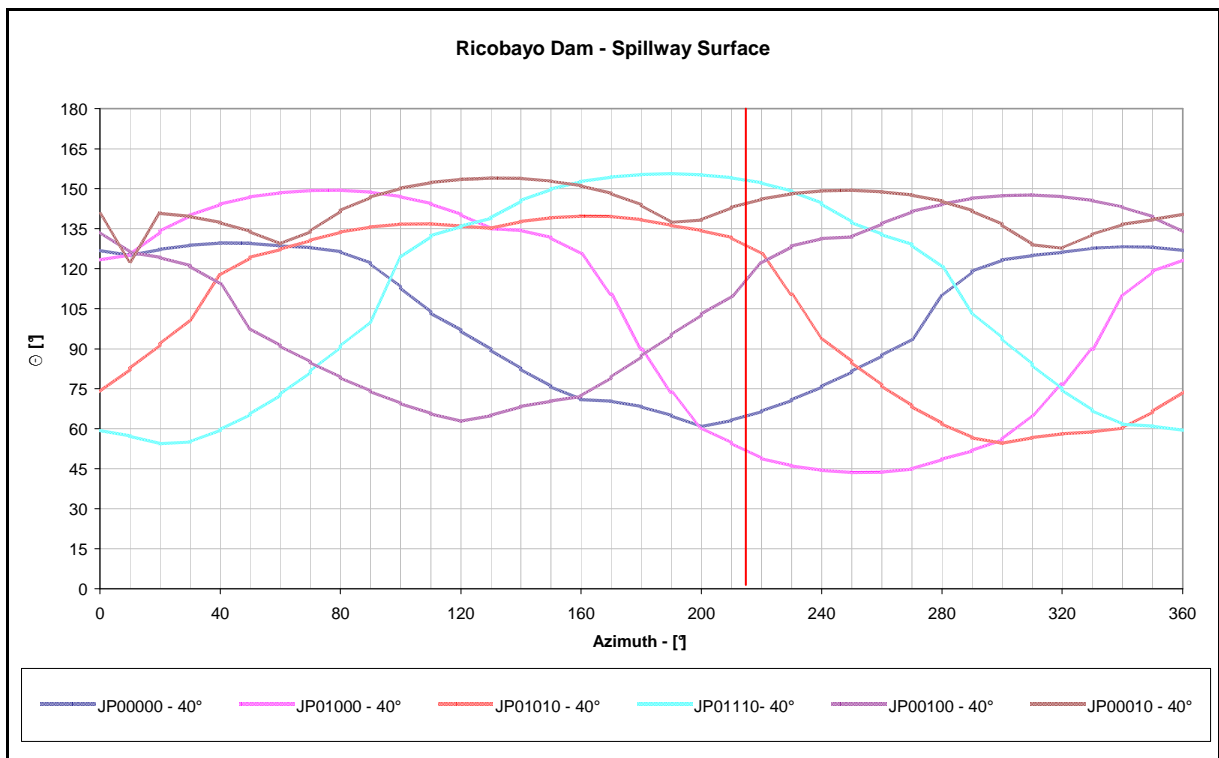


Fig.7 27: Block Erodibility Spectrum for the JPs of the spillway surface at  $\phi = 40^\circ$ . Plot is similar to the one shown in Fig.7.26 with  $30^\circ$  of friction, but shifted to slightly higher values. The spillway flow is indicated by vertical red line.

## 7. Block removability analysis

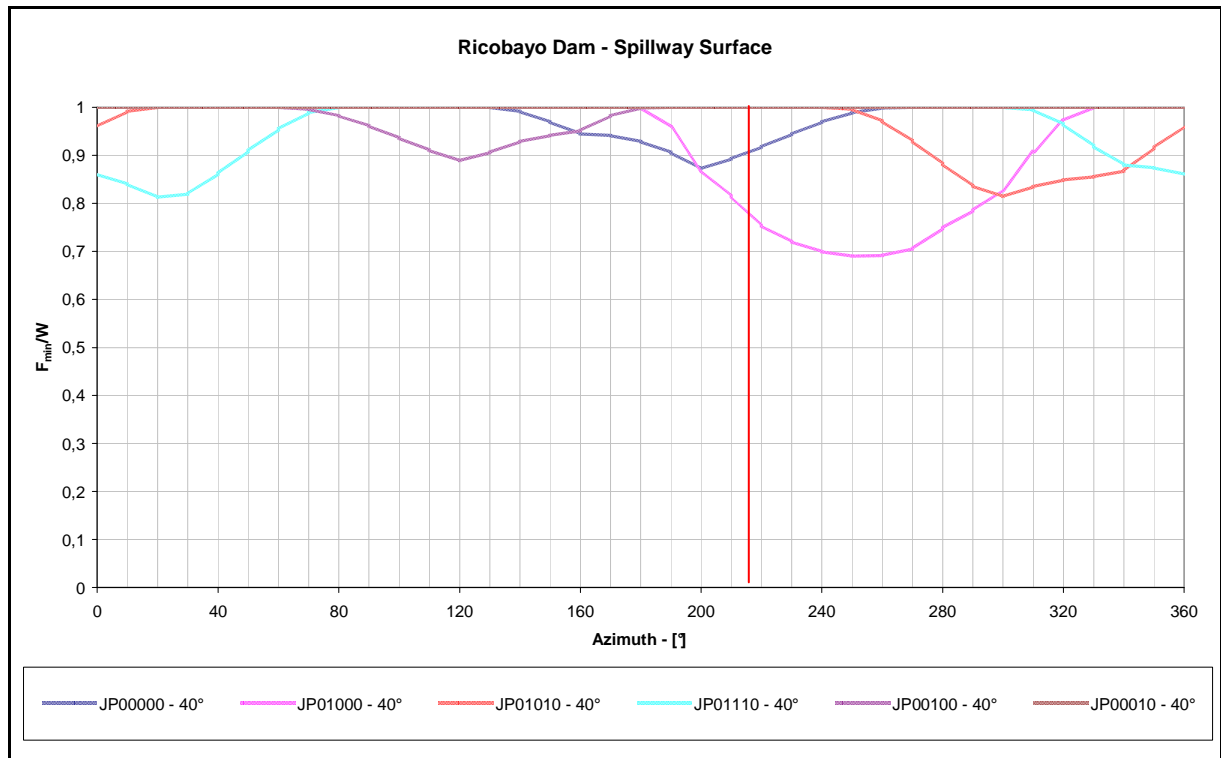


Fig.7 28: Block Erodibility Spectrum for the JPs of the spillway surface showing ratios of weight of individual blocks vs. the  $F_{min}$  at different azimuth orientations. The spillway flow is indicated by vertical red line.

The related stability envelope diagrams are compiled in Fig.7.29 and Fig.7.30.

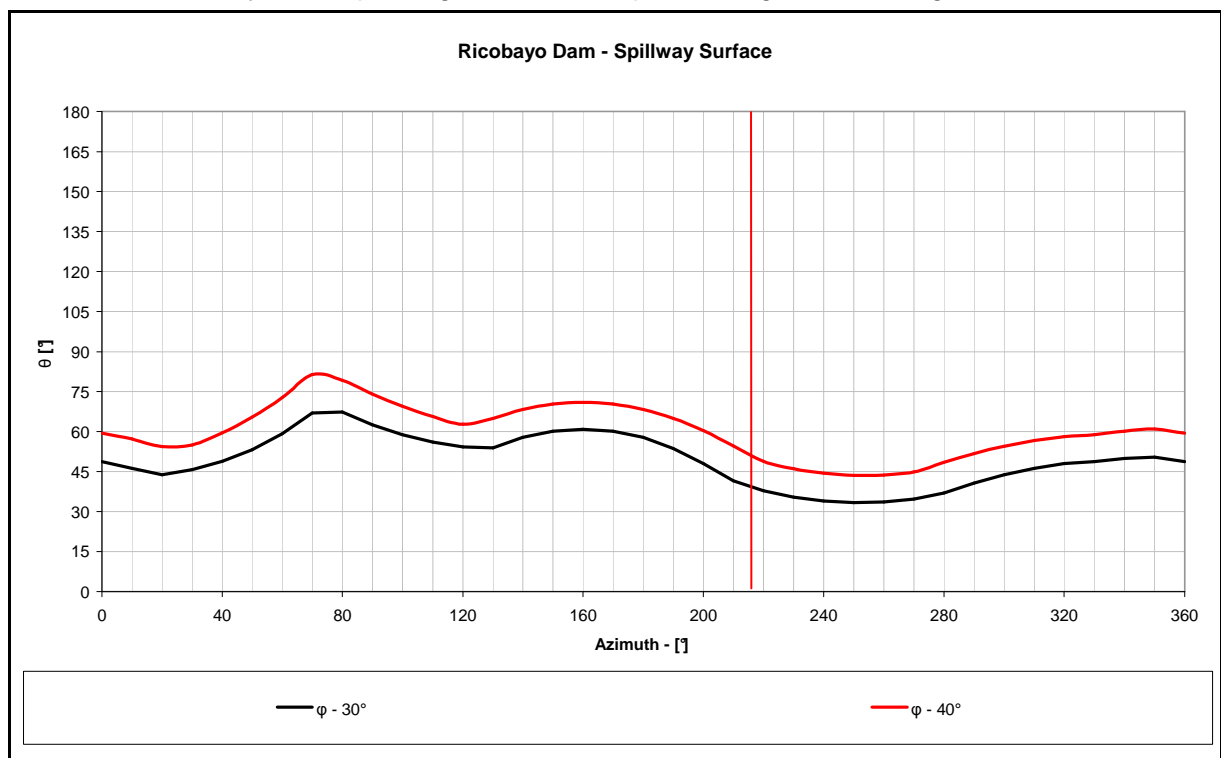


Fig.7 29: Block Erodibility Spectrum Envelope of the angle of rotation for the spillway surface for friction angles of 30° and 40°. The point of the first mobilization is quite uniform over the entire spectrum. The spillway flow is indicated by vertical red line.

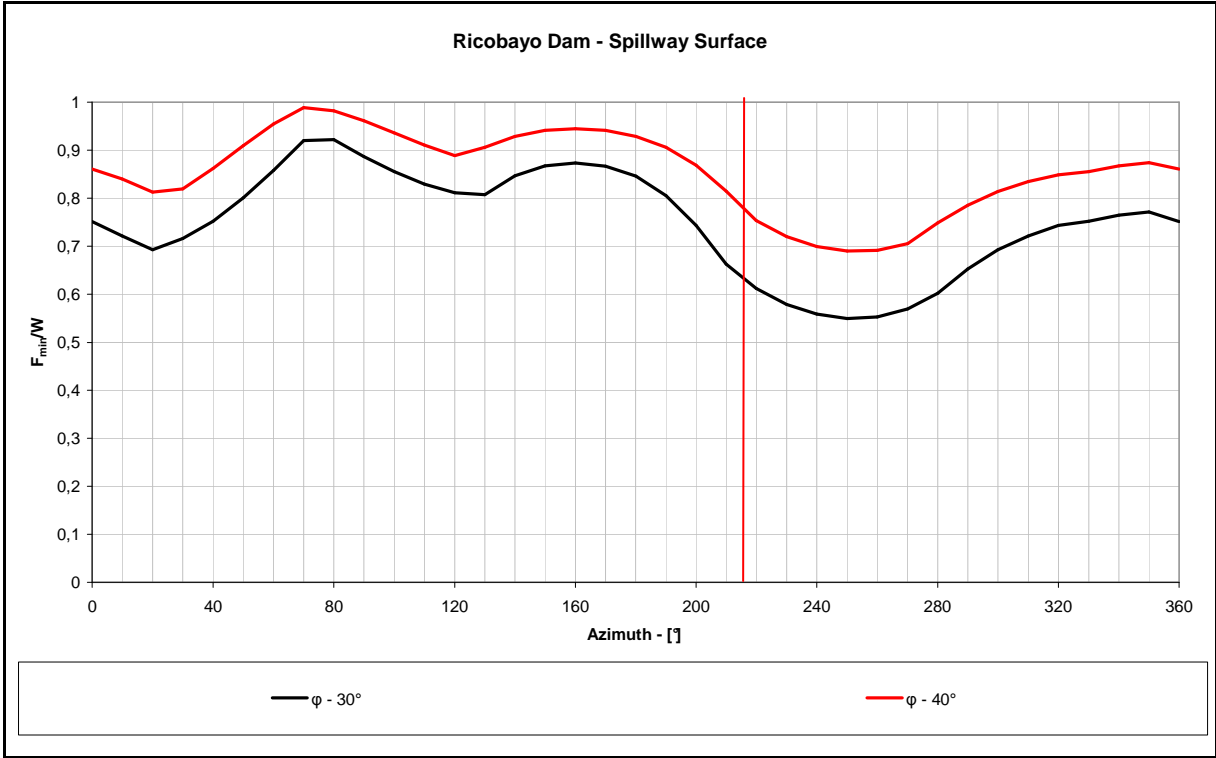
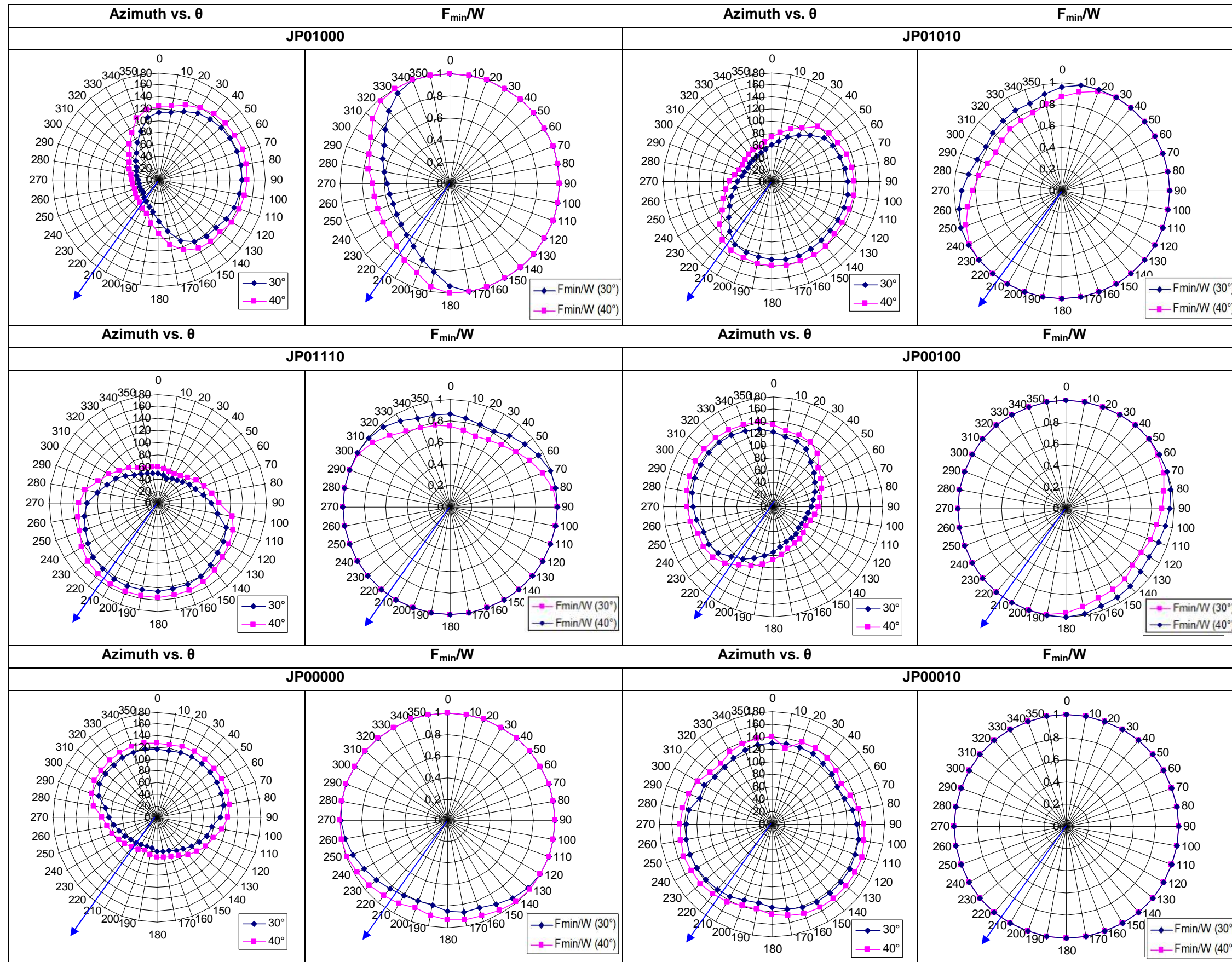


Fig.7 30: Minimal force envelope for the spillway surface for friction angles of 30° and 40°. The spillway flow is indicated by vertical red line.

The radar plots for the spillway surface are shown below (Tab.7.6). Only three JPs that are different from those of the front slope. JP00000, JP01000 and 00010 are the same as on the front slope.



Tab.7 6: Radar plots for the JPs of the spillway surface for friction angles of 30° and 40° and the related  $F_{min}/W$ . Blue arrow indicates the flow direction.

## 7. Block removability analysis

### Compound Slope

Finally, the Block Erodibility Spectrum for the compound slope was compiled (Fig.7.31- Fig.7.36). The compound slope is the combination of the spillway surface and the front slope. The removable JPs are therefore also the combination of the two, yielding 9 removable JPs.

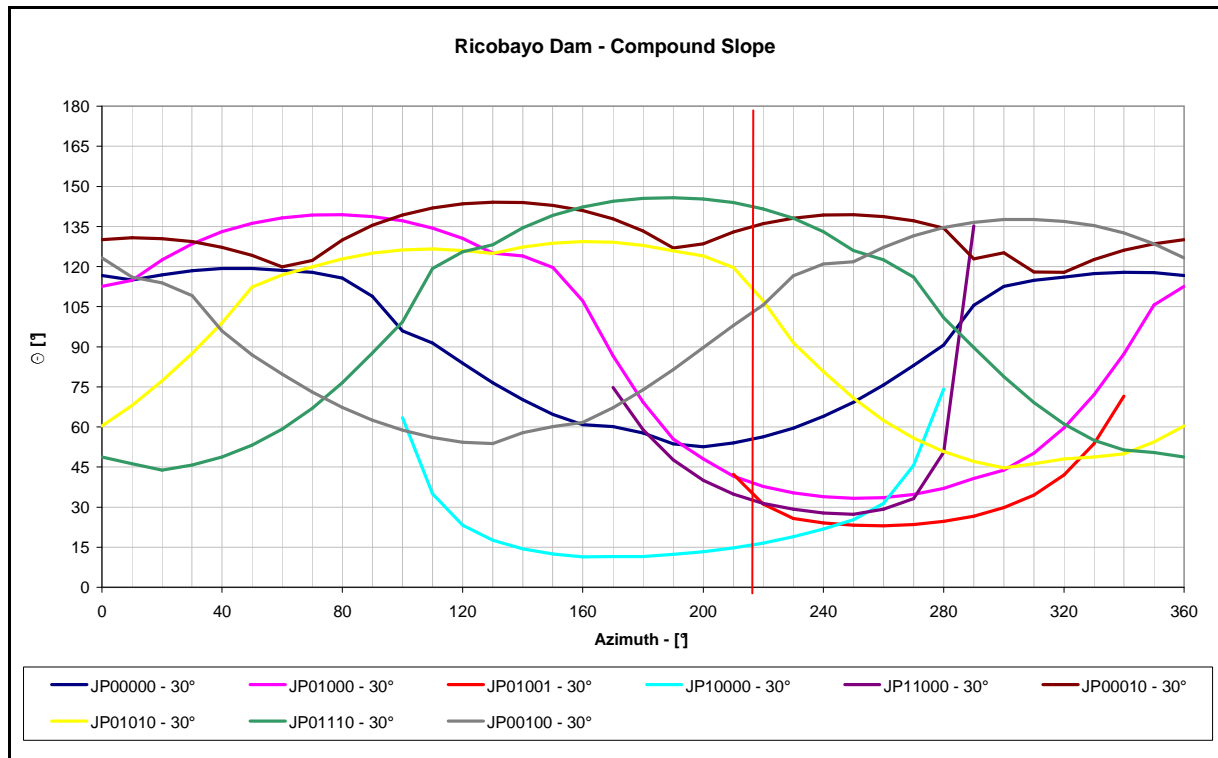


Fig.7 31: Block Erodibility Spectrum for the compound slope for a friction angle of 30°. Vertical red line indicates flow direction.



## 7. Block removability analysis

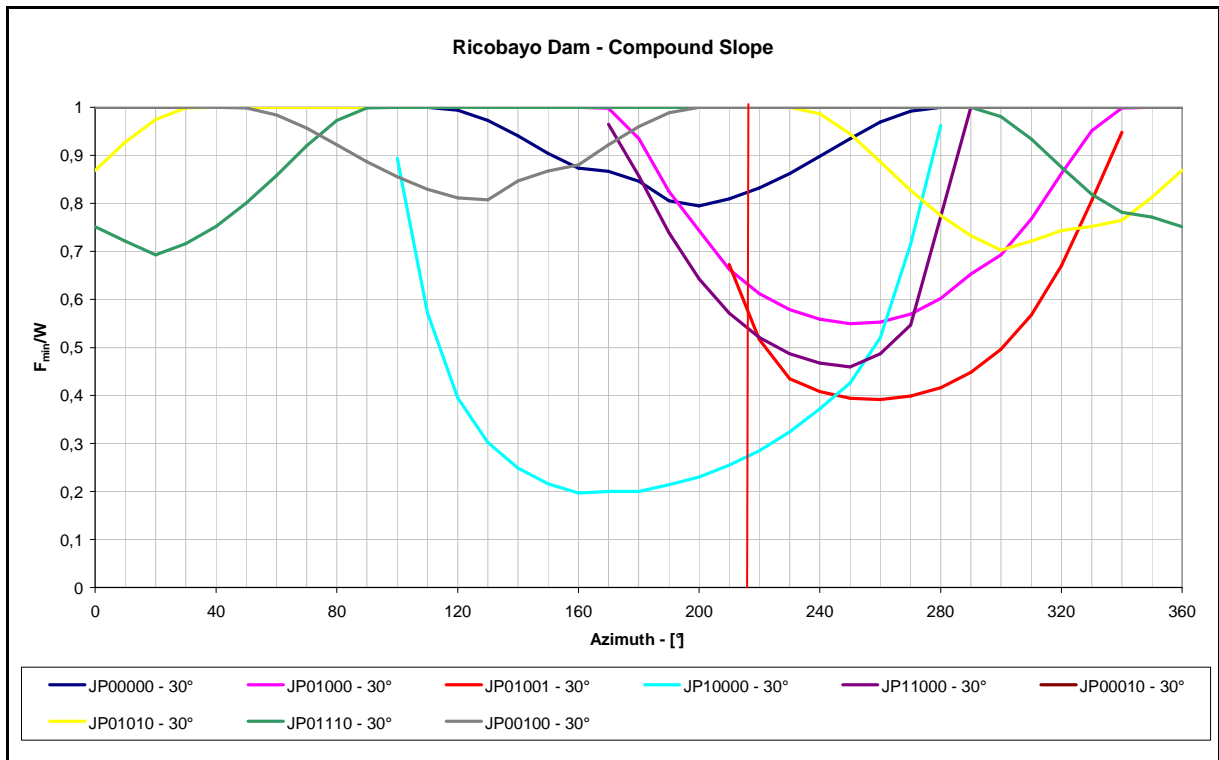


Fig.7 32: Block Erodability Spectrum for the JPs of the compound slope showing ratios of weight of individual blocks vs. the  $F_{min}$  at different azimuth orientations. The spillway flow is indicated by vertical red line.

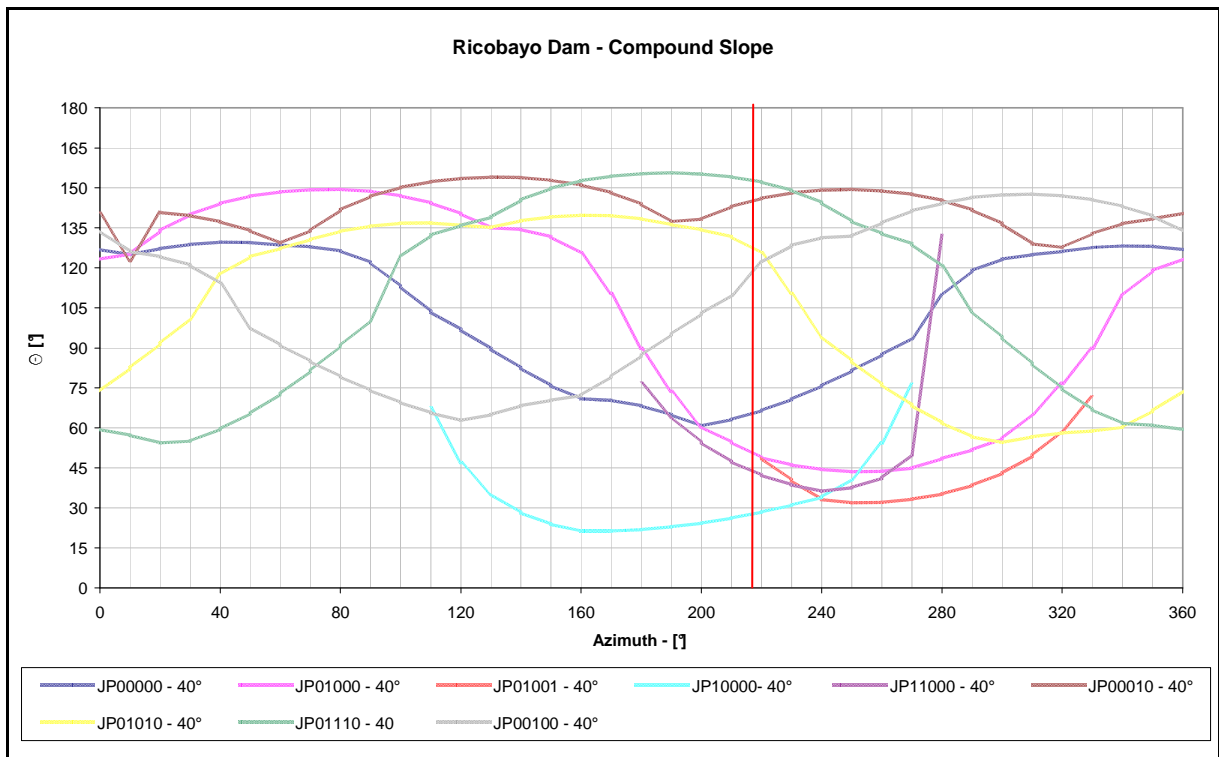


Fig.7 33: Block Erodability Spectrum for the compound slope for a friction angle of 40°. The spillway flow is indicated by vertical red line.

## 7. Block removability analysis

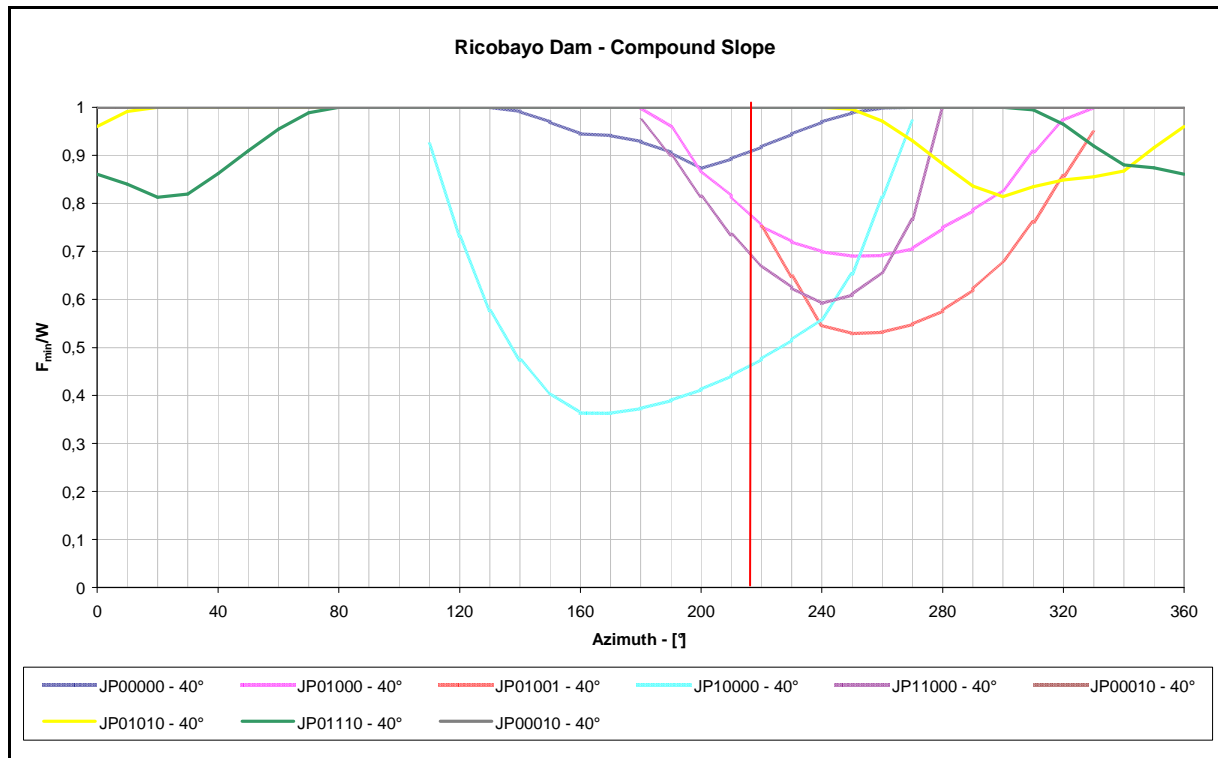


Fig.7 34: Block Erodability Spectrum for the JPs of the compound slope showing ratios of weight of individual blocks vs. the  $F_{min}$  at different azimuth orientations. The spillway flow is indicated by vertical red line.

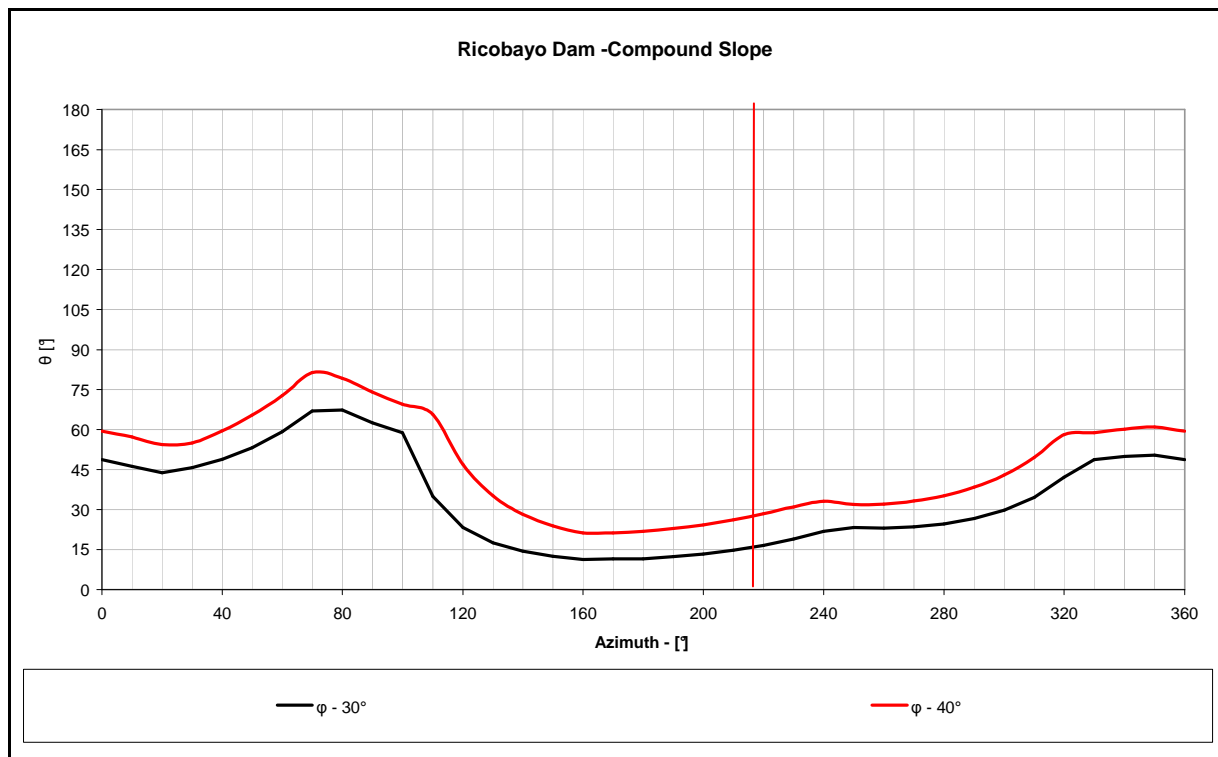


Fig.7 35: Block Erodability Spectrum Envelope of the angle of rotation for the compound slope for friction angles of 30° and 40°. The spillway flow is indicated by vertical red line.

7. Block removability analysis

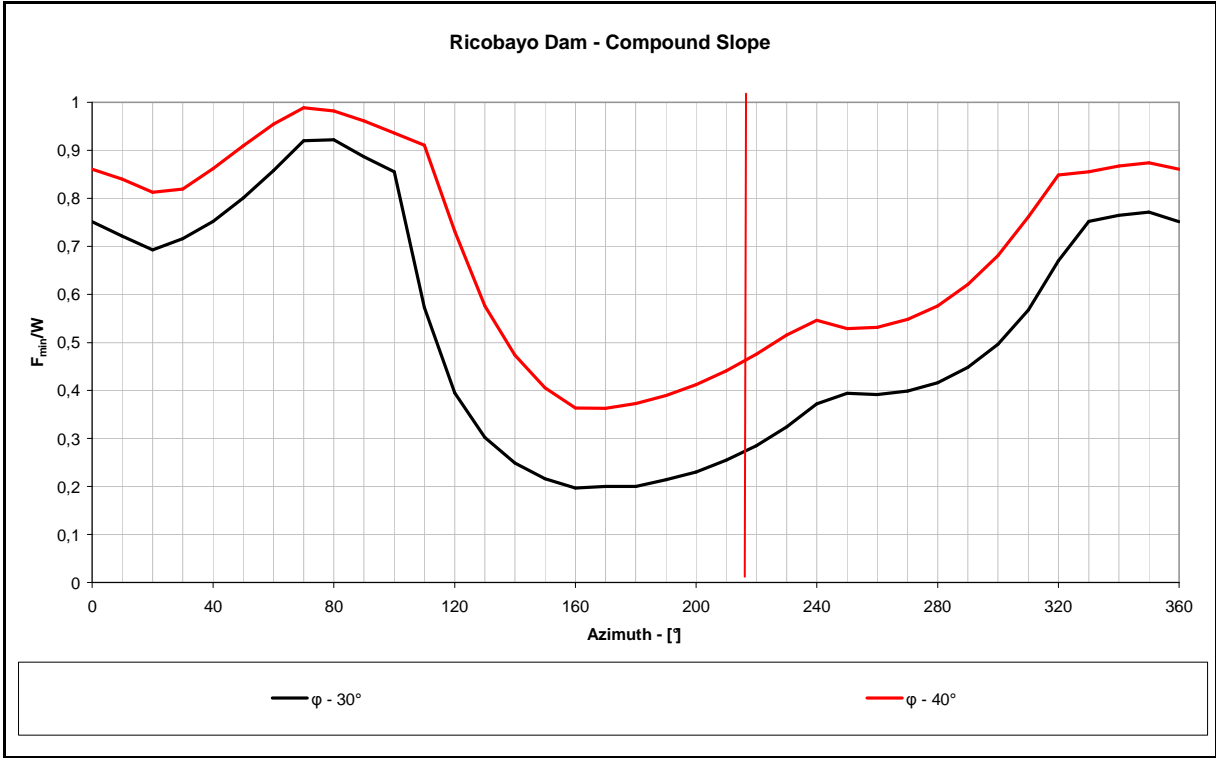
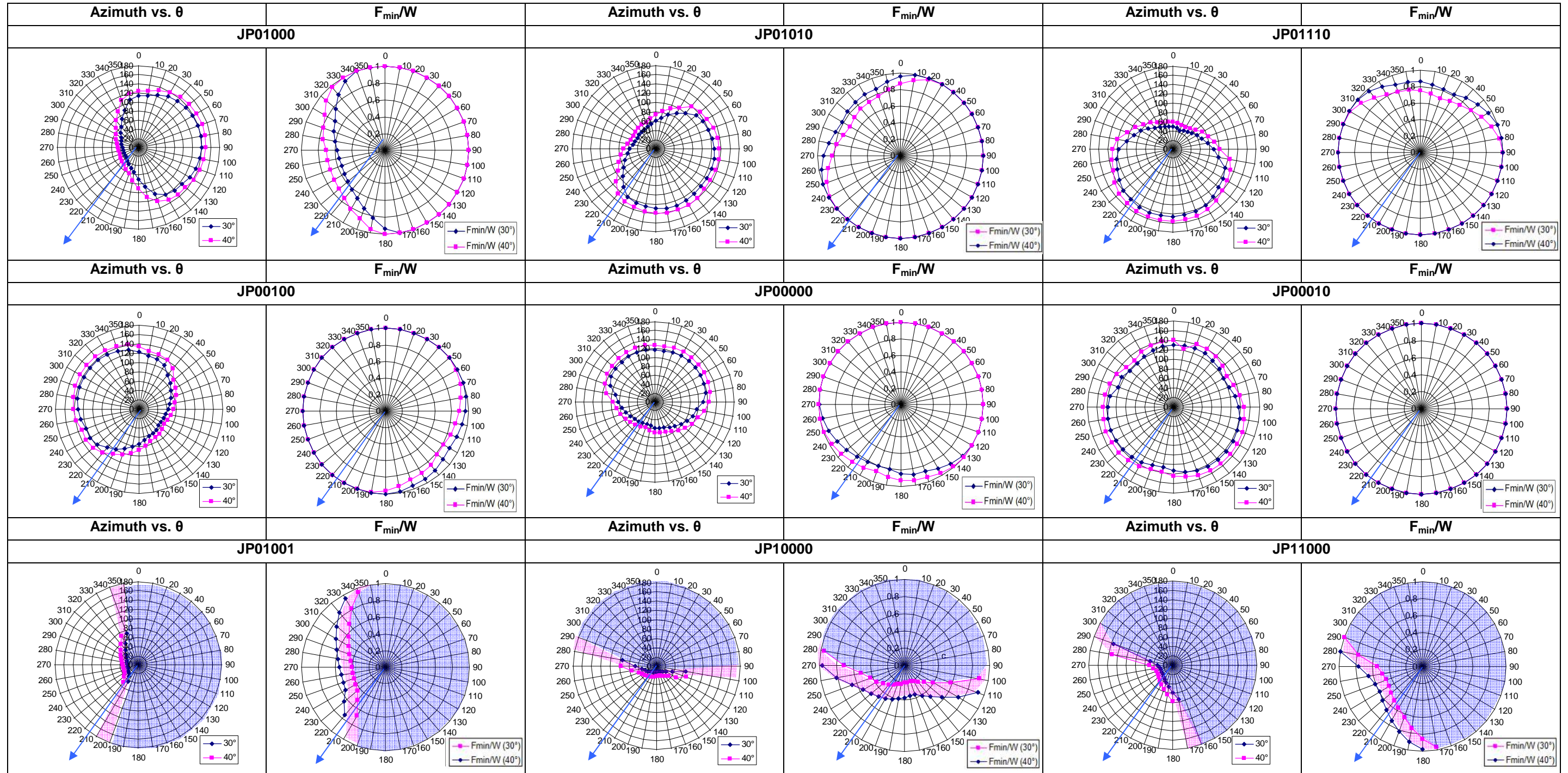


Fig.7 36: Stability Envelope of  $F_{min}$  for the compound slope. The spillway flow is indicated by vertical red line.

Radar plots for the compound are the combination of Tab.7.5 and Tab.7.6 and are presented in Tab.7.7.

7. Block removability analysis



Tab.7.7: Radar plots for the JPs of the compound slope for friction angles of 30° and 40° and the related  $F_{min}/W$ . Blue arrow indicates the flow direction; shaded areas indicate fields of unconditionally stable conditions.

### 8. Discussion and Conclusions

The block removability analysis using Block Theory enables a quite straight forward method to evaluate the removability of blocks from a rock mass. Applying the newly introduced “Block Erodibility Spectrum Analysis (BESA)” (Kieffer, 2011) the direction dependant susceptibility of scour can be recognized.

From the BESA it can be seen that for the mobilization of blocks the alignment of the spillway provides a highly unfavorable direction in terms of scour potential. Especially, the front slope is affected by quite easy mobilization of blocks. This would also support the fast upstream scour development towards the reservoir by a more or less parallel slope retreat due to knickpoint migration. Therefore lowering of the channel and so formed canyon and pool is not produced by lifting of blocks from the horizontal spillway surface. As the Block Erodibility Spectrum indicates mobilization of blocks on the spillway, would require significantly higher hydraulic force. It is also considered unlikely that the large scoured blocks (up to 35t, personal comment F. Faundez; Fig.8.1) could be removed under hydraulic forces operating on the approximately horizontal spillway.

From historical records, it is known that scour occurred in a “landslide/ blockfall” manner (Rocha, 2012). The heavily jointed rock mass enabled significant joint controlled failure of the slopes bounding the developing gorge. 3D stability analyses show that J4 and J1 were of particular importance in forming wedge and block slides. The high persistence and interlocking of the blocks form already blocks that do not require block rupturing to occur.

In the first scour stage in 1933, the inclined front slope started to develop rapids and cascades of its exposed blocks (Fig.8.2). Removal of near surface blocks commenced, leading to steepening and upstream migration of the slope via headcutting. Headcutting continued in scour stage 2 until the front slope, which turned into a head wall at that time, was protected with concrete. From the joint pattern observed in the field and removability analysis it can be concluded that blocks were activated along J4 and J5.

In the 3<sup>rd</sup> scour stage in 1935, the plunge pool began to form. The formation of the pool is linked to the fact that the concrete wall mitigated the scour further upstream, resulting in more local and permanent attack of the channel floor by the impinging waterfall. The lateral growth of the plunge pool was facilitated by block and wedge slides from the sidewalls (Rocha, 2012). Turbulent eddies produced by the impinging waterfall lifted blocks from the plunge pool invert, resulting in deepening of the pool.

In contrast to earlier stages, the 3<sup>rd</sup> scour stage produced quite uniform lowering of the outlet channel, which might be explained by peeling off since this surface was not as smooth as the artificial manmade spillway surface (Fig.8.2). The upstream migration of the front slope produced a more natural channel bed with blocks protruding out of it making the blocks more

## 8. Discussion and Conclusions

---

susceptible to scour. This stage is accompanied by the formation of bedrock terraces, which reflect the pattern of J1 on their flat surfaces.

In the 4<sup>th</sup> stage in 1936, when the concrete wall collapsed upstream migration was triggered again to a certain extent, but also the plunge pool grew significantly in depth during high discharge rates up to 1280m<sup>3</sup>/s.

The asymmetric shape of the plunge pool could be explained by the initial curved alignment of the spillway on the right side. Here the slight curvature (Fig.5.4) created a point bar like feature to the flowing water, which attacked the right wall stronger than the left wall.

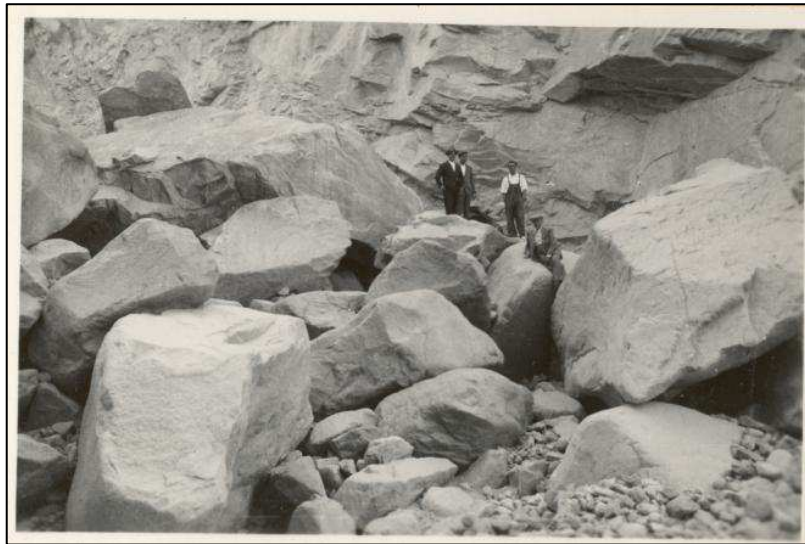


Fig.8 1: Photograph showing the size of scoured blocks after scour stage 2 in 1934.

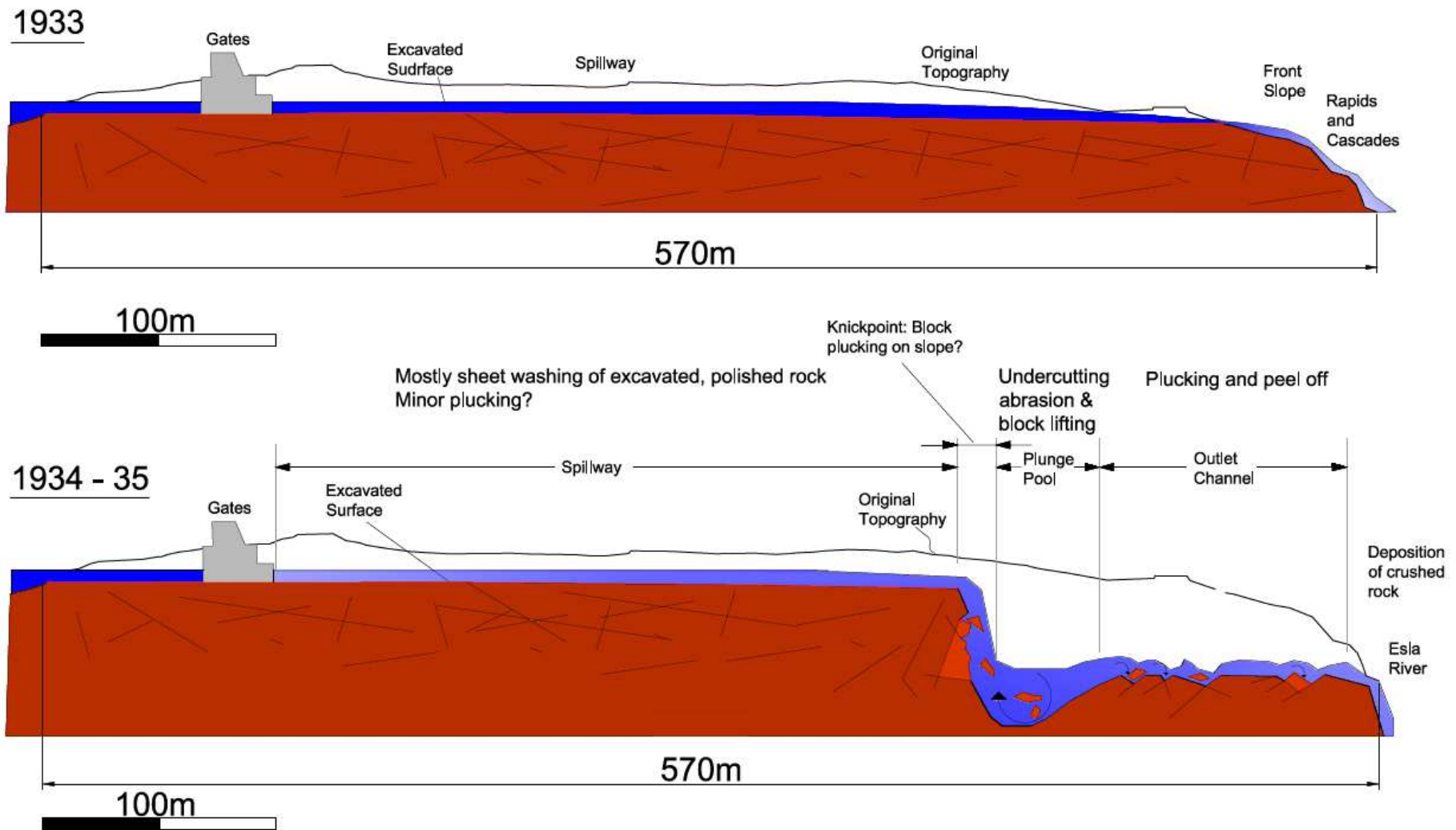


Fig.8 2: Schematic profiles illustrating the scour processes believed having shaped the appearance of the spillway in the years between 1933 and 1934 – 35, respectively.

## 9. References cited

- Annandale, G. W., Melville, B., & Chiew, Y.M., 2002: Scour Case Studies. *Mitteilungsblatt der Bundesanstalt für Wasserbau* Nr. 85.
- Annandale, G. W., 2005: *Scour Technology: Mechanics and Engineering Practice*, McGraw-Hill Professional, NY; 1 edition. 420p.
- Barton, N. R. 1973: Review of a new shear strength criterion for rock joints. *Engin. Geol.*, Elsevier, 7, 287–322.
- Barton, N. 1978: Suggested methods for the quantitative description of discontinuities in rock masses. *International Society of Rock Mechanics Commission on Standardization of Laboratory and Field Tests, International Journal of Rock Mechanics and Mining Sciences and Geomechanical Abstracts*, 15, 319–368.
- Bell, F. G., 2007: *Engineering geology*. 2nd ed., Butterworth-Heinemann. ISBN 0750680776, 9780750680776, 581p.
- Brierley, G., J., & Fryirs, K., A. 2005: *Geomorphology and river management: applications of the river styles framework*. John Wiley & Sons, ISBN 1405115165, 9781405115162, 398p.
- Bollaert, E. F. R. 2002: Transient water pressures in joints and formation of rock scour due to high-velocity jet impact. *Communication of the laboratory of hydraulic construction (LHC)*, No. 13 EPFL, Lausanne, ISSN 1661- 1179
- Bollaert, E. F. R. & Schleiss, A. 2003a: Scour of rock due to the impact of plunging high velocity jets Part II: Experimental results of dynamic pressures at pool bottoms and in one- and two-dimensional closed end rock joints. *Journal of Hydraulic Research* Vol. 00, No. 0 (2003), pp. 1–16
- Breithaupt.de: <http://www.breithaupt.de/en/products/magnetic-compasses/geological-compasses/cocla/>
- Cameron, C. P., Patric, D. M., Kato, K. D. & May, J. H. 1988: Geotechnical aspects of rock erosion in emergency spillway channels, Report 2, Analysis of field and laboratory. Technical Report REMR-GT-3, US Army Corps of Engineers
- Crosby, B. T. & Whipple, K. X. 2006: Knickpoint initiation and distribution within fluvial networks: 236 waterfalls in the Waipaoa River, North Island, New Zealand. *Geomorphology*, Vol. 82, 1–2, pp. 16-38
- Deere, D.U. and Deere, D.W. 1988. The rock quality designation (RQD) index in practice. In *Rock classification systems for engineering purposes*, (ed. L. Kirkaldie), ASTM Special Publication 984, 91-101. Philadelphia: Am. Soc. Test. Mat
- Diego Martín, Y. 2007 in *Nec otium*, XIX, XX, XXI: comercio e industria en Zamora. Museo Etnográfico de Castilla y León, Museo Etnográfico de Castilla y León (Zamora, Espagne), ISBN 849357810X, 9788493578107, 371p.
- Fernandez- Turiel, J., L., Saavedra, J., R. Vaquer, R., Duran, M., E. & Querol, X. 1991: Late and postmagmatic alterations in the tin-bearing batholith of Ricobayo (Iberian Massif, NW Spain). *Acta Geologica Hispanica*, v. 26, no1, p17- 22.



## 9. References cited

---

González Clavijo, E., & Martínez Catalán, J.R., 2002: Stratigraphic record of preorogenic to synorogenic sedimentation, and tectonic evolution of imbricate units in the Alcañices synform (northwestern Iberian Massif), in Martínez Catalán, J.R., Hatcher, R.D., Jr., Arenas, R., and Díaz García, F., eds., Variscan-Appalachian dynamics: The building of the late Paleozoic basement: Boulder, Colorado, Geological Society of America Special Paper 364, p. 17–35.

Google Maps, 2012: Maps and image requests. <http://maps.google.at/>

Goodman, R. E., Shi, G. 1985: Block Theory and its applications to rock mechanics. Prentice- Hall International Series in Civil Engineering and Engineering Mechanics. 338p

Goodman, R., & Shi, G. H. 1989: Block theory software package. University of California-Berkeley.

Grant, G.E., Swanson, F.J. and Wolman, M.G. 1990: Pattern and origin of stepped-bed morphology in high gradient streams, Western Cascades, Oregon. Geological Society of America Bulletin 102, 340–352

Guia Técnica de Seguridad de Presas - Aliviaderos y Desagües - AMI Ricobayo, 1997

Hallet, B., 1996: Glacial quarrying: A simple theoretical model: Annals of Glaciology, v. 22, p. 1–8.

Howard, A. D., 1996, Gradient control in mixed alluvial-bedrock rivers, in: Fort Collins, Colorado State University, Bedrock Channels Conference.

Iberdrola(a), 2011: Iberdrola- a history with deep roots. Information brochure by the company.

Iberdrola(b), 2011: Ricobayo scheme. Information brochure of the dam.

Iberduero S.A., year unknown: Salto de Ricobayo- Aliviadero. 7p

Iberduero S.A, 1937: Planta del aliviadero: modificaciones. Scale 1:500, Plan Nr. 3365.

Iberduero S.A, 1947: Proyecto de Consolidación del Canal Aliviadero. Hoja núm 2, Perfil longitudinal general.

Iberduero S.A, 1984: Salto de Ricobayo II, Estudios y Proyectos, Topografía Aerofotogrametría, Scale 1:1000. Plan Nr. 234.175-8

Iberduero S.A, 1986: Salto de Ricobayo II, Geotechnical report.

IGME (Instituto Geológico y Minero España), 1978: Mapa Geológico de España (Hoja número 368, Carbajales de Alba), Scale 1:50.000.

ISRM, 1981: Rock characterization, testing & monitoring: ISRM suggested methods. E. T. Brown (Ed.), International Society for Rock Mechanics. Commission on Testing Methods. Published for the Commission on Testing Methods, International Society for Rock Mechanics by Pergamon Press. ISBN. 0080273084, 9780080273082. 211p

Kieffer, D.S. 2011: The Block Erodibility Spectrum Analysis personal communication.

Kirsten, H.A.D. 1982: A Classification System for Excavation in Natural Materials, The Civil Engineer in South Africa, pp. 292–308, July (discussion in Vol. 25, No.5, May, 1983).

## 9. References cited

---

- Knighton, A.D. 1998: *Fluvial Forms and Processes: A New Perspective*. Arnold, London.
- Langley, D.E., 2006: Calculation of scour depth at the Parks Highway Bridge on the Tanana River at Nenana, Alaska, using one- and two-dimensional hydraulic models: U.S. Geological Survey Scientific Investigations Report 2006-5023, 19 p.
- Leopold, L. B., Wolman, M. G. & Miller, J. P. 1964: *Fluvial processes in geomorphology*, 2nd Ed., Courier Dover Publications, 1995, ISBN 0486685888, 9780486685885, 522p
- Li, A. & Liu, P., 2010: Mechanism of rock-bed scour due to impinging jet. *Journal of Hydraulic Research* Vol. 48, No. 1, pp. 14–22.
- May, J. H. 1989: Geotechnical aspects of rock erosion in emergency spillway channels; Report 4: geologic and hydrodynamic controls on the mechanics of knickpoint migration. Technical Report REMR-GT-3, US Army Corps of Engineers
- Milne, D., Germain, P., and Potvin, Y., 1992: *Measurement of Rock Mass Properties for Mine Design*, Proceedings of the ISRM- Eurock Symposium on Rock Characterization, A.A. Balkema Publishers, Chester, England.
- Miller, J.R. 1991: The influence of bedrock geology on knickpoint development and channel-bed degradation along downcutting streams in south-central Indiana. *Journal of Geology* 99, 591-605.
- Montgomery, D.R. & Buffington, J.M. 1997: Channel reach morphology in mountain drainage basins. *Geological Society of America Bulletin* 109(5), 596–611
- Obregozo, J. 1924: *Características et bref aperque des projets. (a) Production d' energie hydraulique*. World power conference, London.
- Palmström, A. 1982. The volumetric joint count - a useful and simple measure of the degree of rock jointing. *Proc. 4th Congr. Int. Assn Engrg Geol.*, Delhi 5, 221-228.
- Price, D. G. & De Freitas, M. H. 2009: *Engineering geology: principles and practice*. Springer, ISBN 3540292497, 9783540292494. 450p.
- Rance, H. 2007: *The present is the key to the past: Topics in Historical Geology*. eGeobooks, ISBN 0970442335, 9780970442338, 854p.
- Richardson, E.V. and Davies, S.R. 1995: *Evaluating scour at bridges* fourth edition. Pub. No. FHW NAI-01-001 (HEC 18), Federal Administration, U.S. Department of Transportation, Washington, D.C.
- Riesco Chueca, P. 2009: *El embalse de Ricobayo y la visita en 1934 de Theodor Rehbock*. 11p.
- Revista de Obras Públicas*, 1933: Algunas consideraciones régimen hidráulico pie de presas y su aplicación a los ensayos vertedero del Esla, No. 2629, p397- 403.
- Rocha, L. F. 2012: *Response of Ricobayo Dam spillway walls to extensive rock scour*. Master Thesis, Graz University of Technology.
- Rubio, R. 1940: El túnel aliviadero del salto del Esla, *Revista de Obras Públicas*, No. 2705, pp. 157-161.
- San Román, E. (Compiladora), 2006: *cien años de historia de Iberdrola: la historia económica*. Iberdrola. ISBN 8493498904, 9788493498900. 205p

## 9. References cited

---

Seidl, M. A. & Dietrich, W. E. 1992: The Problem of Channel Erosion into Bedrock, *Catena Supplement* 23, 101- 124, Cremlingen.

SEPREM (Sociedad Española de Presas y Embalses), 2012: Presa: Ricobayo, <http://www.seprem.es/ficha.php?idpresa=912&p=36> Sociedad Hispano Portuguesa de Transpotes Electricos, 1927: Proyecto de aprovechamiento de aguas del Rio Esla, Plano general del aprovechamiento.

Sociedad Hispano Portuguesa de Transpotes Electricos, 1933: Saltol del Duero S.A., Proyecto de Aliviadero y Posible ampliación del embalse del aprovechamiento de Aguas del Rio Esla en Ricobayo (Zamora). Perfil longitudinal del Aliviadero.

Streckeisen, A.L. 1973: Plutonic rocks, classification and nomenclature. *Geotimes* 18: 26- 30

Toros, M. 1981: Les granitoides et les gites d'étain associés dans leur contexte lithostratigraphique et métamorphique cil'Ouest de Zamora (Massif, Hespérique, Espagne). Thesis, Univ.of Lausanne, 216 pp

USBR, 2001: Engineering geological field manual, 2<sup>nd</sup> edition, Vol. 1. U.S. Department of the Interior. Bureau of Reclamation, Washington.

Wallbrecher, E. 1986: Tektonische und gefügeanalytische Arbeitsweisen, Enke, Stuttgart, ISBN 3432956711, 9783432956718, 244p.

Whipple, K. X., Hancock, G. S., & Anderson, R. S. 2000: River incision into bedrock: Mechanics and relative efficacy of plucking, abrasion and cavitation. *GSA Bulletin*; March 2000; v. 112; no. 3.

Wyllie, D. C. & Mah, C. W. 2004: Rock slope engineering: civil and mining. 4<sup>th</sup> Ed. Taylor and Francis. ISBN 041528001X, 9780415280013. 431p.

Wohl, E.E., 2000: Mountain Rivers. American Geophysical Union Water Resources Monograph 14, Washington, D.C. ISBN 0875903185, 9780875903187, 320p

Zimmerman, A. and Church, M. 2001: Channel morphology, gradient profiles and bed stress during flood in a step-pool channel. *Geomorphology* 40, 311–327.

# 10. Appendix

## A1 Removable JPs

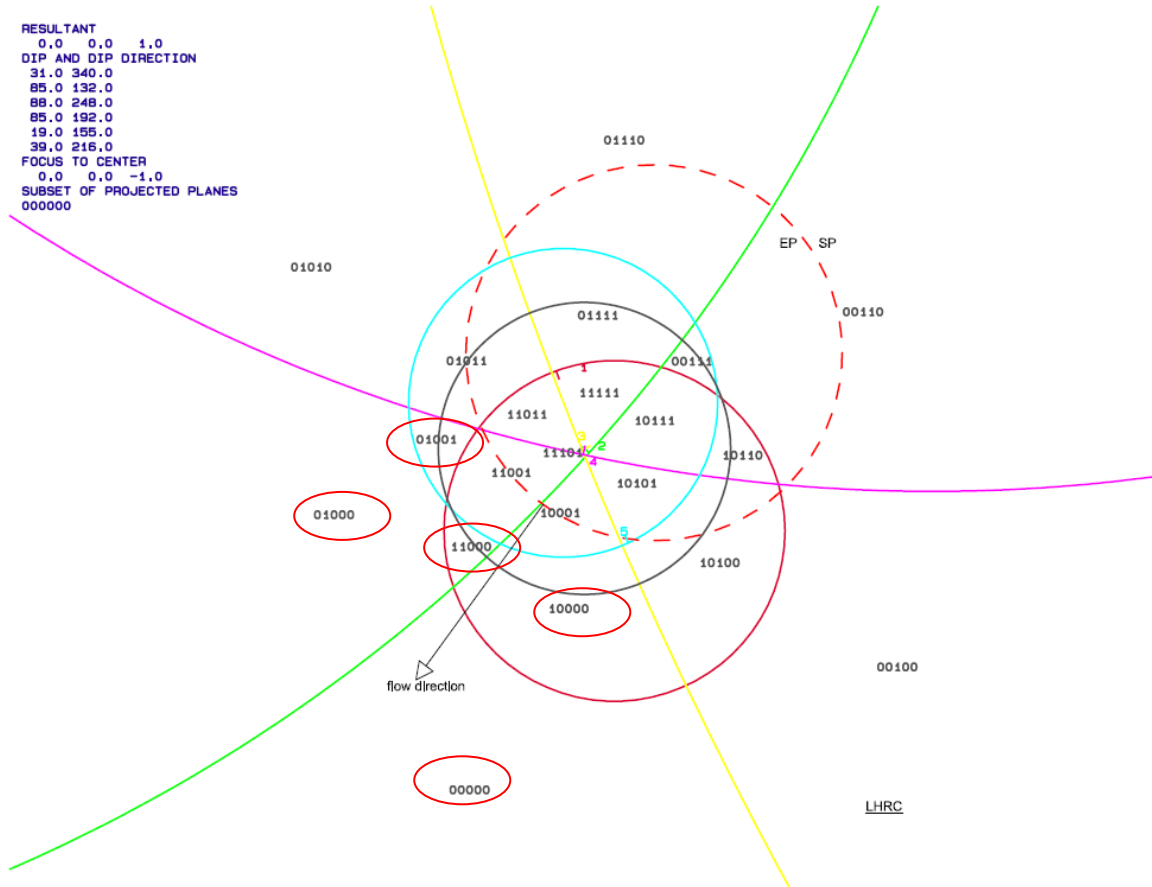


Fig.A1: Removable JPs for the front slope (red ellipses). Arrow shows azimuth of flow direction on front slope

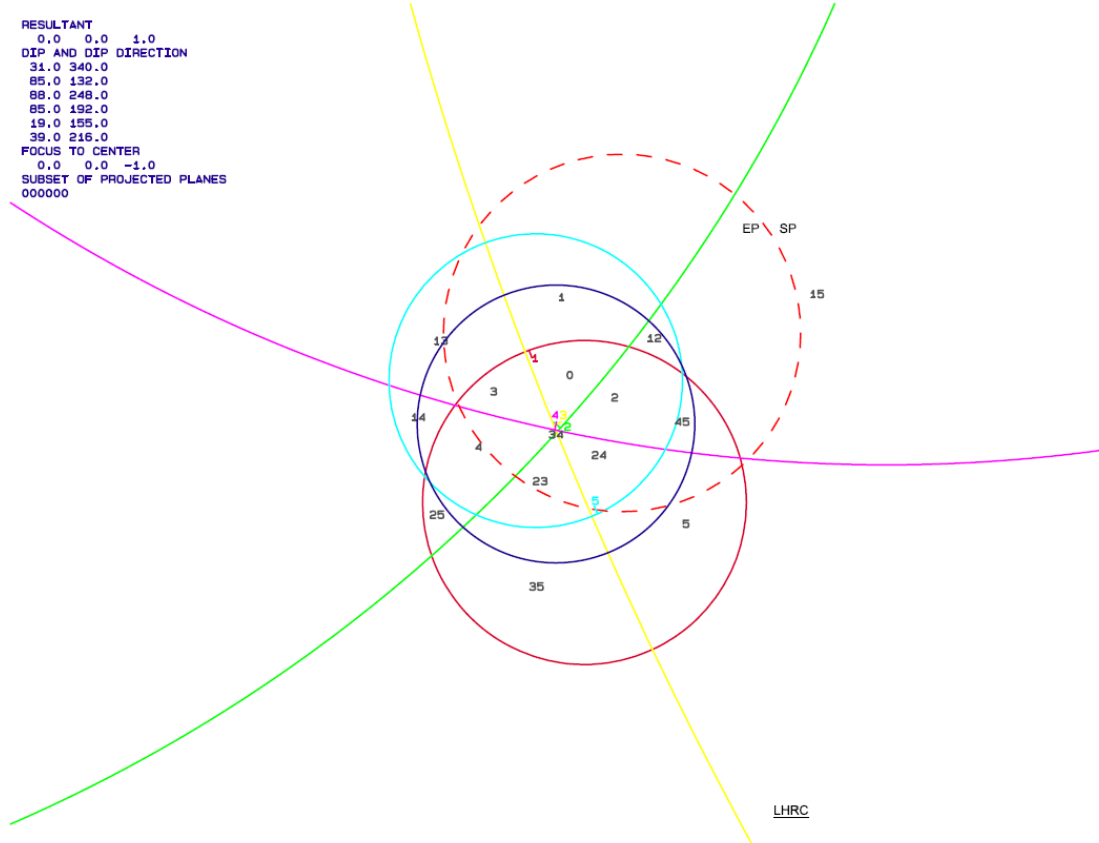


Fig.A2: Failure modes under gravity for removable JPs on the front slope.

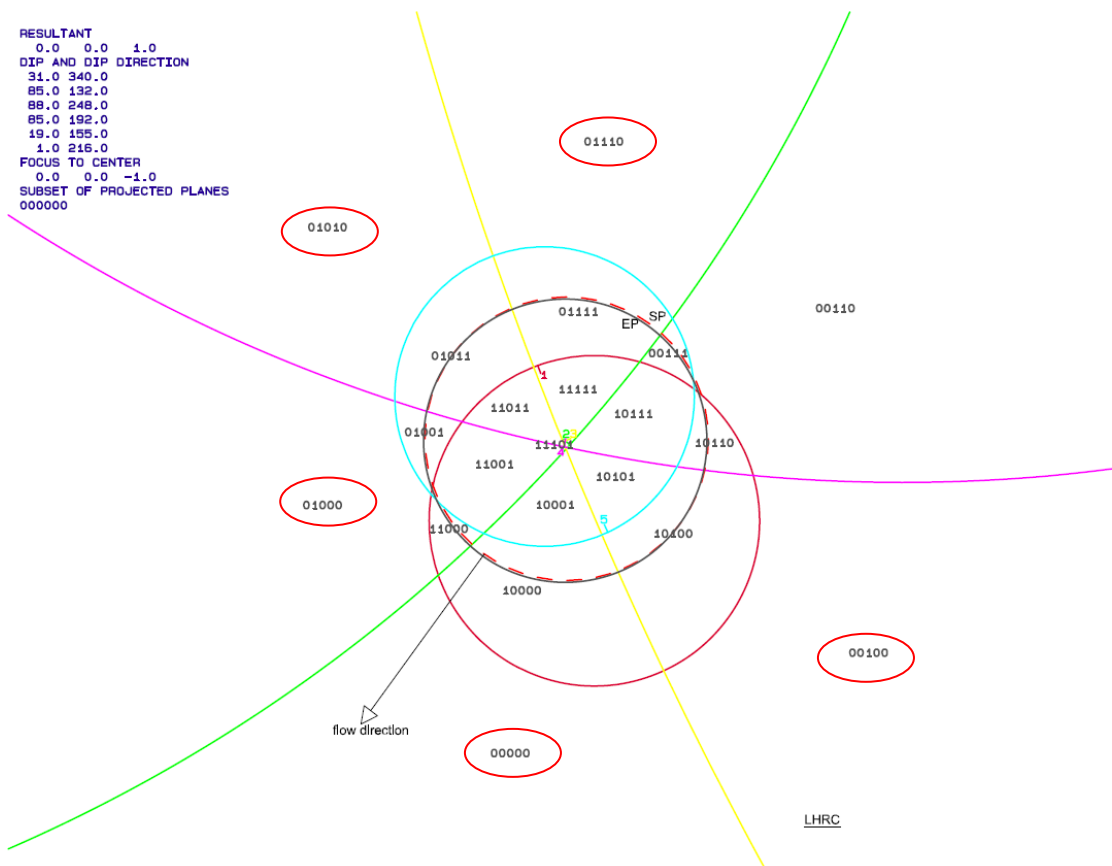


Fig.A3: Removable JPs for the spillway surface (red ellipses). Arrow shows azimuth of flow direction on spillway surface.

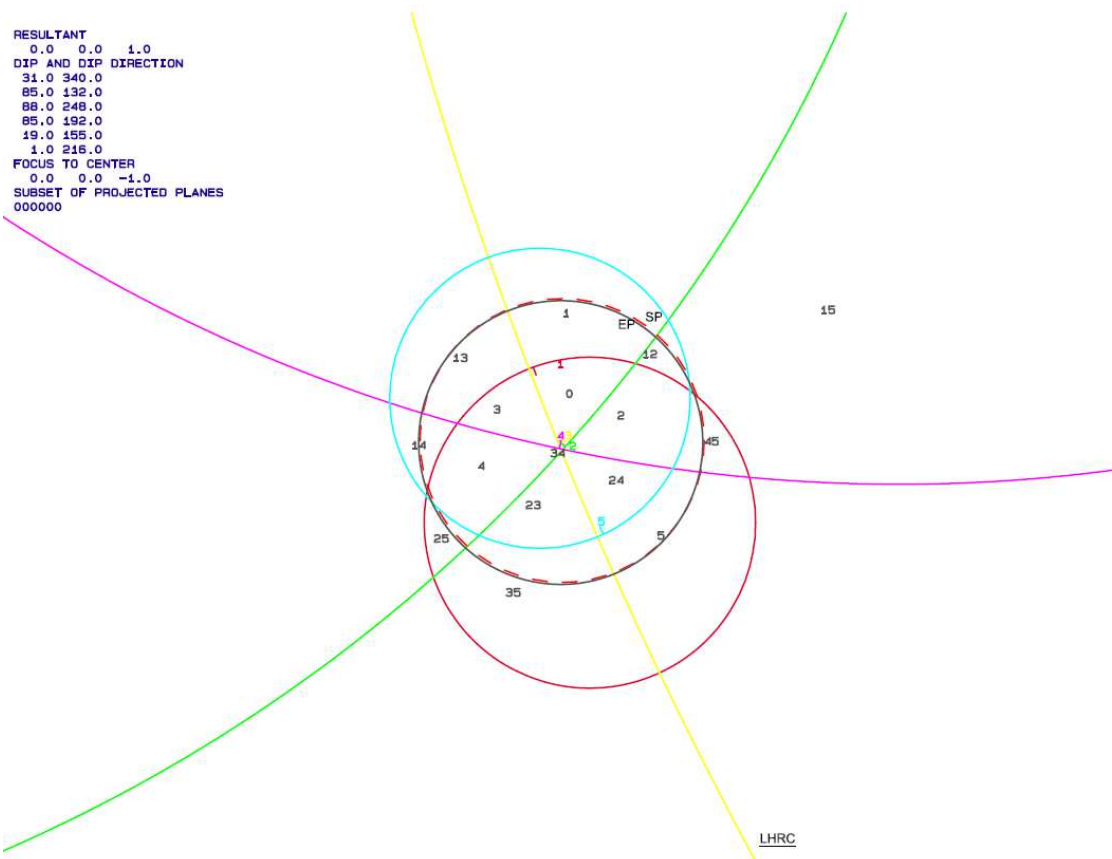


Fig.A4: Failure modes under gravity for removable JPs on the spillway surface.

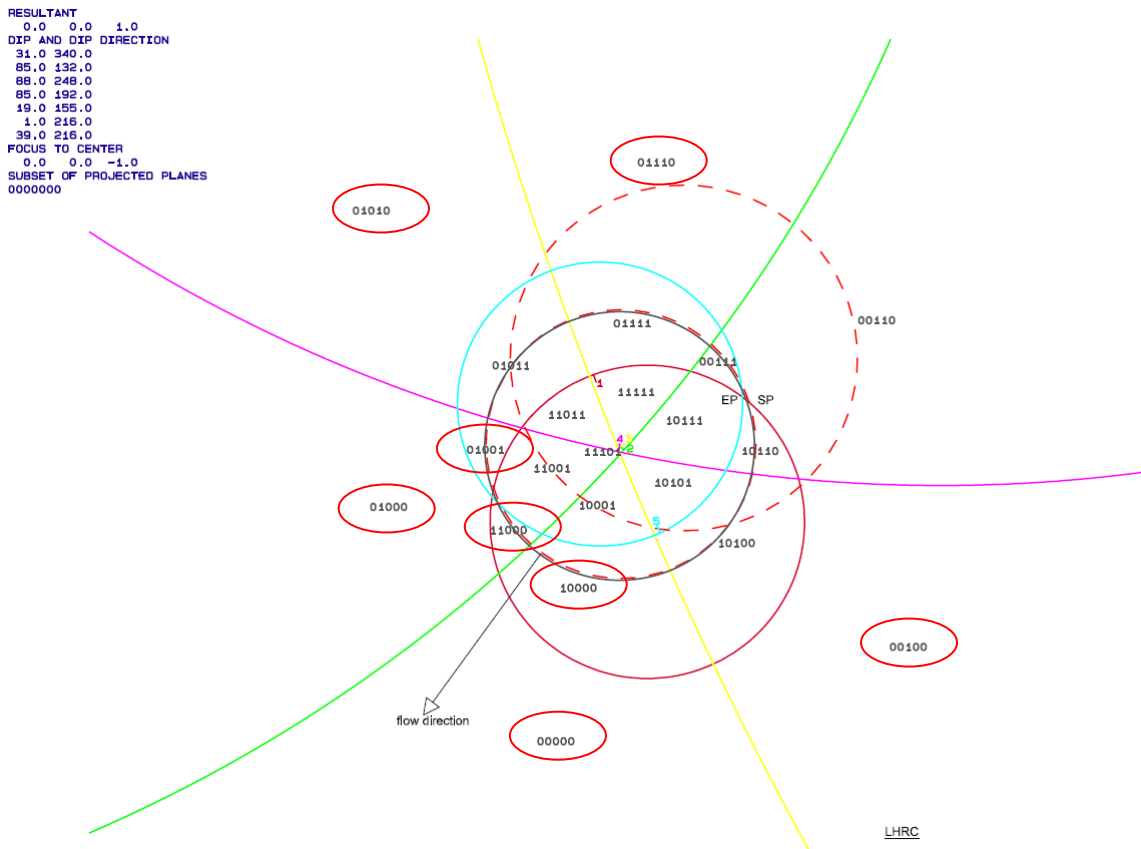


Fig.A5: Removable JPs for the compound slope (red ellipses). Arrow shows azimuth of flow direction on compound slope.

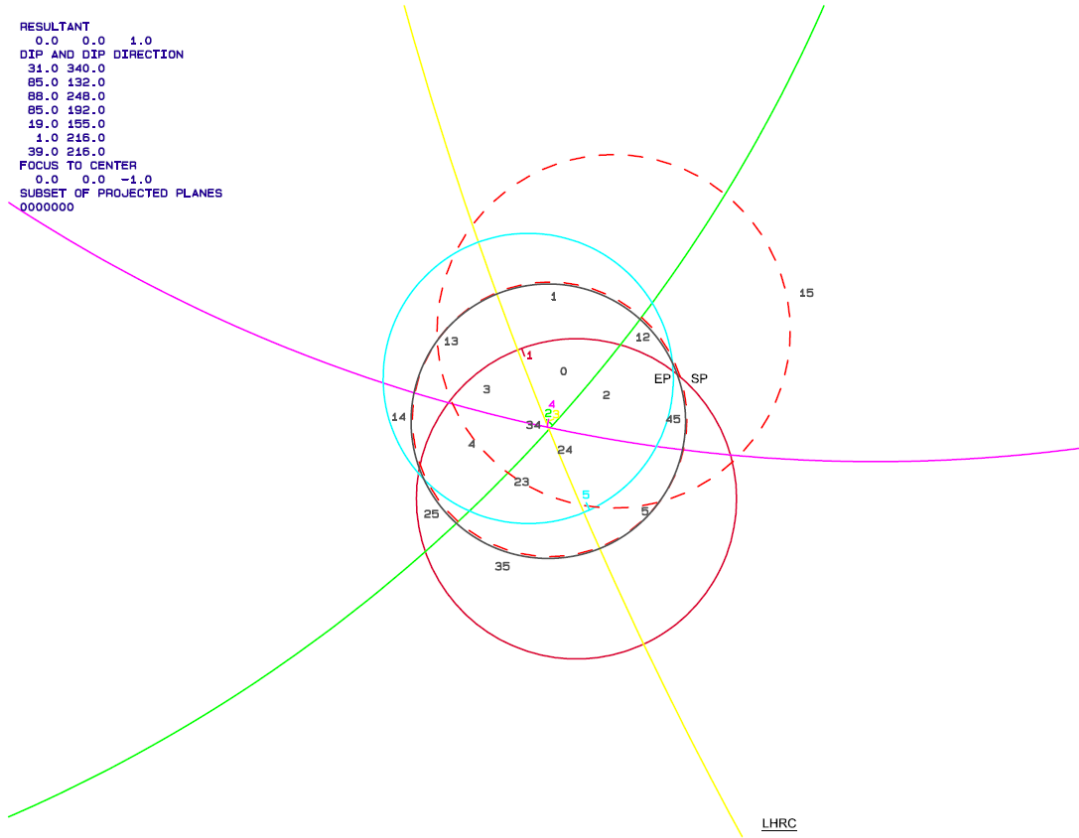


Fig.A6: Failure modes under gravity for removable JPs on the compound slope.

## A2 Compound Friction Cones of Removable JPs

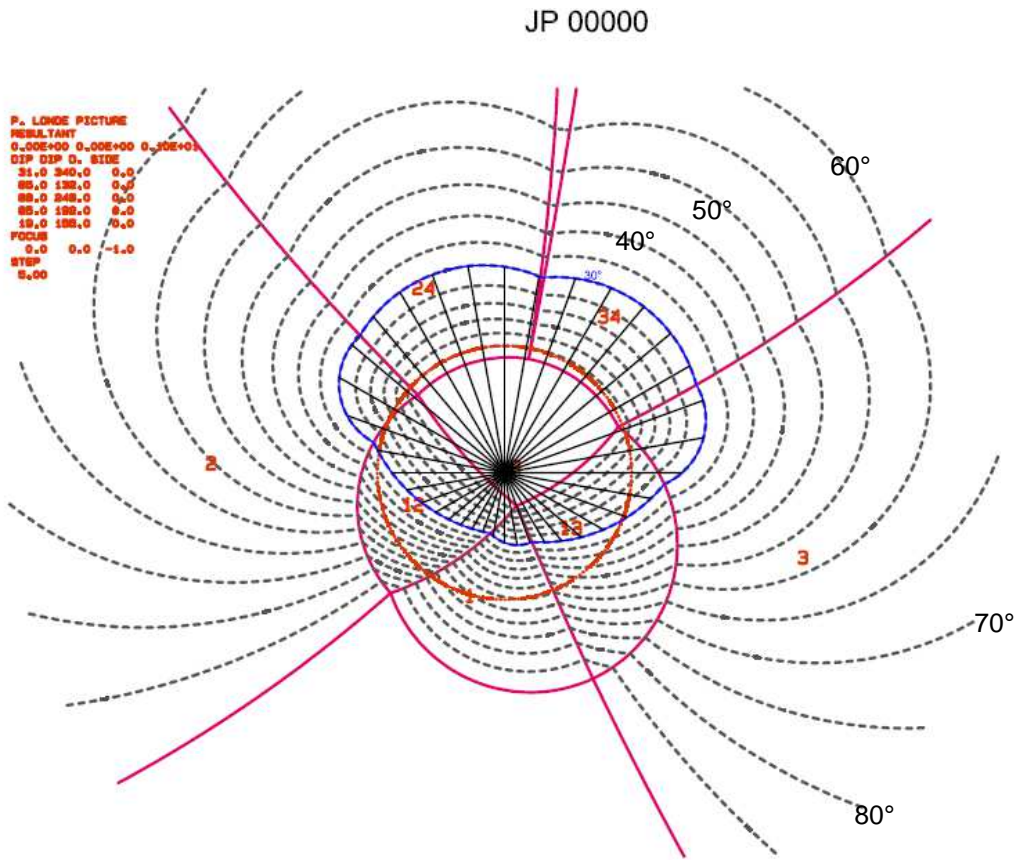


Fig.A7: Compound friction cone JP00000 (30°)



JP 00000

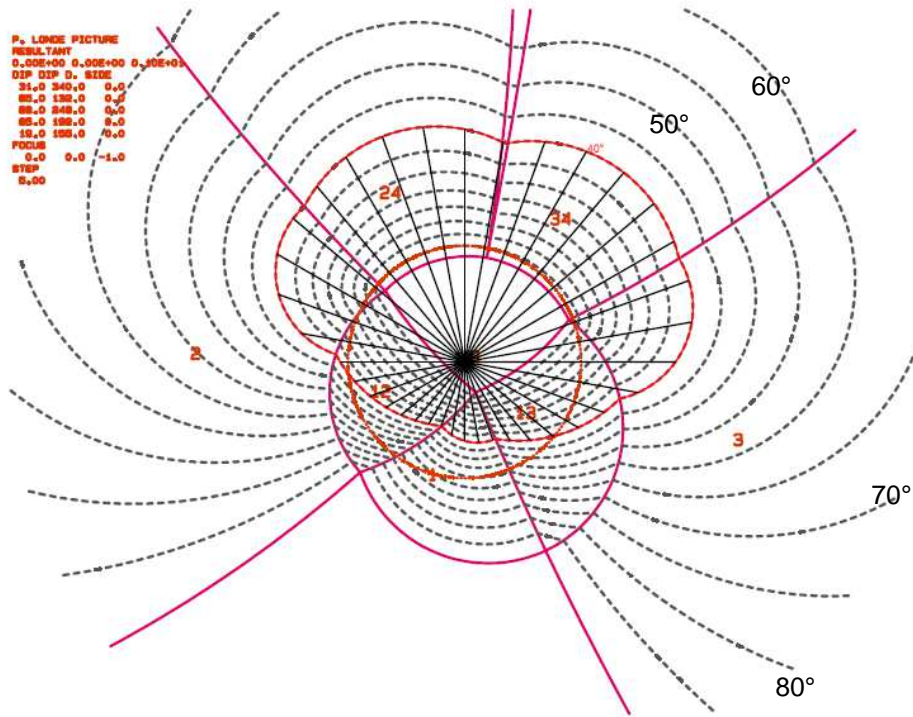


Fig.A8: Compound friction cone JP00000 (40°)

JP 00010

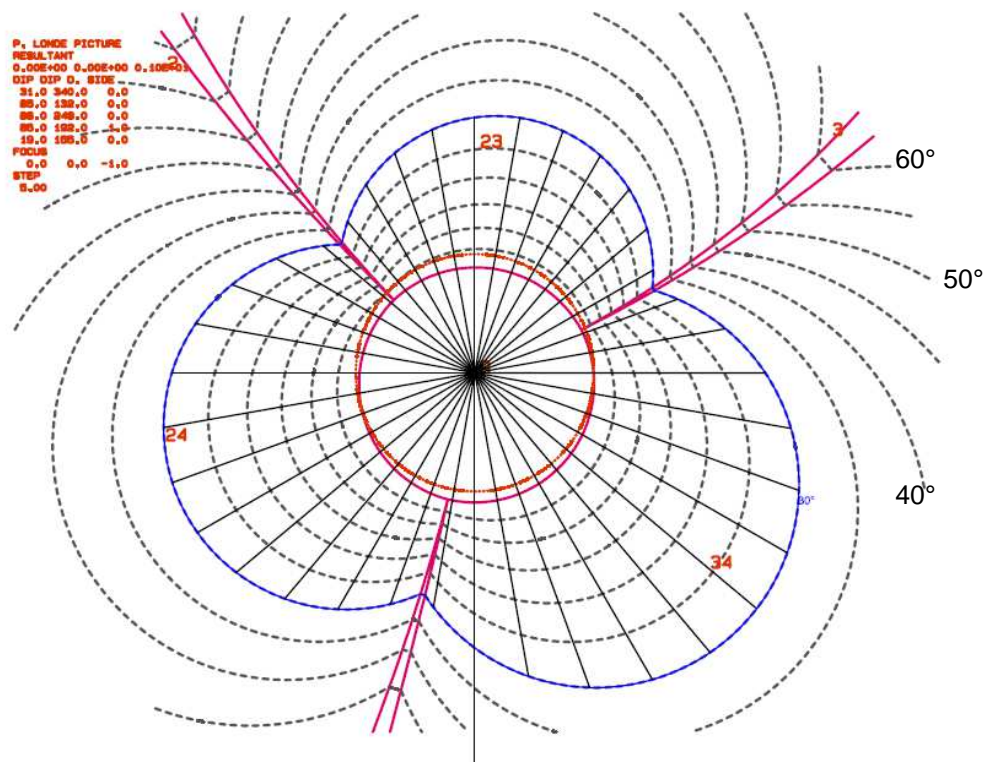


Fig.A9: Compound friction cone JP00010 (30°)

JP 00010

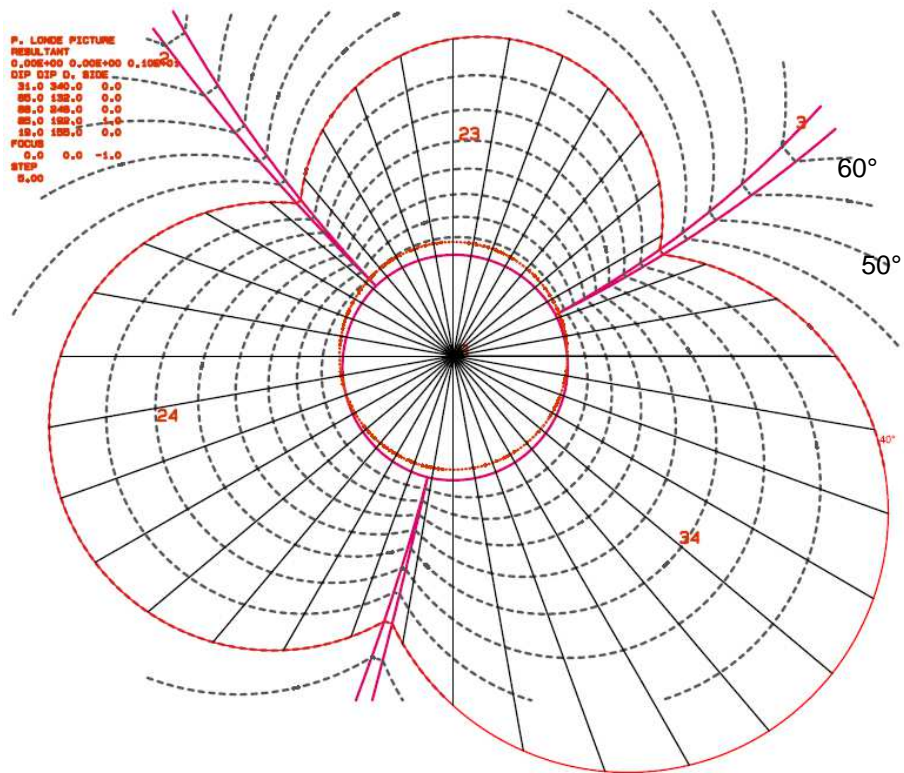


Fig.A10: Compound friction cone JP00010 (40°)

JP 00100

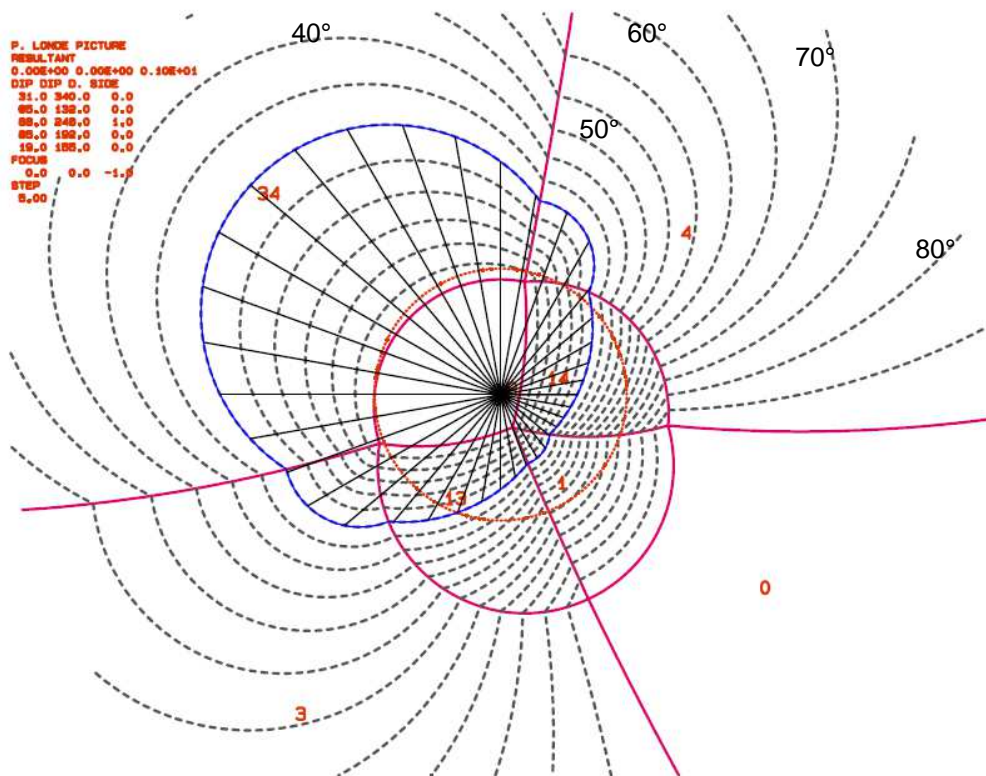


Fig.A11: Compound friction cone JP00100 (30°)

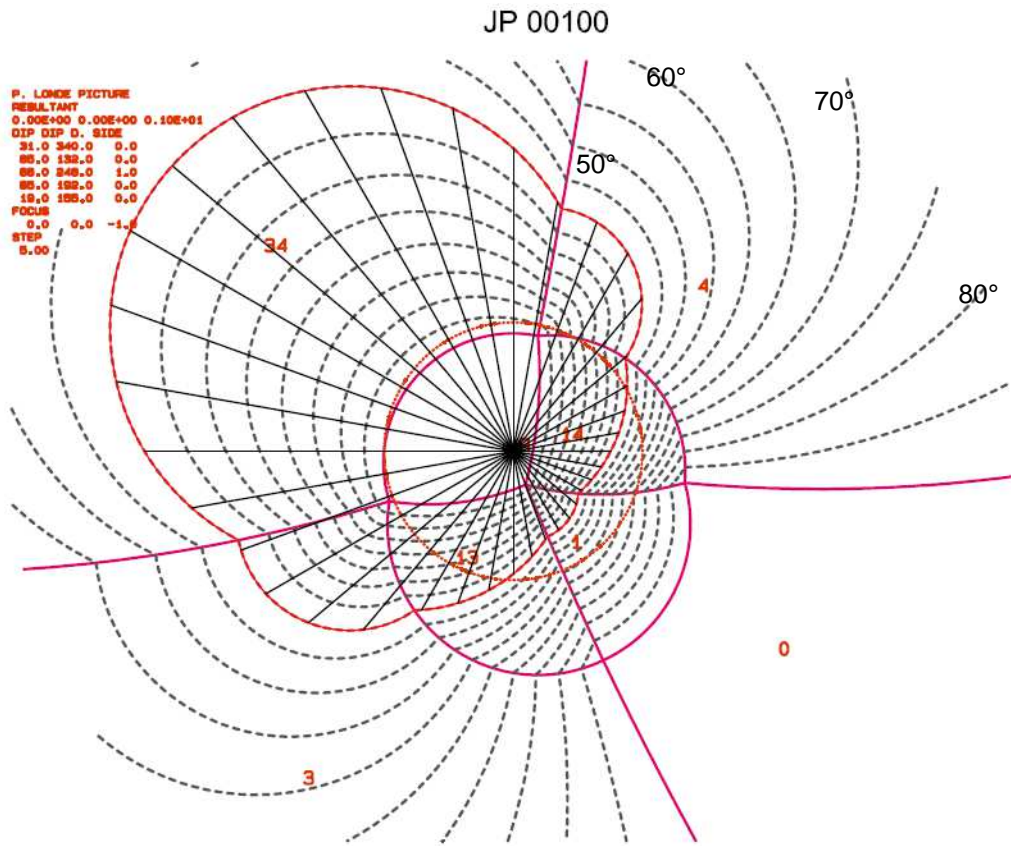


Fig.A12: Compound friction cone JP00100 (40)

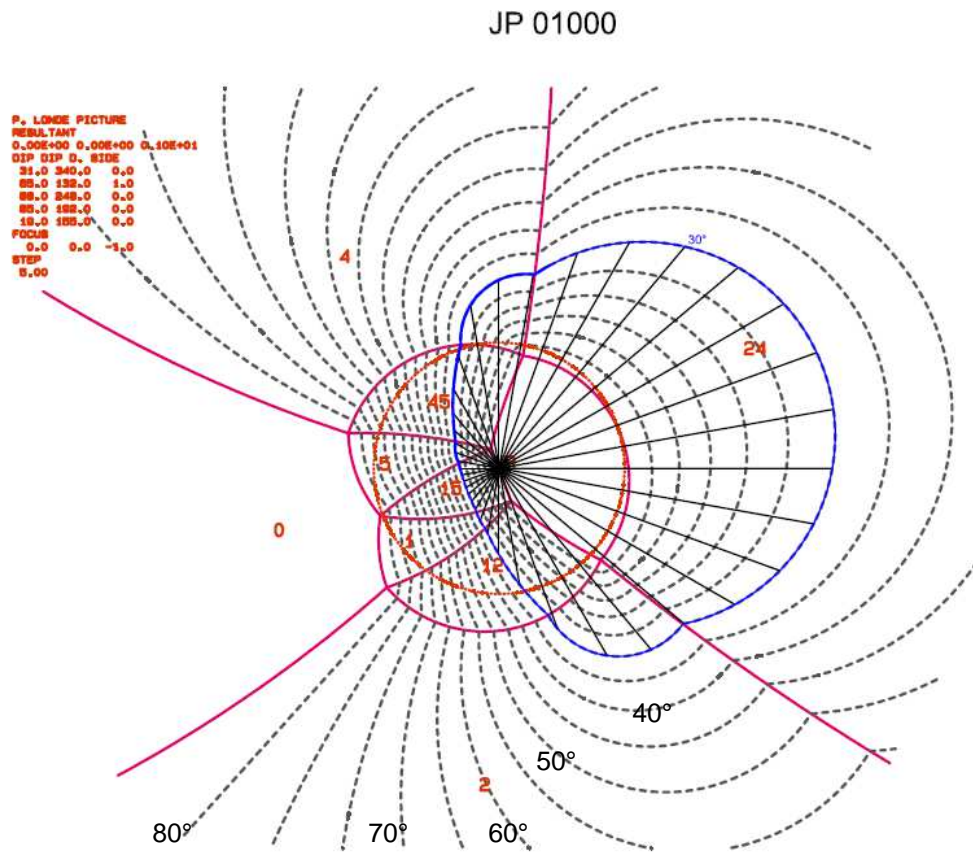


Fig.A13: Compound friction cone JP01000 (30)

JP 01000

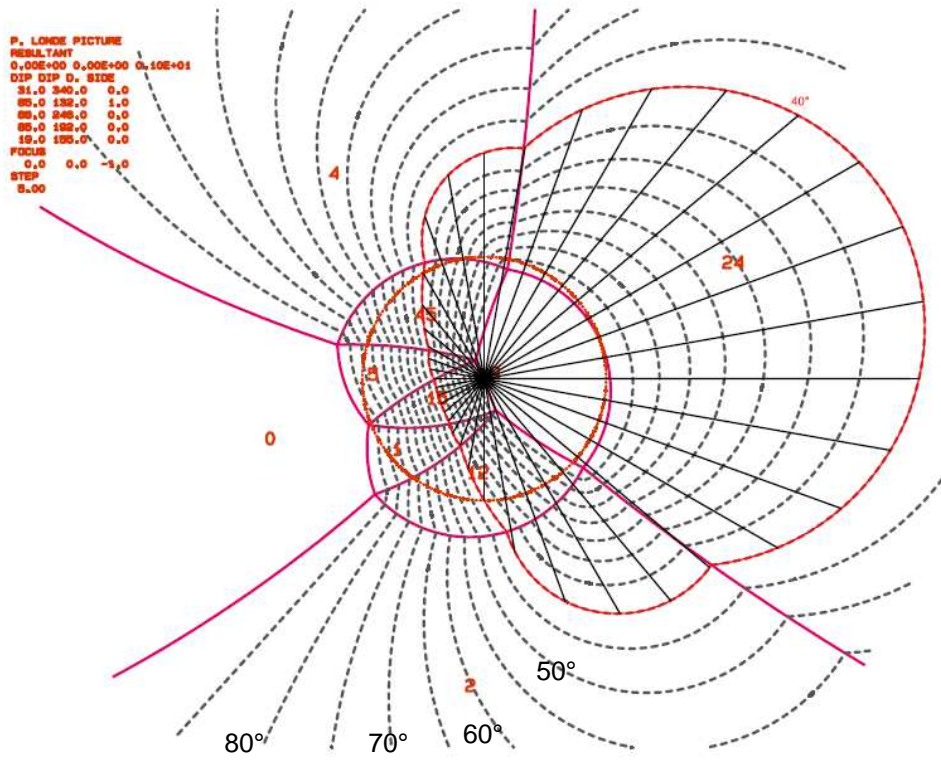


Fig.A14: Compound friction cone JP01000 (40°)

JP 01001

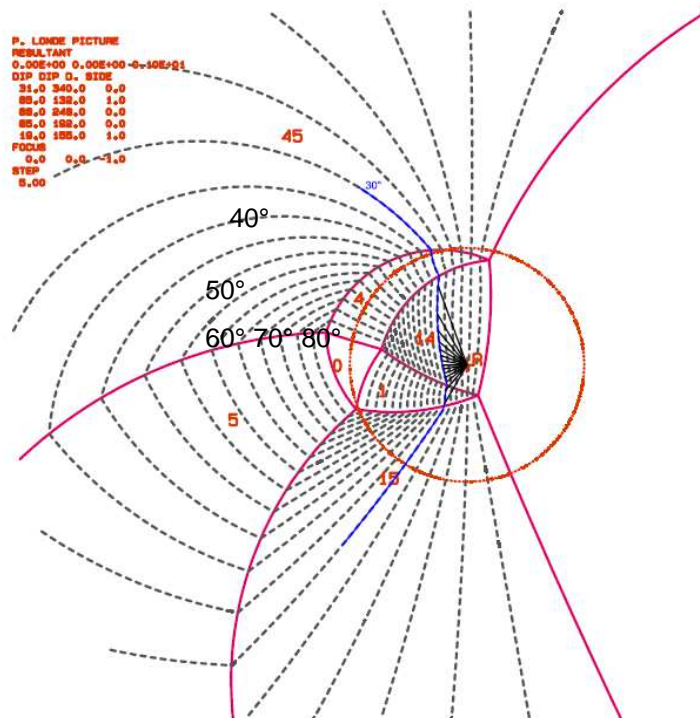


Fig.A15: Compound friction cone JP01001 (30°)

JP 01001

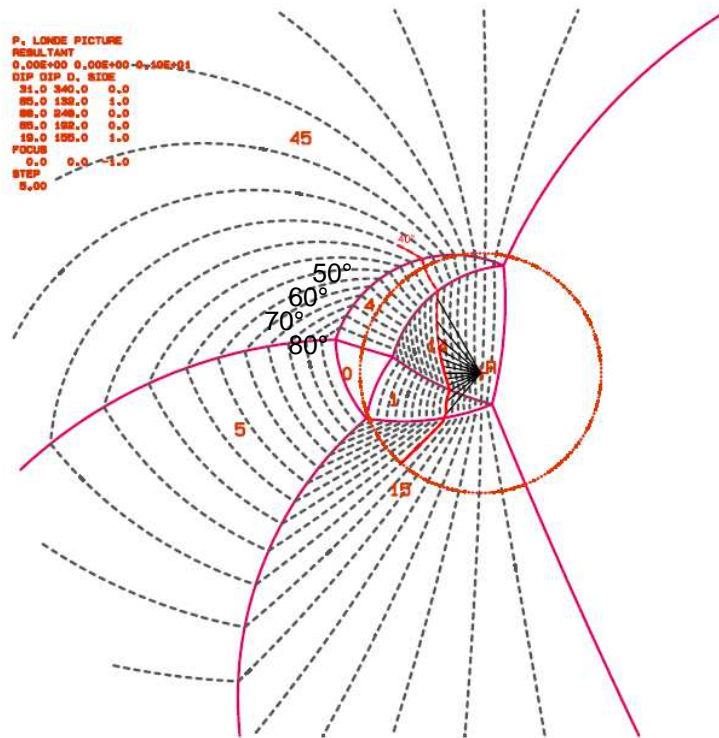


Fig.A16: Compound friction cone JP01001 (40°)

JP 01010

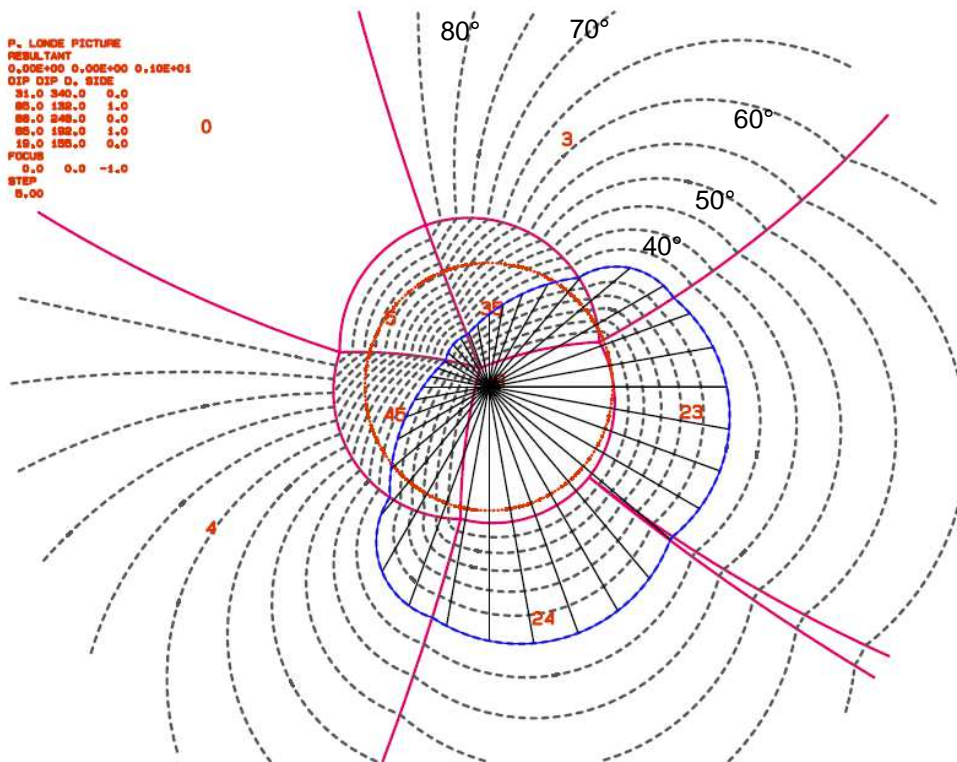


Fig.A17: Compound friction cone JP01010 (30°)

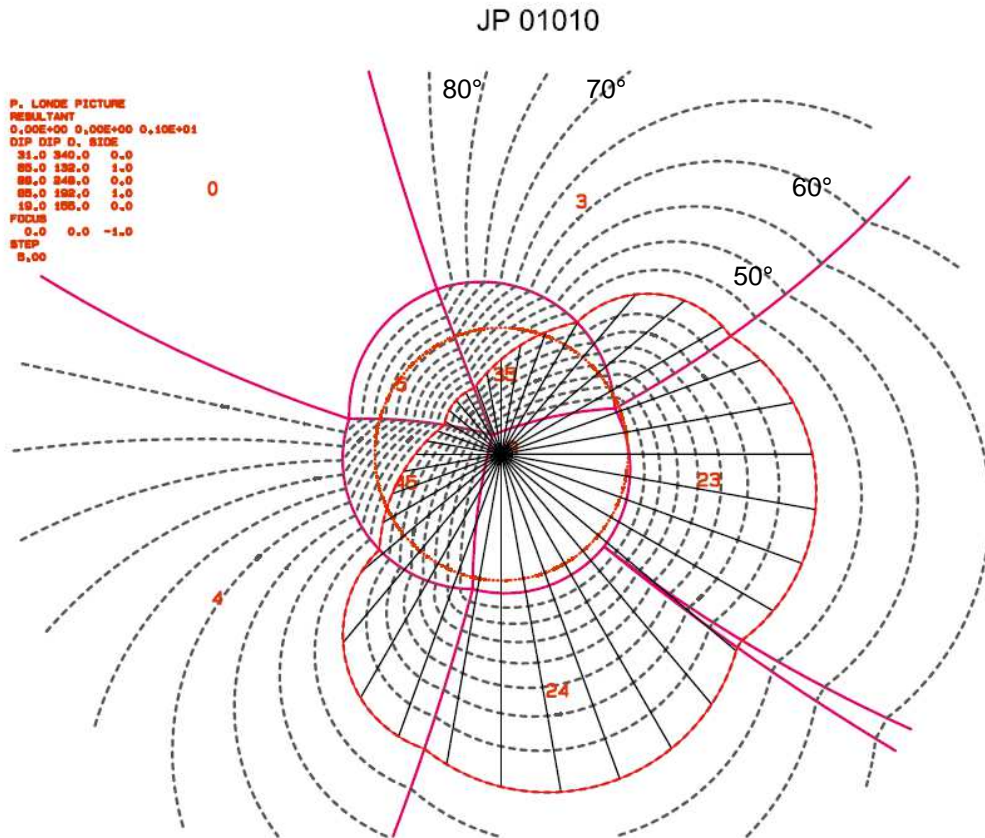


Fig.A18: Compound friction cone JP01010 (40°)

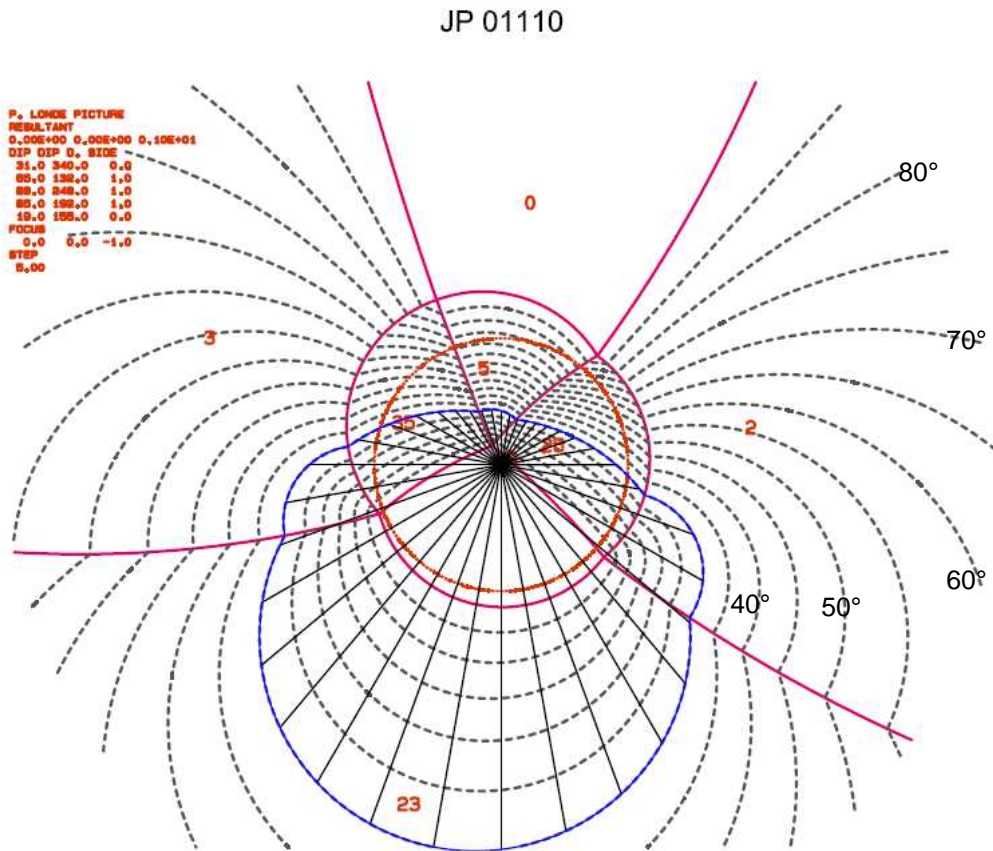


Fig.A19: Compound friction cone JP01110 (30°)

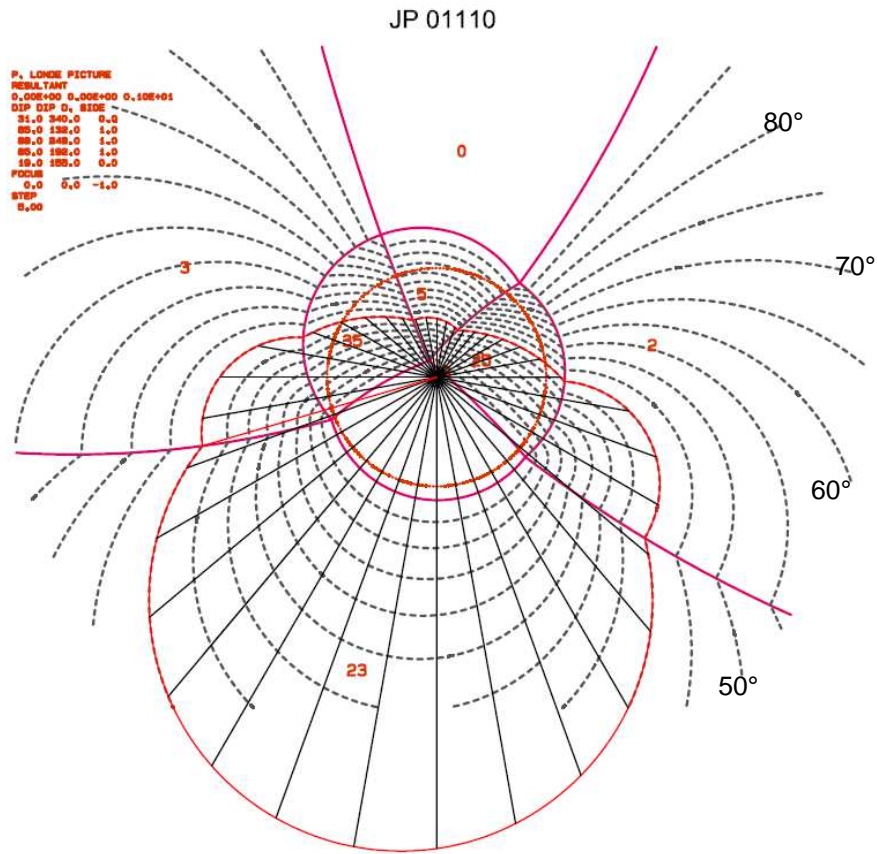


Fig.A20: Compound friction cone JP01110 (40)

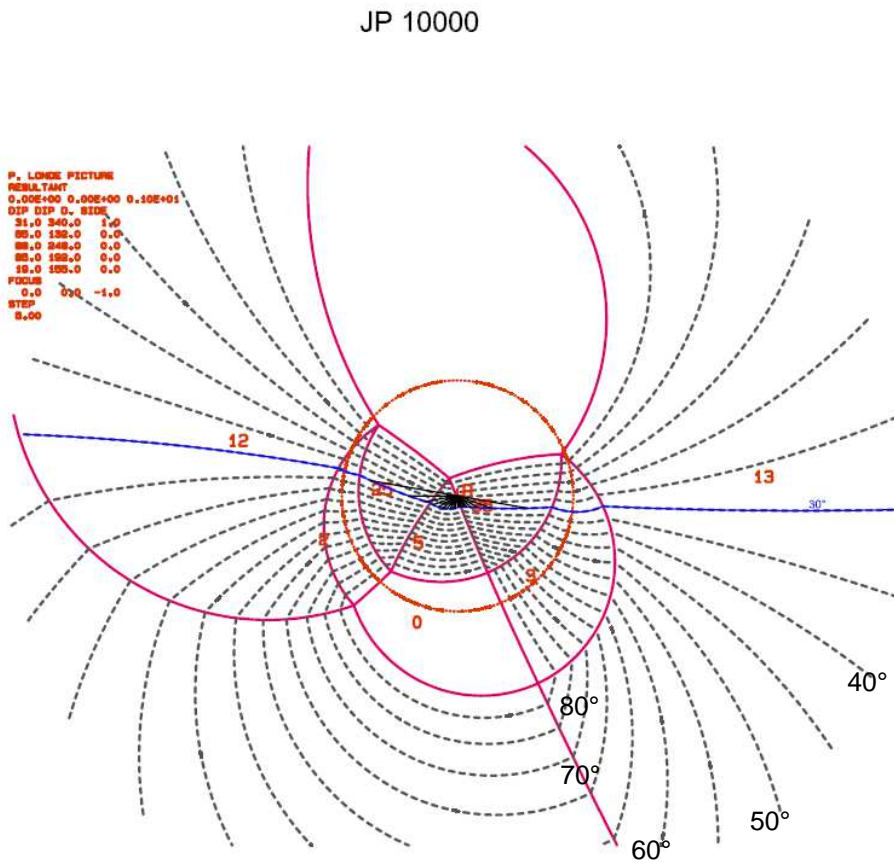


Fig.A21: Compound friction cone JP10000 (30)

JP 10000

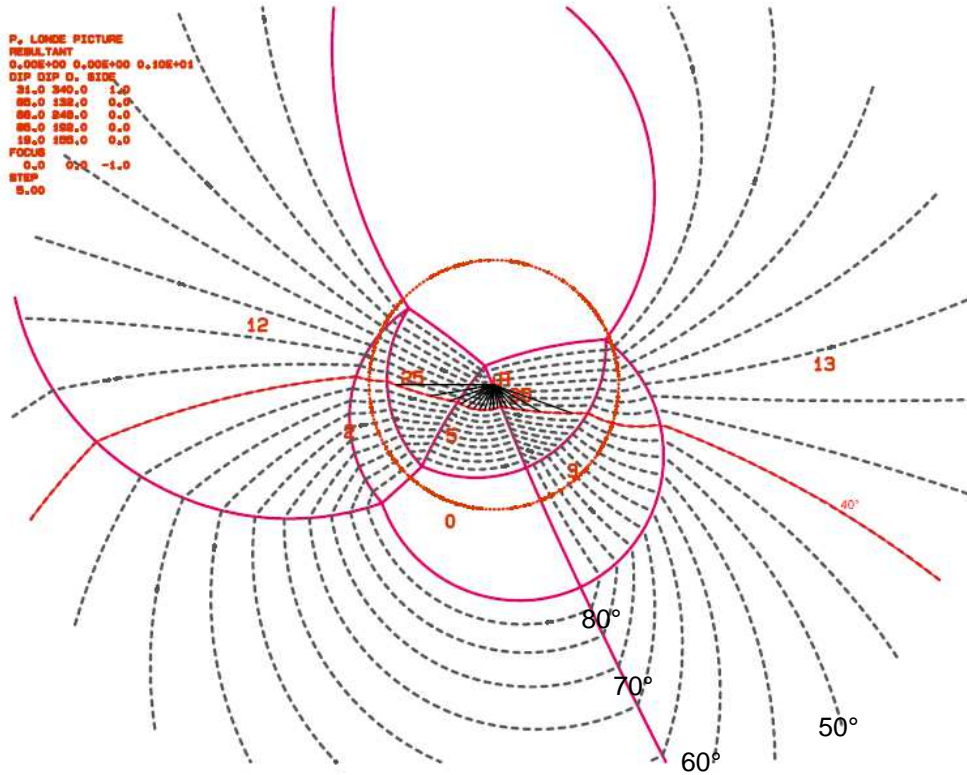


Fig.A22: Compound friction cone JP10000 (40°)

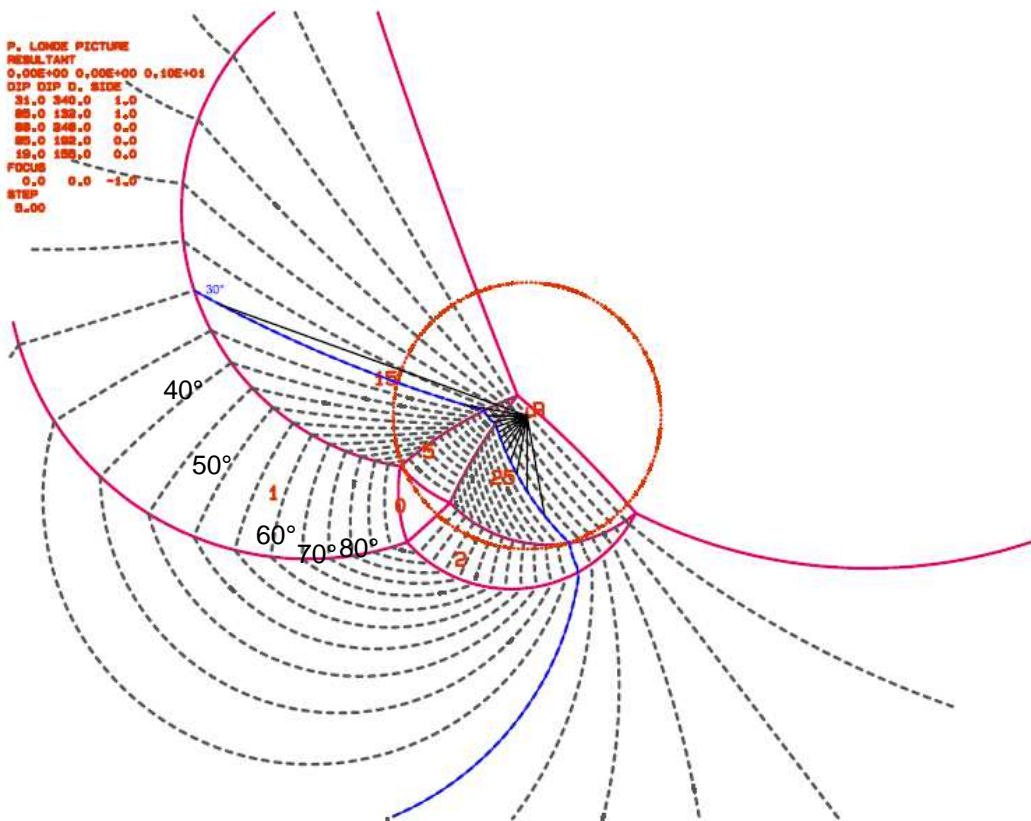


Fig.A23: Compound friction cone JP11000 (30°)



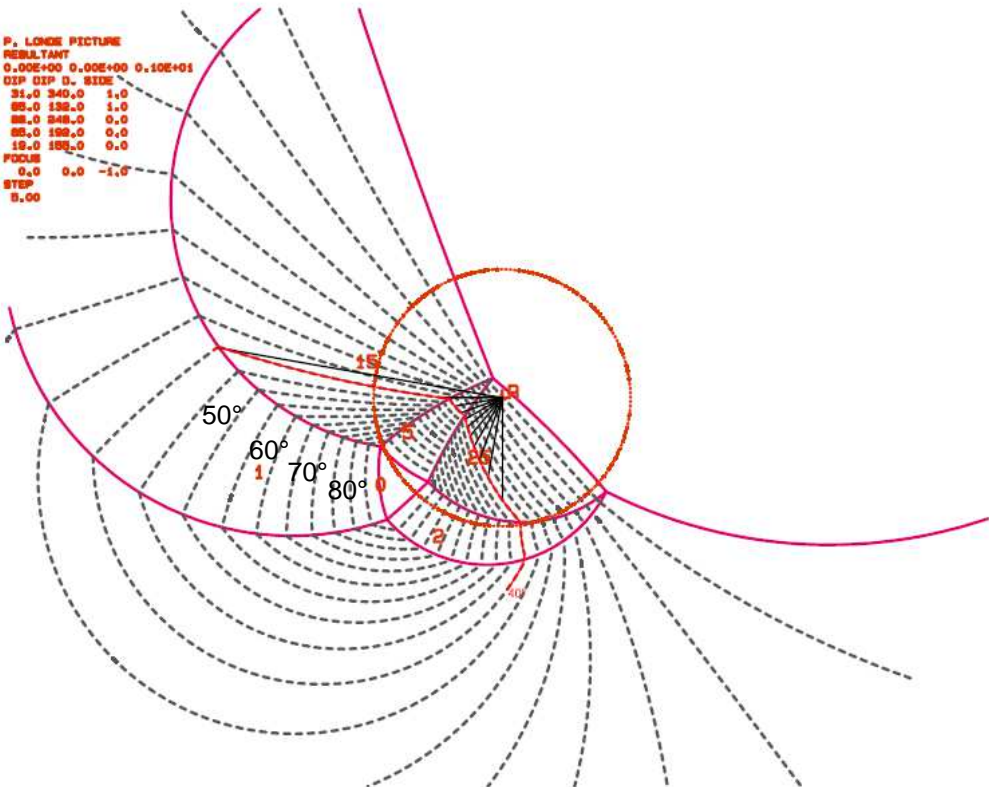
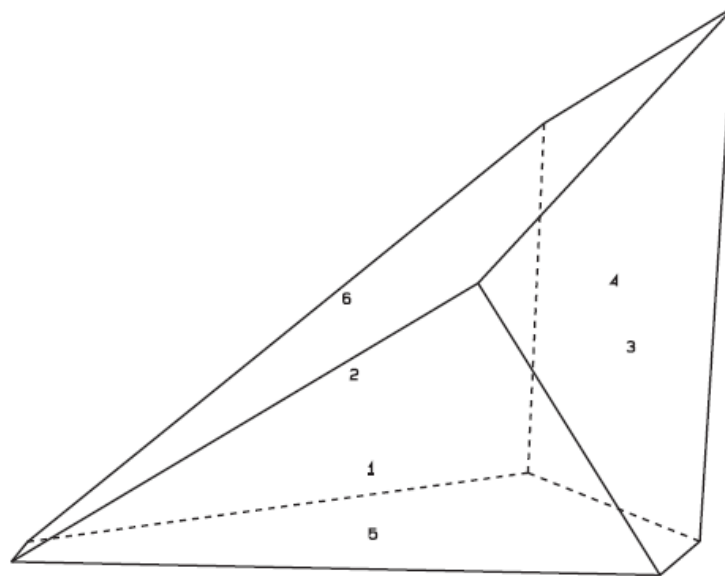


Fig.A24: Compound friction cone JP11000 (40)

### A3 Shapes of Removable Blocks

```

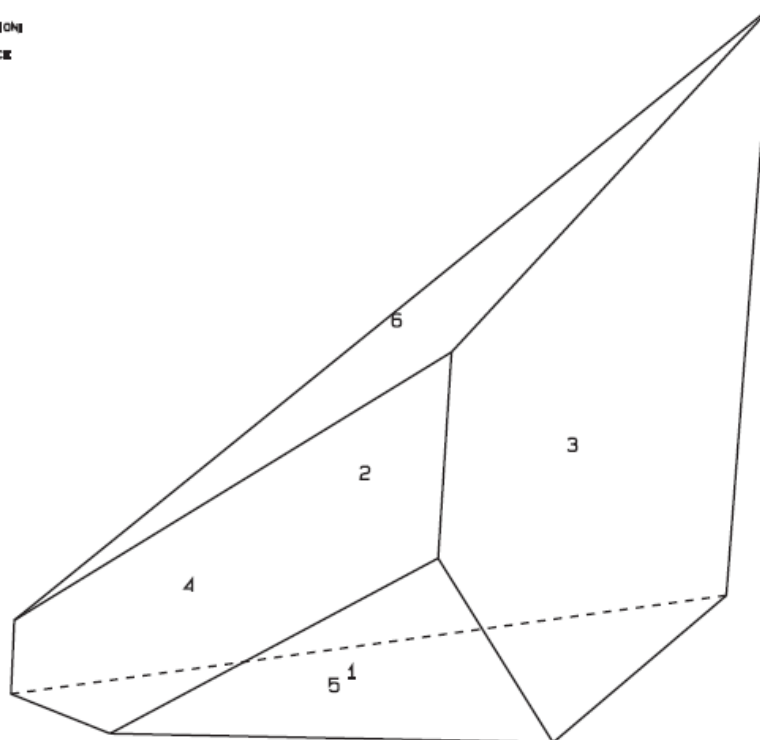
PROJECTIVE DIRECTION
1.0 -1.0 0.0
DIP, DXP D., DISTANCE
31.0 340.0 1.3
88.0 132.0 1.3
88.0 248.0 1.9
88.0 192.0 1.2
19.0 185.0 0.9
39.0 216.0 1.0
VOLUME= 2.420+01
    
```



JP 00000

```

PROJECTIVE DIRECTION
1.0 -1.0 0.0
DIP, DXP D., DISTANCE
31.0 340.0 1.3
88.0 132.0 1.3
88.0 248.0 1.9
88.0 192.0 1.2
19.0 185.0 0.9
39.0 216.0 1.0
VOLUME= 2.780+01
    
```

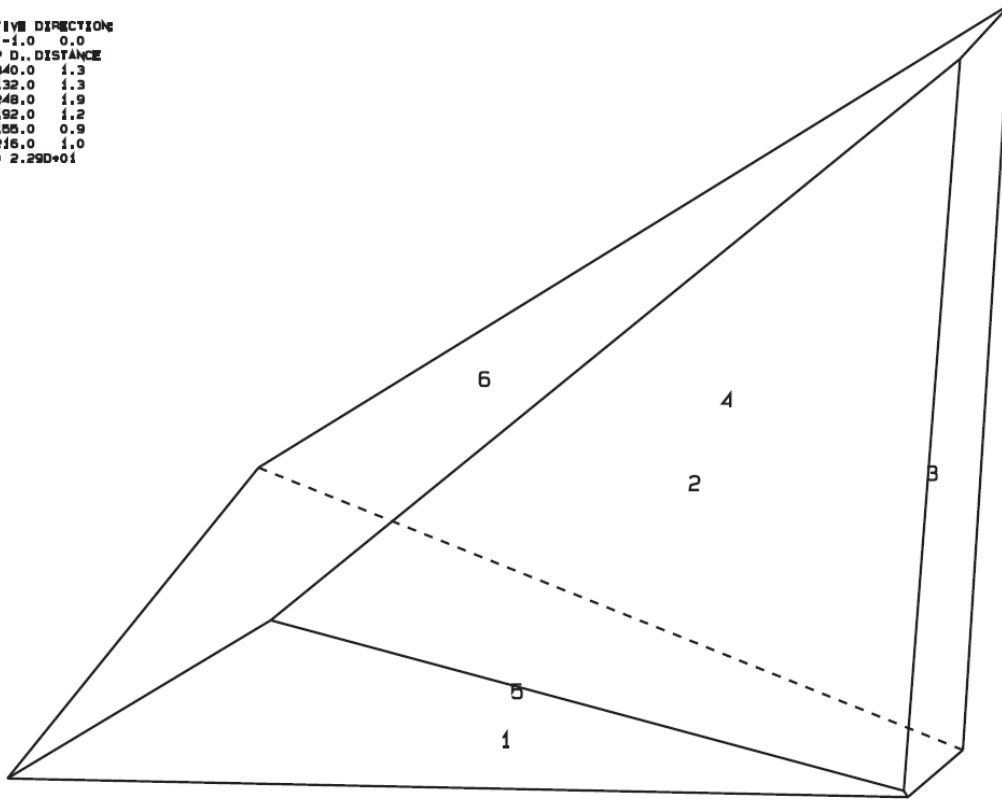


JP 00010

Fig.A25: Shape of JP00000 and JP 00010 on the front slope (6)

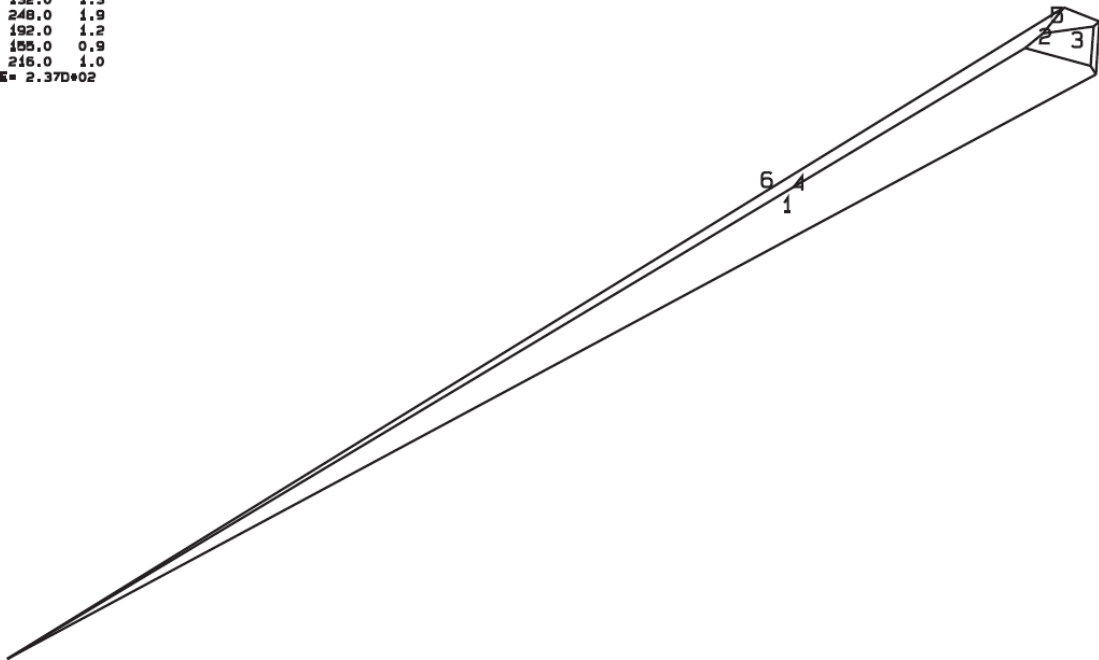
10. Appendix

PROJECTIVE DIRECTION  
 1.0 -1.0 0.0  
 DIP, DIP D., DISTANCE  
 31.0 340.0 1.3  
 85.0 132.0 1.3  
 88.0 248.0 1.9  
 85.0 192.0 1.2  
 19.0 155.0 0.9  
 39.0 216.0 1.0  
 VOLUME= 2.29D+01



JP 01000

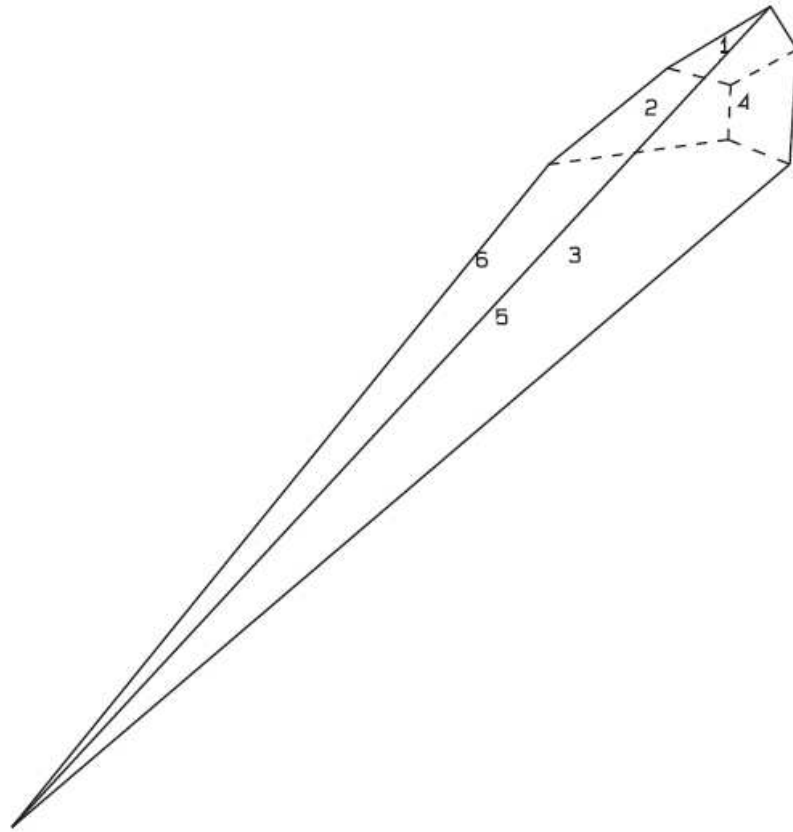
PROJECTIVE DIRECTION  
 1.0 -1.0 0.0  
 DIP, DIP D., DISTANCE  
 31.0 340.0 1.3  
 85.0 132.0 1.3  
 88.0 248.0 1.9  
 85.0 192.0 1.2  
 19.0 155.0 0.9  
 39.0 216.0 1.0  
 VOLUME= 2.37D+02



JP 01001

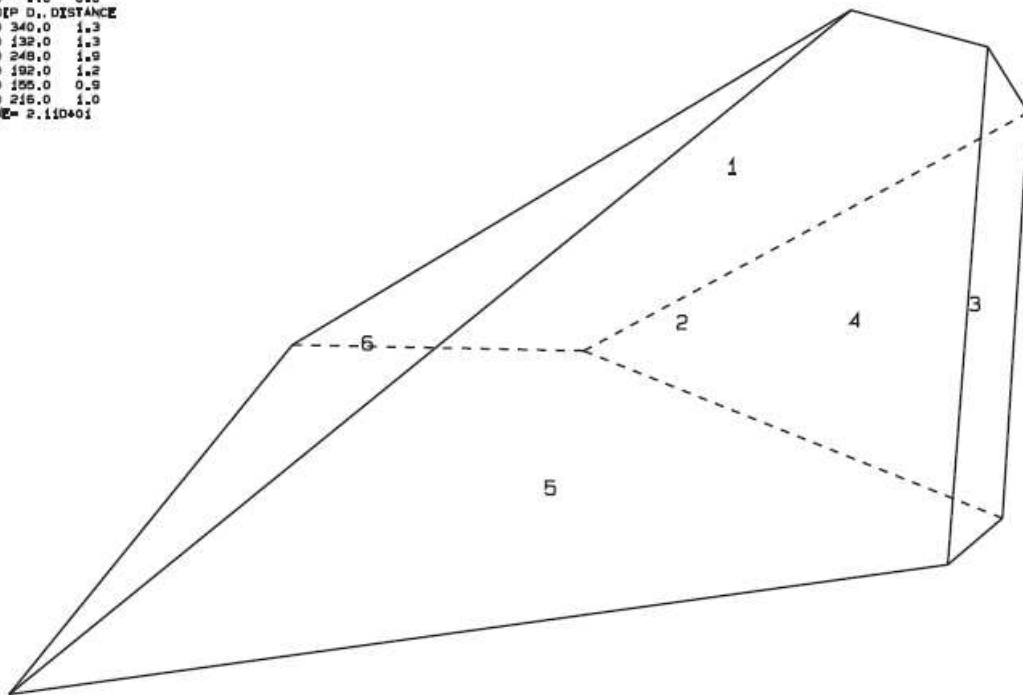
Fig.A26: Shape of JP01000 and JP 01001 on the front slope (6)

PROJECTIVE DIRECTION:  
 1.0 -1.0 0.0  
 DIP, DIP D., DISTANCE  
 31.0 340.0 1.3  
 88.0 132.0 1.3  
 88.0 248.0 1.9  
 88.0 192.0 1.2  
 19.0 188.0 0.9  
 39.0 216.0 1.0  
 VOLUME= 1.220+02



JP 10000

PROJECTIVE DIRECTION:  
 1.0 -1.0 0.0  
 DIP, DIP D., DISTANCE  
 31.0 340.0 1.3  
 88.0 132.0 1.3  
 88.0 248.0 1.9  
 88.0 192.0 1.2  
 19.0 188.0 0.9  
 39.0 216.0 1.0  
 VOLUME= 2.110+01

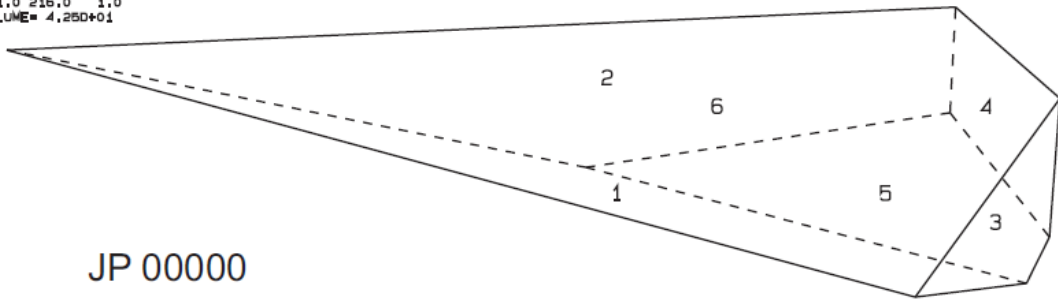


JP 11000

Fig.A27: Shape of JP10000 and JP 11000 on the front slope (6)

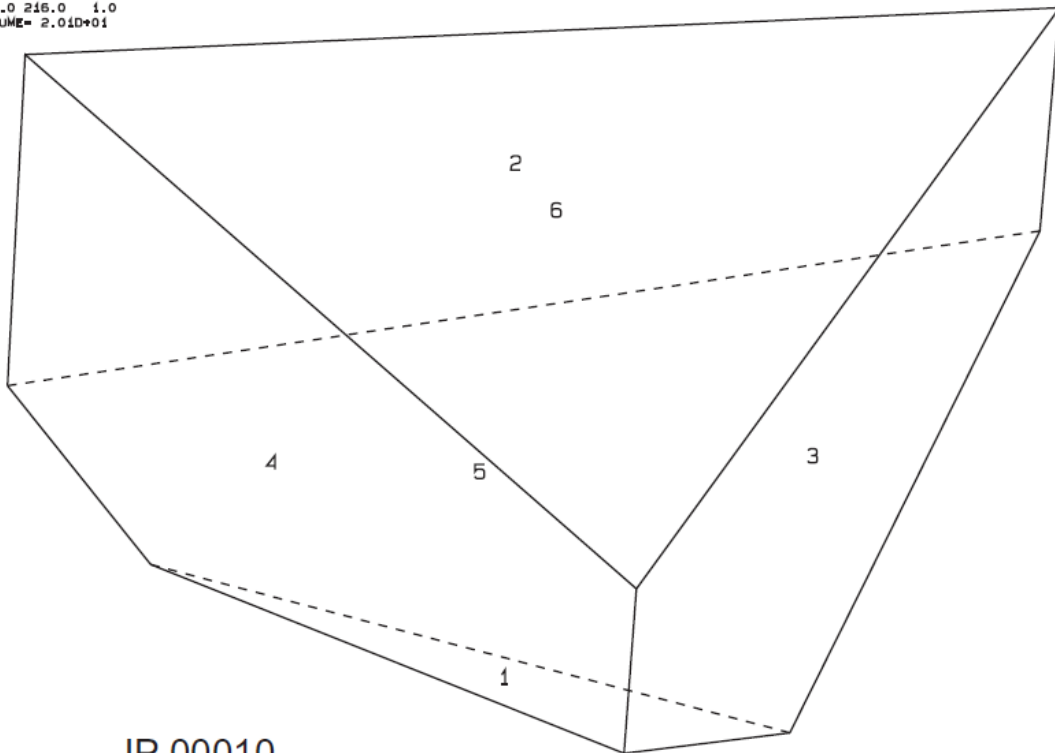
10. Appendix

```
PROJECTIVE DIRECTION:
1.0 -1.0 1.0
DIP, DIP D., DISTANCE
31.0 340.0 1.3
85.0 132.0 1.3
88.0 248.0 1.9
85.0 192.0 1.2
19.0 155.0 0.9
1.0 216.0 1.0
VOLUME= 4.250+01
```



JP 00000

```
PROJECTIVE DIRECTION:
1.0 -1.0 1.0
DIP, DIP D., DISTANCE
31.0 340.0 1.3
85.0 132.0 1.3
88.0 248.0 1.9
85.0 192.0 1.2
19.0 155.0 0.9
1.0 216.0 1.0
VOLUME= 2.010+01
```

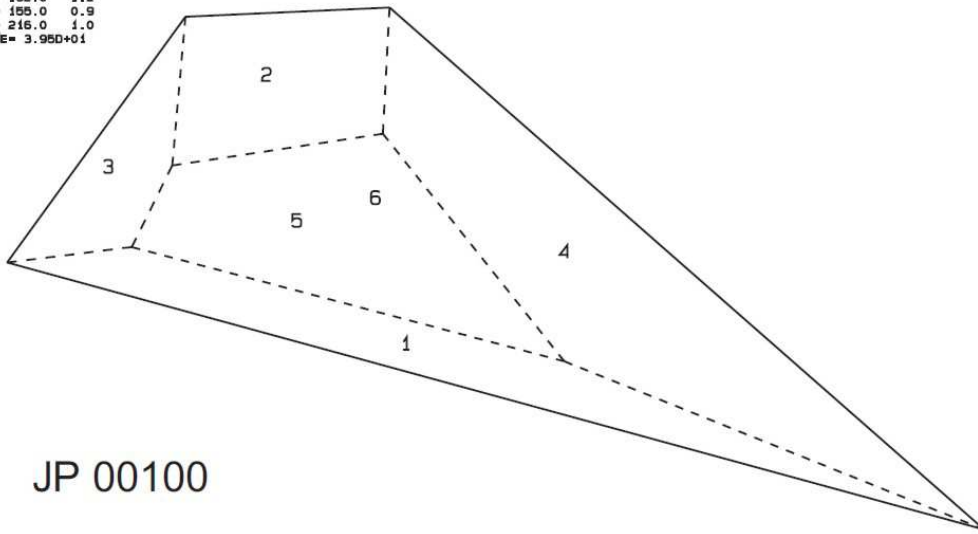


JP 00010

Fig.A28: Shape of JP00000 and JP 00010 on the spillway surface (6)

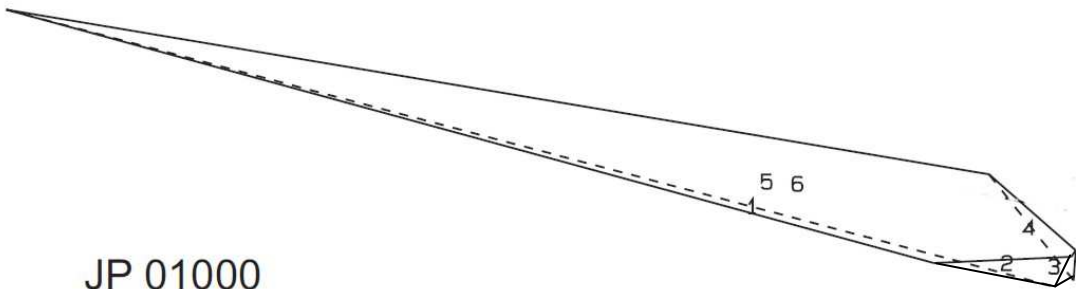
10. Appendix

PROJECTIVE DIRECTION:  
1.0 -1.0 1.0  
DIP, DIP D., DISTANCE  
31.0 340.0 1.3  
85.0 132.0 1.3  
88.0 248.0 1.9  
85.0 192.0 1.2  
19.0 155.0 0.9  
1.0 216.0 1.0  
VOLUME= 3.950+01



JP 00100

PROJECTIVE DIRECTION:  
1.0 -1.0 1.0  
DIP, DIP D., DISTANCE  
31.0 340.0 1.3  
85.0 132.0 1.3  
88.0 248.0 1.9  
85.0 192.0 1.2  
19.0 155.0 0.9  
1.0 216.0 1.0  
VOLUME= 2.240+02



JP 01000

Fig.A29: Shape of JP00100 and JP 01000 on the spillway surface (6)

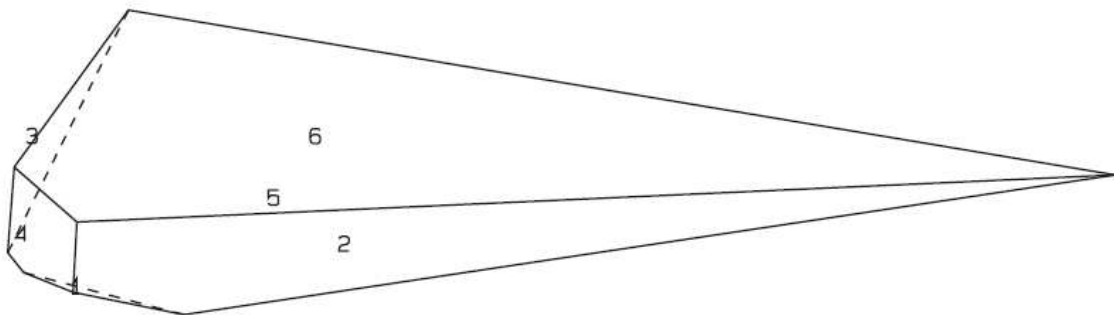
10. Appendix

```
PROJECTIVE DIRECTION:  
1.0 -1.0 1.0  
DIP, DIP D., DISTANCE  
31.0 340.0 1.3  
88.0 132.0 1.3  
88.0 248.0 1.9  
88.0 192.0 1.2  
19.0 155.0 0.9  
1.0 215.0 1.0
```

VOLUME= 4.25D+01

JP 01010

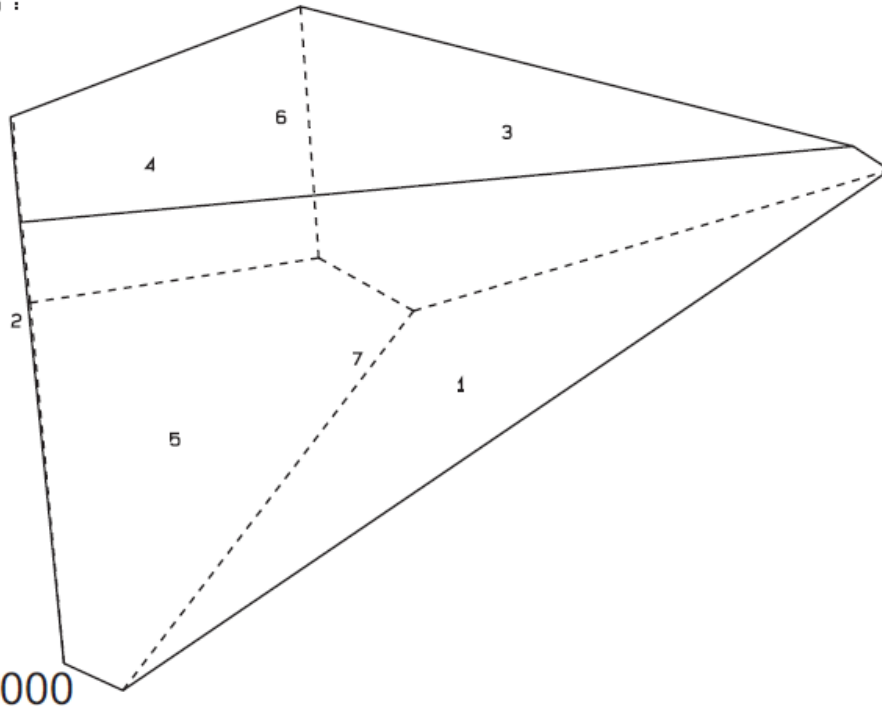
```
PROJECTIVE DIRECTION:  
1.0 -1.0 1.0  
DIP, DIP D., DISTANCE  
31.0 340.0 1.3  
88.0 132.0 1.3  
88.0 248.0 1.9  
88.0 192.0 1.2  
19.0 155.0 0.9  
1.0 215.0 1.0  
VOLUME= 6.79D+01
```



JP 01110

Fig.A30: Shape of JP01010 and JP 01110 on the spillway surface (6)

PROJECTIVE DIRECTION :  
 -1.0 -1.0 1.0  
 DIP, DIP D., DISTANCE  
 31.0 340.0 1.3  
 85.0 132.0 1.3  
 85.0 248.0 1.9  
 85.0 192.0 1.2  
 19.0 185.0 0.9  
 1.0 216.0 1.0  
 39.0 216.0 1.0  
 VOLUME= 1.920+01



PROJECTIVE DIRECTION  
 -1.0 -1.0 1.0  
 DIP, DIP D., DISTANCE  
 31.0 340.0 1.3  
 85.0 132.0 1.3  
 85.0 248.0 1.9  
 85.0 192.0 1.2  
 19.0 185.0 0.9  
 1.0 216.0 1.0  
 39.0 216.0 1.0  
 VOLUME= 1.900+01

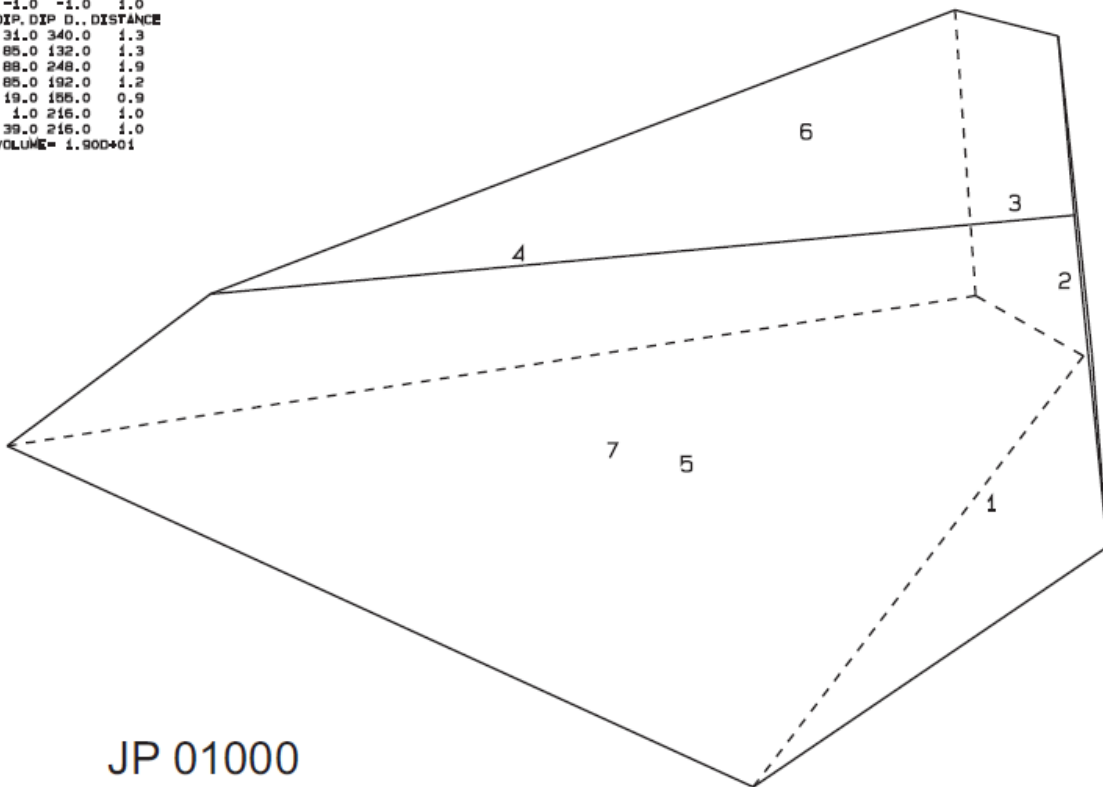
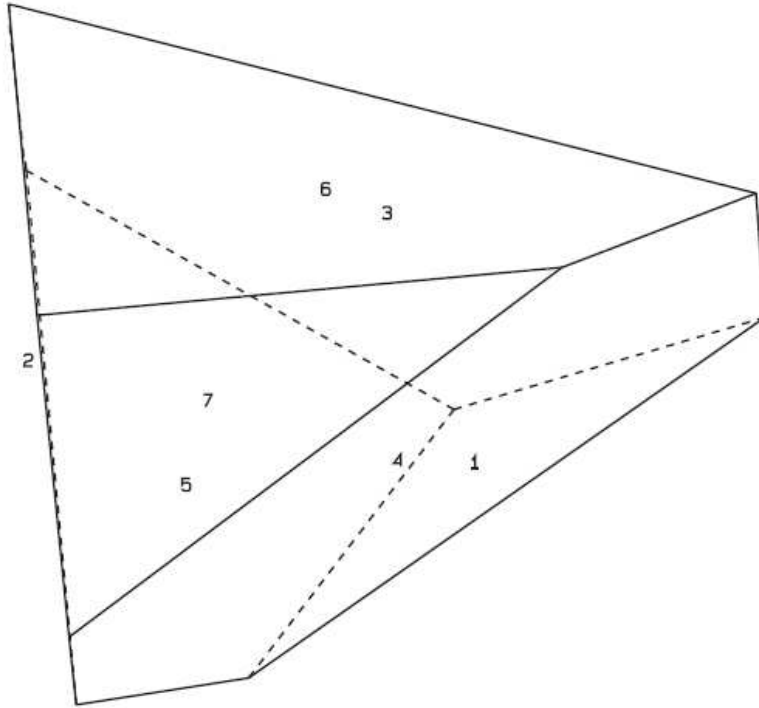


Fig.A31: Shape of JP00000 and JP 01000 on the compound slope (6+7)

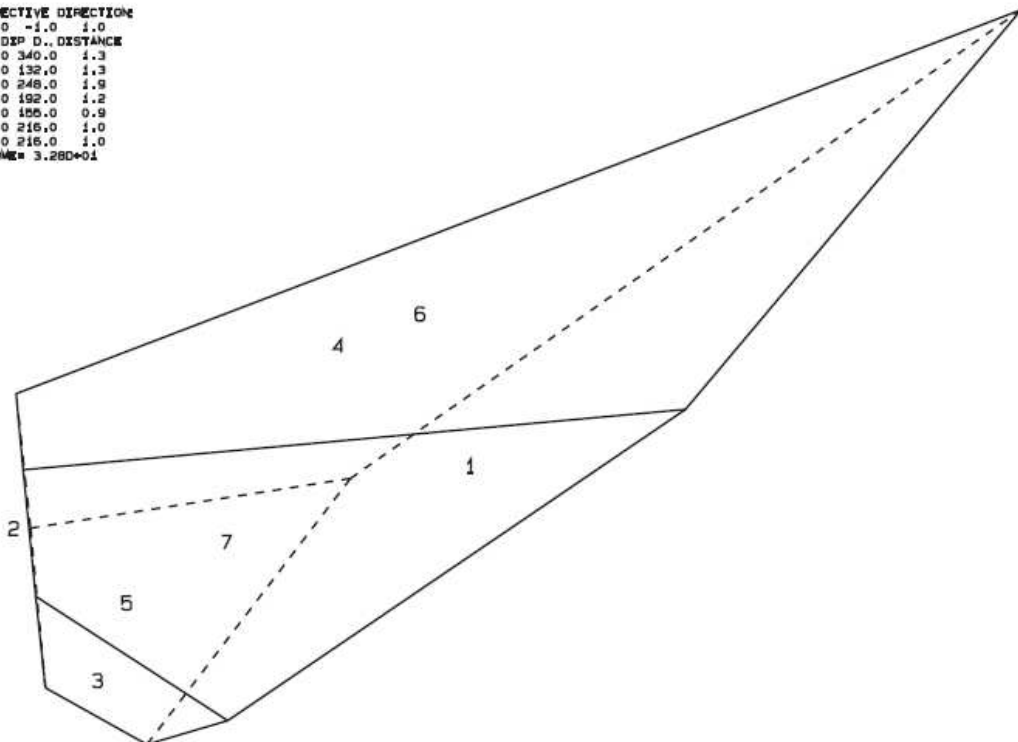


PROJECTIVE DIRECTION:  
 -1.0 -1.0 1.0  
 DXP, DYP D., DISTANCE  
 31.0 340.0 1.3  
 88.0 132.0 1.3  
 88.0 248.0 1.9  
 88.0 192.0 1.2  
 19.0 195.0 0.9  
 1.0 215.0 1.0  
 39.0 215.0 1.0  
 VOLUME= 1.900+01



JP 00010

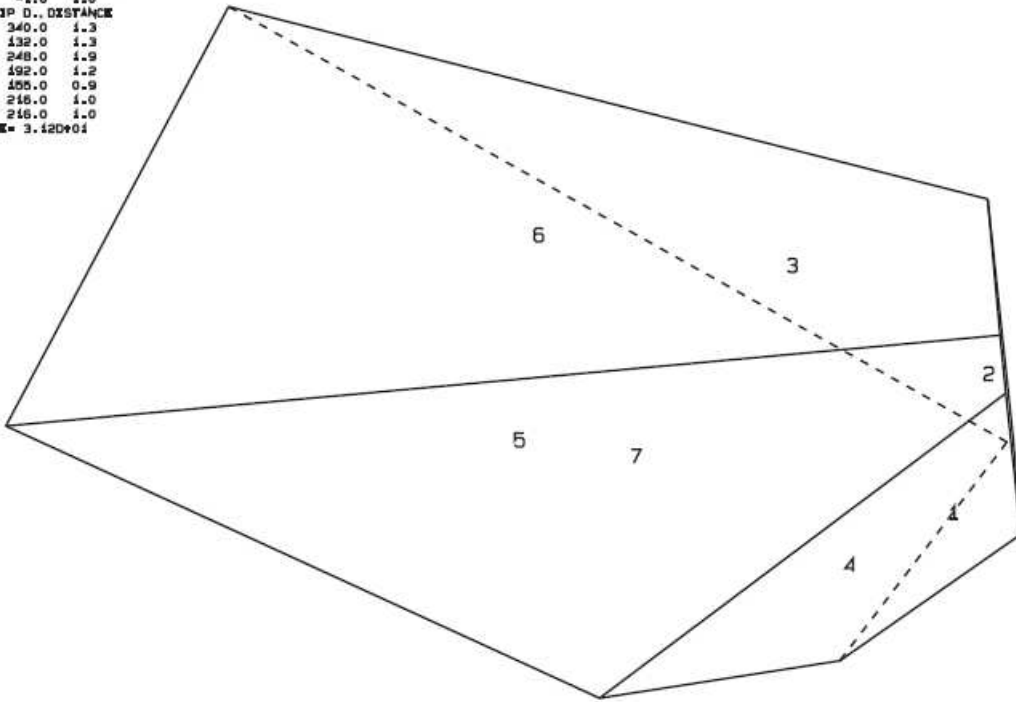
PROJECTIVE DIRECTION:  
 -1.0 -1.0 1.0  
 DXP, DYP D., DISTANCE  
 31.0 340.0 1.3  
 88.0 132.0 1.3  
 88.0 248.0 1.9  
 88.0 192.0 1.2  
 19.0 195.0 0.9  
 1.0 215.0 1.0  
 39.0 215.0 1.0  
 VOLUME= 3.280+01



JP 00100

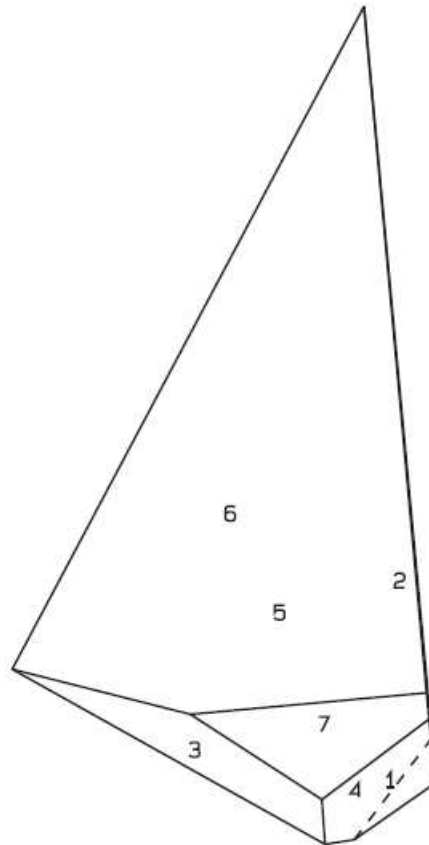
Fig.A32: Shape of JP00010 and JP 00100 on the compound slope (6+7)

PROJECTIVE DIRECTION:  
 -1.0 -1.0 1.0  
 DIP, DIP D., DISTANCE  
 31.0 340.0 1.3  
 88.0 132.0 1.3  
 88.0 248.0 1.9  
 88.0 492.0 1.2  
 19.0 485.0 0.9  
 1.0 216.0 1.0  
 39.0 216.0 1.0  
 VOLUME= 3.42D+01



JP 01010

PROJECTIVE DIRECTION:  
 -1.0 -1.0 1.0  
 DIP, DIP D., DISTANCE  
 31.0 340.0 1.3  
 88.0 132.0 1.3  
 88.0 248.0 1.9  
 88.0 492.0 1.2  
 19.0 485.0 0.9  
 1.0 216.0 1.0  
 39.0 216.0 1.0  
 VOLUME= 6.68D+01

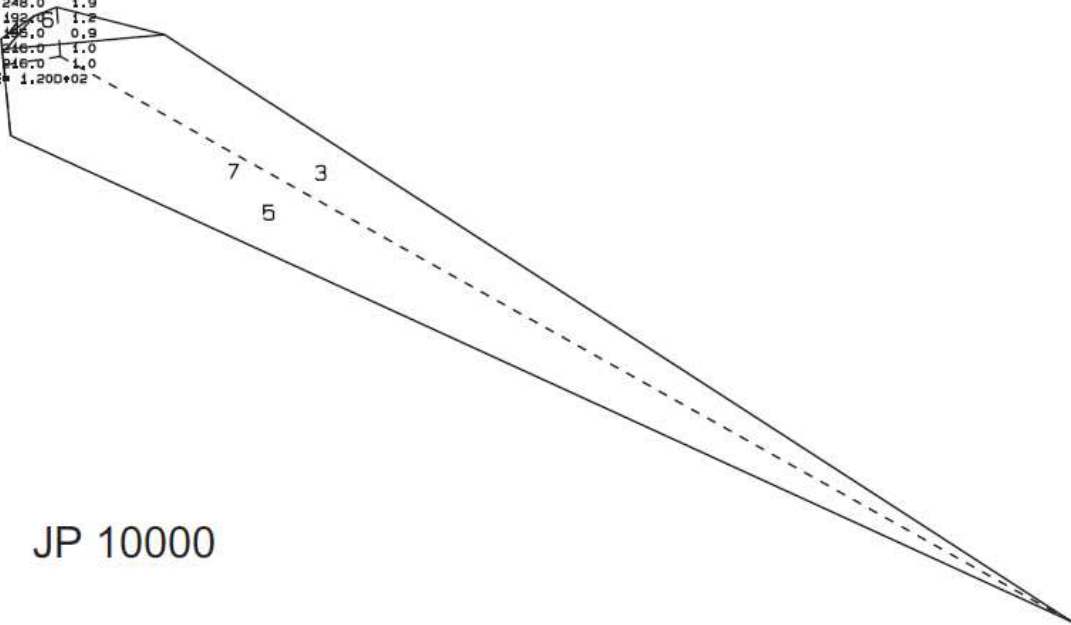


JP 01110

Fig.A33: Shape of JP01010 and JP 01110 on the compound slope (6+7)

```

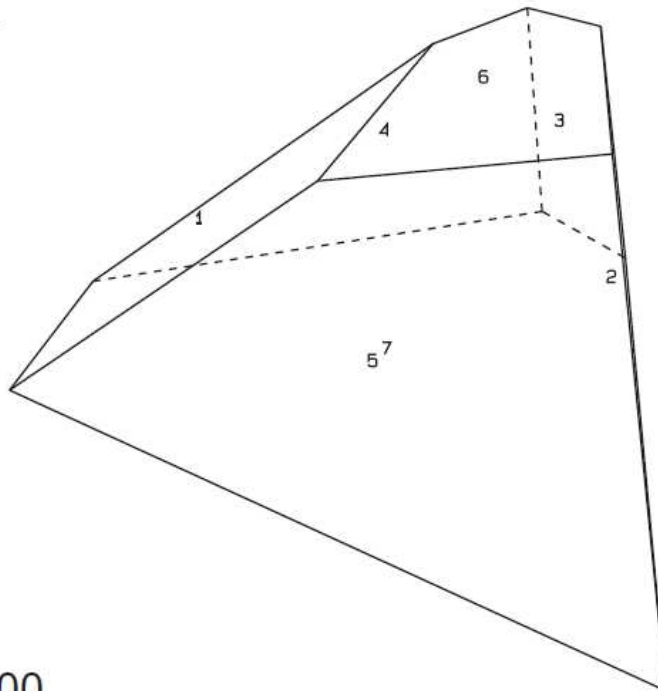
PROJECTIVE DIRECTION:
-1.0 -1.0 1.0
DIP, DIP D., DISTANCE
31.0 340.0 1.3
88.0 132.0 1.3
88.0 248.0 1.9
88.0 192.0 1.2
19.0 196.0 0.9
1.0 216.0 1.0
39.0 216.0 1.0
VOLUME= 1.200*02
    
```



JP 10000

```

PROJECTIVE DIRECTION:
-1.0 -1.0 1.0
DIP, DIP D., DISTANCE
31.0 340.0 1.3
88.0 132.0 1.3
88.0 248.0 1.9
88.0 192.0 1.2
19.0 196.0 0.9
1.0 216.0 1.0
39.0 216.0 1.0
VOLUME= 1.990*01
    
```



JP 11000

Fig.A34: Shape of JP10000 and JP 11000 on the compound slope (6+7)

```
PROJECTIVE DIRECTION  
-1.0 -1.0 1.0  
DIP, DIP D., DISTANCE  
31.0 340.0 1.3  
85.0 132.0 1.3  
88.0 248.0 1.9  
85.0 192.0 1.2  
19.0 155.0 0.9  
1.0 215.0 1.0  
39.0 215.0 1.0  
VOLUME= 2.36D+02
```

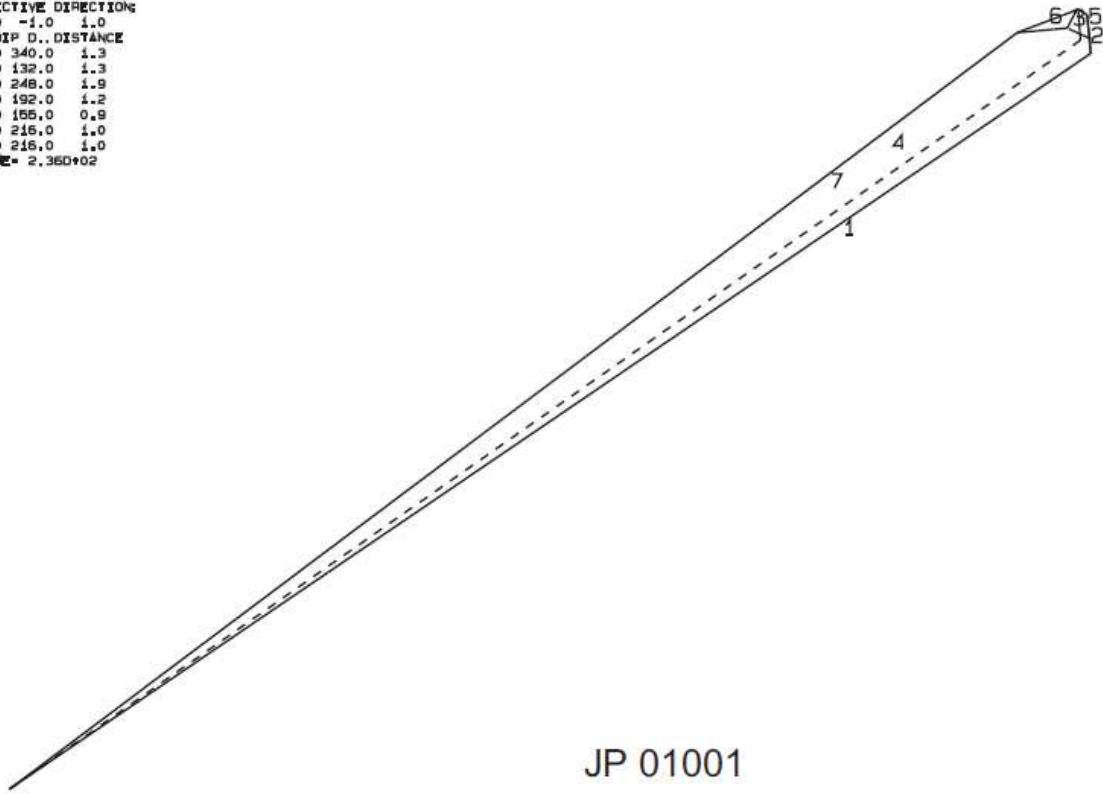


Fig.A35: Shape of JP01001 on the compound slope (6+7)